

UC Berkeley

UC Berkeley Electronic Theses and Dissertations

Title

Catalysis of 6π Electrocyclizations & Catalytic Disproportionation of Lignin Model Compounds

Permalink

<https://escholarship.org/uc/item/6qd2742t>

Author

Bishop, Lee

Publication Date

2010

Peer reviewed|Thesis/dissertation

Catalysis of 6π Electrocyclizations
&
Catalytic Disproportionation of Lignin Model Compounds

by

Lee Bishop

A dissertation submitted in partial satisfaction of the

requirements for the degree of

Doctor of Philosophy

in

Chemistry

in the

Graduate Division

of the

University of California, Berkeley

Committee in charge:

Professor Robert G. Bergman, Chair

Professor Dirk Trauner

Professor Jonathan A. Ellman

Professor Christopher D. Vulpe

Spring 2010

Abstract

Catalysis of 6π Electrocyclizations & Catalytic Disproportionation of Lignin Model Compounds

by

Lee Bishop

Doctor of Philosophy in Chemistry

University of California, Berkeley

Professor Robert G. Bergman, Chair

Part 1 – Chapter 1. The goal of the catalysis of 6π electrocyclizations is introduced in the context of known examples of the catalysis of pericyclic reactions. Recent examples of catalytic electrocyclizations and the computational and experimental precedents used to guide our approach are reviewed.

Part 1 – Chapter 2. The acid-catalyzed and thermal cyclization of an isolable vinyl *ortho*-quinone methide was investigated through DFT calculations and experimental kinetic analysis. We propose that both reactions proceed through rate-limiting *exo*-alkylidene bond isomerization followed by faster oxa- 6π electrocyclization. The vinyl *ortho*-quinone methide was found to be highly basic, allowing for quantitative protonation with weak acids. In addition, we identified a new mode of Diels-Alder dimerization of vinyl *ortho*-quinone methides.

Part 1 – Chapter 3. Density functional theory calculations were performed on the coordination of a Lewis acid to a Lewis basic ester substituent at all positions of a hexatriene molecule and the subsequent 6π electrocyclizations of these molecules. These calculations suggested catalysis of the 6π electrocyclization of 2-carbomethoxy-substituted triene substrates is possible. The electrocyclization of hexatriene substrates with a variety of other Lewis basic substituents in the 2-position were modeled in an analogous fashion.

Part 1 – Chapter 4. A 2-carboethoxy-substituted triene substrate was synthesized and catalysis of its electrocyclization using Me_2AlCl was demonstrated. Evidence is provided suggesting this reaction proceeds through rapid, reversible, exothermic formation of a catalyst-substrate complex, which then undergoes rate-limiting 6π electrocyclization.

Part 1 – Chapter 5. It was demonstrated that ester, ketone, and amide functionalities are useful Lewis-basic docking groups for the catalysis of 6π electrocyclizations. Catalysis using aldehyde moieties as docking groups was unsuccessful, most likely due to the high reactivity of the aldehyde functional group towards intramolecular nucleophilic attack, as demonstrated by the formation of a novel triene dimer. In one clear example, it was demonstrated that the hexatriene

structure must be entropically biased towards electrocyclization in order for catalysis to be successful.

Part 1 – Chapter 6. Moderate levels of enantioselectivity in catalytic 6π electrocyclizations using scandium pyridine-bis-oxazoline catalyst systems were achieved. We have also discovered a catalytic photochemical electrocyclic ring-opening and kinetic resolution of a cyclohexadiene.

Part 2 – Chapter 1. The goal of the depolymerization of lignin *via* catalytic disproportionation was introduced in the context of the development of a liquid fuel source from this biomass input. The structure, methods of isolation, and methods of industrial and environmental degradation of lignin are introduced. Initial results of the catalytic disproportionation of a lignin model compound of the glycerol- β -aryl ether linkage of lignin as well as literature examples of the types of transfer hydrogenation and carbon-oxygen bond cleavage reactions employed in this system are shown.

Part 2 – Chapter 2. Disproportionation of a 1,3-diol model compound was investigated in order to understand and optimize the retro-aldol cleavage process observed in the disproportionation of a glycerol- β -aryl ether model compound. Evidence is provided suggesting the disproportionation of the 1,3-diol model compound proceeds through rate-limiting retro-aldol cleavage. Also active processes in this reaction are dehydration, carbonyl and olefin hydrogenation, dehydrogenation of formaldehyde, and a water-gas-shift reaction. Early metal and aluminum alkoxides and aryloxides were employed as potent co-catalysts in this disproportionation reaction.

Part 2 – Chapter 3. A number of model systems were employed to investigate the carbon-oxygen bond cleavage processes that are observed in the disproportionation of a glycerol- β -aryl ether model compound. These studies suggest this reaction proceeds through ruthenium-enolate intermediates. Attempts at characterizing the catalyst resting state of the carbon-oxygen bond cleavage reaction *via* both NMR and IR analysis were unsuccessful. Experiments were performed which suggest the carbon-oxygen bond cleavage of a 2-phenoxy-1-phenylpropenone substrate proceeds through a novel mechanism.

Catalysis of 6π Electrocyclizations
&
Catalytic Disproportionation of Lignin Model Compounds

Table of Contents

Part 1. Catalysis of 6π Electrocyclizations

Chapter 1. Introduction	1
Chapter 2. Mechanistic investigations of the acid-catalyzed cyclization of a vinyl <i>ortho</i> -quinone methide	5
Chapter 3. Computational analysis of the feasibility of catalytic carba- 6π electrocyclizations	35
Chapter 4. Model substrate synthesis, catalyst development, and mechanistic analysis of a catalytic carba- 6π electrocyclization	66
Chapter 5. Investigations into the substrate scope of catalytic carba- 6π electrocyclizations	79
Chapter 6. Development of a catalytic asymmetric carba- 6π electrocyclization and discovery of a catalytic photochemical electrocyclic ring-opening	134

Part 2. Catalytic Disproportionation of Lignin Model Compounds

Chapter 1. Introduction	147
Chapter 2. Retro-aldol cleavage of a 1-phenylpropane-1,3-diol lignin model compound <i>via</i> β -hydroxypropiophenone	156
Chapter 3. Reductive ether cleavage of 1-aryl-2-aryloxyalkanol lignin model compounds <i>via</i> α -aryloxy ketones	179

Acknowledgements

I would like to begin by thanking Professor Robert Bergman. His curiosity, skepticism, and genuine concern for the safety and education of his students will be a continued source of inspiration for me in my scientific career. I am grateful for the freedom I felt to investigate almost anything that I found interesting. I would also like to thank Professor Dirk Trauner for his abundant enthusiasm, plethora of research ideas, and for always encouraging me to let my “chemical intuition flow.” I am also grateful to Professor Jonathan Ellman for allowing me to join the lignin project over half-way through my graduate career and for his continued focus on performing research that will make an impact outside of academia. It has been a joy and a challenge to work with three such different advisors. I am thankful for everything they have taught me. In addition to my graduate advisors, I would also like to thank my undergraduate advisors, Professors Zhongwu Guo, Rhett Smith, and John Protasiewicz, for giving me the opportunities and encouragement necessary to make it to where I am today.

I have depended on the help of a number of the Berkeley staff as well. Primary among those is the Bergman group administrative assistant Anneke Runtupalit, who never failed to show up with a smiling face and a positive attitude. As a nearly constant user of the NMR facility, I am also highly indebted to Chris Canlas, Rudi Nunlist, and Herman van Halbeek for keeping the facility running around the clock. I have been fortunate enough to obtain three X-ray crystal structures in my time here, and could not have done so without the help of Drs. Allen Oliver and Antonio DiPasquale. Finally, I never would have been able to run a single meaningful DFT calculation without the help of Drs. Kathy Durkin and Jamin Krinsky.

I could not have hoped for a better pair of labmates to enter the Bergman group with than Courtney Hastings and Michael Gribble. Courtney was always available for invigorating discussions, both about our latest confusing research results or the subtleties of our latest immature jokes. Michael, another friend I hope to have for life, is an endlessly entertaining and enlightening individual, and definitely one of the most intelligent people I have ever met. Other friends and colleagues whom I am extremely lucky to have known my entire time at Berkeley are Phil Morganelli, Max Merkle, Stavroula Hatzios, Laura Miller, Rachel Bernstein, Katie Berry, Katrien Brak, Nathan Shapiro, Michael Kienzler, Rob Padilla, Tabitha Clem, Tristan Beaudette, Dylan Domaille, and Lauren Comfort.

I am also indebted to members of the Bergman, Trauner, and Ellman groups, past and present: JP Lumb for being the first colleague to (perhaps foolishly) come to me for scientific advice; Gojko Lalic, who I should have relied on more than I did, for being super smart and liking non-stop NPR as much as I do; Mitch Anstey, my #1 dude in 684 Tan, for being a great labmate and friend; Jennifer Schomaker for putting up with such immature labmates and always keeping things lively; Becca Wilson for terrifying me just the right amount during my first two years; Vince Chan for being an expert complainer, but making up for it by being an awesome dude; Jason Nichols for welcoming me onto his project, and for being patient as I was getting up to speed on a new area of chemistry while also trying to graduate; Elena Arceo for holding the lab together and always laughing at Courtney’s and my jokes; Andy Tsai for organizing the *chemistry in the classroom* outreach group. Finally, I would like to thank Russel Roberson, whose patience and enthusiasm were integral to tolerating my still embryonic mentoring skills.

The graduate student who had perhaps the greatest influence on my career is Marty Mulvihill. Marty showed me that even as an academic researcher, the work I do fits within a broader social context, and it is up to me to decide what impact I will have. I am grateful for having been able to work closely with Courtney Hastings, Laura Miller, Alison Narayan, Akos Kokai, Julian Bigi, Avi Ringer, and Paul Yousefi in the planning of the Green Chemistry & Sustainable Design seminar series. Through this I have also been able to develop fruitful relationships with Berkeley faculty and staff outside of the college of chemistry, including Michael Wilson and Megan Schwarzman from the School of Public Health, Professor Chris Vulpe from the Department of Nutritional Science & Toxicology, and Professor David Sedlak from the Department of Civil & Environmental Engineering.

I owe my thanks to numerous non-chemists as well, not least of which are my parents. I certainly wouldn't be here today if it weren't for their love as well as their emotional and financial support of my continued effort to figure out what I want to do when I grow up (maybe one day I will figure it out). To have arrived at this point in my life with little debt, lots of curiosity, and a state of general emotional well-being and appreciation of life is more than I can ever hope to repay. To my dad I owe my perseverance and work ethic that were necessary to survive in an environment where expectations are so high. To my mom I owe my ability to maintain a positive attitude in the face of frustrating and confusing research results. To my grandad, Floyd Jackson, I owe my penchant for makeshift solutions and my love of distillations. I have also been lucky enough to have spent the past few years with such a beautiful, intelligent, and supportive girlfriend as Elena Spitzer. My graduate school experience has been greatly enriched by her willingness to listen to my most boring stories, her tolerance of my ridiculous working hours, her advice, and her helping me figure out how to combine my creative and scientific energy in a constructive and responsible way.

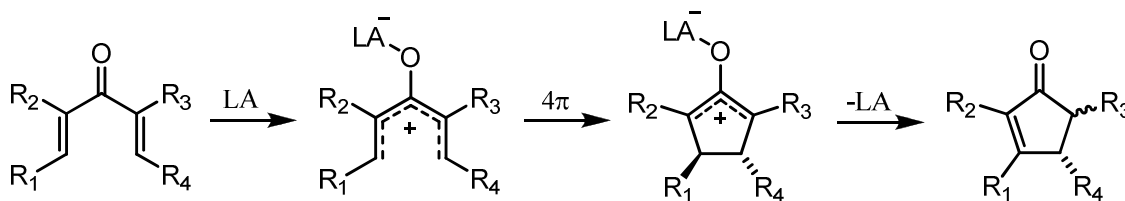
Finally, I would like to thank the entire scientific community, from the dawn of civilization forward, for creating and fostering the knowledge and social momentum on which I have relied to make the small contribution presented herein.

Dedicated to Floyd and Greta Jackson

Part 1 – Chapter 1. *Introduction to the Catalysis of 6 π Electrocyclizations*

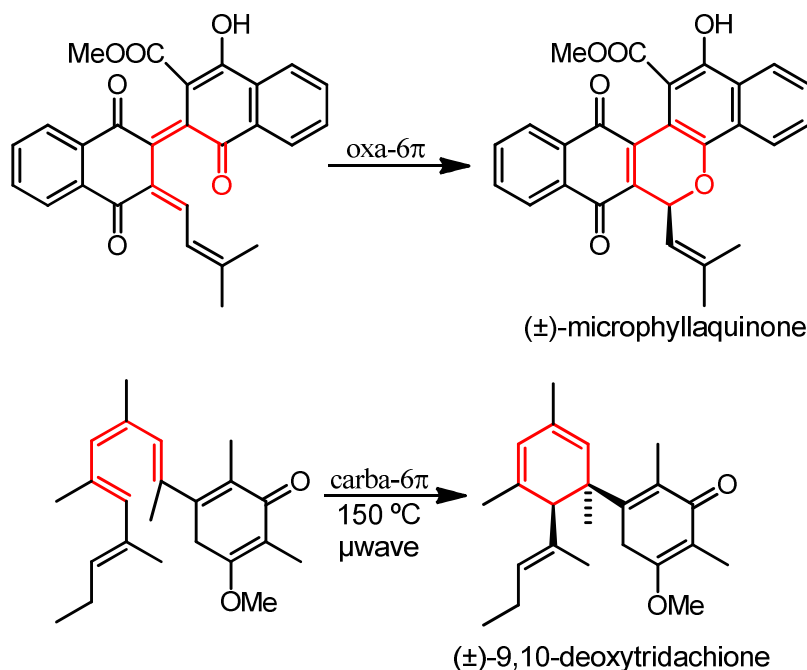
Pericyclic reactions are those that pass through a single transition state possessing a cyclic array of atoms and a corresponding cyclic array of electrons. Pericyclic reactions have been employed widely in synthesis, due in part to their high reliability and stereospecificity.¹⁻⁵ Since the 1965 report by R. B. Woodward and R. Hoffmann that the course of these reactions is governed by the “conservation of orbital symmetry”, pericyclic reactions have been the subject of numerous theoretical analyses.⁶⁻⁹

The emergence of methods to catalyze pericyclic reactions has greatly increased their synthetic power. Of their three main classes, namely cycloadditions, sigmatropic rearrangements, and electrocyclizations, catalytic and catalytic asymmetric cycloadditions¹⁰⁻¹⁴ and sigmatropic rearrangements^{15,16} have been achieved. However, until recently general methods for the catalysis of electrocyclizations has remained elusive, with the notable exception of the acid-catalyzed cyclization of divinyl ketones *via* the 4 π electrocyclization of pentadienylic cations, known as the Nazarov cyclization (Scheme 1).¹⁷⁻¹⁹ First discovered by the cyclization of dibenzylidene acetone under acidic conditions in 1903 and later researched extensively by Nazarov and co-workers,²⁰⁻²⁵ the Nazarov cyclization was first rendered catalytically asymmetric by the Trauner group in 2003 through the use of scandium-pyridine-bis-oxazoline catalysts with substrates capable of bidentate catalyst binding.²⁶⁻²⁹ More recently, catalytic asymmetric 6 π electrocyclizations under phase-transfer and chiral Brønsted acid conditions have been developed for use in the synthesis of indolines and pyrazolines, respectively.^{30,31}



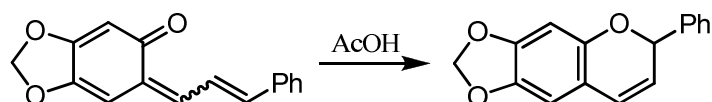
Scheme 1. General mechanism of the Nazarov cyclization. LA = Lewis acid.

The development of general methods for the catalysis of electrocyclizations would enable these reactions to occur under milder conditions and create the possibility of catalytic asymmetric variants. Though in recent years asymmetric 8 π , 6 π , and 4 π electrocyclizations have been achieved by appending chiral auxiliaries to a reacting terminus,³²⁻³⁵ we have focused on achieving asymmetry through catalysis, both as a fundamental synthetic and mechanistic challenge as well as a means of avoiding the stoichiometric waste products associated with auxiliary-based approaches. The Trauner group has employed oxa- and carba-6 π electrocyclizations in the racemic syntheses of a number of natural products, wherein the electrocyclization is the enantio-determining step (Scheme 2).^{2,36-38} We chose therefore to focus first on developing methods for the catalysis of 6 π electrocyclizations, due to our above-described expertise in the application of these reactions in organic synthesis as well as the fact that affecting carba-6 π electrocyclizations often requires the use of high temperatures.³⁸⁻⁴⁰



Scheme 2. Natural products synthesized *via* 6π electrocyclizations.^{36,38}

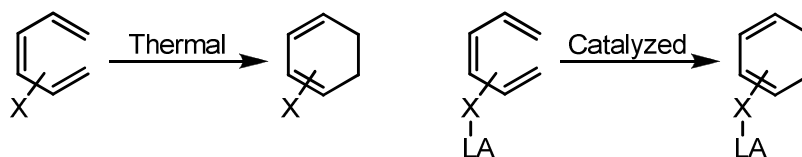
In commencing this work we first investigated a 1977 example of the acid-promoted cyclization of an isolable *ortho*-quinone methide (Scheme 3).⁴¹ As will be outlined in Chapter 2, we determined that this catalysis arises from a catalytic olefin isomerization and not a catalytic oxa- 6π electrocyclization. We published the primary findings of these studies in 2008.⁴²



Scheme 3. Acid-promoted cyclization of an isolable *ortho*-quinone methide.⁴¹

As the work described in Chapter 2 indicate the development of methods for the catalysis of oxa- 6π electrocyclizations is not likely, we turned our attention to the catalysis of carba- 6π electrocyclizations. Though the transition-metal catalyzed cyclization of dienylalkynes is postulated to proceed through 6π electrocyclization of dienyl-substituted metal-vinylidenes,⁴³ and thus could be considered a catalytic electrocyclization, the reaction does not occur in the absence of catalyst, and therefore no rate acceleration can be measured. We focused on developing catalytic methods for the electrocyclization of hexatriene systems where the rate of the thermal electrocyclization can be directly compared to that of the catalyzed process in order to definitively assess whether lowering of the electrocyclization energy barrier occurs.

Experimental and computational studies have shown that the rate of 6π electrocyclizations can be influenced by varying the electronics of the substituents on the triene.^{39,44-50} We envisioned exploiting this effect by using a Lewis acid catalyst to modulate the electronics of a pendant Lewis basic triene substituent, thereby modulating the electrocyclization energy barrier of the catalyst-bound triene (Scheme 4).



Scheme 4. Modulation of the electronics and electrocyclic energy barrier of a triene by Lewis acid catalysis.

We computationally determined that this is a viable approach to the catalysis of 6π electrocyclizations, and these studies are outlined in Chapter 3. We have reduced the predictions of these calculations to practice and experimentally investigated the mechanism of this catalysis, as is outlined in Chapter 4. We have also begun investigations into the substrate scope and a catalytic asymmetric variant of this reaction, which are described in Chapters 5 and 6, respectively. We have previously published the initial reaction discovery, mechanistic and computational analysis, and an initial demonstration of the substrate scope of this reaction.^{51,52}

References

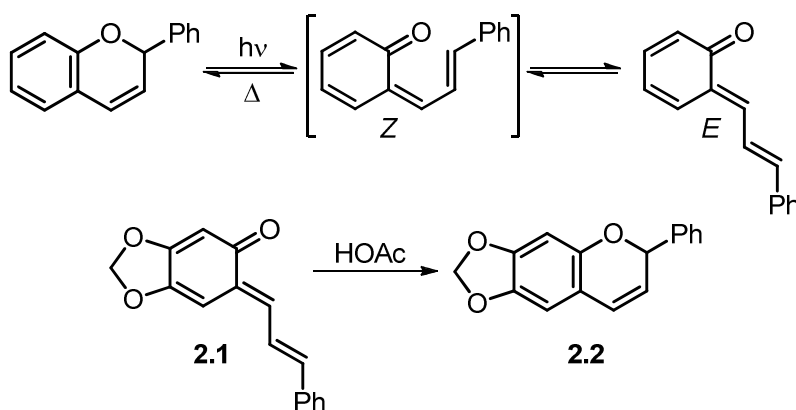
- (1) Miller, A. K.; Trauner, D. *Synlett* **2006**, *14*, 2295.
- (2) Beaudry, C. M.; Malerich, J. P.; Trauner, D. *Chem. Rev.* **2005**, *105*, 4757.
- (3) Arns, S.; Barriault, L. *J. Chem. Soc., Chem. Commun.* **2007**, 2211.
- (4) Stevenson, P. J. *Annu. Rep. Prog. Chem., Sect. B: Org. Chem.* **1999**, *95*, 19.
- (5) Pindur, U.; Schneider, G. H. *Chem. Soc. Rev.* **1994**, *23*, 409.
- (6) Woodward, R. B.; Hoffmann, R. *J. Am. Chem. Soc.* **1965**, *87*, 395.
- (7) Woodward, R. B.; Hoffmann, R. *The Conservation of Orbital Symmetry*; Verlag Chemie: Weinheim, 1970.
- (8) Cunningham, I. D. *Annu. Rep. Prog. Chem., Sect. B: Org. Chem.* **1995**, *92*, 25.
- (9) Tantillo, D. J. *Annu. Rep. Prog. Chem., Sect. B: Org. Chem.* **2006**, *102*, 269.
- (10) Kagan, H. B.; Riant, O. *Chem. Rev.* **1992**, *92*, 1007.
- (11) Gothelf, K. V.; Jørgensen, K. A. *Chem. Rev.* **1998**, *98*, 863.
- (12) Jørgensen, K. A. *Angew. Chem. Int. Ed.* **2000**, *39*, 3558.
- (13) Corey, E. J. *Angew. Chem. Int. Ed.* **2002**, *41*, 1650.
- (14) Kobayashi, S.; Jørgensen, K. A. *Cycloaddition Reactions in Organic Synthesis*; Wiley-VCH: Weinheim, 2002.
- (15) Hiersemann, M.; Abraham, L. *Eur. J. Org. Chem.* **2002**, 1461.
- (16) Nubbemeyer, U. *Synthesis* **2003**, 961.
- (17) Frontier, A. J.; Collison, C. *Tetrahedron* **2005**, *61*, 7577.
- (18) Pelissier, H. *Tetrahedron* **2005**, *61*, 6479.
- (19) Tius, M. A. *Eur. J. Org. Chem.* **2005**, 2193.
- (20) Vorländer, D.; Schroeter, G. *Chem. Ber.* **1903**, *36*, 1490.
- (21) Blomquist, A. T.; Marvel, C. S. *J. Am. Chem. Soc.* **1933**, *55*, 1655.
- (22) Mitchell, D. T.; Marvel, C. S. *J. Am. Chem. Soc.* **1933**, *55*, 4276.
- (23) Nazarov, I. N.; Zaretskaya, I. I. *Bull. Acad. Sci. USSR Div. Chem. Sci.* **1942**, 200.
- (24) Nazarov, I. N.; Zaretskaya, I. I. *Zh. Obshch. Khim* **1957**, *27*, 693.
- (25) Nazarov, I. N.; Zaretskaya, I. I.; Sorkina, T. I. *Zh. Obshch. Khim* **1960**, *30*, 746.
- (26) Liang, G.; Gradl, S. N.; Trauner, D. *Org. Lett.* **2003**, *5*, 4931.
- (27) Aggarwal, V. K.; Belfield, A. J. *Org. Lett.* **2003**, *5*, 5075.

- (28) Liang, G.; Trauner, D. *J. Am. Chem. Soc.* **2004**, *126*, 9544.
- (29) Rueping, M.; Ieawsuwan, W.; Antonchick, A. P.; Nachtsheim, B. J. *Angew. Chem. Int. Ed.* **2007**, *46*, 2097.
- (30) Maciver, E. E.; Thompson, S.; Smith, M. D. *Angew. Chem. Int. Ed.* **2009**, *48*, 9979.
- (31) Müller, S.; List, B. *Angew. Chem. Int. Ed.* **2009**, *48*, 9975.
- (32) Parker, K. A.; Wang, Z. *Org. Lett.* **2006**, *8*, 3553.
- (33) Tanaka, K.; Katsumura, S. *J. Am. Chem. Soc.* **2002**, *124*, 9660.
- (34) Sydorenko, N.; Hsung, R. P.; Vera, E. L. *Org. Lett.* **2006**, *8*, 2611.
- (35) Bongini, A.; Panunzio, M.; Tamanini, E.; Martelli, G.; Vicennati, P.; Monari, M. *Tetrahedron: Asymmetry* **2003**, *14*, 993.
- (36) Lumb, J.-P.; Trauner, D. *Org. Lett.* **2005**, *7*, 5865.
- (37) Malerich, J. P.; Trauner, D. *J. Am. Chem. Soc.* **2003**, *125*, 9554.
- (38) Miller, A. K.; Trauner, D. *Angew. Chem. Int. Ed.* **2005**, *44*, 4602.
- (39) Marvell, E. N. *Thermal Electrocyclic Reactions*; Academic Press: New York, 1980; Vol. 43.
- (40) Ansari, F. L.; Qureshi, R.; Qureshi, M. L. *Electrocyclic Reactions: from fundamentals to research*; Wiley: New York, 1999.
- (41) Jurd, L. *Tetrahedron* **1977**, *33*, 163.
- (42) Bishop, L. M.; Winkler, M.; Houk, K. N.; Bergman, R. G.; Trauner, D. *Chem. Eur. J.* **2008**, *14*, 5405.
- (43) Varela, J. A.; Saá, C. *Chem. Eur. J.* **2006**, *12*, 6450.
- (44) Spangler, C. W.; Jondahl, T. P.; Spangler, B. *J. Org. Chem.* **1973**, *38*, 2478.
- (45) Carpenter, B. K. *Tetrahedron* **1978**, *34*, 1877.
- (46) Evanseck, J. D.; Thomas, B. E. I.; Spellmeyer, D. C.; Houk, K. N. *J. Org. Chem.* **1995**, *60*, 7134.
- (47) Magomedov, N. A.; Ruggiero, P. L.; Tang, Y. *J. Am. Chem. Soc.* **2004**, *126*, 1624.
- (48) Guner, V. A.; Houk, K. N.; Davies, I. W. *J. Org. Chem.* **2004**, *69*, 8024.
- (49) Greshock, T. J.; Funk, R. L. *J. Am. Chem. Soc.* **2006**, *128*, 4946.
- (50) Yu, T.-Q.; Fu, Y.; Liu, L.; Guo, Q.-X. *J. Org. Chem.* **2006**, *71*, 6157.
- (51) Barbarow, J. E., The University of California, 2007.
- (52) Bishop, L. M.; Barbarow, J. E.; Bergman, R. G.; Trauner, D. *Angew. Chem. Int. Ed.* **2008**, *47*, 8100.

Part 1 - Chapter 2. Mechanistic Investigations into the Acid-Catalyzed Cyclization of a Vinyl Ortho-Quinone Methide

Introduction

The reversible ring opening of chromenes to yield vinyl *ortho*-quinone methides (vinyl *o*-QMs) has been the subject of extensive studies. This reaction is one of the first photochromic processes to be investigated and has important applications in certain materials, such as photochromic ophthalmic lenses.¹⁻⁴ Whereas the photochemical ring opening is well understood,¹⁻⁴ the thermal reverse reaction has received relatively little attention. This is mostly due to difficulties with generating isolable vinyl *o*-QMs. These typically contain *E*-configured *exo*-alkylidene bonds preventing them from undergoing *oxa*-6 π electrocyclizations (Scheme 1).⁵⁻⁹ The kinetics of vinyl *o*-QM cyclization or the possibility of catalyzing this processes have not been investigated in detail.

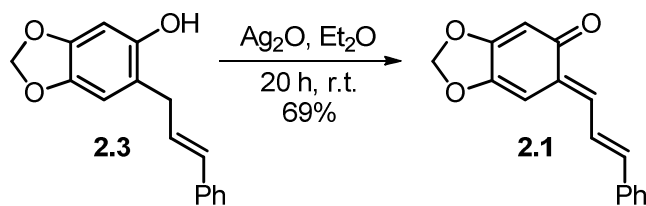


Scheme 1. Cyclization of vinyl *ortho*-quinone methides.⁵

In the context of our ongoing studies on the catalysis of electrocyclizations, we became interested in a report by Jurd describing an acid-promoted cyclization of the isolable vinyl *o*-QM **2.1** to chromene **2.2** (Scheme 1).⁵ We now present a detailed study of this reaction, which has general implications for the thermal cyclization of vinyl *o*-QMs to afford chromenes. This work was published in *Chemistry – A European Journal* in 2008.¹⁰

Results & Discussion

Vinyl *o*-QM **2.1** was prepared through oxidation of phenol **2.3** according to literature procedures (Scheme 2).⁵ The *E*-configuration of the *exo*-alkylidene bond was established by a NØE spectroscopy study which showed cross-peaks between the styrenic and quinoidal protons of **2.1** (Figure 1).



Scheme 2. Synthesis of vinyl *o*-QM **2.1**.

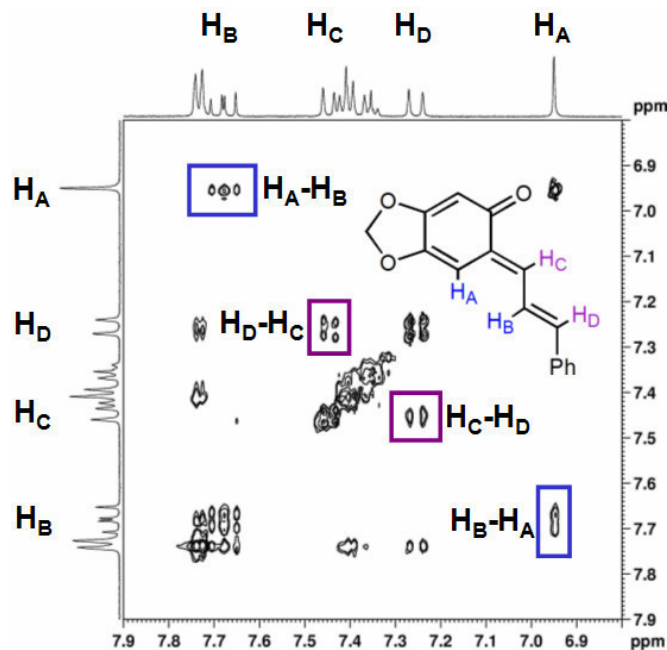


Figure 1. Nuclear Overhauser effect spectrum of vinyl *o*-QM **2.1**.

A single crystal X-ray diffraction study was also carried out on **2.1**, which confirmed the assignment of the *E* configuration of the *exo*-alkylidene bond (Figure 2). In addition, this structure reveals the extended conjugation of the π system of **2.1**, which is evident in the planarity of the molecule. This is also evident in the lengths of the double and single bonds, which are around 0.02-0.04 Å longer and shorter, respectively, than would be expected for those of a non-conjugated system.¹¹ Interestingly, this is not the case for the C1-C2 single bond, which is longer than the other single bonds of **2.1** presumably due to A^{1,3} strain of the O1, C1, C2, C3 system.

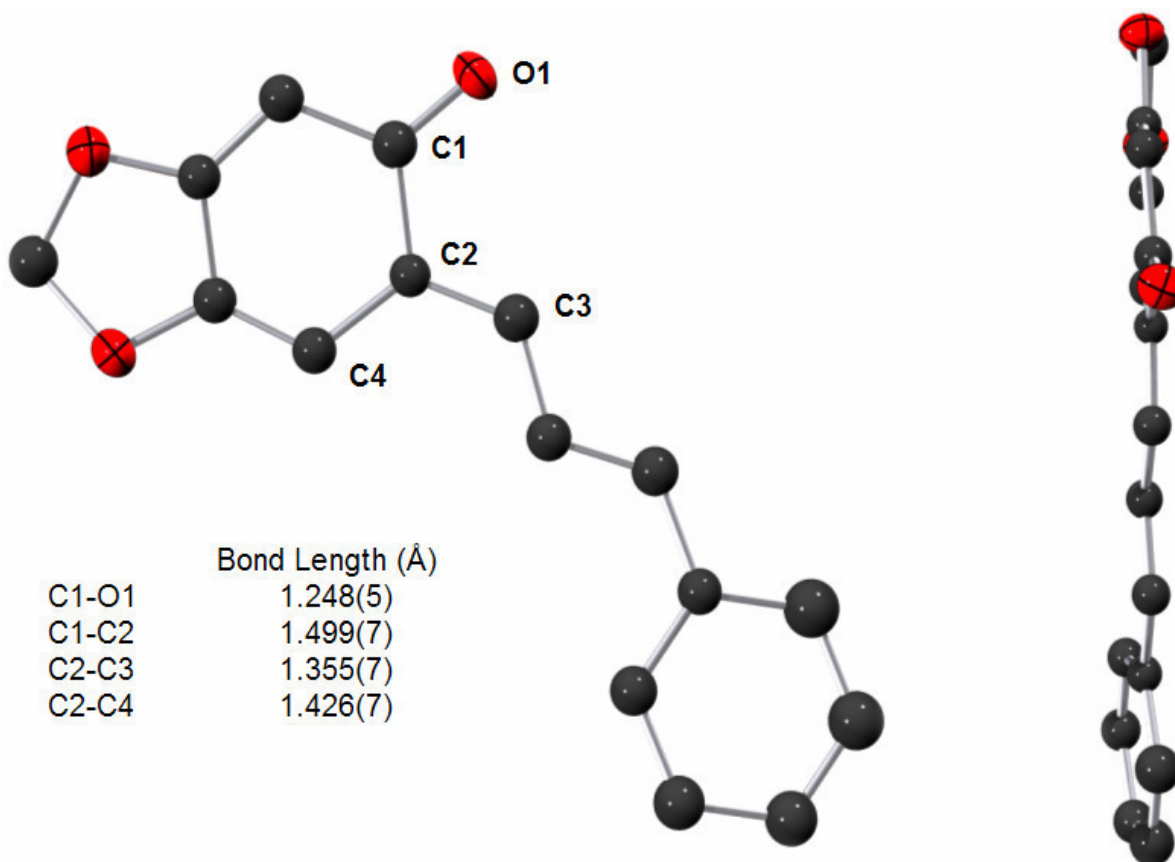
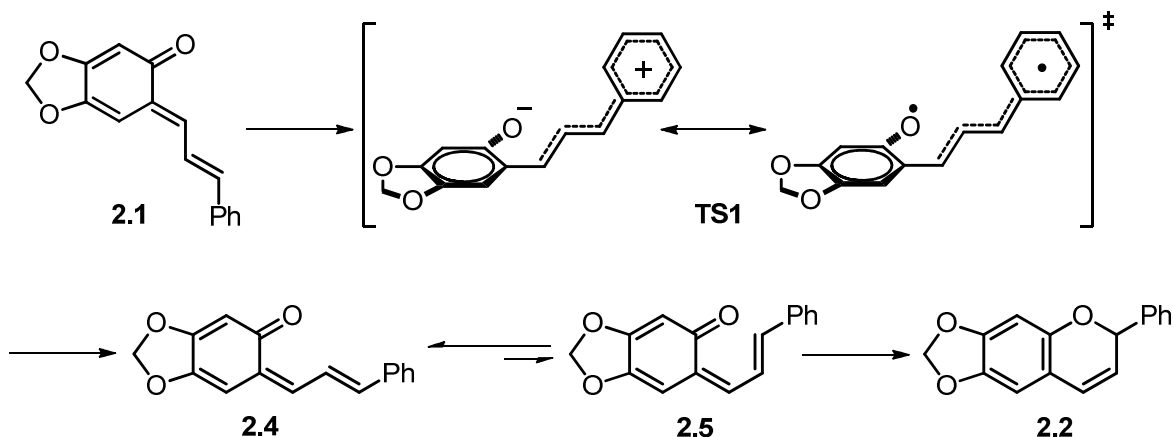


Figure 2. ORTEP diagram of **2.1** at the 50% probability level, with representative bond lengths. Hydrogen atoms have been removed for clarity.

With vinyl *o*-QM **2.1** in hand, we proceeded to study its reactivity. Kinetic investigation of the uncatalyzed cyclization of **2.1** to **2.2** revealed the sensitivity of the rate of this reaction to light, oxygen, and adventitious acid. However, reproducible kinetic data could be obtained in the absence of light, under air-free conditions and in the presence of Proton-sponge™ (1,8-Bis(dimethylamino)naphthalene). Monitoring the cyclization *via* ¹H NMR spectroscopy revealed quantitative formation of **2.2** with no observable intermediates. Kinetic data fit a first order exponential process, with a k_{obs} of $4.2(1) \times 10^{-5} \text{ s}^{-1}$ at 50 °C.



Scheme 3. Proposed mechanism for the thermal cyclization of vinyl *o*-QM **2.1**.

Given the *E*-configuration of the *exo*-alkylidene bond of **2.1**, we hypothesized that the rate-limiting step in the cyclization of **2.1** to **2.2** was the double-bond isomerization and not the subsequent electrocyclization. The activation parameters for the thermal reaction support this hypothesis (Table 1). A relatively modest enthalpy of activation was measured for this process, which we attribute to the aromatization of the quinoidal system in the *exo*-alkylidene bond isomerization transition state (Scheme 3, **TS1**). The reaction also exhibits a highly negative entropy of activation (-38 e.u.), revealing a high degree of order in the transition state of the rate-limiting step, relative to the vinyl *o*-QM reactant. Entropies of activation for *oxa*-6 π electrocyclizations are typically around -12 e.u.¹² However, entropies of activation for the isomerization of push-pull alkenes are quite negative, an effect that has been attributed to solvent reorganization on going from the relatively non-polar reactant to the highly polar transition state, possessing zwitterionic character.¹³ This could also be the case for the cyclization of **2.1**, as DFT calculations suggest the *E/Z* isomerization transition state is highly polar. The calculated dipole moments of **2.1**, **TS1**, and **2.4** are 4.52, 4.56, and 2.86 D, respectively. The charge distribution, as conjectured from natural population analysis, is also comparable for all three stationary points. Because the transition state is polar in all three spatial directions, whereas **2.1** and **2.4** are planar species, stronger solvation of the transition state as compared to the reactant should nevertheless lead to a strongly negative entropy of activation for the *E/Z* isomerization step. Thus, these activation parameters are consistent with a stepwise process, wherein a rate-limiting double bond isomerization step is followed by a faster *oxa*-6 π electrocyclization.

Table 1. Activation parameters for the thermal cyclization of **2.1** in CD₂Cl₂.

	Thermal
ΔH^\ddagger (kcal/mol)	13.3(4)
ΔS^\ddagger (e.u.)	-38(5)
ΔG^\ddagger_{298} (kcal/mol)	24.6(8)

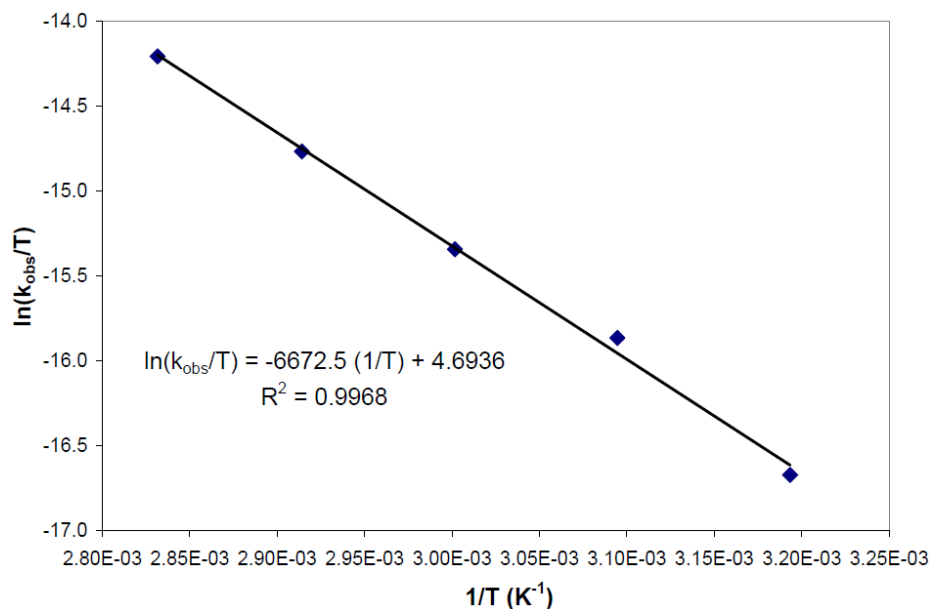


Figure 3. Eyring plot for the thermal cyclization of **2.1** in CD_2Cl_2 .

Next, we proceeded to investigate the influence of Brønsted acids on the rate of the cyclization. Catalytic amounts of chloroacetic acid (0.23 equiv.) led to a 200-fold rate acceleration at 21 °C ($k_{\text{obs}} = 1.31(2) \times 10^{-3} \text{ s}^{-1}$). Interestingly, a shift in the ^1H NMR resonances of **2.1** was observed upon addition of chloroacetic acid, which suggested the vinyl *o*-QM was being appreciably protonated with sub-stoichiometric amounts of acid. Low temperature NMR titration (Figure 4) revealed near quantitative protonation of **2.1** using 9 equivalents of chloroacetic acid. Interestingly, this effect was not observed using acetic acid, which allows us to estimate the $\text{p}K_{\text{a}}$ of the protonated vinyl *o*-QM to be approximately 4.

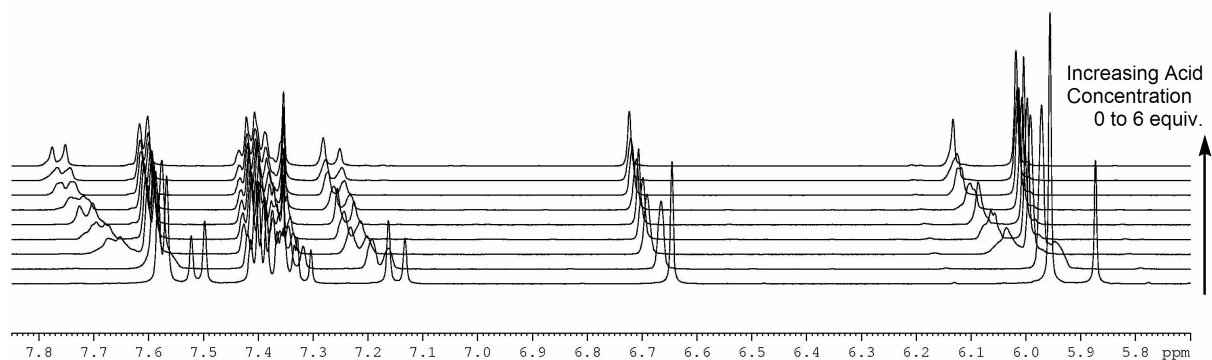


Figure 4. NMR-titration of **2.1** with ClCH_2COOH at $-40\text{ }^\circ\text{C}$.

The unusually high $\text{p}K_{\text{a}}$ of **2.1H** allowed us to observe substrate-saturation kinetics using chloroacetic acid as catalyst (Figure 5). This substrate saturation effect is consistent with a rapid catalyst binding pre-equilibrium followed by rate-limiting transformation of the catalyst-bound substrate species.

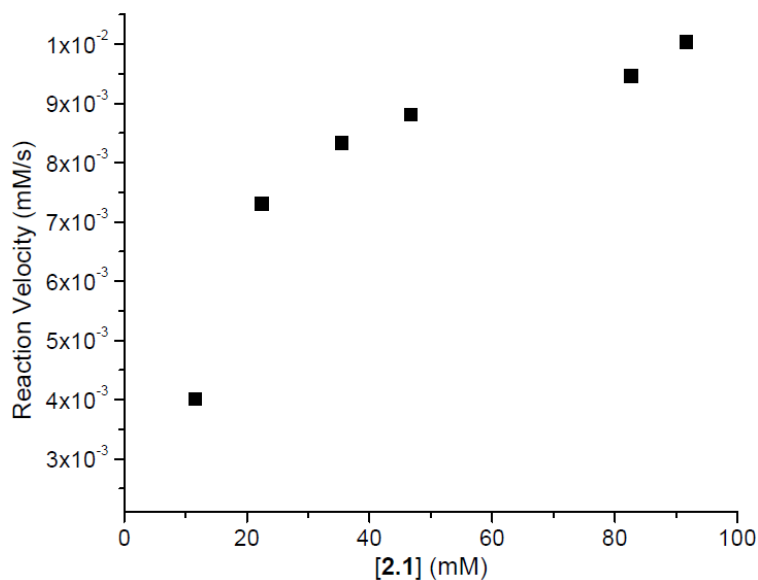


Figure 5. Saturation in **2.1**. Conditions: $[\text{ClCH}_2\text{COOH}] = 0.3 \text{ mM}$

Eyring analysis provides further insight into the mechanism of the catalyzed process. In order to determine the activation parameters for the rate-limiting step in the catalyzed reaction, kinetic data were obtained under acid saturation to assure that we were monitoring only cyclization of the protonated vinyl *o*-QM species with no effect from the protonation pre-equilibrium. Both the enthalpy and entropy of activation for the catalyzed reaction increase dramatically as compared to those of the thermal reaction (Table 2 vs Table 1).

Table 2. Activation parameters for the catalyzed (9 equiv acid) cyclization of **2.1** in CD_2Cl_2 .

	Catalyzed
ΔH^\ddagger (kcal/mol)	20.1(4)
ΔS^\ddagger (e.u.)	-4.1(1)
ΔG^\ddagger_{298} (kcal/mol)	21.3(4)

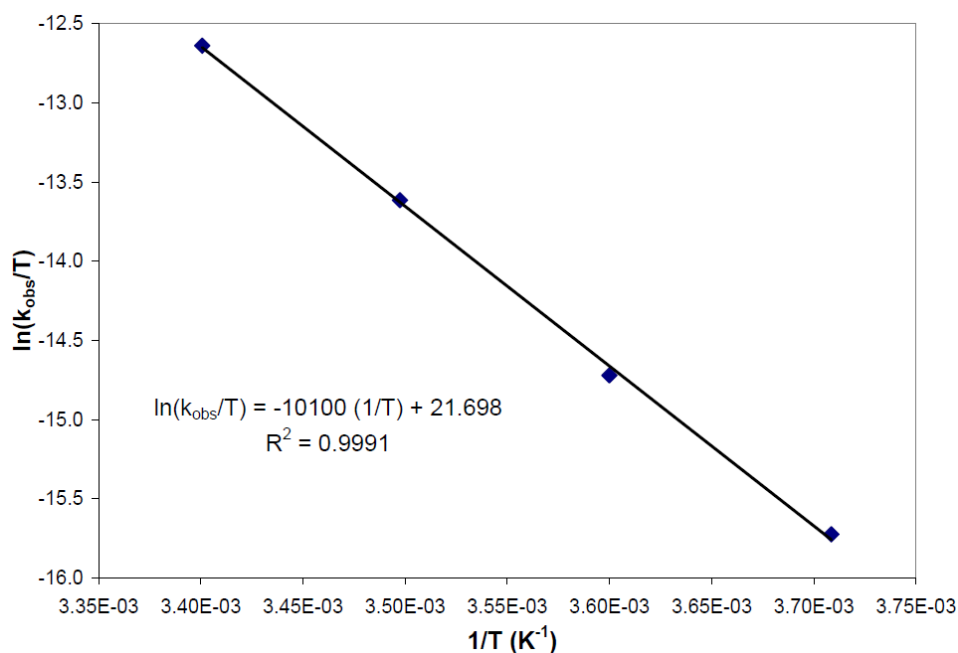
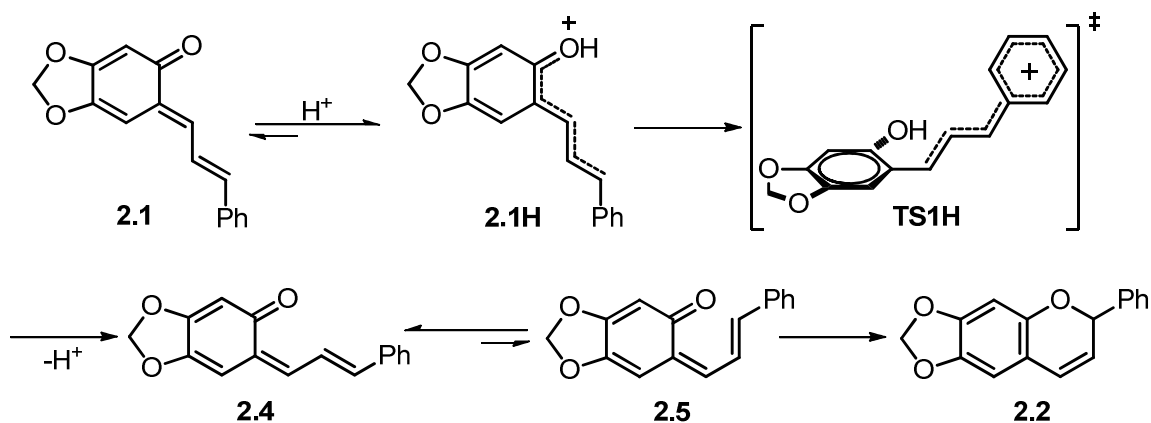


Figure 6. Eyring plot for the catalyzed (9 equiv acid) cyclization of **2.1** in CD_2Cl_2 .

The less negative entropy of activation for the catalyzed reaction suggests only a small change in polarity between the protonated *o*-QM reactant and the isomerization transition state. This observation is consistent with the small polarity change that would be expected under acid-saturated conditions on going from the cationic *o*-QM **1H** to the cationic isomerization transition state **TS1H** (Scheme 4). The increased enthalpy of activation must be understood in terms of the basicity of **2.1**. Protonation of **2.1** results in aromatization of the quinoidal system giving a doubly benzylic cation. This aromatization enthalpically stabilizes the vinyl *o*-QM reactant relative to the isomerization transition state. This is in contrast to the thermal reaction, where aromatization of the quinoidal system occurs only once the transition state is reached, resulting in a lower enthalpy of activation for the thermal process. Thus, based on these activation parameters as well as the substrate saturation and NMR titration data we propose that the catalyzed reaction also proceeds by a rapid protonation pre-equilibrium followed by rate-limiting *exo*-alkylidene bond isomerization. In addition, a kinetic isotope effect of 1 using ClCH_2COOD was measured under acid-saturation conditions. Our post-rate-limiting step mechanistic proposal is based on density functional theory calculations (*vide infra*).



Scheme 4. Proposed mechanism for the acid-catalyzed cyclization of vinyl *o*-QM **2.1**.

In parallel to our experimental work, the energetics of the thermal and catalyzed reactions were modeled by density functional theory calculations by Dr. Michael Winkler at Universität Würzburg. The pathway whereby *E/Z* isomerization precedes *s-cis/s-trans* isomerization was modeled along with the pathway whereby *E/Z* isomerization is preceded by *s-cis/s-trans* isomerization at the UB3LYP/6-31G* level (Figure 7). According to these calculations, the *exo*-alkylidene bond isomerization is the rate-limiting step in the thermal cyclization, having a Gibbs free energy barrier of 29.3 kcal/mol, which is over 10 kcal/mol higher than the electrocyclic barrier. The lowest energy pathway for the thermal reaction occurs *via* *exo*-alkylidene bond isomerization of **2.1** to give the *Z* *o*-QM **2.4**, which can then undergo *s-cis/s-trans* isomerization ($\Delta G^\ddagger = 13.8$ kcal/mol) to give **2.5**, which is poised to undergo an *oxa*-6 π electrocyclic cyclization ($\Delta G^\ddagger = 19.8$ kcal/mol) to give chromene **2.2**. Thus, these calculations mirror our experimental evidence that the isomerization, not the electrocyclic cyclization, is the rate-limiting step of the thermal cyclization.

The catalyzed reaction was modeled by protonation of the carbonyl oxygen of **2.1** *anti* to the *exo*-alkylidene bond. The calculated lowering of the catalyzed *exo*-alkylidene *E/Z* isomerization barrier by 4-5 kcal/mol,¹⁶ relative to the thermal reaction barrier, is in reasonable agreement with the experimental observation of a 3.3 kcal/mol lowering in the Gibbs free energy of activation. The measured activation parameters indicate that acid-catalysis is due to a strong increase in the entropy of activation that more than outweighs the increased enthalpy of activation. The gas phase computations, on the other hand, that do not include solvent effects indicate that the catalyzed reaction is enthalpically more favorable than the thermal isomerization with very minor contributions from entropy. Inasmuch as the DFT calculated energies of **TS1** and **TS1H** are accurate, the comparison of calculated and measured activation parameters gives thus another clue to the decisive role of solvent effects in the *E/Z* isomerization barrier of push-pull substituted alkenes.¹³ The computations also show that upon protonation of **2.1**, the *s-cis/s-trans* isomerization and electrocyclic energy barriers increase, relative to the unprotonated reaction (**TS2H/TS3H** vs **TS2/TS3** and **TS5H** vs **TS5**, respectively). The former remain slightly below the *E/Z* isomerization barrier, whereas the latter increases drastically. We propose that the catalyzed reaction proceeds first by rate-limiting isomerization of **2.1H** to yield protonated *Z* *o*-QM **2.4H**. Because the *s-cis/s-trans* isomerization and electrocyclic energy barriers increase for **2.4H** relative to **2.4**, we believe that the transformation from **2.4H** to product then occurs on the thermal reaction pathway *via* **2.4** to **2.5** to **2.2** (Scheme 4).

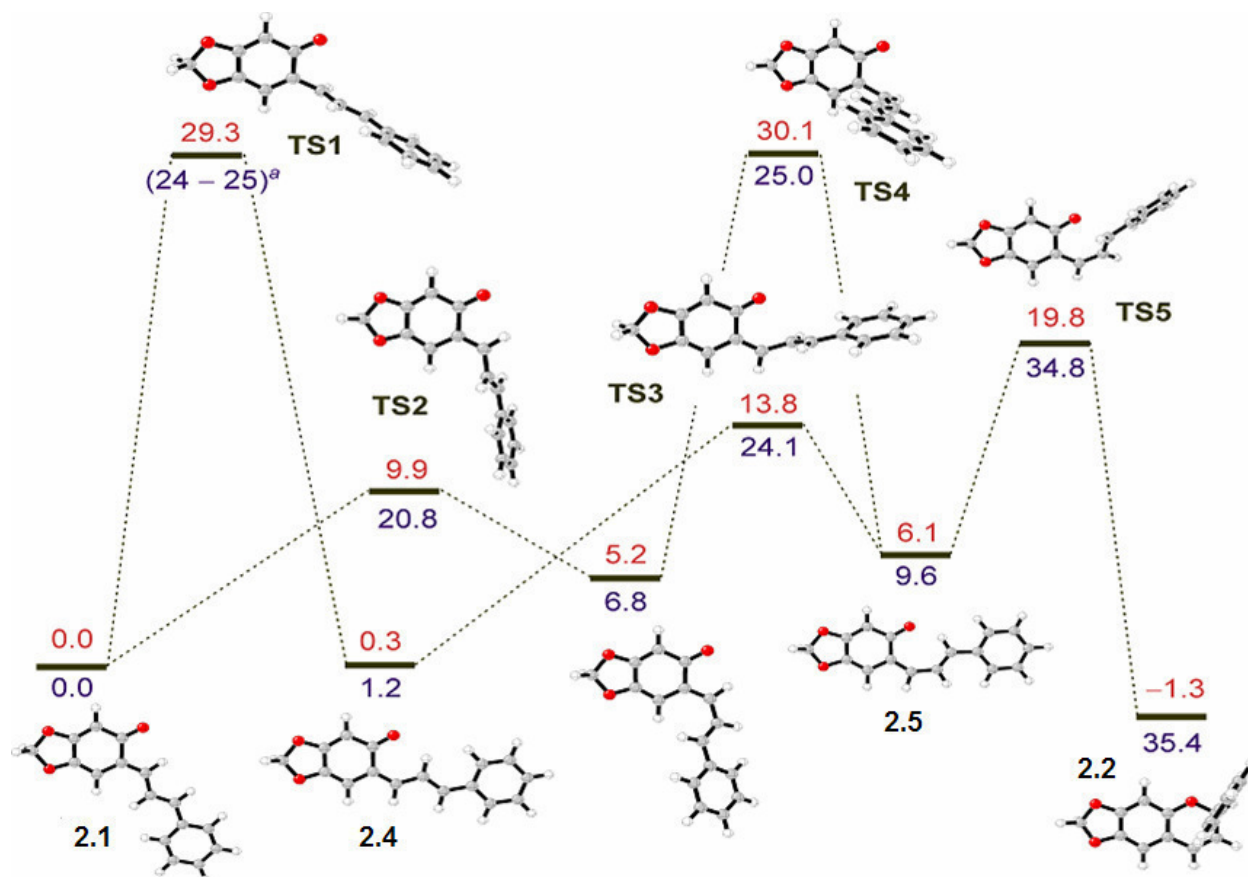
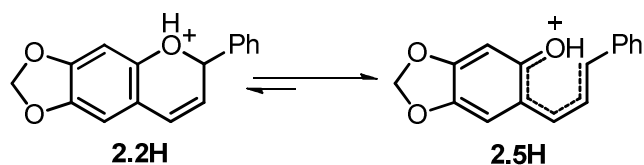


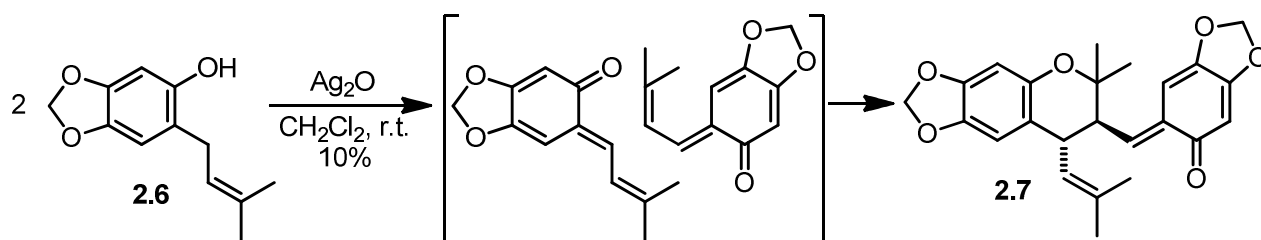
Figure 7. Relative Gibbs free energies (kcal/mol) of the thermal (numbers above line) and carbonyl-protonated (numbers below line) of the cyclization of **2.1** to **2.2** computed at the UB3LYP/6-31G* level of theory using Gaussian 03.^{14,15,16} Structures shown refer to the thermal reaction.

Interestingly, calculations indicate that the chromene product is unstable towards protonation. The protonated chromene **2.2H** occupies a very flat minimum on the potential energy surface and after inclusion of zero-point vibrational energy corrections, the corresponding ring-opening transition state **TS5H** disappears as a stationary point, so that ring-opening of the protonated chromene becomes barrierless. The instability of chromene **2.2** to protonation can be understood in terms of the relative basicity of vinyl *o*-QM **2.5** and chromene **2.2**. Protonation of the sp^2 -hybridized oxygen lone pair of **2.5** results in aromatization of the quinoidal scaffold, giving a highly delocalized, doubly-benzylic cation, while protonation of the sp^3 -hybridized oxygen lone pair on the pyran ring of **2.2** results in highly localized oxonium ion (Scheme 5). One would expect this effect to be partially felt in the *oxa*- 6π transition state as the protonated lone-pair re-hybridizes from sp^2 to sp^3 , which explains the increased electrocyclization energy barrier of the protonated species. Once formed, however, the chromene product is presumably not basic enough to be protonated and is therefore stable under the conditions used in our experiments.



Scheme 5. Ring-opening of protonated chromene **2.2H** to protonated vinyl *o*-QM **2.5H**.

Attempts to prepare a second vinyl *o*-QM from phenol **2.6** under similar conditions resulted in the isolation of compound **2.7**, the result of a Diels-Alder dimerization of two vinyl *o*-QM molecules (Scheme 6).⁶ The structure of this unusual dimer was confirmed by X-ray crystallography (Figure 8). The lower degree of conjugation of the π system of **2.7** as compared to that of **2.1** is evident in the bond lengths, which for **2.7** are within the range that is typically observed for isolated single and double bonds.¹¹ As was the case for **2.1**, the C1-C2 bond of **2.7** is longer than the other single bonds of **2.7**, presumably due to A^{1,3} strain of the O1, C1, C2, C3 system. Whereas *o*-QM dimerization is well established in the literature,¹⁷ with the *exo*-alkylidene alkene acting as dienophile in most cases, this appears to be the first example that leaves an *o*-QM moiety intact. The analogous dimerization was not observed with compound **2.1** under various conditions.



Scheme 6. Formation of novel *o*-QM dimer **2.7**.

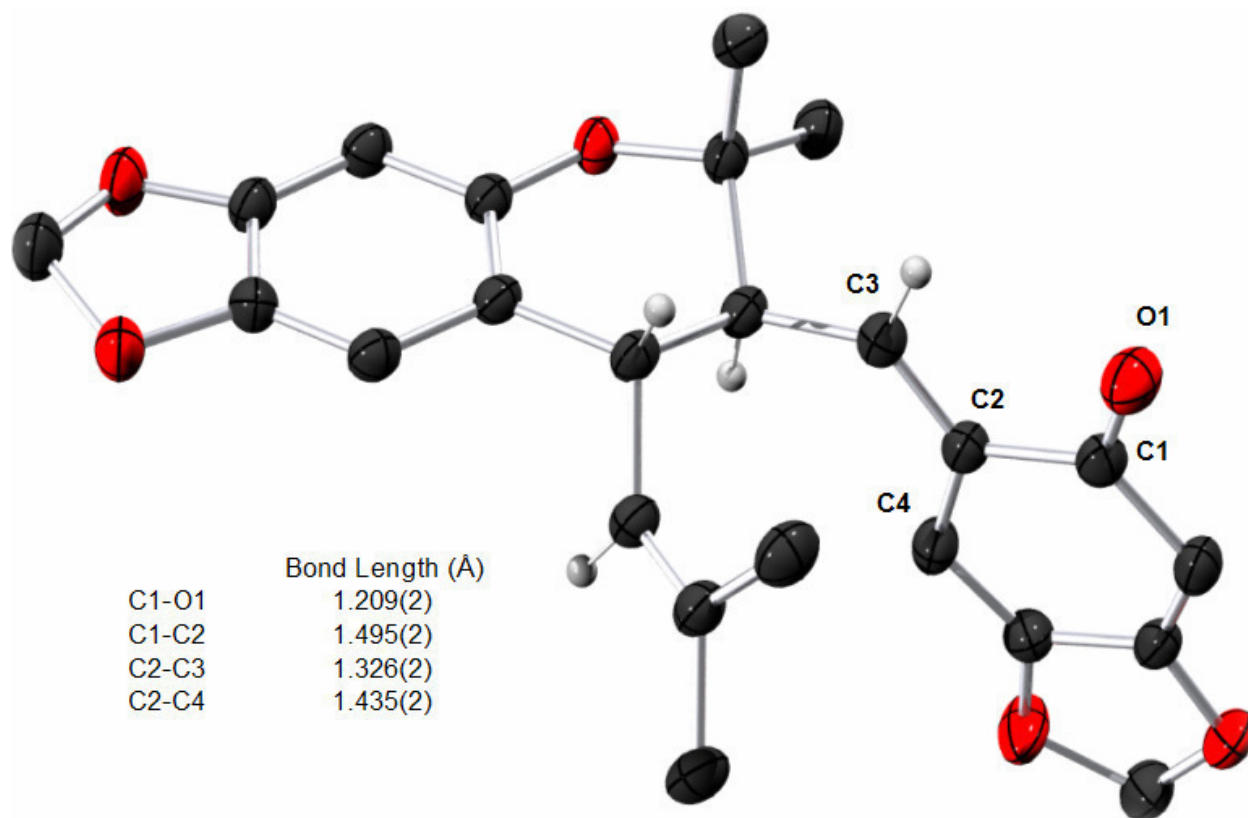


Figure 8. ORTEP diagram of **2.7** at the 50% probability level, with representative bond lengths. Some hydrogen atoms have been removed for clarity.

Summary & Conclusions

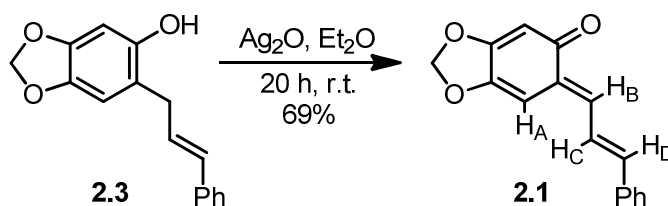
In summary, we have provided evidence that the cyclization of *E*-configured vinyl *o*-QMs involves a relatively slow acid-catalyzed *exo*-alkylidene bond isomerization followed by faster *oxa*- 6π electrocyclization. Computations indicate that the overall reaction is catalyzed by Brønsted acids, but the *oxa*- 6π electrocyclization step itself is not prone to such catalysis. The vinyl *o*-QM was found to be surprisingly basic, allowing for quantitative protonation with relatively weak acids. In addition, we have identified a new mode of Diels-Alder dimerization of vinyl *o*-QMs.

Experimental

General Information. All reactions and manipulations, unless otherwise noted, were carried out in an inert atmosphere (N_2) glovebox or using standard Schlenk and high vacuum techniques. Sealed NMR tubes were prepared by attaching the NMR tube directly to a Kontes high-vacuum stopcock via a cajon ultra-torr reducing union, then flame-sealing on a vacuum line. All glassware was dried in an oven at 150 °C for at least 12 h prior to use or was flame-dried under reduced pressure. 1H NMR and ^{13}C NMR spectra were recorded on Bruker DRX-500 (500 MHz), AV-500 (500 MHz), AVB-400 (400 MHz), and AVQ-400 (400 MHz) spectrometers as

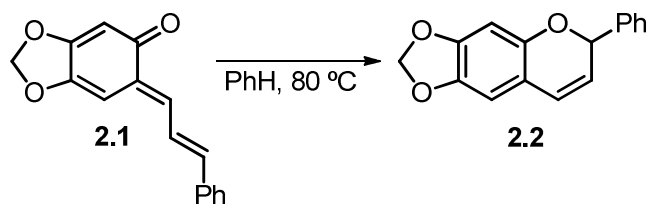
indicated. ^1H NMR chemical shifts (δ) are reported in parts per million relative to residual protiated solvent. Data are reported in the following format: (s = singlet, d = doublet, t = triplet, q = quartet, m = multiplet; coupling constant; integration). ^1H resonance assignments were confirmed by HSQC and HMBC NMR experiments. ^{13}C NMR chemical shifts (δ) are reported in parts per million relative to the carbon resonance of the deuterated solvent. Column chromatography was performed using a Biotage SP1 MPLC purification system and pre-packed silica gel columns. The temperatures of the kinetics experiments carried out in a circulating oil bath were determined from measurements with a calibrated mercury thermometer. The temperatures of the kinetics and titration experiments carried out in an NMR probe were determined from the ^1H NMR chemical shifts of ethylene glycol and MeOH samples. The values for k_{obs} were determined by fitting the concentration versus time plots to the equation $C_t = C_\infty - (C_\infty - C_0)\exp(-k_{\text{obs}}t)$ using the program KaleidaGraph (where C_t , C_∞ , C_0 are the concentration at time t , time infinity, and time zero).¹⁸ All distinct starting material and product ^1H NMR resonances were integrated and fit separately; the k_{obs} values shown are averages of those individual values. All errors in k_{obs} values were calculated from the errors of the fits of experimental data that were propagated through calculations.

Materials. Dichloromethane was dried and purified by passage through a column of activated alumina under N_2 pressure and sparging with N_2 .¹⁹ CD_2Cl_2 , obtained from Cambridge Isotope Labs, Inc., was vacuum transferred from calcium hydride, degassed with three freeze-evacuation-thaw cycles, and run through a plug of anhydrous basic alumina immediately prior to use. CDCl_3 and acetone- d_6 were obtained from Cambridge Isotope Labs, Inc. and were used without further purification. Anhydrous basic alumina was obtained by heating Brockman activity I basic alumina at $150\text{ }^\circ\text{C}$ under vacuum for 12 h. Proton-spongeTM, obtained from Sigma-Aldrich, was recrystallized from ethanol. Chloroacetic acid, hexamethylbenzene, and methanol- d_1 (99.5 atom% CH_3OD) were obtained from Sigma-Aldrich, and silver(I) oxide was obtained from Mallinckrodt; these reagents were used without further purification. 2-cinnamylsesamol²⁰ and 2-(3-methyl-2-butenyl)-sesamol⁶ were synthesized according to literature procedures. Characterization data for these compounds agree with literature values.



Synthesis of vinyl *o*-QM 2.1. This material was synthesized as previously reported.⁵ ^1H spectral data agree with literature values: ^1H NMR (500 MHz, acetone- d_6): δ 7.73 (d, $J = 7.5$ Hz, 2H), 7.68 (dd, $J = 15.2, 12.2$ Hz, 1H; H_C , nOe to H_A), 7.45 (d, $J = 12.5$ Hz, 1H; H_B , nOe to H_D), 7.42 (t, $J = 8$ Hz, 2H), 7.38-7.33 (m, 1H), 7.26 (d, $J = 15.5$ Hz, 1H; H_D , nOe to H_B), 6.95 (s, 1H; H_A , nOe to H_C), 6.05 (s, 2H), 5.83 (s, 1H) ppm.

Further characterization of **2.1**: ^1H NMR (500 MHz, CD_2Cl_2): δ 7.58 (d, $J = 7$ Hz, 2H), 7.53 (d, $J = 12$ Hz, 1H), 7.41 (t, $J = 7$ Hz, 2H), 7.38-7.29 (m, 2H), 7.16 (d, $J = 14$ Hz, 1H), 6.65 (s, 1H), 5.93 (s, 2H), 5.88 (s, 1H) ppm; ^{13}C NMR (100 MHz, CD_2Cl_2) δ 184.9, 162.0, 146.0, 144.1, 140.4, 136.9, 130.8, 130.1, 129.4, 128.0, 123.6, 102.8, 101.9, 98.2 ppm. HRMS (EI^+) Exact mass calcd for $\text{C}_{16}\text{H}_{12}\text{O}_3$ [M]⁺: 252.0786, found 252.0782.



Synthesis of chromene 2.2. This material was synthesized as previously reported.⁵ ¹H NMR (400 MHz, CDCl₃): δ 7.44 (d, *J* = 6.8 Hz, 2H), 7.39-7.27 (m, 3H), 6.51 (s, 1H), 6.43 (d, *J* = 9.6 Hz, 1H), 6.39 (s, 1H), 5.87 (d, *J* = 6 Hz, 2H), 5.80 (broad, 1H), 5.70 (dd, *J* = 9.8, 3.4 Hz, 1H) ppm.

Further characterization of **2.2**: ¹H NMR (500 MHz, CD₂Cl₂): δ 7.46-7.42 (m, 2H), 7.38-7.29 (m, 3H), 6.53 (s, 1H), 6.46 (dd, *J* = 10, 1.5 Hz, 1H), 6.36 (s, 1H), 5.89 (d, *J* = 1.5 Hz, 1H), 5.87 (d, *J* = 1.5 Hz, 1H), 5.80 (dd, *J* = 3.5, 1.5 Hz, 1H), 5.74 (dd, *J* = 9.8, 4 Hz, 1H) ppm; ¹³C NMR (100 MHz, CD₂Cl₂): δ 149.0, 148.5, 142.4, 141.2, 129.0, 128.8, 127.6, 124.7, 122.7, 115.1, 106.3, 101.8, 99.1, 77.2 ppm; HRMS (EI⁺) Exact mass calcd for C₁₆H₁₂O₃ [M]⁺: 252.0786, found 252.0780.

Activation Parameter Measurements for the Thermal Cyclization of 2.1 to 2.2.

Under low-light conditions, a sample of **2.1** (57.4 mg, 0.228 mmol) and hexamethylbenzene (as an internal standard) were dissolved in 10.00 mL CD₂Cl₂. A 5.00 mL sample of this solution was added to a vial containing Proton spongeTM (7.0 mg, 0.033 mmol), and the resulting solution was added to five NMR tubes (600 μL per tube). The tubes were sealed under vacuum and kept frozen in liquid nitrogen in the absence of light. When ready for kinetic analysis, one tube was thawed, completely submerged in a circulating oil bath, and kept completely shielded from light. Kinetic data were obtained on the sample in this tube in the following fashion: with minimal exposure to ambient light, the tube was removed from the oil bath and cooled rapidly to room temperature under a stream of hexanes; the reaction was monitored for disappearance of **2.1** and appearance of **2.2** (via single scan ¹H NMR spectroscopy using an AVB-400 spectrometer) and the tube was replaced in the oil bath. Only time spent in the oil bath was included in the concentration versus time plots. The oil baths used in the above experiments were calibrated to 40.0(1), 50.0(1), 60.0(1), 70.0(1), and 80.0(1) °C. The first order rate constants, activation parameters, and Eyring plot for these experiments can be found in Table 3, Table 1, and Figure 3, respectively.

Table 3. First order rate constants of the thermal cyclization of **2.1** at various temperatures.

Entry	Temperature (°C)	k _{obs} (s ⁻¹)
1	40	1.80(9) × 10 ⁻⁵
2	50	4.2(1) × 10 ⁻⁵
3	60	7.2(3) × 10 ⁻⁵
4	70	1.32(6) × 10 ⁻⁴
5	80	2.39(8) × 10 ⁻⁴

Cyclization of 2.1 in the presence of catalytic chloroacetic acid. Under low-light conditions, a sample of **2.1** (26.8 mg, 0.106 mmol) and hexamethylbenzene (as an internal standard) were dissolved in 3.70 mL CD₂Cl₂. A 400 μL sample of this solution was combined in an NMR tube with 50 μL CD₂Cl₂ and 50 μL of a 57.3 mM solution of chloroacetic acid in CD₂Cl₂. This tube was sealed under vacuum, placed in an AV-500 spectrometer pre-equilibrated

to 20.9(1) °C, and the reaction was monitored for disappearance of **2.1** and appearance of **2.2** (via single scan ¹H NMR spectroscopy). By NMR integration against internal standard, it was determined that 0.23 equivalents of chloroacetic acid were present, relative to **2.1**. The first order rate constant was determined to be 1.31(2)x10⁻³ s⁻¹.

Titration of 2.1 with chloroacetic acid. Under low-light conditions, a sample of **2.1** (4.9 mg, 0.019 mmol) and hexamethylbenzene (as an internal standard) were dissolved in 0.86 mL CD₂Cl₂. A 0.5 mL sample of this solution was added to an NMR tube, which was subsequently sealed with a rubber septum. A sample of chloroacetic acid (28.6 mg, 0.303 mmol) was dissolved in 1.31 mL CD₂Cl₂, and 1.00 mL of this solution was drawn into a gas-tight syringe. The NMR tube was placed in an AV-500 NMR spectrometer pre-equilibrated to -41.1 °C and the shift of the ¹H NMR spectrum of **2.1** was monitored as a function of added chloroacetic acid solution. The acid solution was added by ejecting the sample from the NMR probe, injecting the chloroacetic acid solution through the septum (two 50 μL aliquots, followed by seven 100 μL aliquots), agitating the sample, and replacing it in the NMR probe. The concentration of chloroacetic acid was determined by integration against the internal standard. Stacked NMR spectra are shown in Figure 4 and the graphical representation of the change in chemical shift of a representative resonance is shown in Figure 9.

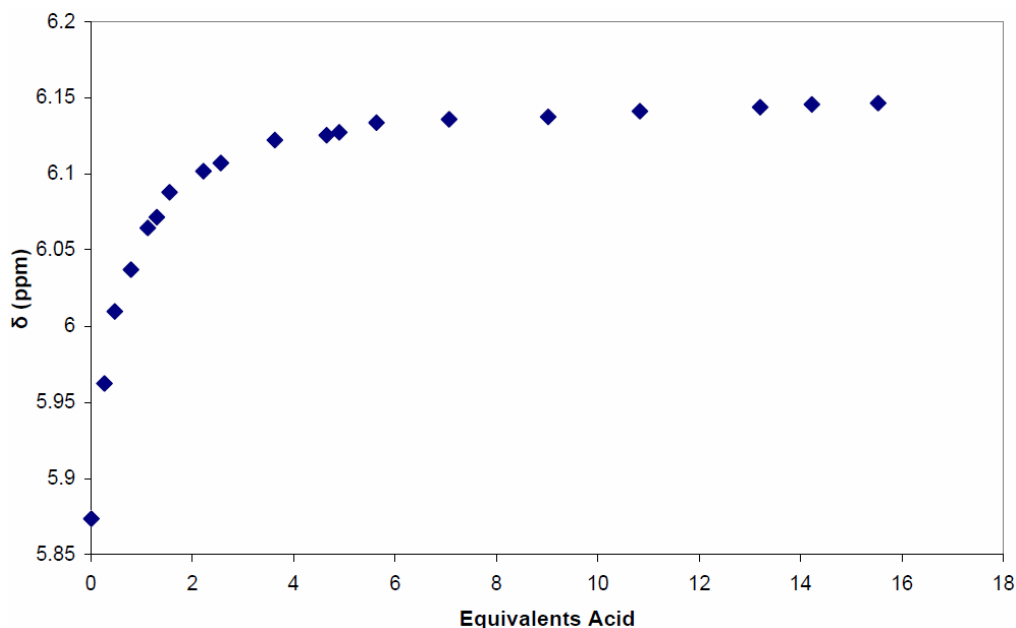


Figure 9. Chemical shift of a representative resonance of **2.1** versus added equivalents of chloroacetic acid in CD₂Cl₂ at -41.1 °C.

Saturation of chloroacetic acid with 2.1. Under low-light conditions, a sample of **2.1** (92.4 mg, 0.366 mmol) and hexamethylbenzene (as an internal standard) were dissolved in 3.00 mL CD₂Cl₂ (solution A). A sample of chloroacetic acid (2.8 mg, 0.030 mmol) was dissolved in 3.22 mL CD₂Cl₂ and a 200 μL aliquot of this solution was added to 1.00 mL CD₂Cl₂ (solution B). Six NMR tubes were then charged with varying amounts of solution A (50, 100, 150, 200, 350, and 400 μL) and the appropriate amount of CD₂Cl₂ such that the total volume in each tube was 400 μL. The tubes were subsequently sealed with rubber septa, and when ready for kinetic

analysis, a sample of solution B (100 μL per tube) was added through the rubber septum via a gas-tight syringe. The tube was then agitated, placed in an AV-500 NMR probe pre-equilibrated to 20.9 $^{\circ}\text{C}$, and the reaction was monitored for disappearance of **2.1** and appearance of **2.2** for at least one half life (via single scan ^1H NMR spectroscopy). The portion of the concentration versus time plots exhibiting zero order dependence on substrate was fit to a line via the least-squares method. The slope of this line was taken as the initial velocity of the reaction. The initial reaction velocity and initial concentration of **2.1** data can be found graphically in Figure 4 and numerically in Table 4.

Table 4. Initial reaction velocity of the catalyzed cyclization of **2.1** at various initial substrate concentrations.

Entry	[2.1] _{initial} (mM)	Velocity (mM/s)
1	12	4.01×10^{-3}
2	22	7.31×10^{-3}
3	35	8.33×10^{-3}
4	47	8.81×10^{-3}
5	83	9.46×10^{-3}
6	92	1.00×10^{-2}

Activation Parameter Measurements for the Catalyzed Cyclization of 2.1 to 2.2.

Under low-light conditions, a sample of **2.1** (20.1 mg, 0.0591 mmol) and hexamethylbenzene (as an internal standard) were dissolved in 2.80 mL CD_2Cl_2 . To this solution was added 800 μL of a 1.14 M solution of chloroacetic acid in CD_2Cl_2 . The resulting solution was added to four NMR tubes (0.5 mL per tube), and the tubes were sealed under vacuum and kept frozen in liquid nitrogen in the absence of light. When ready for kinetic analysis the tube was thawed, placed in an AV-500 spectrometer pre-equilibrated to the desired temperature, and the reaction was monitored for disappearance of **2.1** (via single scan ^1H NMR spectroscopy). The NMR probe for the above experiments was calibrated to -3.5(1), 4.6(1), 12.8(1), and 20.9(1) $^{\circ}\text{C}$. By NMR integration against internal standard, it was determined that 9.1 equivalents of chloroacetic acid were present, relative to **2.1**. The first order rate constants, activation parameters, and Eyring plot for these experiments can be found in Table 5, Table 2, and Figure 6, respectively.

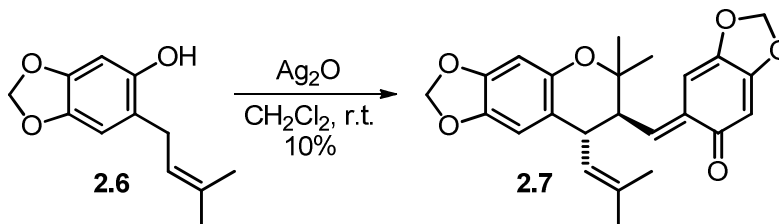
Table 5. First order rate constants of the catalyzed cyclization of **2.1** at various temperatures.

Entry	Temperature ($^{\circ}\text{C}$)	k_{obs} (s^{-1})
1	-3.5	$4.00(4) \times 10^{-5}$
2	4.6	$1.123(8) \times 10^{-4}$
3	12.8	$3.50(4) \times 10^{-4}$
4	20.9	$9.55(4) \times 10^{-4}$

Kinetic isotope effect study. Under low-light conditions, a sample of **2.1** (6.8 mg, 0.027 mmol), ClCH_2COOD (25.8 mg, 0.270 mmol), and hexamethylbenzene (as an internal standard) were dissolved in 1.20 mL CD_2Cl_2 . This solution was added to two NMR tubes (0.5 mL per tube), and the tubes were sealed under vacuum and kept frozen in liquid nitrogen in the absence of light. When ready for kinetic analysis the sample was thawed, placed in an AV-500 spectrometer pre-equilibrated to 20.9 $^{\circ}\text{C}$, and the reaction was monitored for disappearance of **2.1** (via single scan ^1H NMR spectroscopy). By NMR integration against internal standard, it

was determined that 9.4 equivalents of chloroacetic acid- d_1 were present, relative to **2.1**. The first order rate constants were determined to be $9.66(9) \times 10^{-4} \text{ s}^{-1}$ and $9.7(1) \times 10^{-4} \text{ s}^{-1}$. These rates are within experimental error of the rate measured using ClCH_2COOH under similar conditions (Table 5, entry 4).

Chloroacetic acid- d_1 was obtained by dissolving a sample of chloroacetic acid (490 mg, 5.2 mmol) in methanol- d_1 (20 mL) and concentrating the resulting solution under reduced pressure overnight. **HRMS** (EI^+) Exact mass calcd for $\text{C}_2\text{H}_2\text{DO}_2\text{Cl}$ $[\text{M}]^+$: 94.9884, found 94.9885.



Synthesis of vinyl *o*-QM dimer **2.7.** 2-(3-methyl-2-butenyl)-sesamol (**2.3**) (220 mg, 1.1 mmol) and silver(I) oxide (792 mg, 3.4 mmol) were placed into a Schlenk flask, to which 15 mL dichloromethane was added. This suspension was stirred for 4 h, opened to air, and run through a plug of Celite® 521. The resulting solution was concentrated under reduced pressure, and the resulting residue was purified by silica gel chromatography (20 to 33% EtOAc in hexanes) to afford 45 mg of **2.7** as a yellow solid (10%). **^1H NMR** (CDCl_3 , 500 MHz): δ 6.79 (d, $J = 11.5$ Hz, 1H), 6.48 (s, 1H), 6.33 (s, 1H), 6.23 (s, 1H), 5.88-5.82 (m, 5H), 4.79 (d, $J = 10$ Hz, 1H), 3.55 (t, $J = 10$ Hz, 1H), 2.65 (t, $J = 11$ Hz, 1H), 1.63 (s, 3H), 1.61 (s, 3H), 1.29 (s, 3H), 1.23 (s, 3H) ppm; **^{13}C NMR** (CDCl_3 , 100 MHz): δ 184.3, 161.9, 147.3, 146.8, 145.5, 144.7, 141.4, 134.8, 133.6, 125.3, 115.1, 107.9, 101.8, 101.5, 100.8, 98.7, 98.0, 76.8, 48.2, 37.67, 28.9, 25.8, 20.3, 18.4 ppm; **HRMS** (FAB^+) Exact mass calcd for $\text{C}_{24}\text{H}_{24}\text{NaO}_6$ $[\text{M}+\text{Na}]^+$: 431.1471, found 431.1475.

X-Ray crystal structure determination of **2.1.** This work was performed by Dr. Allen Oliver at the UC Berkeley CHEXRAY X-Ray crystallographic facility. A single crystal was mounted on a glass fiber using Paratone N hydrocarbon oil. All measurements were made on a Bruker APEX²¹ CCD area detector and the data were collected at a temperature of -100 °C. An arbitrary hemisphere of data was collected and integrated by the program SAINT.²² The data were corrected for Lorentz and polarization effects and were analyzed for agreement and possible absorption using XPREP.²³ An empirical absorption correction based on comparison of redundant and equivalent reflections was applied using SADABS.²⁴ The structure was solved by direct methods²⁵ and expanded using Fourier techniques.²⁶ Some non-hydrogen atoms were refined anisotropically, while the rest were refined isotropically. Hydrogen atoms were included but not refined. All calculations were performed using the teXsan crystallographic software package.²⁷ ORTEP diagrams were created using the ORTEP-3 software package.²⁸ Crystallographic data for vinyl *o*-QM **2.1** are summarized in Tables 6-12.

Table 6. X-Ray crystallographic data for vinyl *o*-QM **2.1**.

Empirical Formula	$\text{C}_{16}\text{H}_{12}\text{O}_3$
Formula Weight	252.27

Crystal Color, Habit	red, tablet
Crystal Dimensions	0.21 X 0.17 X 0.10 mm
Crystal System	orthorhombic
Lattice Type	primitive
Lattice Parameters	a = 7.632(3) Å b = 12.566(5) Å c = 25.201(1) Å,
Volume	2416(1) Å ³
Space Group	P2 ₁ 2 ₁ 2 ₁ (#19)
Z value	8
D _{calc}	1.386 g/cm ³
F ₀₀₀	1056.00
M(MoKα)	0.95 cm ⁻¹
Radiation	MoKα (λ = 0.71069 Å) graphite monochromated
Detector Position	60.00 mm
Exposure Time	20.0 seconds per frame
Scan Type	ω (0.3 degrees per frame)
2θ _{max}	46.6 °
No. of Reflections Measured	Total: 0
Corrections	Lorentz-polarization Absorption (T _{max} = 1.00 T _{min} = 0.93)
Refinement	Full-matrix least-squares
Function Minimized	Σω(F _o - F _c) ²
Least Squares Weights	ω = 1/[σ ² (F _o)] = [σ _c ² (F _o) + (p ² /4)(F _o) ²] ⁻¹
p-factor	0.0300
Anomalous Dispersion	All non-hydrogen atoms
No. Observations (I>3.00σ(I))	1447
No. Variables	183
Reflection/Parameter Ratio	7.91
Residuals: R; R _w ; R _{all}	0.043; 0.051; 0.068
Goodness of Fit Indicator	1.65
Max Shift/Error in Final Cycle	0.00
Maximum peak in Final Diff. Map	0.18 e ⁻ /Å ³
Minimum peak in Final Diff. Map	-0.23 e ⁻ /Å ³

Table 7. Atomic coordinates and Beq for **2.1**. Beq = 8/3 p²(U₁₁(aa*)² + U₂₂(bb*)² + U₃₃(cc*)² + 2U₁₂(aa*bb*)cos g + 2U₁₃(aa*cc*)cos b + 2U₂₃(bb*cc*)cos a)

atom	x	y	z	Beq
O(1)	-0.0447(5)	0.1523(2)	0.7957(1)	2.86(9)
O(2)	-0.2982(4)	-0.1216(2)	0.9000(1)	2.92(9)
O(3)	-0.2244(5)	-0.2533(2)	0.8402(1)	2.96(9)
O(4)	0.5460(5)	-0.6097(3)	0.7035(1)	2.95(9)
O(5)	0.8002(5)	-0.3357(2)	0.6003(1)	2.90(9)
O(6)	0.7264(4)	-0.2038(2)	0.6600(1)	2.80(9)

C(1)	-0.0747(7)	0.0565(4)	0.8049(2)	2.42(10)
C(2)	-0.1651(6)	0.0251(3)	0.8535(2)	2.5(1)
C(3)	-0.2062(7)	-0.0776(4)	0.8590(2)	2.20(10)
C(4)	-0.3220(8)	-0.2317(4)	0.8873(2)	2.9(1)
C(5)	-0.1603(6)	-0.1578(4)	0.8223(2)	2.3(1)
C(6)	-0.0667(7)	-0.1382(4)	0.7788(2)	2.39(10)
C(7)	-0.0196(6)	-0.0296(3)	0.7674(2)	2.04(9)
C(8)	0.0761(7)	-0.0007(4)	0.7237(2)	2.50(9)
C(9)	0.1511(6)	-0.0696(4)	0.6856(2)	2.44(10)
C(10)	0.2355(7)	-0.0337(4)	0.6423(2)	2.7(1)
C(11)	0.3189(6)	-0.0964(4)	0.6001(2)	2.36(10)
C(12)	0.3265(7)	-0.2067(4)	0.6014(2)	2.7(1)
C(13)	0.4058(7)	-0.2625(4)	0.5609(2)	3.2(1)
C(14)	0.4786(7)	-0.2103(4)	0.5176(2)	3.3(1)
C(15)	0.4717(8)	-0.1012(4)	0.5161(2)	3.8(1)
C(16)	0.3922(8)	-0.0442(4)	0.5567(2)	3.8(1)
C(17)	0.5764(7)	-0.5137(4)	0.6946(2)	2.15(9)
C(18)	0.6675(7)	-0.4831(4)	0.6465(2)	2.6(1)
C(19)	0.7101(7)	-0.3807(4)	0.6412(2)	2.31(10)
C(20)	0.8221(7)	-0.2254(4)	0.6127(2)	3.2(1)
C(21)	0.6625(7)	-0.2992(4)	0.6780(2)	2.2(1)
C(22)	0.5683(7)	-0.3182(3)	0.7214(2)	2.40(10)
C(23)	0.5190(6)	-0.4285(4)	0.7325(2)	2.26(10)
C(24)	0.4256(7)	-0.4576(4)	0.7751(2)	2.50(10)
C(25)	0.3507(6)	-0.3880(3)	0.8144(2)	2.39(10)
C(26)	0.2632(7)	-0.4245(4)	0.8571(2)	2.63(10)
C(27)	0.1813(7)	-0.3639(4)	0.8996(2)	2.4(1)
C(28)	0.1748(7)	-0.2533(4)	0.8993(2)	2.46(10)
C(29)	0.0943(7)	-0.1976(4)	0.9404(2)	2.9(1)
C(30)	0.0161(7)	-0.2525(4)	0.9820(2)	3.3(1)
C(31)	0.0207(7)	-0.3619(4)	0.9826(2)	3.2(1)
C(32)	0.1033(7)	-0.4166(4)	0.9420(2)	3.1(1)
H(1)	-0.1937	0.0757	0.8801	2.9737
H(2)	-0.2804	-0.2747	0.9156	3.4708
H(3)	-0.4427	-0.2460	0.8814	3.4708
H(4)	-0.0319	-0.1943	0.7559	2.8695
H(5)	0.0939	0.0734	0.7184	3.0078
H(6)	0.1415	-0.1443	0.6909	2.9286
H(7)	0.2420	0.0414	0.6386	3.1970
H(8)	0.2766	-0.2441	0.6305	3.2223
H(9)	0.4107	-0.3380	0.5626	3.8324
H(10)	0.5321	-0.2492	0.4896	4.0226
H(11)	0.5217	-0.0642	0.4869	4.5066
H(12)	0.3879	0.0313	0.5549	4.5718
H(13)	0.6956	-0.5338	0.6198	3.1324
H(14)	0.9427	-0.2101	0.6180	3.8940

H(15)	0.7783	-0.1829	0.5844	3.8940
H(16)	0.5340	-0.2620	0.7444	2.8786
H(17)	0.4068	-0.5317	0.7798	2.9944
H(18)	0.3635	-0.3133	0.8100	2.8649
H(19)	0.2538	-0.4997	0.8598	3.1526
H(20)	0.2259	-0.2152	0.8706	2.9444
H(21)	0.0929	-0.1220	0.9401	3.5222
H(22)	-0.0402	-0.2147	1.0099	3.9385
H(23)	-0.0329	-0.3999	1.0109	3.8464
H(24)	0.1067	-0.4922	0.9432	3.6886

Table 8. Anisotropic displacement parameters for **2.1**. The general temperature factor expression: $\exp(-2p2(a^2U_{11}h^2 + b^2U_{22}k^2 + c^2U_{33}l^2 + 2a*b*U_{12}hk + 2a*c*U_{13}hl + 2b*c*U_{23}kl))$

atom	U11	U22	U33	U12	U13	U23
O(1)	0.042(2)	0.022(2)	0.045(2)	-0.003(1)	0.005(2)	0.002(1)
O(2)	0.044(2)	0.032(2)	0.035(2)	0.001(2)	0.007(2)	0.004(2)
O(3)	0.048(2)	0.026(2)	0.038(2)	-0.001(2)	0.006(2)	0.002(2)
O(4)	0.046(2)	0.028(2)	0.038(2)	-0.001(2)	0.001(2)	-0.001(2)
O(5)	0.046(3)	0.027(2)	0.036(2)	-0.002(2)	0.010(2)	0.003(2)
O(6)	0.046(2)	0.024(2)	0.037(2)	-0.003(2)	0.007(2)	0.002(1)

Table 9. Bond lengths (Å) for **2.1**.

atom	atom	distance	atom	atom	distance
O1	C1	1.246(5)	O2	C3	1.365(6)
O2	C4	1.431(6)	O3	C4	1.426(6)
O3	C5	1.372(6)	O4	C17	1.248(5)
O5	C19	1.362(6)	O5	C20	1.431(6)
O6	C20	1.426(6)	O6	C21	1.371(5)
C1	C2	1.459(7)	C1	C7	1.497(7)
C2	C3	1.336(6)	C3	C5	1.413(7)
C5	C6	1.332(7)	C6	C7	1.440(6)
C7	C8	1.371(7)	C8	C9	1.413(6)
C9	C10	1.345(7)	C10	C11	1.469(7)
C11	C12	1.388(6)	C11	C16	1.393(7)
C12	C13	1.380(7)	C13	C14	1.389(8)
C14	C15	1.372(7)	C15	C16	1.388(8)
C17	C18	1.450(7)	C17	C23	1.501(7)
C18	C19	1.334(6)	C19	C21	1.430(7)
C21	C22	1.330(7)	C22	C23	1.463(6)
C23	C24	1.339(7)	C24	C25	1.439(7)
C25	C26	1.347(7)	C26	C27	1.457(7)
C27	C28	1.391(6)	C27	C32	1.391(7)
C28	C29	1.394(7)	C29	C30	1.389(7)
C30	C31	1.375(7)	C31	C32	1.384(7)
C2	H1	0.95	C4	H2	0.95

C4	H3	0.95	C6	H4	0.95
C8	H5	0.95	C9	H6	0.95
C10	H7	0.95	C12	H8	0.95
C13	H9	0.95	C14	H10	0.95
C15	H11	0.95	C16	H12	0.95
C18	H13	0.95	C20	H14	0.95
C20	H15	0.95	C22	H16	0.95
C24	H17	0.95	C25	H18	0.95
C26	H19	0.95	C28	H20	0.95
C29	H21	0.95	C30	H22	0.95
C31	H23	0.95	C32	H24	0.95

Table 10. Bond angles (°) for **2.1**.

atom	atom	atom	angle	atom	atom	atom	angle
C3	O2	C4	106.7(4)	C4	O3	C5	107.1(4)
C19	O5	C20	107.2(4)	C20	O6	C21	107.0(4)
O1	C1	C2	120.3(5)	O1	C1	C7	121.9(5)
C2	C1	C7	117.8(4)	C1	C2	C3	117.4(4)
O2	C3	C2	126.3(4)	O2	C3	C5	109.5(4)
C2	C3	C5	124.3(5)	O2	C4	O3	107.7(4)
O3	C5	C3	108.6(4)	O3	C5	C6	128.7(4)
C3	C5	C6	122.7(5)	C5	C6	C7	118.3(4)
C1	C7	C6	119.2(4)	C1	C7	C8	117.8(4)
C6	C7	C8	123.0(4)	C7	C8	C9	126.8(4)
C8	C9	C10	122.6(4)	C9	C10	C11	128.0(4)
C10	C11	C12	122.4(4)	C10	C11	C16	119.4(4)
C12	C11	C16	118.2(5)	C11	C12	C13	120.5(5)
C12	C13	C14	121.1(5)	C13	C14	C15	118.6(5)
C14	C15	C16	120.8(5)	C11	C16	C15	120.8(5)
O4	C17	C18	119.7(4)	O4	C17	C23	121.4(4)
C18	C17	C23	118.9(4)	C17	C18	C19	117.1(5)
O5	C19	C18	126.8(4)	O5	C19	C21	108.9(4)
C18	C19	C21	124.3(5)	O5	C20	O6	107.9(4)
O6	C21	C19	108.7(4)	O6	C21	C22	128.4(4)
C19	C21	C22	122.9(4)	C21	C22	C23	117.8(4)
C17	C23	C22	118.6(4)	C17	C23	C24	118.1(4)
C22	C23	C24	123.3(4)	C23	C24	C25	126.6(4)
C24	C25	C26	122.7(4)	C25	C26	C27	128.6(4)
C26	C27	C28	122.2(4)	C26	C27	C32	120.0(4)
C28	C27	C32	117.8(4)	C27	C28	C29	120.8(4)
C28	C29	C30	120.1(5)	C29	C30	C31	119.6(5)
C30	C31	C32	120.0(5)	C27	C32	C31	121.7(5)
C1	C2	H1	121.3	C3	C2	H1	121.3
O2	C4	H2	109.9	O2	C4	H3	109.9
O3	C4	H2	109.9	O3	C4	H3	109.9
H2	C4	H3	109.5	C5	C6	H4	120.8

C7	C6	H4	120.9	C7	C8	H5	116.6
C9	C8	H5	116.6	C8	C9	H6	118.7
C10	C9	H6	118.7	C9	C10	H7	116.0
C11	C10	H7	116.0	C11	C12	H8	119.7
C13	C12	H8	119.8	C12	C13	H9	119.4
C14	C13	H9	119.4	C13	C14	H10	120.7
C15	C14	H10	120.7	C14	C15	H11	119.6
C16	C15	H11	119.6	C11	C16	H12	119.6
C15	C16	H12	119.6	C17	C18	H13	121.4
C19	C18	H13	121.5	O5	C20	H14	109.9
O5	C20	H15	109.9	O6	C20	H14	109.8
O6	C20	H15	109.8	H14	C20	H15	109.5
C21	C22	H16	121.1	C23	C22	H16	121.1
C23	C24	H17	116.7	C25	C24	H17	116.7
C24	C25	H18	118.7	C26	C25	H18	118.7
C25	C26	H19	115.7	C27	C26	H19	115.7
C27	C28	H20	119.6	C29	C28	H20	119.6
C28	C29	H21	119.9	C30	C29	H21	119.9
C29	C30	H22	120.2	C31	C30	H22	120.2
C30	C31	H23	120.0	C32	C31	H23	120.0
C27	C32	H24	119.2	C31	C32	H24	119.2

Table 11. Torsion Angles (°) for **2.1**.

atom	atom	atom	atom	angle	atom	atom	atom	atom	angle
O1	C1	C2	C3	174.6(5)	O1	C1	C7	C6	-176.6(5)
O1	C1	C7	C8	4.2(7)	O2	C3	C2	C1	-176.4(5)
O2	C3	C5	O3	0.1(5)	O2	C3	C5	C6	-178.6(5)
O2	C4	O3	C5	-6.1(5)	O3	C4	O2	C3	6.2(5)
O3	C5	C3	C2	-179.5(5)	O3	C5	C6	C7	177.8(4)
O4	C17	C18	C19	-174.3(4)	O4	C17	C23	C22	176.2(4)
O4	C17	C23	C24	-3.5(7)	O5	C19	C18	C17	177.7(5)
O5	C19	C21	O6	-1.0(5)	O5	C19	C21	C22	177.8(5)
O5	C20	O6	C21	5.1(5)	O6	C20	O5	C19	-5.7(5)
O6	C21	C19	C18	-179.5(5)	O6	C21	C22	C23	-178.7(4)
C1	C2	C3	C5	3.2(7)	C1	C7	C6	C5	0.9(7)
C1	C7	C8	C9	175.2(5)	C2	C1	C7	C6	3.7(7)
C2	C1	C7	C8	-175.5(5)	C2	C3	O2	C4	175.7(5)
C2	C3	C5	C6	1.8(8)	C3	C2	C1	C7	-5.6(7)
C3	C5	O3	C4	3.8(5)	C3	C5	C6	C7	-3.8(7)
C4	O2	C3	C5	-3.9(5)	C4	O3	C5	C6	-177.6(5)
C5	C6	C7	C8	-179.9(5)	C6	C7	C8	C9	-4.0(8)
C7	C8	C9	C10	176.4(5)	C8	C9	C10	C11	179.9(5)
C9	C10	C11	C12	-2.9(8)	C9	C10	C11	C16	176.6(5)
C10	C11	C12	C13	179.9(5)	C10	C11	C16	C15	-179.9(5)
C11	C12	C13	C14	-0.5(8)	C11	C16	C15	C14	0.5(8)
C12	C11	C16	C15	-0.4(8)	C12	C13	C14	C15	0.6(8)

C13	C12	C11	C16	0.4(7)	C13	C14	C15	C16	-0.6(8)
C17	C18	C19	C21	-4.0(7)	C17	C23	C22	C21	-0.2(7)
C17	C23	C24	C25	-176.5(4)	C18	C17	C23	C22	-4.4(6)
C18	C17	C23	C24	175.9(5)	C18	C19	O5	C20	-177.4(5)
C18	C19	C21	C22	-0.8(8)	C19	C18	C17	C23	6.3(7)
C19	C21	O6	C20	-2.6(5)	C19	C21	C22	C23	2.9(8)
C20	O5	C19	C21	4.1(5)	C20	O6	C21	C22	178.7(5)
C21	C22	C23	C24	179.5(5)	C22	C23	C24	C25	3.8(8)
C23	C24	C25	C26	-177.7(5)	C24	C25	C26	C27	180.0(5)
C25	C26	C27	C28	4.2(8)	C25	C26	C27	C32	-177.0(5)
C26	C27	C28	C29	179.5(5)	C26	C27	C32	C31	-178.5(5)
C27	C28	C29	C30	-1.3(7)	C27	C32	C31	C30	-0.8(8)
C28	C27	C32	C31	0.3(7)	C28	C29	C30	C31	0.8(8)
C29	C28	C27	C32	0.7(7)	C29	C30	C31	C32	0.2(7)

Table 12. Non-bonded Contacts out to 3.60 Å for **2.1**.

atom	atom	distance	ADC	atom	atom	distance	ADC
O1	C19	3.036(6)	65604	O1	C21	3.052(6)	65604
O1	O5	3.221(5)	65604	O1	O6	3.227(4)	65604
O1	C20	3.253(6)	65604	O1	C6	3.345(6)	55604
O2	O4	3.224(5)	55604	O2	C31	3.273(6)	44703
O2	C29	3.305(6)	1	O2	C17	3.468(6)	55604
O2	C18	3.513(6)	55604	O2	C30	3.569(6)	1
O3	O4	3.240(5)	55604	O3	C28	3.391(6)	1
O3	C22	3.484(6)	45501	O3	C10	3.552(5)	54604
O3	C29	3.575(6)	1	O4	C3	3.062(6)	54604
O4	C5	3.075(6)	54604	O4	C4	3.241(7)	54604
O4	C22	3.348(6)	64604	O5	C13	3.301(6)	1
O5	C15	3.306(7)	54603	O5	C14	3.317(7)	54603
O5	C1	3.454(6)	64604	O5	C2	3.489(6)	64604
O5	C14	3.585(6)	1	O6	C12	3.391(7)	1
O6	C6	3.483(6)	65501	O6	C26	3.537(5)	65604
O6	C13	3.574(6)	1	C1	C19	3.195(7)	65604
C1	C24	3.357(8)	55604	C1	C18	3.377(8)	65604
C1	C23	3.525(7)	55604	C2	C17	3.400(7)	55604
C2	C23	3.512(7)	55604	C3	C17	3.234(7)	55604
C3	C29	3.427(7)	1	C4	C29	3.474(8)	1
C4	C30	3.523(8)	44703	C4	C30	3.525(8)	1
C5	C28	3.427(7)	1	C5	C29	3.591(7)	1
C7	C24	3.400(7)	55604	C7	C18	3.504(7)	65604
C7	C17	3.521(7)	65604	C8	C17	3.362(7)	65604
C8	C23	3.405(7)	65604	C8	C26	3.430(7)	55604
C10	C24	3.455(7)	65604	C12	C21	3.414(7)	1
C13	C19	3.420(7)	1	C13	C20	3.467(8)	1
C13	C21	3.574(7)	1	C14	C20	3.557(8)	1
C14	C20	3.585(8)	44603				

X-Ray crystal structure determination of 2.7. This work was performed by Dr. Allen Oliver at the UC Berkeley CHEXRAY X-Ray crystallographic facility. A single crystal was mounted on a glass fiber using Paratone N hydrocarbon oil. All measurements were made on a Bruker Platinum 200²⁹ CCD area detector and the data were collected at a temperature of -80 °C. An arbitrary hemisphere of data was collected and integrated by the program SAINT.²² The data were corrected for Lorentz and polarization effects and were analyzed for agreement and possible absorption using XPREP.²³ An empirical absorption correction based on comparison of redundant and equivalent reflections was applied using SADABS.²⁴ The structure was solved by direct methods³⁰ and expanded using Fourier techniques.³¹ Some non-hydrogen atoms were refined anisotropically, while the rest were refined isotropically. Hydrogen atoms were included but not refined. All calculations were performed using the SHELXTL crystallographic software package.³² ORTEP diagrams were created using the ORTEP-3 software package.²⁸ Crystallographic data for vinyl *o*-QM dimer **2.7** are summarized in Tables 13-18.

Table 13. X-Ray crystallographic data for vinyl *o*-QM dimer **2.7**.

Empirical Formula	C ₂₄ H ₂₄ O ₆	
Formula Weight	408.43	
Crystal Color, Habit	colorless, rod	
Crystal Dimensions	0.10 X 0.04 X 0.03 mm	
Crystal System	monoclinic	
Lattice Type	primitive	
Lattice Parameters	a = 9.825(1) Å	α = 90 °
	b = 18.291(1) Å	β = 94.927(2) °
	c = 10.517(1) Å	γ = 90 °
Volume	1883.0(2) Å ³	
Space Group	P2(1)/n	
Z value	4	
D _{calc}	1.441 g/cm ³	
F ₀₀₀	864	
M(MoKα)	0.12 cm ⁻¹	
Radiation	synchrotron (λ = 0.77490 Å)	
	Channel-cut Si-<111> crystal	
Detector Position	74.00 mm	
Exposure Time	2 seconds per frame	
Scan Type	ω (0.3 degrees per frame)	
2θ _{max}	31.12 °	
No. of Reflections Measured	Total: 24323	
	Unique: 4656 (R _{int} = 0.0627)	
Corrections	Lorentz-polarization	
	Absorption (T _{max} = 0.9963, T _{min} = 0.9877)	
Refinement	Full-matrix least-squares	
Function Minimized	Σω(F _o ² - F _c ²) ²	
Least Squares Weights	ω = 1/[σ ² (F _o) ² + (qP) ² + 0.4236P]	
	where P = [(F _o) ² + 2(F _c) ²]/3	
p-factor	0.0585	
Anomalous Dispersion	All non-hydrogen atoms	

No. Observations ($I > 2.00\sigma(I)$)	4025
No. Variables	275
Reflection/Parameter Ratio	14.64
Residuals: R; R_w ; R_{all}	0.0430; 0.1151; 0.0490
Goodness of Fit Indicator	1.041
Max Shift/Error in Final Cycle	0.001
Maximum peak in Final Diff. Map	$0.315 e^-/\text{\AA}^3$
Minimum peak in Final Diff. Map	$-0.185 e^-/\text{\AA}^3$

Table 14. Atomic coordinates, U_{iso}/U_{eq} , and occupancy for **2.7**. U_{eq} is defined as one third of the orthogonalized U_{ij} tensor.

atom	x	y	z	U_{eq}	Occupancy
O1	0.4582(1)	0.1981(1)	0.6116(1)	0.028(1)	1
O2	0.0778(1)	0.1024(1)	0.8020(1)	0.036(1)	1
O3	0.0354(1)	0.0146(1)	0.6502(1)	0.037(1)	1
O4	0.4486(1)	0.3026(1)	-0.0431(1)	0.047(1)	1
O5	0.6310(1)	0.2733(1)	-0.1509(1)	0.037(1)	1
O6	0.8018(1)	0.1060(1)	0.1564(1)	0.038(1)	1
C1	0.3588(1)	0.1470(1)	0.6132(1)	0.024(1)	1
C2	0.2785(1)	0.1530(1)	0.7146(1)	0.027(1)	1
C3	0.1746(1)	0.1052(1)	0.7179(1)	0.028(1)	1
C4	0.0084(1)	0.0360(1)	0.7742(1)	0.036(1)	1
C5	0.1496(1)	0.0526(1)	0.6269(1)	0.028(1)	1
C6	0.2271(1)	0.0464(1)	0.5280(1)	0.027(1)	1
C7	0.3351(1)	0.0949(1)	0.5199(1)	0.025(1)	1
C8	0.4206(1)	0.0908(1)	0.4092(1)	0.025(1)	1
C9	0.5047(1)	0.1610(1)	0.4019(1)	0.025(1)	1
C10	0.5668(1)	0.1852(1)	0.5327(1)	0.026(1)	1
C11	0.6085(1)	0.1494(1)	0.3108(1)	0.027(1)	1
C12	0.6083(1)	0.1764(1)	0.1938(1)	0.027(1)	1
C13	0.5083(1)	0.2272(1)	0.1393(1)	0.032(1)	1
C14	0.5262(1)	0.2539(1)	0.0260(1)	0.032(1)	1
C15	0.5143(1)	0.3185(1)	-0.1523(1)	0.038(1)	1
C16	0.6380(1)	0.2344(1)	-0.0435(1)	0.029(1)	1
C17	0.7308(1)	0.1854(1)	-0.0052(1)	0.031(1)	1
C18	0.7208(1)	0.1520(1)	0.1165(1)	0.028(1)	1
C19	0.6633(1)	0.1307(1)	0.5979(1)	0.031(1)	1
C20	0.6337(1)	0.2585(1)	0.5239(1)	0.032(1)	1
C21	0.3346(1)	0.0811(1)	0.2868(1)	0.027(1)	1
C22	0.3604(1)	0.0415(1)	0.1876(1)	0.028(1)	1
C23	0.2677(1)	0.0450(1)	0.0686(1)	0.038(1)	1
C24	0.4815(1)	-0.0059(1)	0.1806(1)	0.035(1)	1
H2A	0.2959	0.1892	0.7788	0.033	1
H4A	0.0407	-0.0020	0.8367	0.044	1
H4B	-0.0911	0.0427	0.7787	0.044	1
H6A	0.2083	0.0097	0.4650	0.033	1

H8A	0.4844	0.0483	0.4217	0.030	1
H9A	0.4419	0.2006	0.3672	0.031	1
H11A	0.6839	0.1193	0.3390	0.033	1
H13A	0.4320	0.2410	0.1835	0.038	1
H15A	0.5414	0.3706	-0.1524	0.046	1
H15B	0.4523	0.3089	-0.2297	0.046	1
H17A	0.8020	0.1727	-0.0568	0.037	1
H19A	0.6923	0.1479	0.6843	0.046	1
H19B	0.7434	0.1252	0.5493	0.046	1
H19C	0.6171	0.0834	0.6029	0.046	1
H20A	0.6622	0.2764	0.6099	0.048	1
H20B	0.5688	0.2930	0.4809	0.048	1
H20C	0.7139	0.2540	0.4750	0.048	1
H21A	0.2503	0.1068	0.2796	0.032	1
H23A	0.1852	0.0724	0.0847	0.057	1
H23B	0.2423	-0.0047	0.0408	0.057	1
H23C	0.3143	0.0695	0.0018	0.057	1
H24A	0.5314	-0.0092	0.2652	0.053	1
H24B	0.5413	0.0150	0.1200	0.053	1
H24C	0.4522	-0.0548	0.1521	0.053	1

Table 15. Anisotropic displacement parameters for **2.7**. The general temperature factor expression: $\exp(-2\Pi^2(a^2U_{11}h^2 + b^2U_{22}k^2 + c^2U_{33}l^2 + 2a*b*U_{12}hk + 2a*c*U_{13}hl + 2b*c*U_{23}kl))$.

atom	U_{11}	U_{22}	U_{33}	U_{12}	U_{13}	U_{23}
O1	0.029(1)	0.029(1)	0.026(1)	-0.005(1)	0.009(1)	-0.004(1)
O2	0.036(1)	0.043(1)	0.032(1)	-0.005(1)	0.016(1)	-0.007(1)
O3	0.035(1)	0.047(1)	0.031(1)	-0.004(1)	0.009(1)	-0.013(1)
O4	0.036(1)	0.066(1)	0.039(1)	0.026(1)	0.010(1)	0.012(1)
O5	0.040(1)	0.047(1)	0.025(1)	0.008(1)	0.007(1)	-0.002(1)
O6	0.039(1)	0.044(1)	0.032(1)	0.001(1)	0.008(1)	0.010(1)
C1	0.026(1)	0.026(1)	0.022(1)	0.000(1)	0.003(1)	0.001(1)
C2	0.031(1)	0.029(1)	0.023(1)	-0.003(1)	0.005(1)	0.001(1)
C3	0.028(1)	0.034(1)	0.022(1)	0.001(1)	0.007(1)	0.002(1)
C4	0.035(1)	0.042(1)	0.034(1)	-0.001(1)	0.011(1)	-0.007(1)
C5	0.027(1)	0.032(1)	0.026(1)	0.002(1)	0.003(1)	-0.004(1)
C6	0.031(1)	0.030(1)	0.022(1)	-0.002(1)	0.003(1)	-0.002(1)
C7	0.027(1)	0.028(1)	0.019(1)	0.001(1)	0.003(1)	0.001(1)
C8	0.028(1)	0.027(1)	0.019(1)	-0.001(1)	0.004(1)	0.001(1)
C9	0.028(1)	0.028(1)	0.021(1)	0.002(1)	0.005(1)	0.001(1)
C10	0.027(1)	0.029(1)	0.022(1)	-0.001(1)	0.006(1)	-0.001(1)
C11	0.027(1)	0.031(1)	0.025(1)	0.000(1)	0.004(1)	0.000(1)
C12	0.026(1)	0.031(1)	0.023(1)	-0.001(1)	0.004(1)	-0.003(1)
C13	0.028(1)	0.041(1)	0.027(1)	0.005(1)	0.007(1)	0.002(1)
C14	0.027(1)	0.039(1)	0.028(1)	0.005(1)	0.002(1)	-0.001(1)
C15	0.040(1)	0.045(1)	0.031(1)	0.011(1)	0.005(1)	-0.002(1)

C16	0.032(1)	0.036(1)	0.021(1)	0.000(1)	0.004(1)	-0.009(1)
C17	0.032(1)	0.038(1)	0.026(1)	-0.003(1)	0.009(1)	-0.004(1)
C18	0.028(1)	0.032(1)	0.024(1)	-0.004(1)	0.003(1)	-0.003(1)
C19	0.032(1)	0.034(1)	0.025(1)	0.002(1)	0.002(1)	0.001(1)
C20	0.035(1)	0.032(1)	0.029(1)	0.001(1)	0.007(1)	-0.006(1)
C21	0.028(1)	0.032(1)	0.021(1)	0.000(1)	0.004(1)	0.001(1)
C22	0.032(1)	0.031(1)	0.022(1)	0.000(1)	0.005(1)	-0.002(1)
C23	0.042(1)	0.049(1)	0.022(1)	-0.004(1)	0.002(1)	0.000(1)
C24	0.042(1)	0.036(1)	0.027(1)	-0.004(1)	0.007(1)	0.006(1)

Table 16. Bond lengths (Å) for **2.7**.

atom	atom	distance	atom	atom	distance
O1	C1	1.3537(13)	O1	C10	1.4270(13)
O2	C3	1.3546(14)	O2	C4	1.4110(16)
O3	C5	1.3607(14)	O3	C4	1.4078(16)
O4	C14	1.3444(15)	O4	C15	1.3950(16)
O5	C16	1.3308(14)	O5	C15	1.4127(17)
O6	C18	1.2088(15)	C1	C7	1.3737(15)
C1	C2	1.3839(15)	C2	C3	1.3474(17)
C2	H2A	0.9500	C3	C5	1.3639(17)
C4	H4A	0.9900	C4	H4B	0.9900
C5	C6	1.3454(16)	C6	C7	1.3915(16)
C6	H6A	0.9500	C7	C8	1.4940(15)
C8	C21	1.4884(15)	C8	C9	1.5325(15)
C8	H8A	1.0000	C9	C11	1.4735(15)
C9	C10	1.5218(15)	C9	H9A	1.0000
C10	C20	1.4998(16)	C10	C19	1.5005(16)
C11	C12	1.3259(16)	C11	H11A	0.9500
C12	C13	1.4354(17)	C12	C18	1.4946(16)
C13	C14	1.3138(17)	C13	H13A	0.9500
C14	C16	1.4162(17)	C15	H15A	0.9900
C15	H15B	0.9900	C16	C17	1.3171(18)
C17	C18	1.4293(17)	C17	H17A	0.9500
C19	H19A	0.9800	C19	H19B	0.9800
C19	H19C	0.9800	C20	H20A	0.9800
C20	H20B	0.9800	C20	H20C	0.9800
C21	C22	1.3133(16)	C21	H21A	0.9500
C22	C24	1.4785(17)	C22	C23	1.4847(17)
C23	H23A	0.9800	C23	H23B	0.9800
C23	H23C	0.9800	C24	H24A	0.9800
C24	H24B	0.9800	C24	H24C	0.9800

Table 17. Bond Angles (°) for **2.7**.

atom	atom	atom	angle	atom	atom	atom	angle
C1	O1	C10	117.95(8)	C3	O2	C4	104.53(9)
C5	O3	C4	104.42(9)	C14	O4	C15	107.57(10)

C16	O5	C15	107.72(10)	O1	C1	C7	123.31(10)
O1	C1	C2	114.44(10)	C7	C1	C2	122.21(11)
C3	C2	C1	116.86(10)	C3	C2	H2A	121.6
C1	C2	H2A	121.6	C2	C3	O2	128.18(11)
C2	C3	C5	122.01(11)	O2	C3	C5	109.73(10)
O3	C4	O2	107.78(10)	O3	C4	H4A	110.2
O2	C4	H4A	110.2	O3	C4	H4B	110.2
O2	C4	H4B	110.2	H4A	C4	H4B	108.5
C6	C5	O3	128.76(11)	C6	C5	C3	121.54(11)
O3	C5	C3	109.58(10)	C5	C6	C7	118.59(11)
C5	C6	H6A	120.7	C7	C6	H6A	120.7
C1	C7	C6	118.78(10)	C1	C7	C8	121.27(10)
C6	C7	C8	119.93(10)	C21	C8	C7	111.36(9)
C21	C8	C9	108.97(9)	C7	C8	C9	109.81(9)
C21	C8	H8A	108.9	C7	C8	H8A	108.9
C9	C8	H8A	108.9	C11	C9	C10	112.53(9)
C11	C9	C8	108.58(9)	C10	C9	C8	111.98(9)
C11	C9	H9A	107.9	C10	C9	H9A	107.9
C8	C9	H9A	107.9	O1	C10	C20	103.96(9)
O1	C10	C19	108.56(9)	C20	C10	C19	111.06(10)
O1	C10	C9	108.20(9)	C20	C10	C9	110.37(9)
C19	C10	C9	114.13(9)	C12	C11	C9	127.18(11)
C12	C11	H11A	116.4	C9	C11	H11A	116.4
C11	C12	C13	123.88(11)	C11	C12	C18	116.84(11)
C13	C12	C18	119.28(10)	C14	C13	C12	117.52(11)
C14	C13	H13A	121.2	C12	C13	H13A	121.2
C13	C14	O4	128.50(12)	C13	C14	C16	123.03(12)
O4	C14	C16	108.47(11)	O4	C15	O5	107.57(10)
O4	C15	H15A	110.2	O5	C15	H15A	110.2
O4	C15	H15B	110.2	O5	C15	H15B	110.2
H15A	C15	H15B	108.5	C17	C16	O5	127.39(12)
C17	C16	C14	124.10(11)	O5	C16	C14	108.51(11)
C16	C17	C18	117.74(11)	C16	C17	H17A	121.1
C18	C17	H17A	121.1	O6	C18	C17	120.98(11)
O6	C18	C12	120.95(11)	C17	C18	C12	118.07(11)
C10	C19	H19A	109.5	C10	C19	H19B	109.5
H19A	C19	H19B	109.5	C10	C19	H19C	109.5
H19A	C19	H19C	109.5	H19B	C19	H19C	109.5
C10	C20	H20A	109.5	C10	C20	H20B	109.5
H20A	C20	H20B	109.5	C10	C20	H20C	109.5
H20A	C20	H20C	109.5	H20B	C20	H20C	109.5
C22	C21	C8	128.25(11)	C22	C21	H21A	115.9
C8	C21	H21A	115.9	C21	C22	C24	125.01(11)
C21	C22	C23	119.96(11)	C24	C22	C23	114.96(10)
C22	C23	H23A	109.5	C22	C23	H23B	109.5
H23A	C23	H23B	109.5	C22	C23	H23C	109.5

H23A	C23	H23C	109.5	H23B	C23	H23C	109.5
C22	C24	H24A	109.5	C22	C24	H24B	109.5
H24A	C24	H24B	109.5	C22	C24	H24C	109.5
H24A	C24	H24C	109.5	H24B	C24	H24C	109.5

Table 18. Torsion angles (°) for **2.7**.

atom	atom	atom	atom	angle	atom	atom	atom	atom	angle
C10	O1	C1	C7	-18.72(16)	C10	O1	C1	C2	163.63(10)
O1	C1	C2	C3	177.49(10)	C7	C1	C2	C3	-0.19(17)
C1	C2	C3	O2	-175.87(11)	C1	C2	C3	C5	0.62(18)
C4	O2	C3	C2	-171.21(13)	C4	O2	C3	C5	11.96(14)
C5	O3	C4	O2	19.38(14)	C3	O2	C4	O3	-19.40(14)
C4	O3	C5	C6	171.94(13)	C4	O3	C5	C3	-12.03(14)
C2	C3	C5	C6	-0.67(19)	O2	C3	C5	C6	176.40(11)
C2	C3	C5	O3	-177.04(11)	O2	C3	C5	O3	0.03(14)
O3	C5	C6	C7	175.86(12)	C3	C5	C6	C7	0.25(18)
O1	C1	C7	C6	-177.67(10)	C2	C1	C7	C6	-0.20(17)
O1	C1	C7	C8	0.71(17)	C2	C1	C7	C8	178.19(10)
C5	C6	C7	C1	0.17(17)	C5	C6	C7	C8	-178.24(10)
C1	C7	C8	C21	-134.74(11)	C6	C7	C8	C21	43.62(14)
C1	C7	C8	C9	-13.96(14)	C6	C7	C8	C9	164.41(10)
C8	C9	C11		-69.78(11)	C7	C8	C9	C11	168.00(9)
C21	C8	C9	C10	165.35(9)	C7	C8	C9	C10	43.14(12)
C1	O1	C10	C20	164.52(9)	C1	O1	C10	C19	-77.18(12)
C1	O1	C10	C9	47.18(13)	C11	C9	C10	O1	177.36(9)
C8	C9	C10	O1	-60.00(12)	C11	C9	C10	C20	64.22(13)
C8	C9	C10	C20	-173.14(9)	C11	C9	C10	C19	-61.68(13)
C8	C9	C10	C19	60.96(12)	C10	C9	C11	C12	-129.44(13)
C8	C9	C11	C12	106.02(13)	C9	C11	C12	C13	4.9(2)
C9	C11	C12	C18	-175.62(11)	C11	C12	C13	C14	174.88(12)
C18	C12	C13	C14	-4.63(18)	C12	C13	C14	O4	-178.83(13)
C12	C13	C14	C16	0.43(19)	C15	O4	C14	C13	175.33(14)
C15	O4	C14	C16	-4.02(15)	C14	O4	C15	O5	3.99(15)
C16	O5	C15	O4	-2.42(15)	C15	O5	C16	C17	179.63(13)
C15	O5	C16	C14	-0.02(14)	C13	C14	C16	C17	3.5(2)
O4	C14	C16	C17	-177.10(12)	C13	C14	C16	O5	-176.83(12)
O4	C14	C16	O5	2.56(14)	O5	C16	C17	C18	177.79(11)
C14	C16	C17	C18	-2.61(19)	C16	C17	C18	O6	179.04(12)
C16	C17	C18	C12	-1.73(17)	C11	C12	C18	O6	5.05(17)
C13	C12	C18	O6	-175.40(11)	C11	C12	C18	C17	-174.18(11)
C13	C12	C18	C17	5.37(16)	C7	C8	C21	C22	-142.58(12)
C9	C8	C21	C22	96.14(14)	C8	C21	C22	C24	3.4(2)
C8	C21	C22	C23	-173.63(12)					

References

- (1) Delbaere, S.; Micheau, J.-C.; Vermeersch, G. *J. Org. Chem.* **2003**, *68*, 8968.
- (2) Van Gemert, B. In *Organic Photochromic and Thermochromic Compounds*; Crano, J. C., Guglielmetti, R., Eds.; Plenum Press: New York, 1999; Vol. 1, p 111.
- (3) Hepworth, J. D.; Heron, B. M. In *Progress in Heterocyclic Chemistry*; Gribble, G., Joule, J., Eds.; Elsevier Science: New York, 2005; Vol. 17, p 33.
- (4) Samat, A.; Guglielmetti, R. In *Kirk-Othmer encyclopedia of chemical technology*; 5th ed.; Seidel, A., Ed.; John Wiley & Sons: Hoboken, 2004; Vol. 6, p 587.
- (5) Jurd, L. *Tetrahedron* **1977**, *33*, 163.
- (6) Iyer, M. R.; Trivedi, G. K. *Bull. Chem. Soc. Jpn.* **1992**, *65*, 1662.
- (7) Arduini, A.; Pochini, A.; Ungaro, R.; Domiano, P. *J. Chem. Soc. Perkin Trans. I* **1986**, 1391.
- (8) Inoue, T.; Inoue, S.; Sato, K. *Bull. Chem. Soc. Jpn.* **1990**, *63*, 1062.
- (9) Banwell, M. G.; Lambert, J. N.; Gravatt, G. L. *J. Chem. Soc. Perkin Trans. I* **1993**, 2817.
- (10) Bishop, L. M.; Winkler, M.; Houk, K. N.; Bergman, R. G.; Trauner, D. *Chem. Eur. J.* **2008**, *14*, 5405.
- (11) Allen, F. H.; Kennard, O.; Watson, D. G.; Brammer, L.; Orpen, A. G.; Taylor, R. *J. Chem. Soc. Perkin Trans. II* **1987**, S1.
- (12) Schiess, P.; Seeger, R.; Suter, C. *Helv. Chim. Acta* **1970**, *53*, 1713.
- (13) Sandstrom, J. In *Topics in Stereochemistry*; Allinger, N. L., Eliel, E. L., Wilen, S. H., Eds.; John Wiley & Sons: New York, 1983; Vol. 14, p 83.
- (14) Frisch, M. J.; Trucks, G. W.; Schlegel, H. B.; Scuseria, G. E.; Robb, M. A.; Cheeseman, J. R.; Montgomery, J., J. A.; Vreven, T.; Kudin, K. N.; Burant, J. C.; Millam, J. M.; Lyengar, S. S.; Tomasi, J.; Barone, V.; Mennucci, B.; Cossi, M.; Scalmani, G.; Rega, N.; Petersson, G. A.; Nakatsuji, H.; Hada, M.; Ehara, M.; Toyota, K.; Fukuda, R.; Hasegawa, J.; Ishida, M.; Nakajima, T.; Honda, Y.; Kitao, O.; Nakai, H.; Klene, M.; Li, X.; Knox, J. E.; Hratchian, H. P.; Cross, J. B.; Bakken, V.; Adamo, C.; Jaramillo, J.; Gomperts, R.; Stratmann, R. E.; Yazyev, O.; Austin, A. J.; Cammi, R.; Pomelli, C.; Ochterski, J. W.; Ayala, P. Y.; Morokuma, K.; Voth, G. A.; Salvador, P.; Dannenberg, J. J.; Zakrzewski, V. G.; Dapprich, S.; Daniels, A. D.; Strain, M. C.; Farkas, O.; Malick, D. K.; Rabuck, A. D.; Raghavachari, K.; Foresman, J. B.; Ortiz, J. V.; Cui, Q.; Baboul, A. G.; Clifford, S.; Cioslowski, J.; Stefanov, B. B.; Liu, G.; Liashenko, A.; Piskorz, P.; Komaromi, I.; Martin, R. L.; Fox, D. J.; Keith, T.; Al-Laham, M. A.; Peng, C. Y.; Nanayakkara, A.; Challacombe, M.; Gill, P. M. W.; Johnson, B.; Chen, W.; Wong, M. W.; Gonzalez, C.; Pople, J. A., *Gaussian 03*, Gaussian Inc.: Wallingford, **2004**.
- (15) All RDFT stationary points have been checked for triplet instabilities by calculating the eigenvalues of the Hermitian stability matrices. UDFT energies are reported throughout whenever an external instability was found.
- (16) Despite several attempts, TS1H could not be located as a stationary point on the PES at the RB3LYP or UB3LYP level. Given the almost identical energies of TS1 and TS4, and according to single point energy calculations, the energy of TS1H relative to 1H is estimated to be 24 - 25 kcal/mol.
- (17) Van De Water, R. W.; Pettus, T. R. R. *Tetrahedron* **2002**, *58*, 5367.
- (18) *KaleidaGraph*, Synergy Software: Reading, PA, **2003**.
- (19) Alaimo, P. J.; Peters, D. W.; Arnold, J.; Bergman, R. G. *J. Chem. Ed.* **2001**, *78*, 64.

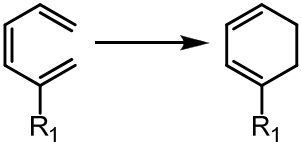
- (20) Jurd, L.; Stevens, K.; Manners, G. *Tetrahedron* **1973**, *29*, 2347.
- (21) *SMART: Area-Detector Software Package*, Bruker Analytical X-ray Systems, Inc.: Madison, WI, **2001-03**.
- (22) *SAINTE v. 7.23: SAX Area-Detector Integration Program*, Siemens Industrial Automation, Inc.: Madison, WI, **2005**.
- (23) *XPREP v. 6.12*, Bruker Analytical X-ray Systems, Inc.: Madison, WI, **2001**.
- (24) *SADABS v. 2.05: Bruker-Nonius Area Detector Scaling and Absorption*, Bruker Analytical X-ray Systems, Inc.: Madison, WI, **2003**.
- (25) Altomare, A.; Burla, M. C.; Camalli, M.; Cascarano, G. L.; Giacovazzo, C.; Guagliardi, A.; Moliterni, A. G. G.; Polidori, G.; Spagna, R. *J. Appl. Cryst.* **1999**, *32*, 115.
- (26) Beurskens, P. T.; Admiraal, G.; Beurskens, G.; Bosman, W. P.; de Gelder, R.; Israel, R.; Smits, J. M. M., *DIRDIF-94*, Nijmegen, Netherlands, **1994**.
- (27) *teXsan: Crystal Structure Analysis Package*, Molecular Structure Corporation: **1985, 1992**.
- (28) Farrugia, L. J. *J. Appl. Cryst.* **1997**, *30*, 565.
- (29) *APEX-II v2.0.2: Area-Detector Software Package*, Bruker Analytical X-ray Systems Inc.: Madison, WI, **2006**.
- (30) *XS: Program for the solution of X-ray crystal structures, part of the SHELXTL Crystal Structure Determination Package*, Bruker Analytical X-Ray Systems, Inc.: Madison, WI, **1995-1999**.
- (31) *XL: Program for the solution of X-ray crystal structures, part of the SHELXTL Crystal Structure Determination Package*, Bruker Analytical X-Ray Systems, Inc.: Madison, WI, **1995-1999**.
- (32) *XP: Program for the solution of X-ray crystal structures, part of the SHELXTL Crystal Structure Determination Package*, Bruker Analytical X-Ray Systems, Inc.: Madison, WI, **1995-1999**.

Part 1 - Chapter 3. Computational Analysis of the Feasibility of Catalytic Carba-6 π Electrocyclizations

Introduction

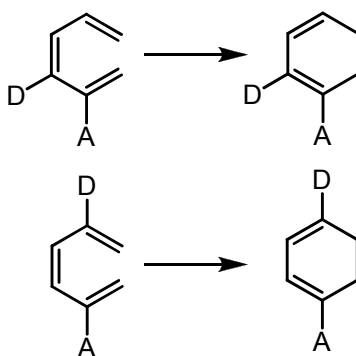
Experimental and computational studies have shown that the rates of 6 π electrocyclizations can be influenced by varying the electronics of the pendant triene substituents.¹⁻⁸ Electron-withdrawing groups located in the 2-position of hexatriene systems have been shown to lower their electrocyclization energy barriers,⁵⁻⁸ sometimes by as much as 10 kcal/mol relative to the hexatriene analogue in which the electron withdrawing group is replaced by a hydrogen atom.⁶ The results of the calculations shown in Table 1 predict a ~3 kcal/mol lowering of the electrocyclization energy barrier for 2-electron-withdrawing-group-substituted triene systems (entries 6-8) relative to their roughly isosteric methyl analogue (entry 2).⁸

Table 1. Gibbs free energies of activation of the electrocyclization of 2-substituted triene systems computed at the B3LYP/6-31G+** level of theory.⁸



Entry	R ₁	$\Delta G_{298}^{\ddagger}$ (kcal/mol)
1	H	30.7
2	CH ₃	27.7
3	NH ₂	27.1
4	OH	29.8
5	F	30.0
6	CHO	25.3
7	CN	24.9
8	NO ₂	24.8

Fu and Liu further discovered that calculations predict unusually low electrocyclization energy barriers for 2-electron-acceptor-, 3-electron-donor- and 2-electron-acceptor-, 5-electron acceptor-triene systems (Scheme 1). The authors found that this “captodative substitution” effect is greater than the sum of the mono-substituted effects of the type described in Table 1, and is attributed to a greater electronic “affinity” between the donor and acceptor groups in the electrocyclization transition state as compared to that of the ground state. Systems such as this can be thought of as “push-pull” triene systems, in which electron density is able to flow from donor to acceptor substituent more readily the electrocyclization transition state than in the ground state.



Scheme 1. Triene substrates with unusually low calculated electrocyclization energy barriers due to “captodative substitution”.⁸ D = electron-donating substituent; A = electron-accepting substituent.

This chapter describes our computational analysis of the feasibility of the catalysis of carba- 6π electrocyclizations. Parts of this work were published in *Angewandte Chemie* in 2008.⁹

Results & Discussion

We envisioned exploiting the above-described substituent effect to catalyze 6π electrocyclizations *via* the coordination of a Lewis acid to a Lewis basic electron-withdrawing group located in the 2-position of a hexatriene system. This should increase the electron-withdrawing effect of the substituent, thereby decreasing the electrocyclization energy barrier.

We began our investigations by computationally assessing the viability of this approach in the catalysis of 6π electrocyclizations. Hexatriene systems with methyl ester substitution at all possible positions and orientations were modeled *via* density functional theory (Figure 1). These calculations were carried out in Gaussian 03 using the B3LYP functional and the 6-31G** basis set.¹⁰⁻¹⁶ This level of theory has been shown to accurately predict the activation energies of pericyclic reactions.¹⁷ Global minima were located by performing 1000-step conformational searches on reactants and products using the OPLS_2005 force field in the program MacroModel.¹⁸

The thermal electrocyclization energy barriers predicted by these calculations (Figure 1) are consistent with those found in the literature.^{3,8} In order to model the catalyzed process, a proton, serving as the simplest Lewis acid, was bonded to the sp^2 -hybridized oxygen on the lone pair *anti* to the hexatriene. Proton coordination to the sp^2 -hybridized oxygen *syn* to the triene as well as proton coordination on the sp^3 -hybridized oxygen were also modeled. However, these coordination sites were found to have less pronounced effects on the electrocyclization energy barriers (results not shown). As can be seen in Figure 1, these calculations predict a slight increase and decrease of the electrocyclization energy barrier for the (*E,Z*) and (*Z,Z*) 1-carbomethoxy-substituted hexatriene systems (Figures 1A and 1B) upon proton coordination, respectively. Calculations further predict a small decrease of the electrocyclization energy barrier for the 3-substituted system (Figure 1D) upon proton coordination. However, we were pleased to find that the electrocyclization energy barrier is predicted to decrease by 10 kcal/mol upon protonation of the 2-carbomethoxy-substituted triene system (Figure 1C). An intrinsic

reaction coordinate search in both directions from the protonated electrocyclization transition state of this system suggests that the catalyzed pathway is a concerted process, as no stationary points other than the transition state were located between the protonated triene and protonated cyclohexadiene.

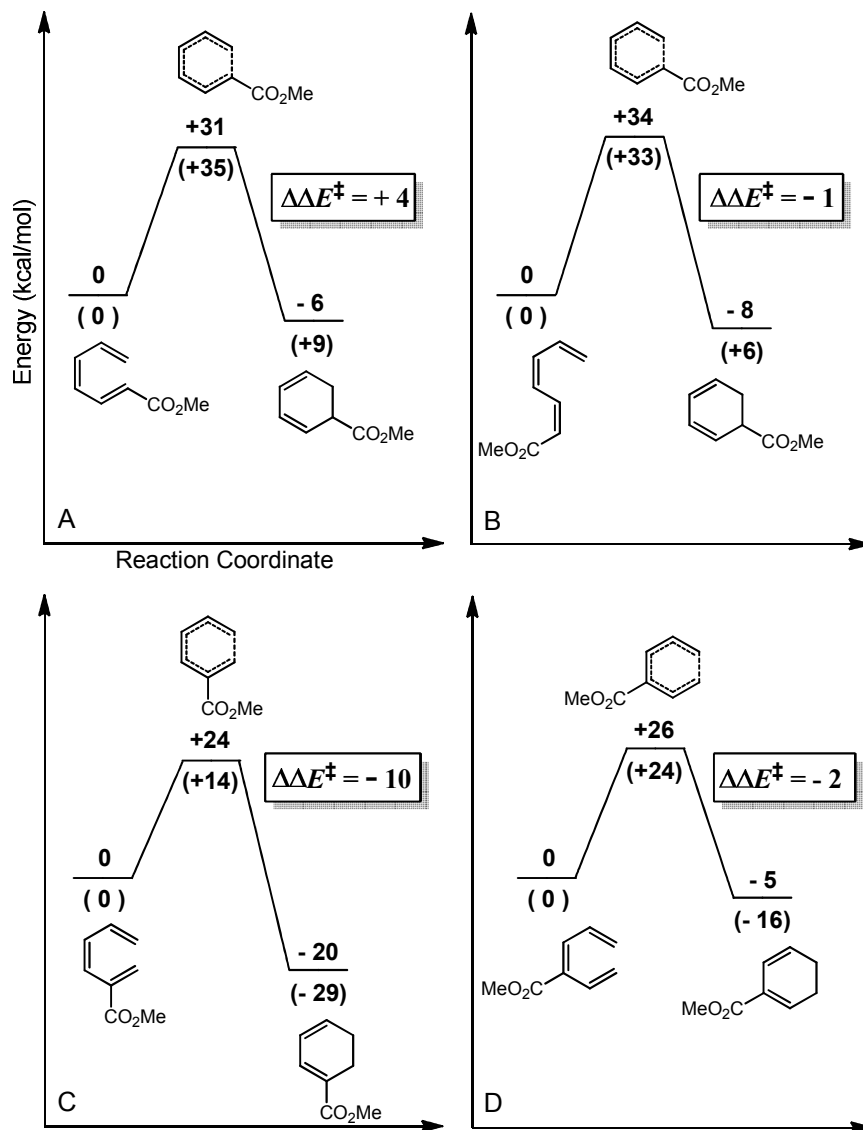


Figure 1. Relative zero-point corrected electronic energies of the thermal (numbers above line) and carbonyl-protonated (numbers below line) electrocyclization pathways computed at the B3LYP/6-31G** level of theory using Gaussian 03.¹⁰ Conformational analyses were performed using Macromodel.¹⁸

Calculations indicate it is possible to extend this catalysis concept to Lewis basic groups other than esters. A 2-substituted formyl-triene was modeled (Figure 2A), and calculations predict a significant 16 kcal/mol lowering of the electrocyclization energy barrier upon protonation of the formyl oxygen *anti* to the hexatriene skeleton. Calculations further indicate a slight (4 kcal/mol) lowering of the electrocyclization energy barrier upon protonation of a model 2-substituted imino-triene substrate (Figure 2B). We also investigated whether similar effects

would be observed upon methylation of a tertiary amine in the 2-position of a hexatriene. Indeed, calculations predict a 7 kcal/mol lowering of the electrocyclization energy barrier for such a system (Figure 2C). Whereas the systems in Figures 1C, 2A, and 2B demonstrate the possibility for catalysis *via* increasing the electron-withdrawing capability of an electron-withdrawing substituent, the system in Figure 2C can alternatively be thought of as demonstrating catalysis *via* decreasing the electron-donating ability of an electron-donating substituent.

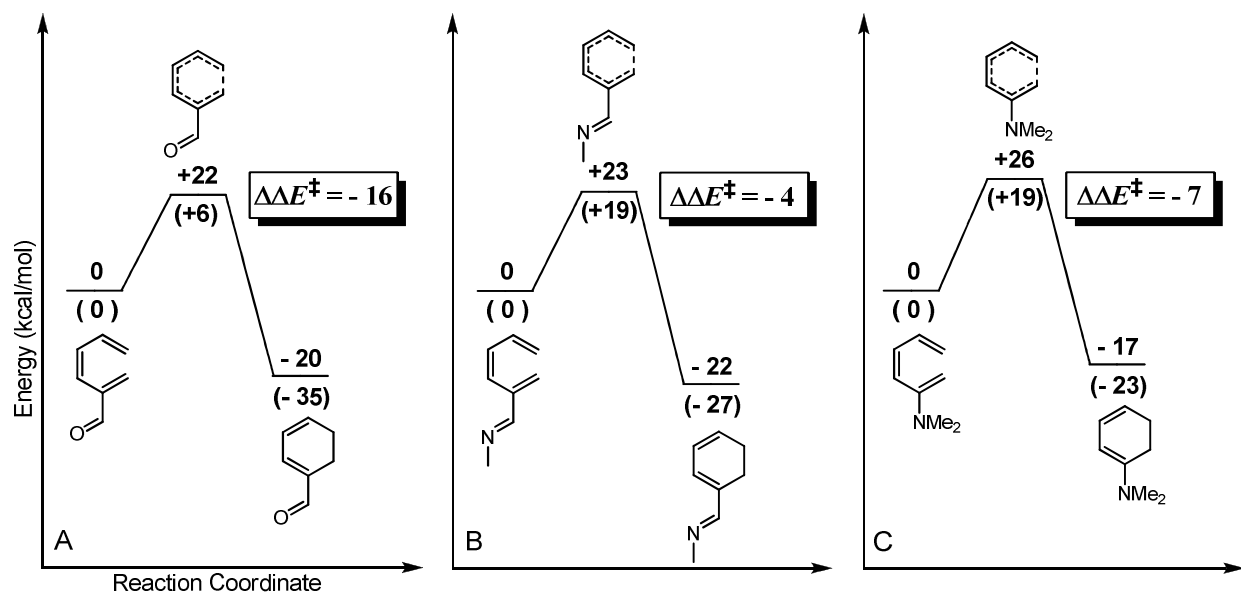


Figure 2. Relative zero-point corrected electronic energies of the thermal (numbers above line) and substrate-protonated/methylated (numbers below line) electrocyclization pathways computed at the B3LYP/6-31G** level of theory using Gaussian 03.¹⁰ A-carbonyl protonated *anti* to triene; B-imine protonated *syn* to triene; C-amine methylated. Conformational analyses were performed using MacroModel.¹⁸

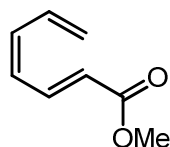
Summary & Conclusions

We have completed a suite of calculations that indicate catalysis of 6π electrocyclizations is possible for 2-carbomethoxy-substituted triene systems. Our calculations further indicate this catalysis should be applicable to other triene substrates possessing Lewis basic substituents such as aldehydes, imines, and amines in the 2-position of triene systems. Varying levels of catalysis have been predicted for the systems studied (from 4-16 kcal/mol).

Experimental

Molecules were first submitted to 1000-step conformational searches using the OPLS_2005 force field in the program MACROMODEL.¹⁸ The potential energy surfaces were further investigated by performing density functional theory geometry optimizations, energy minimizations, and frequency calculations, in GAUSSIAN 03 at the B3LYP/6-31G** level of theory,¹⁰⁻¹⁶ on molecules in conformations similar to the minimum energy conformations

obtained from MACROMODEL. All energies reported are those of the lowest energy conformation obtained *via* this method. Intrinsic reaction coordinate searches were performed in GAUSSIAN 03 by the method of Schlegel and Gonzalez.^{19,20}

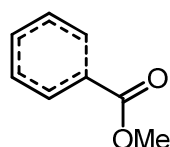


$E_{\text{SCF}} = -461.280415991$ Hartrees

Zero-Point Correction = 0.162729 Hartrees

No Imaginary Frequencies

C	-1.37343577	-1.13728222	-0.00027238
H	-1.04710001	-2.17571813	-0.00050229
C	-2.71006841	-0.89562431	-0.00014188
H	-3.37607074	-1.75740162	-0.00027934
C	-3.36763823	0.39688102	0.00017164
H	-2.74557384	1.28844520	0.00031327
C	-4.70321715	0.53760483	0.00029800
H	-5.17342520	1.51509823	0.00053647
H	-5.36487023	-0.32487448	0.00016654
C	-0.33123509	-0.14017951	-0.00013050
H	-0.60033115	0.91296170	0.00005578
C	0.98957962	-0.42631070	-0.00022080
H	1.31941453	-1.45945898	-0.00041385
C	1.97686785	0.67826846	-0.00009328
O	1.66640086	1.85185892	-0.00022814
O	3.30593481	0.37028245	-0.00000050
C	3.76479196	-0.98140696	0.00043729
H	3.44041070	-1.52326324	0.89568143
H	4.85396688	-0.92099707	0.00079577
H	3.44102501	-1.52362623	-0.89481320



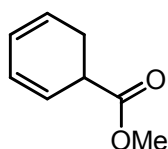
$E_{\text{SCF}} = -461.230263158$ Hartrees

Zero-Point Correction = 0.162477 Hartrees

Single Imaginary Frequency = $-515.8687 \text{ cm}^{-1}$

C	2.86206658	0.14819491	-0.07905338
H	3.93374611	0.03083982	0.07069430
C	2.21098743	1.13784975	0.65201883
H	2.70719777	1.47656713	1.56205211
C	2.20687815	-0.94999033	-0.67672245
H	2.84564416	-1.78741304	-0.94990656
C	0.84690170	-1.20516091	-0.54831041

H	0.55534878	-2.24103573	-0.37978005
C	-0.17000993	-0.23385695	-0.41638171
H	-0.29138037	0.46206757	-1.22839919
C	0.90627437	1.58085883	0.40254618
H	0.67818895	1.93896693	-0.58891372
H	0.37967373	2.11530523	1.19181316
C	-1.41087842	-0.67739799	0.28483514
O	-1.45624820	-1.67400194	0.97365783
O	-2.54017990	0.08206745	0.18313589
C	-2.60174269	1.22573678	-0.66719506
H	-1.87682739	1.99323625	-0.37673962
H	-3.60802058	1.62926903	-0.54531680
H	-2.45500958	0.96026821	-1.72027619

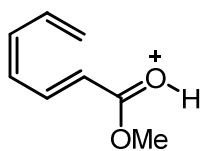


$E_{\text{SCF}} = -461.292089491$ Hartrees

Zero-Point Correction = 0.165446 Hartrees

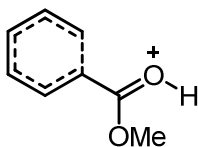
No Imaginary Frequencies

C	-2.78599769	-0.48742626	0.07782539
H	-3.80597897	-0.85068323	0.16601300
C	-2.41946248	0.68426163	0.62229479
H	-3.14132786	1.30172039	1.15044293
C	-1.81964416	-1.27544473	-0.68949911
H	-2.18513756	-2.08824986	-1.31176158
C	-0.50477845	-1.01126453	-0.63192447
H	0.20749446	-1.59518974	-1.20796198
C	0.01265913	0.09394702	0.28281338
H	0.19068958	-0.35090134	1.27476222
C	-1.02299849	1.22196743	0.43306259
H	-0.73687390	1.87168139	1.26628999
H	-0.98788718	1.85523501	-0.46530677
C	1.33588253	0.64922248	-0.24913586
O	1.42742912	1.69682860	-0.84182635
O	2.46054682	-0.10275849	-0.09147218
C	2.49613965	-1.25041767	0.76364787
H	2.35214363	-0.97084368	1.81275471
H	3.49599318	-1.66960133	0.64433893
H	1.75627679	-2.00480086	0.48230939



$E_{\text{SCF}} = -461.653133826$ Hartrees
 Zero-Point Correction = 0.176010 Hartrees
 No Imaginary Frequencies

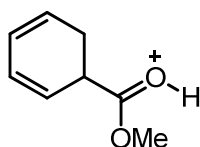
C	1.40764995	-1.14970499	0.00001473
H	1.10844629	-2.19434597	0.00003875
C	2.75603699	-0.86997604	0.00002006
H	3.42855622	-1.72626289	0.00005004
C	3.39756126	0.41489211	-0.00000806
H	2.79380183	1.31795277	-0.00003688
C	4.74271329	0.52269349	-0.00000069
H	5.23593838	1.48876670	-0.00002385
H	5.38270663	-0.35540668	0.00002797
C	0.38376691	-0.17594843	-0.00001838
H	0.66044010	0.87486594	-0.00004258
C	-0.96441931	-0.48281447	-0.00003108
H	-1.29004372	-1.51521375	0.00000085
C	-1.94876271	0.52123926	-0.00005932
O	-3.24134605	0.33337091	0.00002297
C	-3.82270077	-1.00129047	0.00000362
H	-3.52030262	-1.53563037	-0.90221833
H	-4.89703981	-0.83345478	-0.00008626
H	-3.52044295	-1.53559214	0.90229612
O	-1.59715145	1.78896538	0.00001996
H	-2.38515403	2.36108815	0.00012560



$E_{\text{SCF}} = -461.597697796$ Hartrees
 Zero-Point Correction = 0.175567 Hartrees
 Single Imaginary Frequency = $-407.1270 \text{ cm}^{-1}$

C	2.84523581	0.11763171	0.13417271
H	3.84352982	-0.11773712	0.49567468
C	2.14021038	1.13130043	0.75429975
H	2.46584523	1.46906315	1.73602360
C	2.25206343	-0.86317949	-0.71497891
H	2.90011285	-1.67277571	-1.03761008
C	0.89848694	-1.08203657	-0.80512939
H	0.59191877	-2.10945705	-0.99810204
C	-0.16944676	-0.12452601	-0.56101837
H	-0.41710454	0.58491681	-1.33490796
C	0.96003168	1.65225607	0.20862766
H	0.96206080	1.88940239	-0.84604257
H	0.31574853	2.28121284	0.81847624
C	-1.28275204	-0.56354491	0.20637845

O	-2.45560531	0.00188517	0.28742983
C	-2.84124993	1.09679288	-0.59188863
H	-2.20930828	1.96489474	-0.39796700
H	-3.87325555	1.31324130	-0.32617193
H	-2.77437816	0.77727555	-1.63312678
O	-1.12767676	-1.59771707	0.99627906
H	-1.95438998	-1.80154629	1.47130311

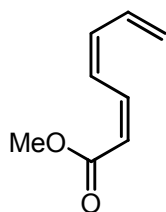


$E_{\text{SCF}} = -461.640920445$ Hartrees

Zero-Point Correction = 0.178140 Hartrees

No Imaginary Frequencies

C	-2.83464941	-0.41310578	-0.15875259
H	-3.86860547	-0.66935825	-0.36440403
C	-2.05646899	-1.22555984	0.57227628
H	-2.42961181	-2.15690247	0.98614759
C	-2.30647716	0.85446858	-0.66448693
H	-3.00202999	1.59950808	-1.03849614
C	-0.98867957	1.10287983	-0.69993521
H	-0.58816387	2.02987485	-1.09493502
C	-0.02823138	0.00256281	-0.27470175
H	0.13720822	-0.68760944	-1.11385432
C	-0.64280084	-0.82310928	0.91654415
H	-0.02458848	-1.69935962	1.13391488
H	-0.64772396	-0.19088749	1.81610067
C	1.28860141	0.50778723	0.17483454
O	2.43136241	-0.05420749	-0.00923231
C	2.61009282	-1.29210064	-0.78476332
H	2.01333652	-2.08853753	-0.34193238
H	3.67177100	-1.50743283	-0.69492950
H	2.33778936	-1.10443152	-1.82332197
O	1.31093199	1.59962929	0.86948752
H	2.21394183	1.82882430	1.16757761

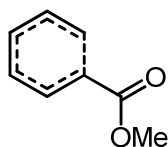


$E_{\text{SCF}} = -461.277110556$ Hartrees

Zero-Point Correction = 0.162893 Hartrees

No Imaginary Frequencies

C	2.54036342	0.61868143	0.00007920
H	3.03056367	1.59147677	0.00029480
C	1.18079329	0.61216643	-0.00021535
H	0.64999491	1.55615351	-0.00011856
C	0.36298387	-0.57838060	-0.00063847
H	0.88723914	-1.53200156	-0.00111579
C	-0.99253146	-0.65882678	-0.00060357
H	-1.42582485	-1.65152539	-0.00104677
C	3.43997749	-0.51918882	0.00018955
H	3.01057540	-1.51837834	0.00016984
C	4.77734170	-0.39431840	0.00037057
H	5.25487980	0.58210513	0.00043523
H	5.43216216	-1.25923169	0.00045246
C	-1.91163468	0.50029780	-0.00011640
O	-1.56505287	1.66523576	-0.00001683
O	-3.25621529	0.25382794	0.00020484
C	-3.79447629	-1.06754551	0.00052714
H	-3.50451156	-1.62834114	-0.89491256
H	-4.87825699	-0.94179162	0.00108373
H	-3.50358053	-1.62828860	0.89569751



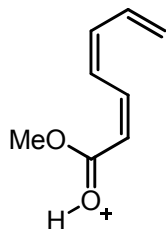
$E_{\text{SCF}} = -461.222944393$ Hartrees

Zero-Point Correction = 0.162355 Hartrees

Single Imaginary Frequency = $-485.0193 \text{ cm}^{-1}$

C	2.66046775	0.19875581	0.20087930
H	3.74193713	0.22245224	0.32176180
C	1.98535031	1.41500587	0.14384841
H	2.57270859	2.29431225	-0.12240088
C	2.12842336	-1.02343695	-0.25794169
H	2.85116986	-1.82343994	-0.40518641
C	0.91792926	-1.13918539	-0.93246965
H	0.93408918	-1.80533279	-1.79773576
C	-0.25252891	-0.36857678	-0.76208004
H	-0.83794327	-0.25524499	-1.67403887
C	0.59989814	1.53887412	0.26862462
H	0.12429438	2.46842299	-0.04003059
H	0.14559401	1.05426172	1.11710783
C	-1.08782885	-0.53278318	0.46040031
O	-0.72081432	-1.04969401	1.49249745
O	-2.37641988	-0.07440400	0.40571232
C	-2.88801884	0.63745792	-0.71970659
H	-2.23930520	1.47041484	-1.00925578

H	-3.85506813	1.03181519	-0.40313615
H	-3.04175629	-0.02154584	-1.58209143

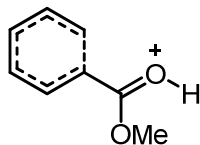


$E_{SCF} = -461.648353678$ Hartrees

Zero-Point Correction = 0.176257 Hartrees

No Imaginary Frequencies

C	2.59910104	0.58965823	0.00009245
H	3.09569046	1.55882231	0.00034716
C	1.22012371	0.61395733	0.00017999
H	0.73673528	1.58199031	0.00029987
C	0.41984806	-0.55188264	0.00022225
H	0.94761853	-1.50229881	0.00014032
C	-0.96254975	-0.68428714	0.00025785
H	-1.36545665	-1.68800017	0.00033415
C	3.48057980	-0.54403762	-0.00023483
H	3.07051344	-1.54986353	-0.00063719
C	4.82049842	-0.38180591	-0.00009923
H	5.27286443	0.60616717	0.00026495
H	5.49623621	-1.23034405	-0.00035323
C	-1.90846736	0.35589013	-0.00002532
O	-3.20711535	0.20080071	-0.00022420
C	-3.83241555	-1.11377882	-0.00001005
H	-3.54825151	-1.65802093	-0.90220404
H	-4.90038264	-0.90907471	-0.00009907
H	-3.54837194	-1.65766705	0.90243111
O	-1.53753962	1.61764447	-0.00012129
H	-2.32026610	2.19844661	-0.00005872



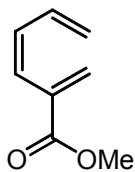
$E_{SCF} = -461.595323975$ Hartrees

Zero-Point Correction = 0.175350 Hartrees

Single Imaginary Frequency = $-347.5207 \text{ cm}^{-1}$

C	2.78295995	0.26453320	0.00781738
H	3.85926437	0.34791684	-0.12585207
C	2.04701005	1.42248247	0.18209391
H	2.49624816	2.37587172	-0.08778936
C	2.22243043	-1.00401483	-0.32054100

H	2.92973205	-1.80912092	-0.49666833
C	0.95665031	-1.18071294	-0.82751763
H	0.84230911	-2.01595501	-1.52042879
C	-0.20726684	-0.31592539	-0.73369819
H	-0.64937429	-0.05108391	-1.69432703
C	0.72166235	1.38945120	0.61931336
H	0.10781071	2.28483695	0.56474295
H	0.47520565	0.69142799	1.40673933
C	-1.16290878	-0.45843498	0.28399595
O	-2.38949656	0.00431551	0.26243850
C	-2.89598832	0.77359409	-0.86123911
H	-2.26000328	1.64320736	-1.03692813
H	-3.89302886	1.08435176	-0.55772874
H	-2.95089158	0.13887214	-1.74805730
O	-0.87383354	-1.11892897	1.38790567
H	-1.63792625	-1.11925422	1.99219611

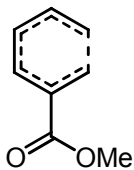


$E_{\text{SCF}} = -461.282039183$ Hartrees

Zero-Point Correction = 0.162560 Hartrees

No Imaginary Frequencies

H	2.41269506	0.80343701	0.92855585
C	2.84929608	-0.04426606	0.40582081
C	1.96150399	-0.85188113	-0.41583121
C	4.15444118	-0.31113707	0.56760078
H	2.39398701	-1.77632320	-0.79693824
C	0.66545588	-0.61334912	-0.71503619
H	0.12502682	-1.38475618	-1.25601020
C	-0.12604817	0.57629597	-0.36325615
C	-1.56574727	0.39541196	0.03480093
C	0.32009285	1.84400407	-0.41658819
H	-0.33850319	2.66040914	-0.14145115
H	1.32245392	2.07967909	-0.75423425
H	4.63218920	-1.14499414	0.05934973
H	4.78520725	0.29631799	1.20809580
O	-2.31703831	1.29116902	0.36269897
O	-1.94330329	-0.90258714	-0.01399504
C	-3.31095438	-1.15480516	0.34624503
H	-3.50459336	-0.82458713	1.36951611
H	-3.44393238	-2.23277824	0.25857004
H	-3.99003845	-0.62670013	-0.32762000

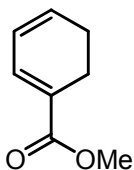


$E_{\text{SCF}} = -461.243865583$ Hartrees

Zero-Point Correction = 0.162468 Hartrees

Single Imaginary Frequency = $-528.5674 \text{ cm}^{-1}$

H	3.22932103	-0.98395604	1.48693261
C	2.77002224	-0.57049002	0.58645407
C	1.90848584	-1.44871026	-0.09232391
C	2.92432908	0.79434855	0.35291610
H	2.08042624	-2.51513070	0.04177939
C	0.64051999	-1.09474108	-0.56291742
H	-0.05596766	-1.90906301	-0.73551596
C	0.12005814	0.21166367	-0.46899718
C	-1.28586870	0.41928058	-0.01779338
C	0.92017470	1.35220047	-0.59087238
H	3.19867554	1.14201629	-0.62848739
H	3.33389527	1.40677108	1.15543662
H	0.51878588	2.29553562	-0.23136242
H	1.55633580	1.42131120	-1.45720491
O	-1.74316093	1.48187073	0.35944653
O	-2.02951662	-0.71408060	-0.08570801
C	-3.40408060	-0.56205489	0.29576916
H	-3.48265333	-0.23961692	1.33697716
H	-3.85612739	-1.54536368	0.16530974
H	-3.90311514	0.17619305	-0.33718328



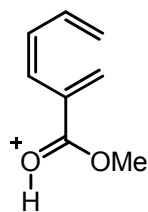
$E_{\text{SCF}} = -461.316767056$ Hartrees

Zero-Point Correction = 0.165806 Hartrees

No Imaginary Frequencies

H	-4.03545257	-0.62129757	0.04658302
C	-2.96518732	-0.42970503	0.04903990
C	-2.09139903	-1.43537667	-0.13912067
C	-2.47717523	0.96461181	0.35815457
H	-2.43827934	-2.45101089	-0.30738607
C	-0.65450898	-1.19311262	-0.06430107
H	0.02057700	-2.03959130	0.00505473
C	-0.15919108	0.06446893	-0.08673966
C	1.28957037	0.35719850	-0.03934707
C	-1.09769152	1.24022619	-0.25959543

H	-2.43047118	1.07673430	1.45419451
H	-3.19801399	1.71272117	0.01172383
H	-1.20897537	1.43585818	-1.33744206
H	-0.64931992	2.14078231	0.16590392
O	1.76057290	1.47947728	-0.10070235
O	2.05968803	-0.75480243	0.08101104
C	3.47239373	-0.51183919	0.13005432
H	3.81218240	-0.01456207	-0.78202281
H	3.93696965	-1.49335144	0.22559196
H	3.72783022	0.11748689	0.98646020

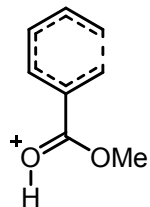


$E_{\text{SCF}} = -461.617780626$ Hartrees

Zero-Point Correction = 0.174701 Hartrees

No Imaginary Frequencies

H	2.47190529	0.82585837	0.93748709
C	2.89192108	-0.02558882	0.40705286
C	2.01416371	-0.82974618	-0.42313800
C	4.19347042	-0.31537023	0.56526925
H	2.46080398	-1.73880748	-0.82200826
C	0.71199133	-0.62523791	-0.72872222
H	0.19460681	-1.39308655	-1.29517382
C	-0.09202467	0.55192652	-0.36369603
C	-1.48456701	0.31749424	-0.00401281
C	0.32903477	1.84357796	-0.36630567
H	-0.30901826	2.66239425	-0.05458369
H	1.33237771	2.08863403	-0.69312632
H	4.65626972	-1.15412487	0.05247660
H	4.83498721	0.28011778	1.20559659
O	-1.90420201	-0.90290703	0.02968165
C	-3.28684784	-1.25208316	0.34761558
H	-3.51828491	-0.94639954	1.37131351
H	-3.32032535	-2.33592582	0.26985658
H	-3.96147380	-0.80420492	-0.38674167
O	-2.26240001	1.33130105	0.25783810
H	-3.17188306	1.09855797	0.51036771

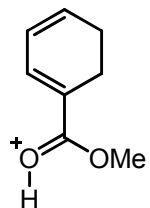


$E_{\text{SCF}} = -461.594966929$ Hartrees

Zero-Point Correction = 0.174555 Hartrees

Single Imaginary Frequency = $-392.0461 \text{ cm}^{-1}$

H	3.07716277	-0.98821499	1.58796776
C	2.72820340	-0.56749710	0.64294355
C	1.92383162	-1.44616113	-0.13830439
C	2.98339162	0.76479811	0.40059895
H	2.15256416	-2.50853477	-0.09528504
C	0.69202395	-1.10168503	-0.64627619
H	0.04522565	-1.89988284	-0.99644744
C	0.13844973	0.21687056	-0.47103466
C	-1.21013369	0.33399467	-0.04246017
C	0.93076770	1.37097600	-0.57234280
H	3.22325691	1.10055991	-0.59591905
H	3.39048565	1.38077276	1.19827412
H	0.61221456	2.30515813	-0.12114351
H	1.57494207	1.45980071	-1.43091443
O	-1.94385446	-0.74253708	0.05979893
C	-3.37812846	-0.67324450	0.28850368
H	-3.58044527	-0.31589016	1.30258700
H	-3.72470008	-1.69965538	0.19387488
H	-3.85492417	-0.04752394	-0.47056202
O	-1.70313649	1.53033868	0.19842076
H	-2.59028979	1.52268828	0.59204245



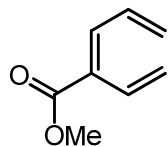
$E_{\text{SCF}} = -461.667677047$ Hartrees

Zero-Point Correction = 0.178148 Hartrees

No Imaginary Frequencies

H	4.09968617	-0.16887860	0.07873184
C	3.01575728	-0.09108391	0.04400399
C	2.43514227	1.12303786	-0.13714180
C	2.20894068	-1.32688371	0.30102538
H	3.03427448	2.01857014	-0.25799256
C	1.00994851	1.24643165	-0.06245644
H	0.57757325	2.24053541	0.00561537

C	0.18705883	0.14120933	-0.06774549
C	-1.21454502	0.32086316	0.01182941
C	0.78233463	-1.24109671	-0.26929292
H	2.19067517	-1.48078567	1.39256554
H	2.71977385	-2.20474609	-0.10602362
H	0.80639059	-1.44985548	-1.34744628
H	0.15258141	-2.01004293	0.18192725
O	-1.97857996	-0.73722478	-0.06951728
C	-3.42617133	-0.64891330	0.01416303
H	-3.72587075	-0.24013057	0.98344768
H	-3.77341535	-1.67587941	-0.07157043
H	-3.81854403	-0.06024971	-0.82020852
O	-1.71732419	1.52855519	0.16606740
H	-2.68668673	1.55943343	0.18224176

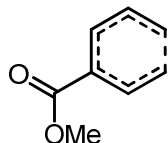


$E_{\text{SCF}} = -461.284504052$ Hartrees

Zero-Point Correction = 0.162432 Hartrees

No Imaginary Frequencies

C	-0.16543043	0.16038579	-0.06707443
C	-1.24692719	-0.66098554	-0.00424621
H	-1.03290485	-1.71484253	0.16254084
C	-2.63772613	-0.30287468	-0.18716849
H	-2.86133113	0.71653976	-0.48979545
C	-3.64049619	-1.18138491	-0.01956343
H	-4.67593662	-0.90132791	-0.18305744
H	-3.45242644	-2.20528250	0.29265804
C	-0.19382249	1.62159344	-0.24965936
H	0.56954129	2.02691177	-0.90960131
C	-1.03368871	2.46839169	0.35880662
H	-0.98883510	3.53535839	0.16393411
H	-1.76669959	2.13354085	1.08614174
C	1.16502608	-0.51703041	0.03277923
O	1.33970151	-1.70708185	0.21402857
O	2.18894756	0.36032386	-0.10378495
C	3.50117138	-0.21659506	-0.02679558
H	3.65057444	-0.70411262	0.93959163
H	4.19540177	0.61468009	-0.14852788
H	3.64478566	-0.95640324	-0.81830346

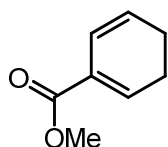


$E_{\text{SCF}} = -461.242282722$ Hartrees

Zero-Point Correction = 0.162062 Hartrees

Single Imaginary Frequency = $-567.7264 \text{ cm}^{-1}$

C	0.68042053	-1.14709511	0.02782572
H	-0.05894015	-1.93125428	-0.10169091
C	2.00640327	-1.45215668	-0.27717532
H	2.14222516	-2.28919853	-0.96480904
C	0.16420707	0.16624492	0.09380255
C	0.95898731	1.30545319	-0.11684162
H	0.50367786	2.08893311	-0.72012246
C	2.29486912	1.41817635	0.25679910
H	2.89351506	2.21350108	-0.18327032
H	2.55715461	1.19248788	1.27750053
C	3.13540357	-0.68955375	0.04186286
H	4.03365561	-0.83264438	-0.55859683
H	3.35000303	-0.47012020	1.07411955
C	-1.31046268	0.37490682	-0.03308424
O	-1.83629744	1.43834199	-0.30253716
O	-2.02546986	-0.75107146	0.21032245
C	-3.44928817	-0.60038364	0.11319315
H	-3.73941798	-0.30811792	-0.89924177
H	-3.80481972	0.16061804	0.81206856
H	-3.86615520	-1.57592156	0.36346722



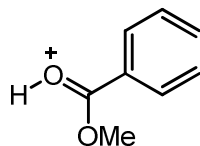
$E_{\text{SCF}} = -461.295210321$ Hartrees

Zero-Point Correction = 0.165060 Hartrees

No Imaginary Frequencies

C	-0.49063558	-0.89629614	-0.79185319
H	0.16168671	-1.47090255	-1.44300491
C	-1.76221112	-1.27206787	-0.58759963
H	-2.15199695	-2.17333267	-1.05343141
C	0.04297069	0.32917778	-0.16936707
C	-0.80464208	1.23659331	0.35609158
H	-0.41014534	2.17097666	0.74492622
C	-2.29332479	1.01330047	0.33112226
H	-2.77581191	1.52666815	1.16934048
H	-2.68766313	1.48892227	-0.58245746
C	-2.65743561	-0.48181440	0.33794175

H	-2.55384908	-0.88359457	1.35907404
H	-3.71017435	-0.61276540	0.06768184
C	1.50737716	0.65213248	-0.19396840
O	1.93488673	1.76421769	-0.40375136
O	2.39877722	-0.36313427	-0.00030191
C	2.04563039	-1.53640999	0.74260675
H	1.75372698	-2.35379759	0.07702447
H	1.23569037	-1.34149605	1.45014298
H	2.94285085	-1.82703952	1.29328551

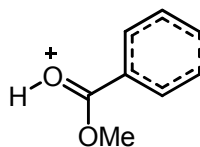


$E_{SCF} = -461.628708815$ Hartrees

Zero-Point Correction = 0.175269 Hartrees

No Imaginary Frequencies

C	0.05661094	0.02073461	0.14873345
C	1.29930354	-0.54801164	-0.06602786
H	1.32782898	-1.59577565	-0.35414929
C	2.57180061	0.09450469	0.07225023
H	2.60814725	1.11605947	0.43462091
C	3.71370467	-0.56827606	-0.21555301
H	4.68547552	-0.10362439	-0.08590443
H	3.70455717	-1.58851504	-0.58987132
C	-0.15404415	1.44453789	0.51218444
H	-0.75673999	1.62792930	1.40028350
C	0.37468491	2.48340832	-0.14228593
H	0.22012979	3.49869907	0.20770641
H	0.96506029	2.36065717	-1.04562829
C	-1.06320655	-0.87824631	0.08921343
O	-2.32717699	-0.58918121	0.01515592
C	-2.90231503	0.69943655	-0.38296887
H	-3.02700342	1.31915511	0.50320299
H	-3.87040155	0.43468666	-0.80349101
H	-2.26786128	1.18309279	-1.12191822
O	-0.83593641	-2.16982801	0.15227470
H	-1.66351921	-2.66881907	0.02242853

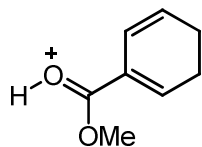


$E_{SCF} = -461.589710442$ Hartrees

Zero-Point Correction = 0.174857 Hartrees

Single Imaginary Frequency = $-513.5010 \text{ cm}^{-1}$

C	-1.02938094	-1.18911367	0.27141109
H	-0.67278397	-2.20540338	0.39784291
C	-2.36741735	-1.02040990	-0.04453127
H	-2.83277566	-1.90008797	-0.49567684
C	-0.03078663	-0.18484459	0.06940876
C	-0.38555045	1.13633081	-0.33368286
H	0.16706276	1.58759656	-1.15538254
C	-1.53256040	1.75079421	0.12359531
H	-1.77363899	1.62995723	1.17043406
H	-1.88497105	2.66654175	-0.33990739
C	-3.14412860	0.14734803	-0.04375266
H	-3.36019801	0.67158281	0.87329635
H	-3.94049167	0.22919962	-0.78313684
C	1.32147500	-0.64437223	-0.03869334
O	2.41024549	0.06427272	-0.11108638
C	2.54695267	1.49498637	0.15565323
H	1.78020751	1.82402199	0.85568622
H	2.48234730	2.03348746	-0.78891150
H	3.54374900	1.59694651	0.58080790
O	1.55327532	-1.93503928	-0.04492909
H	2.51170633	-2.11202429	-0.02337823



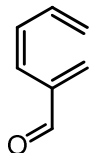
$E_{SCF} = -461.657937455$ Hartrees

Zero-Point Correction = 0.177606 Hartrees

No Imaginary Frequencies

C	-0.73156060	-1.25023587	-0.17541556
H	-0.05800908	-2.07579075	-0.36939038
C	-2.04686146	-1.44326748	-0.00643204
H	-2.45182992	-2.44975290	-0.05484188
C	-0.17423994	0.11055899	-0.06874848
C	-0.99267410	1.20586783	-0.05449458
H	-0.57348558	2.20651394	-0.00042541
C	-2.46767985	1.04617785	-0.19025426
H	-2.98770675	1.88163612	0.28797996
H	-2.67783595	1.15363237	-1.27021273
C	-2.98943582	-0.31198711	0.31635512
H	-3.13573345	-0.27910460	1.40604347
H	-3.97825220	-0.50248365	-0.10975405
C	1.24489329	0.31013851	0.00416473
O	2.01136458	-0.73689088	-0.02286370
C	3.46407515	-0.64350726	0.04515604
H	3.84408239	-0.09036607	-0.81808713

H	3.80913754	-1.67367946	0.00218866
H	3.76549970	-0.19263091	0.99459006
O	1.72726001	1.52500658	0.09423267
H	2.69603652	1.57462746	0.13897169



$E_{\text{SCF}} = -346.722682804$ Hartrees

Zero-Point Correction = 0.128722 Hartrees

No Imaginary Frequencies

C	0.09822336	-1.01074779	0.36112985
C	-0.95098105	0.00868760	0.23885153
C	-0.85220054	1.30819669	0.58116670
C	-2.28020771	-0.47797947	-0.25836003
H	0.04554482	1.72782895	1.01960540
H	-1.71069702	1.95794473	0.44321341
H	3.99521639	1.26715965	-0.68915632
H	-2.33607292	-1.57526134	-0.43251723
H	4.11745849	-0.44162062	0.00775749
O	-3.24374857	0.23050494	-0.46712605
C	1.43128510	-0.87561468	0.17837762
H	-0.26513914	-2.00880794	0.60566565
C	2.14909592	0.30533383	-0.27191604
H	2.04656309	-1.75869078	0.34642266
H	1.55703474	1.15348449	-0.60683229
C	3.48813160	0.38111104	-0.32210803



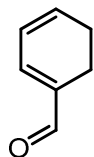
$E_{\text{SCF}} = -346.687759861$ Hartrees

Zero-Point Correction = 0.128721 Hartrees

Single Imaginary Frequency = $-529.8278 \text{ cm}^{-1}$

H	0.23792066	2.37236204	-0.16385313
C	-2.23815898	0.81883415	-0.17708369
H	-2.35640780	1.15920302	0.83812358
C	-2.09633279	-0.54630512	-0.41607036
H	-2.78588742	1.41734533	-0.90313762
H	-2.65977978	-0.98302812	-1.24264708
C	-1.14264404	-1.39126583	0.17564021
H	-1.30079546	-2.46470476	0.09097009
C	0.15561657	-0.98759528	0.49295975
H	0.90109148	-1.76732184	0.62757638

C	0.64691161	0.30957217	0.24650130
C	2.01769449	0.42647487	-0.30350946
C	-0.11907048	1.47843600	0.34924199
H	-0.61974159	1.68798129	1.27938960
O	2.87593451	-0.43568675	-0.24517581
H	2.23202548	1.41475128	-0.77109379

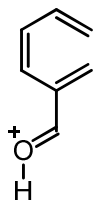


$E_{\text{SCF}} = -346.757384676$ Hartrees

Zero-Point Correction = 0.132073 Hartrees

No Imaginary Frequencies

H	0.00547372	-2.24770004	0.08676428
C	-1.75855906	-0.99552035	0.31140403
H	-2.50692306	-1.70417809	-0.05853836
C	-2.18740117	0.42568869	0.03625322
H	-1.72097426	-1.13776806	1.40420923
H	-3.24954573	0.65781265	0.03297746
C	-1.27400511	1.40401525	-0.11670283
H	-1.58253259	2.43592900	-0.25803217
C	0.14647653	1.10120292	-0.03054083
H	0.86890821	1.90550007	0.07952483
C	0.59735282	-0.17484221	-0.08301318
C	2.04203774	-0.45615083	0.00921360
C	-0.38662498	-1.30408666	-0.30978532
H	-0.50697366	-1.45347547	-1.39451395
O	2.91343549	0.38460318	0.15889536
H	2.30942276	-1.53478642	-0.06452636



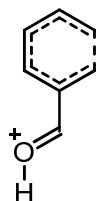
$E_{\text{SCF}} = -347.055152007$ Hartrees

Zero-Point Correction = 0.141751 Hartrees

No Imaginary Frequencies

C	0.12635800	-1.35910788	-0.33859178
C	-1.06719498	-0.56176798	-0.00456317
C	-2.22015772	-1.08757822	0.52070877
C	-1.09289119	0.80650851	-0.40556647
H	-2.28125750	-2.14199077	0.77210883
H	-3.11209630	-0.48662339	0.66380774
H	3.50919989	1.64768524	0.65805148

H	-0.31045095	1.19670220	-1.05766975
H	3.91410231	0.11258011	-0.29062410
O	-2.03749769	1.60557562	-0.03425342
C	1.40746072	-0.93664011	-0.24190526
H	-0.06966829	-2.37072953	-0.68011734
C	1.88768565	0.31972647	0.30937273
H	2.17715222	-1.62380936	-0.58717232
H	1.18912651	0.94085687	0.87152585
C	3.16834750	0.71638567	0.21904628
H	-1.97377428	2.49556492	-0.42688959

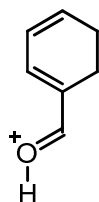


$E_{SCF} = -347.045197619$ Hartrees

Zero-Point Correction = 0.141799 Hartrees

Single Imaginary Frequency = $-296.5153 \text{ cm}^{-1}$

H	-0.02229523	2.40050502	0.11985503
C	2.39607876	0.73271215	0.22934699
H	2.49014506	1.05194441	-0.79825188
C	2.03358233	-0.55314716	0.53257910
H	2.94362418	1.32553841	0.95633973
H	2.40032479	-0.98112950	1.46757692
C	1.12361799	-1.39142469	-0.19993755
H	1.33514058	-2.45845952	-0.22672504
C	-0.12145959	-0.99077168	-0.59419346
H	-0.82465544	-1.73521715	-0.95436425
C	-0.61179309	0.34066287	-0.27699106
C	-1.87818461	0.53068687	0.26768898
C	0.18647627	1.48925538	-0.43509724
H	0.74904308	1.61161063	-1.34626684
O	-2.75571875	-0.43879134	0.29379497
H	-2.17768694	1.50834783	0.64629955
H	-3.61779841	-0.16065189	0.64480252

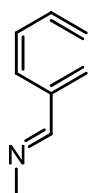


$E_{SCF} = -347.115519581$ Hartrees

Zero-Point Correction = 0.145601 Hartrees

No Imaginary Frequencies

H	0.13111255	-2.28907903	-0.06966906
C	1.83744438	-0.96399625	-0.29940754
H	2.62619843	-1.61078799	0.09817916
C	2.19689358	0.46927040	-0.08971644
H	1.84749917	-1.13833735	-1.38924760
H	3.24166422	0.75513678	-0.19173458
C	1.25770938	1.43959686	0.12890876
H	1.54452243	2.48150652	0.21752676
C	-0.11825691	1.09488609	0.09279192
H	-0.85731686	1.88960140	0.02930616
C	-0.54773852	-0.23491217	0.10361362
C	-1.89746925	-0.53238669	-0.02130897
C	0.48037547	-1.33073725	0.32375260
H	0.61309336	-1.46171989	1.40572518
O	-2.80720601	0.40566293	-0.16066093
H	-2.23722915	-1.56822944	-0.00940559
H	-3.70564487	0.04627964	-0.23719677



$E_{\text{SCF}} = -366.161831724$ Hartrees

Zero-Point Correction = 0.168952 Hartrees

No Imaginary Frequencies

H	-4.51765204	1.08407415	1.09092326
C	-4.02567166	0.25537243	0.59257311
C	-2.69684832	0.23386758	0.40549696
H	-4.66246264	-0.55543943	0.24747016
H	-2.09621680	1.06844311	0.75876937
C	-1.99354815	-0.87230388	-0.22387055
C	-0.68117652	-0.94083610	-0.54065733
H	-2.59849224	-1.75681299	-0.42079573
C	0.34692785	0.10663014	-0.42100868
H	-0.31567625	-1.89829654	-0.91233580
C	0.14232263	1.41006304	-0.69399411
C	1.69848920	-0.37499488	-0.02398549
H	1.78686558	-1.46567594	0.11851294
N	2.69169638	0.40097511	0.14886328
H	-0.81268255	1.77473278	-1.05328510
H	0.95678409	2.11820837	-0.58642927
C	3.95709538	-0.18719145	0.53695577
H	4.71931174	0.07253366	-0.20715305
H	3.92900611	-1.28368863	0.64607784
H	4.28379786	0.25145432	1.48714440

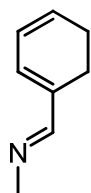


$E_{\text{SCF}} = -366.200743316$ Hartrees

Zero-Point Correction = 0.172459 Hartrees

Single Imaginary Frequency = $-513.7444 \text{ cm}^{-1}$

H	3.87681157	-0.27316590	0.01506731
C	2.80077076	-0.12139827	-0.01941623
C	2.28127525	1.11636217	0.07547891
C	1.90516579	-1.31101422	-0.26726690
H	2.92632056	1.98217109	0.19837011
C	0.84271810	1.32654759	-0.03020392
H	0.47117214	2.34069937	-0.16316531
C	-0.02957637	0.29225040	0.04487175
C	-1.46541580	0.52995854	-0.04405496
C	0.49477391	-1.10402142	0.30795261
H	0.51378874	-1.25659642	1.39800836
H	1.84650256	-1.47641754	-1.35601645
H	-0.20601774	-1.84297666	-0.08720945
H	2.34780208	-2.22257941	0.14870837
N	-2.32603896	-0.41262534	0.03473985
H	-1.76708772	1.58258241	-0.18451411
C	-3.72698694	-0.05824454	-0.06096290
H	-3.91112152	1.01961262	-0.20255160
H	-4.24794493	-0.38440095	0.84751540
H	-4.18430127	-0.60319272	-0.89578171



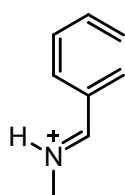
$E_{\text{SCF}} = -366.124795103$ Hartrees

Zero-Point Correction = 0.168903 Hartrees

No Imaginary Frequencies

H	3.19606559	0.24399947	1.58637599
C	2.66452570	0.05720689	0.65104101
C	2.10694115	1.19520903	0.04493565
C	2.43049110	-1.26638006	0.29029044
H	2.56656045	2.15609670	0.26991539
C	0.81253872	1.24870980	-0.47869594
H	0.39267273	2.24645858	-0.60069089
C	-0.08626335	0.15974414	-0.48746137

C	-1.48133202	0.45191644	-0.10595917
C	0.32719962	-1.16460526	-0.67269512
H	-0.36207414	-1.95171369	-0.37707794
H	2.59667769	-1.57983191	-0.72596614
H	0.93740388	-1.38807865	-1.53121134
H	2.63637317	-2.04520263	1.02335518
N	-2.36642080	-0.45390597	0.05017872
H	-1.71675664	1.52004317	0.04169859
C	-3.69149237	-0.04129655	0.46360225
H	-3.81160131	1.04990727	0.56786229
H	-3.93686104	-0.50957110	1.42465532
H	-4.42916605	-0.40779204	-0.26051388

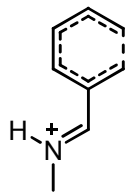


$E_{\text{SCF}} = -366.552736613$ Hartrees

Zero-Point Correction = 0.183278 Hartrees

No Imaginary Frequencies

H	-3.26807706	-1.68871871	-1.41150903
C	-3.03267911	-1.09845556	-0.53250203
C	-1.91638110	-0.35709238	-0.45997910
H	-3.75041017	-1.12779454	0.28290303
H	-1.23627404	-0.33657140	-1.30995916
C	-1.59431516	0.46765183	0.69629290
C	-0.48148315	1.21100902	0.88757484
H	-2.35546823	0.51021285	1.47339996
C	0.68171894	1.28669304	-0.03666623
H	-0.41616721	1.83889717	1.77221485
C	1.11626087	2.43547011	-0.60801739
C	1.49136912	0.11201600	-0.27888311
H	2.34343018	0.17530102	-0.95314016
H	0.59439374	3.37368215	-0.44957548
H	2.00047493	2.46580613	-1.23856643
C	2.06068139	-2.25804108	0.11309617
H	2.87906244	-2.07065106	-0.58206490
H	1.41567142	-3.04822325	-0.27854178
H	2.46217045	-2.56793797	1.08088228
N	1.27292822	-1.03497804	0.28711805
H	0.46966515	-1.07466205	0.91863410

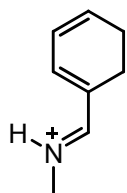


$E_{\text{SCF}} = -366.598948062$ Hartrees

Zero-Point Correction = 0.186986 Hartrees

Single Imaginary Frequency = $-383.2396 \text{ cm}^{-1}$

H	3.91576594	-0.21455744	-0.03959281
C	2.83604792	-0.08937523	-0.02928536
C	2.30231382	1.15163596	0.08691389
C	1.98408542	-1.30334717	-0.24923820
H	2.93475013	2.02744142	0.17956654
C	0.88134204	1.32354223	-0.00783948
H	0.49019558	2.33260559	-0.11928677
C	0.00682879	0.26015012	0.03579965
C	-1.37251136	0.55428586	-0.05479658
C	0.54820194	-1.13630013	0.28449035
H	0.53559490	-1.32246365	1.36752639
H	1.97667405	-1.50368212	-1.33266582
H	-0.08597156	-1.90385428	-0.17305171
H	2.44932508	-2.18266790	0.20598592
H	-1.67929824	1.58746123	-0.20363671
C	-3.77939862	-0.00970258	-0.06569682
H	-3.90768861	1.06190236	-0.22010020
H	-4.28406221	-0.30575099	0.85739989
H	-4.21963431	-0.55185636	-0.90639147
N	-2.35097934	-0.31929144	0.02976691
H	-2.11025504	-1.29487214	0.17379368



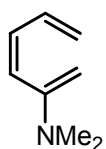
$E_{\text{SCF}} = -366.522286907$ Hartrees

Zero-Point Correction = 0.182950 Hartrees

No Imaginary Frequencies

H	3.04819391	0.24591030	1.71908475
C	2.63032867	0.05672416	0.72858770
C	2.11702122	1.20706748	0.06999310
C	2.53529692	-1.25344970	0.31352046
H	2.60347940	2.15860869	0.27185863
C	0.86466209	1.26966826	-0.50316919
H	0.47803272	2.25740529	-0.74356191
C	-0.05046382	0.15602406	-0.51853800

C	-1.38761469	0.46768253	-0.13412883
C	0.39203484	-1.15349114	-0.74606643
H	-0.18317760	-2.01925830	-0.42424073
H	2.69696570	-1.51219859	-0.72051123
H	1.03816175	-1.33491392	-1.58806420
H	2.73741539	-2.05257644	1.02210854
H	-1.64860643	1.51799336	-0.01859278
C	-3.73007124	-0.00680539	0.48873043
H	-3.81153974	1.07910985	0.54040005
H	-3.94809625	-0.43302312	1.47122287
H	-4.44817759	-0.39197776	-0.23922216
N	-2.37118306	-0.37285597	0.07887744
H	-2.19153377	-1.36560906	-0.03619936

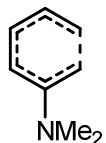


$E_{\text{SCF}} = -367.378907208$ Hartrees

Zero-Point Correction = 0.193200 Hartrees

No Imaginary Frequencies

C	-0.33899265	1.39784321	0.40206155
C	0.94464771	0.78064129	0.00853939
C	1.96672099	1.59482607	-0.33928918
H	1.81976399	2.66825452	-0.36136724
H	2.93836372	1.22918584	-0.64452289
H	-3.67221421	-1.54200905	-0.95354547
H	-4.14000341	0.00634308	-0.05697426
C	-1.60519238	0.94808116	0.24590831
H	-0.22528038	2.38939533	0.83389256
C	-2.05965339	-0.28574646	-0.37755696
H	-2.40004325	1.60440778	0.60054640
H	-1.29727288	-0.93465281	-0.79813111
C	-3.35527120	-0.62540740	-0.46671495
N	1.01859053	-0.63068539	-0.04621420
C	2.18660380	-1.19712741	-0.70115692
H	2.03766840	-2.27465787	-0.81802231
H	2.30853694	-0.75246648	-1.69194544
H	3.12201530	-1.04489228	-0.13449328
C	0.69015341	-1.33755782	1.19450140
H	1.51364490	-1.28895856	1.92648523
H	-0.20045651	-0.90769147	1.65146365
H	0.49104584	-2.39077606	0.97235777

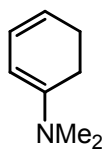


$E_{\text{SCF}} = -367.409783782$ Hartrees

Zero-Point Correction = 0.196307 Hartrees

Single Imaginary Frequency = $-484.8333 \text{ cm}^{-1}$

H	-0.07703787	-2.04602802	0.49796999
C	-2.00490769	-1.07621376	0.45848416
H	-2.59547458	-1.96154838	0.19772828
C	-2.64739265	0.18451893	-0.06494371
H	-1.98348865	-1.03870614	1.56071409
H	-3.72831624	0.23168899	-0.16049044
C	-1.87278590	1.25094326	-0.32712495
H	-2.31872111	2.18609074	-0.65823468
C	-0.42335366	1.21603173	-0.16355898
H	0.11479819	2.15558047	-0.20762708
C	0.23381114	0.03676388	-0.00015646
C	-0.57211555	-1.25385302	-0.07129948
H	-0.61203610	-1.59060657	-1.11885482
N	1.60617333	-0.07160795	0.24074668
C	2.36063289	1.16065057	0.38656195
H	1.87642434	1.80486445	1.12486937
H	3.36703417	0.92175182	0.74169406
H	2.45476286	1.72681154	-0.55617848
C	2.35489939	-1.12752932	-0.43312032
H	3.30377885	-1.28823548	0.08815384
H	1.80199462	-2.06692636	-0.41933513
H	2.58034045	-0.88135507	-1.48468909



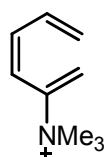
$E_{\text{SCF}} = -367.336344537$ Hartrees

Zero-Point Correction = 0.192052 Hartrees

No Imaginary Frequencies

H	-0.24226758	2.19394221	0.41910523
C	2.47671825	1.02911412	0.36975235
H	2.56442350	1.51739002	-0.58672715
C	2.56189286	-0.35941382	0.42740118
H	2.87956027	1.61625647	1.19473221
H	3.15285915	-0.81903249	1.22060759
C	1.76825073	-1.22170375	-0.34327295
H	2.09042862	-2.25859975	-0.43906571
C	0.46083871	-0.94919854	-0.75683685

H	-0.10216230	-1.79731667	-1.13923503
C	-0.28748538	0.18658639	-0.34057464
C	0.28844010	1.46746266	-0.19511575
H	0.77586961	1.90087378	-1.05428759
N	-1.59404808	-0.01984846	0.09428116
C	-2.07173573	-1.30717722	0.56405179
H	-1.23585856	-1.90882177	0.92323259
H	-2.77177007	-1.15919019	1.39685435
H	-2.60352482	-1.87775776	-0.21458127
C	-2.63160869	0.98422792	-0.06500350
H	-2.99610155	1.36198584	0.90147570
H	-2.24955140	1.82625167	-0.64263073
H	-3.49543339	0.56357127	-0.60185811



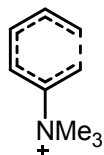
$E_{\text{SCF}} = -407.052725754$ Hartrees

Zero-Point Correction = 0.235120 Hartrees

No Imaginary Frequencies

H	-3.95550387	0.18740901	-0.43182637
C	-2.98172606	0.03377328	0.03127969
C	-2.79638749	-1.05693381	0.78294093
C	-2.03849149	1.14404224	-0.15331862
C	-0.70614862	1.14759351	-0.36764842
H	-2.50525159	2.12874088	-0.13170994
C	0.15849503	-0.02127287	-0.62077745
H	-0.23328204	2.12416546	-0.44543422
C	-0.10041490	-0.99293589	-1.49470900
H	-1.02543640	-0.94101825	-2.05554603
H	0.52872317	-1.85234028	-1.68018794
H	-3.58107987	-1.79642947	0.90093536
H	-1.87479519	-1.23666853	1.32819503
N	1.47518316	-0.01767425	0.15968757
C	2.33466002	1.14156573	-0.30653421
H	1.83922313	2.08041036	-0.07081171
H	3.29135107	1.09320607	0.21441046
H	2.48048959	1.05060022	-1.38241652
C	2.27281096	-1.28305710	-0.02669475
H	3.16276627	-1.21390013	0.59834169
H	1.66892575	-2.13578032	0.27991689
H	2.56675765	-1.37617508	-1.07081579
C	1.18428184	0.13764429	1.63767097
H	0.62247931	-0.73414736	1.97201580
H	2.13227812	0.20484004	2.17209076

H 0.59359700 1.03829085 1.79177475

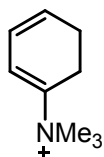


$E_{\text{SCF}} = -407.094139675$ Hartrees

Zero-Point Correction = 0.239169 Hartrees

Single Imaginary Frequency = $-519.5469 \text{ cm}^{-1}$

H	-0.26759936	-2.08243693	0.03664900
C	-2.20201510	-1.15420426	0.26409800
H	-2.79207979	-1.97673545	-0.14961479
C	-2.87860913	0.16871058	0.02130132
H	-2.15693844	-1.32910572	1.35046613
H	-3.96385061	0.20438315	0.01237250
C	-2.15688202	1.29375787	-0.10384834
H	-2.63120462	2.26102689	-0.22840227
C	-0.69699582	1.25785400	-0.00202351
H	-0.19238980	2.20730798	0.12786256
C	-0.03789110	0.08968139	-0.06800211
C	-0.78715600	-1.19909725	-0.34490526
H	-0.86728977	-1.33148464	-1.43420905
N	1.46663368	0.01371533	0.02218775
C	2.12094829	1.37046973	0.10769345
H	1.78175541	1.87774004	1.00926630
H	3.19914341	1.22081588	0.15365831
H	1.86328484	1.94909766	-0.77797313
C	2.01528105	-0.68427064	-1.20708192
H	3.10122298	-0.73440227	-1.12303461
H	1.60381029	-1.68930459	-1.26717215
H	1.72762597	-0.10782185	-2.08598206
C	1.86541078	-0.76517915	1.26168314
H	2.95391732	-0.81461213	1.30832572
H	1.46781262	-0.24631998	2.13305470
H	1.45379810	-1.77048899	1.20593000



$E_{\text{SCF}} = -407.022740787$ Hartrees

Zero-Point Correction = 0.235557 Hartrees

No Imaginary Frequencies

H	-0.10935490	-2.18677702	-0.34393811
C	-2.65110551	-1.09713932	0.22893742
H	-2.81333004	-1.52385720	-0.74669112

C	-2.74808314	0.28030405	0.42024099
H	-2.97523493	-1.74812650	1.04026885
H	-3.36022115	0.62485412	1.25579141
C	-2.00777611	1.28947086	-0.20966595
H	-2.39227742	2.30416396	-0.14109974
C	-0.65478132	1.18366263	-0.56912517
H	-0.13948628	2.12403538	-0.72439372
C	0.05115525	-0.02245817	-0.48461964
C	-0.56522712	-1.25756344	-0.67296910
H	-1.13945014	-1.35281051	-1.57944670
N	1.47149016	-0.01130319	0.08871442
C	2.06462430	1.37454428	0.14718737
H	1.46610112	1.99877900	0.80738061
H	3.07808946	1.28847304	0.53830355
H	2.09220507	1.79514194	-0.85727424
C	2.38870336	-0.85876071	-0.76665203
H	3.39430696	-0.82314382	-0.34580748
H	2.02765256	-1.88418750	-0.77885893
H	2.38337358	-0.45542663	-1.77876640
C	1.43856983	-0.56172462	1.49898546
H	2.45014728	-0.54461612	1.90755976
H	0.77528552	0.06404769	2.09500702
H	1.06528496	-1.58344079	1.47704816

References

- (1) Spangler, C. W.; Jondahl, T. P.; Spangler, B. *J. Org. Chem.* **1973**, *38*, 2478.
- (2) Carpenter, B. K. *Tetrahedron* **1978**, *34*, 1877.
- (3) Marvell, E. N. *Thermal Electrocyclic Reactions*; Academic Press: New York, 1980; Vol. 43.
- (4) Evanseck, J. D.; Thomas, B. E. I.; Spellmeyer, D. C.; Houk, K. N. *J. Org. Chem.* **1995**, *60*, 7134.
- (5) Magomedov, N. A.; Ruggiero, P. L.; Tang, Y. *J. Am. Chem. Soc.* **2004**, *126*, 1624.
- (6) Guner, V. A.; Houk, K. N.; Davies, I. W. *J. Org. Chem.* **2004**, *69*, 8024.
- (7) Greshock, T. J.; Funk, R. L. *J. Am. Chem. Soc.* **2006**, *128*, 4946.
- (8) Yu, T.-Q.; Fu, Y.; Liu, L.; Guo, Q.-X. *J. Org. Chem.* **2006**, *71*, 6157.
- (9) Bishop, L. M.; Barbarow, J. E.; Bergman, R. G.; Trauner, D. *Angew. Chem. Int. Ed.* **2008**, *47*, 8100.
- (10) Frisch, M. J.; Trucks, G. W.; Schlegel, H. B.; Scuseria, G. E.; Robb, M. A.; Cheeseman, J. R.; Montgomery, J., J. A.; Vreven, T.; Kudin, K. N.; Burant, J. C.; Millam, J. M.; Lyengar, S. S.; Tomasi, J.; Barone, V.; Mennucci, B.; Cossi, M.; Scalmani, G.; Rega, N.; Petersson, G. A.; Nakatsuji, H.; Hada, M.; Ehara, M.; Toyota, K.; Fukuda, R.; Hasegawa, J.; Ishida, M.; Nakajima, T.; Honda, Y.; Kitao, O.; Nakai, H.; Klene, M.; Li, X.; Knox, J. E.; Hratchian, H. P.; Cross, J. B.; Bakken, V.; Adamo, C.; Jaramillo, J.; Gomperts, R.; Stratmann, R. E.; Yazyev, O.; Austin, A. J.; Cammi, R.; Pomelli, C.; Ochterski, J. W.; Ayala, P. Y.; Morokuma, K.; Voth, G. A.; Salvador, P.; Dannenberg, J. J.; Zakrzewski,

- V. G.; Dapprich, S.; Daniels, A. D.; Strain, M. C.; Farkas, O.; Malick, D. K.; Rabuck, A. D.; Raghavachari, K.; Foresman, J. B.; Ortiz, J. V.; Cui, Q.; Baboul, A. G.; Clifford, S.; Cioslowski, J.; Stefanov, B. B.; Liu, G.; Liashenko, A.; Piskorz, P.; Komaromi, I.; Martin, R. L.; Fox, D. J.; Keith, T.; Al-Laham, M. A.; Peng, C. Y.; Nanayakkara, A.; Challacombe, M.; Gill, P. M. W.; Johnson, B.; Chen, W.; Wong, M. W.; Gonzalez, C.; Pople, J. A.; Gaussian Inc.: Wallingford, 2004.
- (11) Becke, A. D. *J. Chem. Phys.* **1993**, *98*, 5648.
- (12) Lee, C.; Yang, W.; Parr, R. G. *Phys. Rev. B* **1988**, *37*, 785.
- (13) Vosko, S. H.; Wilk, L.; Nusair, M. *Can. J. Phys.* **1980**, *58*, 1200.
- (14) Stephens, P. J.; Devlin, F. J.; Chabalowski, C. F.; Frisch, M. J. *J. Phys. Chem.* **1994**, *98*, 11623.
- (15) Dill, J. D.; Pople, J. A. *J. Chem. Phys.* **1975**, *62*, 2921.
- (16) Francl, M. M.; Pietro, W. J.; Hehre, W. J.; Binkley, J. S.; Gordon, M. S.; DeFrees, D. J.; Pople, J. A. *J. Chem. Phys.* **1982**, *77*, 3654.
- (17) Ess, D. H.; Houk, K. N. *J. Phys. Chem. A* **2005**, *109*, 9542.
- (18) Mohamadi, F.; Richards, N. G. J.; Guida, W. C.; Liskamp, R.; Caufield, C.; Chang, G.; Hendrickson, T.; Still, W. C. *J. Comput. Chem.* **1990**, *11*, 440.
- (19) Gonzalez, C.; Schlegel, H. B. *J. Chem. Phys.* **1989**, *90*, 2154.
- (20) Gonzalez, C.; Schlegel, H. B. *J. Phys. Chem.* **1990**, *94*, 5523.

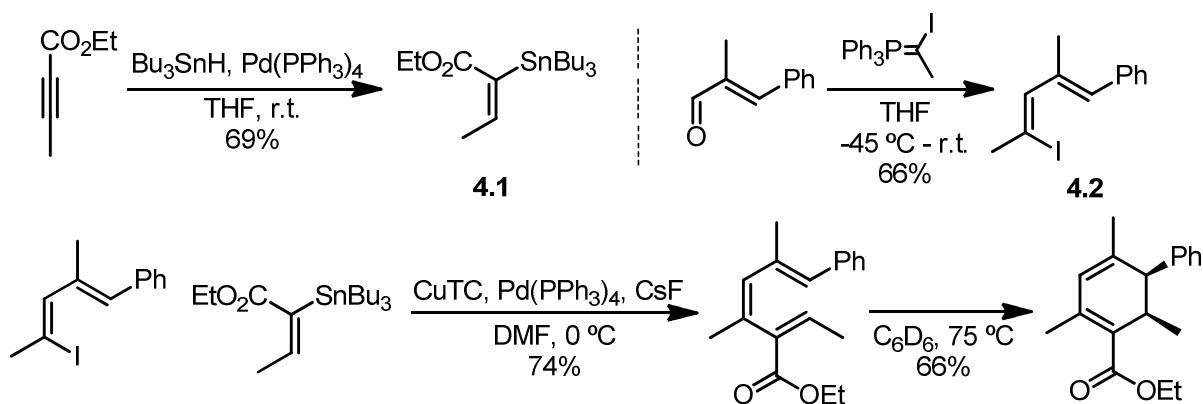
Part 1 - Chapter 4. Model Substrate Synthesis, Catalyst Development, and Mechanistic Analysis of a Catalytic 6π Electrocyclization

Introduction

The calculations performed in Chapter 3 indicate that catalysis of 6π electrocyclizations is possible by binding a Lewis acid to trienes substituted in the 2-position with Lewis basic groups. This chapter describes the synthesis of a model substrate using low-temperature cross coupling conditions, the development of experimental conditions resulting in the first example of catalysis of a 6π electrocyclization, as well as investigations into the mechanism of this catalysis. This work was published in *Angewandte Chemie* in 2008.¹

Results & Discussion

We focused our initial synthetic efforts on 2-carboethoxy-substituted hexatriene system **4.3** (Scheme 1). Triene **4.3** and other similar substrates were first synthesized by Trauner student Dr. Jennifer Barbarow.² Hydrostannylation of ethyl butynoate yielded a 3:1 mixture of α : β stannylated alkenes, from which stannane **4.1** was isolated *via* reverse-phase HPLC. Stork-Zhao olefination furnished (*Z*)-vinyl iodide **4.2**, which was coupled with stannane **4.1** using modified Liebeskind coupling conditions.^{3,4} Among the variety of available olefin cross-coupling methodologies, these are to our knowledge the mildest conditions, and were crucial in cleanly isolating triene **4.3** and all other trienes described in this chapter as well as in Chapter 5.



Scheme 1. Synthesis and thermal cyclization of triene substrate **4.3**. CuTC = copper(I) thiophene-2-carboxylate.

Triene **4.3** cyclizes thermally to *cis*-substituted cyclohexadiene **4.4** (Scheme 1). This reaction proceeds quantitatively (*via* ^1H NMR) with a half-life of four hours at $50\text{ }^\circ\text{C}$. After investigating a variety of Lewis acids (Table 1) we found that dimethylaluminum chloride (Me_2AlCl) proved to be an excellent catalyst for this reaction. The discovery of Me_2AlCl catalysis was first accomplished by Trauner student Dr. Jennifer Barbarow.² The addition of one equivalent of Me_2AlCl results in a significant rate increase, giving a half-life of 21 minutes at $50\text{ }^\circ\text{C}$ (Figure 1). The reaction in the presence of Me_2AlCl yields *cis*-cyclohexadiene **4.4**, indicating that the catalyzed reaction also proceeds *via* the expected thermal disrotatory pathway.^{5,6}

Table 1. Screen for catalysis of the electrocyclization of **4.3** in C₆D₆ in the presence of 2,6-di-*tert*-butyl-4-methylpyridine (0.5 equiv) and Lewis Acid (1 equiv). Tf = trifluoromethanesulfonyl.

Entry	Lewis Acid	Approx t _{1/2} , temperature	Approx. rate acceleration
1	Cu(OTf) ₂	2 h, 50 °C	2
2	Sc(OTf) ₃	2 h, 50 °C	2
3	Me ₃ Al*	40 min, 50 °C	6
4	Me ₂ AlCl*	20 min, 50 °C	13
5	AlBr ₃	Decomposition at r.t.	N/A
6	AlBr ₃ :Me ₃ Al 6:1*	30 min, 35 °C [†]	50
7	BF ₃ ·OEt ₂	2.5 h, 55 °C	None
8	TMSOTf	2.5 h, 55 °C	None
9	MgBr ₂ ·OEt ₂	2 h, 55 °C	1.5
10	TiCl ₄ ·2THF	2 h, 55 °C	1.5
11	Yb(OTf) ₃	2.5 h, 55 °C	None
12	Pr(OTf) ₃	2.5 h, 55 °C	None
13	ZnBr ₂	2.5 h, 55 °C	None

* no 2,6-di-*tert*-butyl-4-methylpyridine added.

[†] slight substrate decomposition observed.

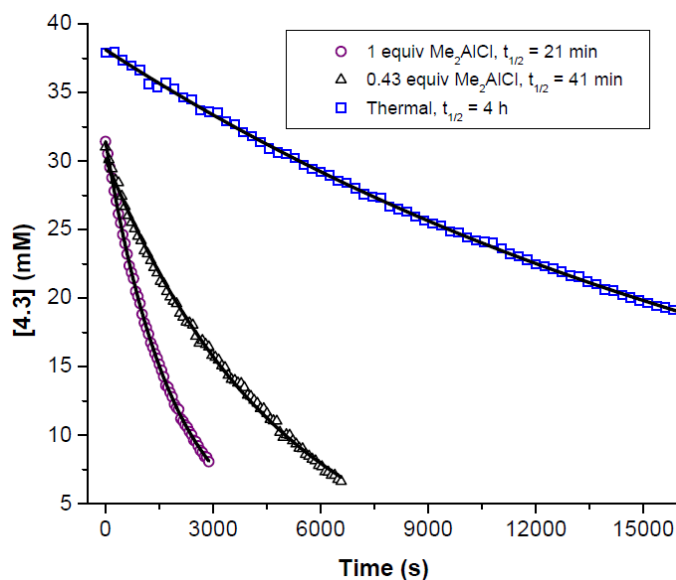


Figure 1. Kinetic plots (with first order exponential decay fits) and half-lives of the electrocyclization of **4.3** at 50 °C in the presence and absence of Me₂AlCl.

A plot of the observed first order rate constant for the electrocyclization of **4.3** in benzene-*d*₆ at constant initial substrate concentration versus varying Me₂AlCl concentration is shown in Figure 2. For reference, the thermal first order rate constant in benzene-*d*₆ at this temperature is 4.75(4) × 10⁻⁵ s⁻¹. The data in Figure 2 provide clear evidence in support of catalytic turnover—the rate of the reaction is increased at catalyst loadings as low as 17 mol% (*k*_{obs} = 1.27(4) × 10⁻⁴ s⁻¹) and all kinetic data fit a first order exponential process. A plot of the logarithm of the rate constant versus the logarithm of Me₂AlCl concentration at sub-stoichiometric catalyst loadings yields a straight line with a slope of 0.88(4), indicating the

reaction is first order in catalyst. Also evident in Figure 2 is the fact that the rate increase begins to level off at approximately one equivalent of catalyst, suggesting tight binding of the catalyst to the triene substrate.

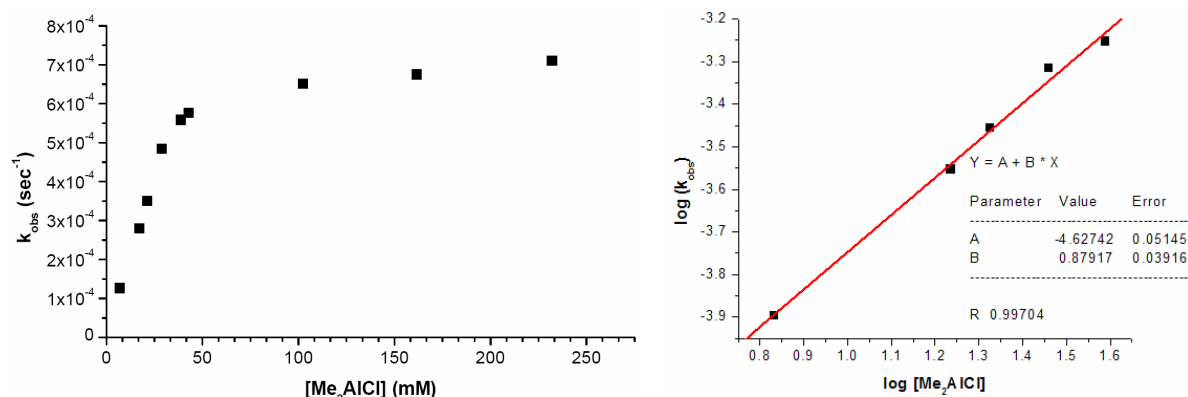


Figure 2. Saturation and kinetic order in Me_2AlCl . Conditions: $[\mathbf{4.3}] = 40 \text{ mM}$ in C_6D_6 at $50 \text{ }^\circ\text{C}$.

The nature of the catalyst-substrate binding was further investigated by conducting a ^1H NMR titration of $\mathbf{4.3}$ with Me_2AlCl at $10 \text{ }^\circ\text{C}$ (Figure 3). A shift in all resonances of the ^1H NMR spectrum of $\mathbf{4.3}$ is observed. This shift levels off at approximately one equivalent of Me_2AlCl for all resonances (Figure 4), which provides further evidence for an energetically favorable 1:1 binding of Me_2AlCl to $\mathbf{4.3}$. The observation of a time-averaged mixture of bound and unbound triene reveals that even though catalyst binding is exothermic, it is rapid and reversible.

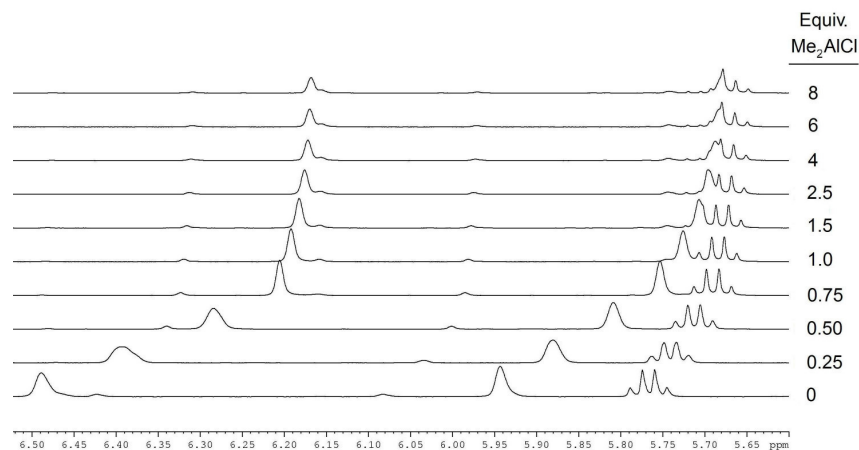


Figure 3. Stacked ^1H NMR spectra of three representative resonances of $\mathbf{4.3}$ versus added equivalents of Me_2AlCl in C_6D_6 at $10 \text{ }^\circ\text{C}$.

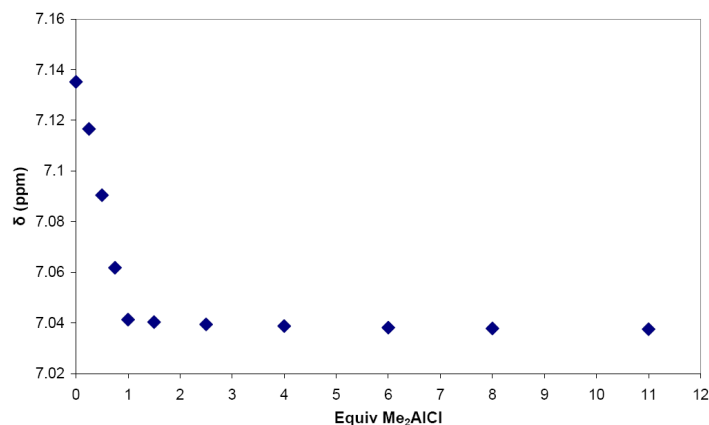


Figure 4. Chemical shift of a representative ¹H NMR resonance of **4.3** versus added equivalents of Me₂AlCl in C₆D₆ at 10 °C.

A substrate-saturation curve was assembled to measure the order in substrate and to extract a rate acceleration and Michaelis constant for the catalyzed reaction (Figure 5). A plot of the logarithm of the initial reaction velocity versus the logarithm of the initial substrate concentration (where [4.3] < [Me₂AlCl]) yields a straight line with a slope of 0.99(3), confirming the reaction is first order in triene **4.3**. The substrate-saturation curve also provides further evidence for the high affinity of Me₂AlCl for **4.3**, as this curve can be fit to the Michaelis-Menten equation to give a Michaelis constant of 38(3) mM. Furthermore, a first order rate constant (k_{cat}) of $6.2(2) \times 10^{-4} \text{ s}^{-1}$ for the electrocyclicization of the Me₂AlCl-bound substrate at 50 °C can be extracted, which is in excellent agreement with the data obtained under catalyst-saturation conditions (Figure 2). This represents a 13-fold rate increase of the catalyzed 6 π electrocyclicization over the thermal reaction (thermal $k_{\text{obs}} = 4.75(4) \times 10^{-5} \text{ s}^{-1}$ at 50 °C).

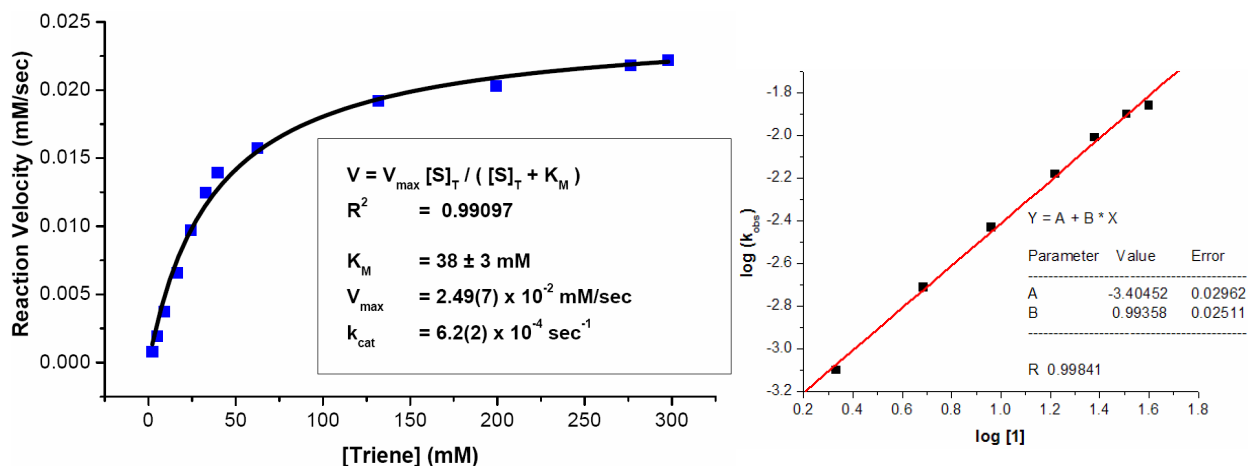


Figure 5. Saturation (with Michaelis-Menten fit) and kinetic order in **4.3**. Conditions: [Me₂AlCl] = 40 mM in C₆D₆ at 50 °C.

An Eyring plot of the rate constant for the thermal reaction reveals activation parameters typical of a carba-6 π electrocyclicization (Figure 6).⁷ The Eyring plot of the catalyzed reaction was assembled under saturation conditions (2 equiv Me₂AlCl) to assure the parameters being measured are those for the electrocyclicization of the catalyst-bound triene, with no effect from the catalyst-binding pre-equilibrium. Under these conditions, a 1.7 kcal/mol decrease in the Gibbs

free energy of activation is measured (Table 2) for the catalyzed electrocyclization relative to that of the thermal reaction. This corresponds to a 2.5 kcal/mol decrease in the enthalpy of activation, and a 0.8 kcal/mol decrease in $T\Delta S^\ddagger$ (298 K), which indicates that the catalysis is primarily enthalpic in nature. Additionally, the data obtained from the Eyring plots can be compared to the data obtained in the substrate-saturation experiments. An 11-fold rate acceleration would be expected at 50 °C based on the measured activation parameters. This is in good agreement with the 13-fold rate acceleration that is measured in the substrate-saturation experiments.

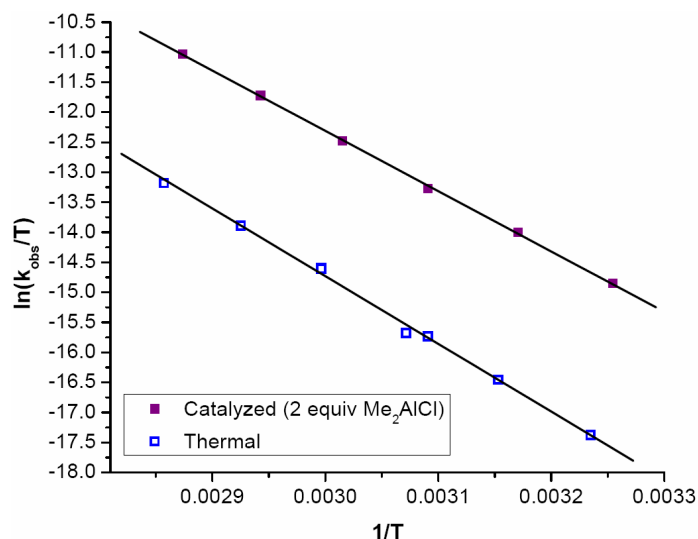


Figure 6. Catalyzed and thermal Eyring plots for the electrocyclization of **4.3** in C₆D₆.

Table 2. Activation parameters of the thermal and catalyzed (2 equiv. Me₂AlCl) electrocyclization of **4.3**. Conditions: [**4.3**] = 40 mM in C₆D₆.

	Thermal	Catalyzed
ΔH^\ddagger (kcal/mol)	22.4(5)	20.0(2)
ΔS^\ddagger (e.u.)	-9.2(4)	-11.8(2)
ΔG^\ddagger_{298} (kcal/mol)	25.2(5)	23.5(2)

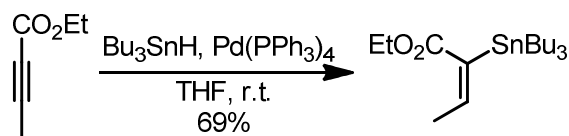
Summary & Conclusion

We have synthesized a 2-carboethoxy-substituted triene substrate and demonstrated the catalysis of its electrocyclization using Me₂AlCl. Based on both the substrate- and catalyst-saturation experiments we can conclude that triene **4.3** forms an energetically favorable complex with Me₂AlCl. This is in agreement with the observations from the NMR titrations. The fact that we do not observe two distinct species in the ¹H NMR spectrum, but instead observe a time-averaged mixture of the bound and unbound triene indicates a rapid equilibrium is present between the two species. This, along with the fact that the reaction is overall first order in catalyst and substrate, leads us to conclude that the catalyzed reaction proceeds through rate-limiting electrocyclization of the catalyst-bound triene.

Experimental

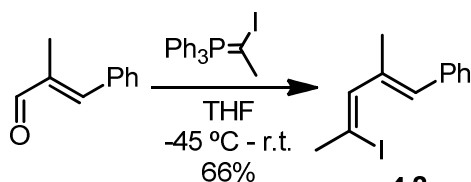
General Information. All reactions and manipulations, unless otherwise noted, were carried out in an inert atmosphere (N_2) glovebox or using standard Schlenk and high vacuum techniques. Sealed NMR tubes were prepared by attaching the NMR tube directly to a Kontes high-vacuum stopcock via a cajon ultra-torr reducing union, then flame-sealing on a vacuum line. All glassware was dried in an oven at 150 °C for at least 12 h prior to use or was flame-dried under reduced pressure. 1H NMR and ^{13}C NMR spectra were recorded on Bruker DRX-500 (500 MHz), AV-500 (500 MHz), AVB-400 (400 MHz), AVQ-400 (400 MHz), and AV-300 (300 MHz) spectrometers as indicated. 1H NMR chemical shifts (δ) are reported in parts per million relative to residual protiated solvent. Data are reported in the following format: (s = singlet, d = doublet, t = triplet, q = quartet, m = multiplet; coupling constant; integration). ^{13}C NMR chemical shifts (δ) are reported in parts per million relative to the carbon resonance of the deuterated solvent. Column chromatography was performed using a Biotage SP1 MPLC purification system and pre-packed silica gel columns. HPLC was performed using an Alltech Econosil C18 10u column (250mm x 22mm). IR spectra were obtained on neat samples on NaCl plates using a ThermoNicolet Avatar 370 FT-IR spectrometer. The temperatures of the kinetics experiments carried out in a circulating oil bath were measured using a calibrated mercury thermometer, and varied ± 0.1 °C. The temperatures of the kinetics and titration experiments carried out in an NMR probe were determined from the 1H NMR chemical shifts of ethylene glycol and MeOH samples, and varied ± 0.1 °C. The values for k_{obs} were determined by fitting the concentration versus time plots to the equation $C_t = C_\infty - (C_\infty - C_0)\exp(-k_{obs}t)$ using the program KaleidaGraph (where C_t , C_∞ , C_0 are the concentration at time t , time infinity, and time zero).⁸ All well-resolved starting material and product 1H NMR resonances were integrated and fit separately; which 1H NMR resonances are well-resolved depends on the Me_2AlCl :Triene ratio (see 1H NMR titrations). However, the vinyl proton resonances of **4.3** and **4.4** were integrated in all cases; the k_{obs} values shown are averages of those individual values. The reported errors in the k_{obs} values are one standard deviation of the k_{obs} values obtained from each integrated resonance.

Materials. Tetrahydrofuran was dried and purified by passage through a column of activated alumina under N_2 pressure followed by sparging with N_2 .⁹ Dry DMF was obtained from EMD and used without further purification. C_6D_6 and $CDCl_3$ were obtained from Cambridge Isotope Labs, Inc. C_6D_6 for use as a reaction solvent was sparged with N_2 and stored over activated 4 Å molecular sieve pellets overnight prior to use. Activated 4 Å molecular sieve pellets were obtained from Sigma-Aldrich and heated at 150 °C under vacuum for 24 h. Hexamethylbenzene was obtained from Sigma-Aldrich and was sublimed prior to use. $Pd(PPh_3)_4$ was obtained from Strem Chemicals; ethyl 2-butynoate was obtained from Fluka; Bu_3SnH , $n-BuLi$, $NaHMDS$, α -methyl-*trans*-cinnamaldehyde, $Cu(OTf)_2$, $Sc(OTf)_3$, Me_3Al , Me_2AlCl , $AlBr_3$, $BF_3 \cdot OEt_2$, $TMSOTf$, $MgBr_2 \cdot OEt_2$, $TiCl_4 \cdot 2THF$, $Yb(OTf)_3$, $Pr(OTf)_3$, and $ZnBr_2$ were obtained from Sigma-Aldrich; CsF was obtained from Acros Organics; I_2 was obtained from Fisher Scientific; these reagents were used without further purification. (Ethyl)triphenylphosphonium iodide^{10,11} and copper(I) thiophene-2-carboxylate³ were synthesized according to literature procedures. Characterization data for these compounds agree with literature values.



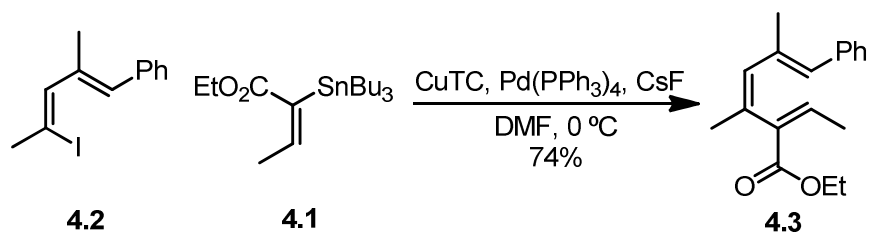
4.1

Synthesis of ethyl 2-tributylstannyl-2-butenate 4.1. A round bottom flask was charged with Pd(PPh₃)₄ (17 mg, 0.015 mmol), THF (10 mL), and ethyl 2-butynoate (0.10 mL, 0.86 mmol). To this solution was added Bu₃SnH (1 mL, 0.86 M in THF, 0.86 mmol) dropwise over 2 h at room temperature. The reaction mixture was stirred for an additional 1 h, concentrated *in vacuo*, and purified by silica gel chromatography (2-4% EtOAc in hexanes) to yield a 3:1 mixture of α:β stannylated isomers. These isomers were separated by reverse-phase HPLC (96:4 MeCN:H₂O) to yield 239 mg product as a clear oil (69%). ¹H NMR (CDCl₃, 300 MHz): δ 6.17 (q, *J*_{H-H} = 6.1 Hz, *J*_{Sn-H} = 31 Hz, 1H), 4.15 (q, *J* = 7.1 Hz, 2H), 2.00 (d, *J* = 6.9 Hz, 3H) 1.55-1.40 (m, 6H), 1.38-1.20 (m, 12H), 0.98-0.80 (m, 12H) ppm; ¹³C NMR (CDCl₃, 100 MHz): δ 171.4, 148.2, 137.1, 60.1, 29.1 (*J*_{Sn-C} = 9.8 Hz), 27.5 (*J*_{Sn-C} = 29 Hz), 18.4 (*J*_{Sn-C} = 22 Hz), 14.6, 13.9, 10.4 (*J*_{Sn-C} = 170 Hz) ppm; IR 2957, 2926, 2872, 2853, 1708, 1608, 1464, 1183, 1035 cm⁻¹; HRMS (EI⁺) Exact mass calcd for C₁₈H₃₅O₂Sn [M-H]⁺: 403.1659, found 403.1660.

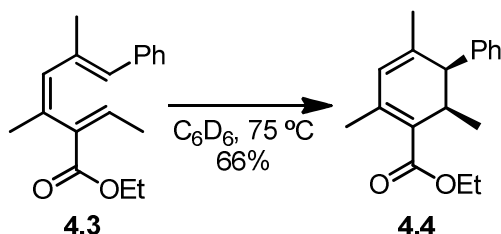


4.2

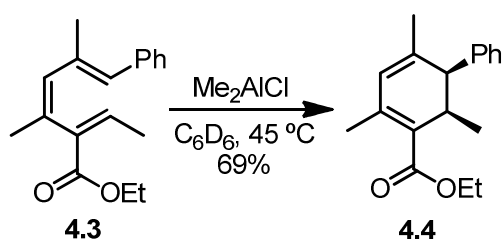
Synthesis of 2-iodo-4-methyl-5-phenyl-2,4-pentadiene 4.2. Synthesized according to the procedure developed by Zhao et. al.¹² To a Schlenk flask charged with ethyl(triphenyl)phosphonium iodide (1.5 g, 3.6 mmol) and THF (10 mL) was added *n*-BuLi (2.25 mL, 1.6 M in hexanes, 3.6 mmol) at room temperature. The resulting suspension was stirred for 5 min, during which the reaction mixture became a red, homogeneous solution. This solution was slowly cannulated into a round bottom flask charged with iodine (0.91 g, 3.6 mmol) and THF (30 mL) at -78 °C, resulting in an orange suspension. The temperature of this suspension was raised to -45 °C and NaHMDS (5.60 mL, 0.6 M in toluene, 3.4 mmol) was added dropwise over 5 min. The resulting suspension was stirred for 5 min, during which the reaction mixture again became a red, homogeneous solution. To this solution was added α-methyl-*trans*-cinnamaldehyde (0.25 mL, 1.8 mmol) dropwise. The reaction mixture was allowed to warm to room temperature over 20 min. Hexanes (100 mL) was added, and the reaction mixture was filtered through a plug of Celite, concentrated *in vacuo*, and purified by silica gel chromatography (0-2% EtOAc in hexanes), yielding 334 mg product as a yellow oil (66%). ¹H NMR (CDCl₃, 500 MHz): δ 7.42-7.31 (m, 4H), 7.28 (t, *J* = 7.2 Hz, 1H), 6.61 (s, 1H), 6.20 (s, 1H), 2.67 (s, 3H), 2.07 (s, 3H) ppm; ¹³C NMR (125 MHz, CDCl₃): δ 138.6, 137.5, 136.3, 131.3, 129.2, 128.3, 126.9, 98.0, 35.4, 18.0 ppm; HRMS (EI⁺) Exact mass calcd for C₁₂H₁₃I [M]⁺: 284.0062, found 284.0062.



Synthesis of triene 4.3. A Schlenk flask was charged with ethyl 2-tributylstannyl-2-butenolate **4.1** (775 mg, 1.9 mmol), 2-iodo-4-methyl-5-phenyl-2,4-pentadiene **4.2** (600 mg, 2.1 mmol), DMF (22 mL), and Pd(PPh₃)₄ (111 mg, 0.1 mmol). This solution was cooled to 0 °C and copper(I) thiophene-2-carboxylate (403 mg, 2.1 mmol) was added. The reaction mixture was stirred for 10 min, after which CsF (583 mg, 3.8 mmol) was added. After a further 50 min of stirring, the reaction mixture was diluted with Et₂O and the organic phase was washed three times with 10% aqueous KF and once with brine. The organic solution was then dried over MgSO₄, filtered, concentrated *in vacuo*, and purified by silica gel chromatography (4-5% EtOAc in hexanes). The resulting orange oil was further purified by reverse-phase HPLC (67:33 MeCN:H₂O) yielding 384 mg product as a clear oil (74%). ¹H NMR (400 MHz, C₆D₆): δ 7.26 (d, *J* = 8.0 Hz, 2H), 7.18-7.10 (m, 2H), 7.01 (t, *J* = 7.2 Hz, 1H), 6.54 (s, 1H), 5.99 (s, 1H), 5.80 (q, *J* = 7.2 Hz, 2H), 3.94 (q, *J* = 7.1 Hz, 2H), 1.98-1.85 (m, 9H), 0.88 (t, *J* = 7.1 Hz, 3H) ppm; ¹³C NMR (100 MHz, C₆D₆): δ 167.1, 138.8, 137.4, 136.3, 136.2, 135.1, 133.9, 131.5, 129.9, 128.7, 127.0, 60.5, 26.2, 18.7, 15.9, 14.5 ppm; IR 3021, 2977, 2922, 1715, 1444, 1243, 1222, 1184, 1031, 748, 700 cm⁻¹; HRMS (FAB⁺) Exact mass calcd for C₁₈H₂₂O₂ [M]⁺: 270.1620, found 270.1625.



Thermal synthesis of cyclohexadiene 4.4. A solution of triene **4.3** (0.84 mL, 40 mM in benzene-*d*₆, 0.034 mmol; containing 5 mol% hexamethylbenzene as an internal standard) was heated in a sealed NMR tube at 75 °C for 4 h. The reaction mixture was concentrated *in vacuo* and purified by silica gel chromatography (4-5% EtOAc in hexanes) yielding 6 mg product (66%). Quantitative conversion was observed by ¹H NMR. ¹H NMR (400 MHz, C₆D₆): δ 7.20-7.00 (m, 5H), 5.70 (s, 1H), 4.06 (m, 2H), 3.38 (d, *J* = 7.6 Hz, 1H), 3.17 (quintet, *J* = 7.0 Hz, 1H), 2.36 (s, 3H), 1.55 (s, 3H), 1.06 (d, *J* = 7.0 Hz, 3H), 0.98 (t, *J* = 7.2 Hz, 3H) ppm; ¹³C NMR (100 MHz, C₆D₆): δ 168.4, 143.2, 140.0, 139.9, 130.8, 129.8, 128.0, 127.3, 127.0, 60.1, 52.4, 36.2, 22.5, 21.0, 14.8, 14.0 ppm; IR 3028, 2967, 2934, 1701, 1575, 1444, 1366, 1259, 1222, 1071, 1048, 786, 707 cm⁻¹; HRMS (FAB⁺) Exact mass calcd for C₁₈H₂₂O₂ [M]⁺: 270.1620, found 270.1620.



Catalyzed synthesis of cyclohexadiene 4.4. A solution of triene **4.3** (400 μL , 48 mM in benzene- d_6 , 0.019 mmol; containing 5 mol% hexamethylbenzene as an internal standard) was combined in an NMR tube with benzene- d_6 (10 μL) and a solution of Me_2AlCl (70 μL , 240 mM in benzene- d_6 , 0.017 mmol). The NMR tube was sealed and heated at 45 $^\circ\text{C}$ for 5 h. The reaction mixture was quenched with water and extracted three times with dichloromethane. The organic solution was then dried over MgSO_4 , filtered, concentrated *in vacuo*, and purified by silica gel chromatography (4-5% EtOAc in hexanes) yielding 3.6 mg product (69%). Quantitative conversion was observed by ^1H NMR. Spectral data were identical to those listed above.

Screen for catalysis of the electrocyclic cyclization of triene 4.3—representative procedure. An NMR tube was charged with 2,6-di-*tert*-butyl-4-methylpyridine (2 mg, 0.0097 mmol), Lewis acid (0.0192 mmol), benzene- d_6 (80 μL), and triene **4.3** (400 μL , 48 mM in benzene- d_6 , 0.0192 mmol; containing 5 mol% hexamethylbenzene as an internal standard). The NMR tube was then sealed under vacuum and the reaction was monitored at regular intervals *via* ^1H NMR. The reaction mixture was kept at room temperature initially, and heated in a circulating oil bath at increasing temperatures until significant conversion was observed.

Saturation and kinetic order in Me_2AlCl for triene 4.3. A solution of triene **4.3** (400 μL , 48 mM in benzene- d_6 , 0.0192 mmol; containing 5 mol% hexamethylbenzene as an internal standard) was combined in a J-Young NMR tube with varying amounts of a solution of Me_2AlCl in benzene- d_6 . Benzene- d_6 was then added such that the total volume of the solution in the tube was 480 μL . A 240 mM Me_2AlCl solution was used for the kinetic runs with the four lowest Me_2AlCl concentrations, and a 1.44 M Me_2AlCl solution was used for the remaining runs. The J-Young tube was then sealed and the reaction mixture was frozen in ice-water until ready for kinetic analysis. Once ready for analysis, the solution was thawed and agitated, the tube was placed in an AV-500 NMR probe pre-equilibrated to 50.4 $^\circ\text{C}$, and the reaction was monitored for disappearance of **4.3** and appearance of **4.4** (*via* single scan ^1H NMR spectroscopy). The concentration of Me_2AlCl was determined by integration against the internal standard. The first order rate constants and Me_2AlCl concentrations can be found in Table 3.

Table 3. First order rate constants of the electrocyclic cyclization of **4.3** in the presence of varying concentrations of Me_2AlCl .

Entry	$[\text{Me}_2\text{AlCl}]$ (mM)	k_{obs} (s^{-1})
1	6.80	$1.27(4)\times 10^{-4}$
2	17.2	$2.8(1)\times 10^{-4}$
3	21.2	$3.51(5)\times 10^{-4}$
4	28.8	$4.8(2)\times 10^{-4}$
5	38.8	$5.6(1)\times 10^{-4}$
6	42.8	$5.77(4)\times 10^{-4}$

7	102	$6.5(1)\times 10^{-4}$
8	162	$6.8(3)\times 10^{-4}$
9	232	$7(1)\times 10^{-4}$

Saturation and kinetic order in 4.3. A solution of Me_2AlCl (80 μL , 240 mM in benzene- d_6 , 0.0192 mmol) was combined in a J-Young NMR tube with varying amounts of a solution of **4.3** in benzene- d_6 (containing 5 mol% hexamethylbenzene as an internal standard). Benzene- d_6 was then added such that the total volume of the solution in the tube was 480 μL . A 48 mM solution of **4.3** was used for the kinetic runs with the seven lowest concentrations of **4.3**, and a 384 mM solution of **4.3** was used for the remainder. The J-Young tube was then sealed, the solution was agitated, the tube was placed in an AV-500 NMR probe pre-equilibrated to 50.4 $^\circ\text{C}$, and the reaction was monitored for disappearance of **4.3** and appearance of **4.4** (via single scan ^1H NMR spectroscopy). The concentration of **4.3** was determined by integration against Me_2AlCl and the internal standard. The portion of the concentration versus time plots exhibiting zero order dependence on substrate was fit to a line via the least-squares method. The slope of this line was taken as the initial velocity of the reaction. These, as well as the concentrations of **4.3**, can be found in Table 4.

Table 4. The initial reaction rate versus at varying initial concentrations of **4.3**. Conditions: $[\text{Me}_2\text{AlCl}] = 40 \text{ mM}$ in C_6D_6 at 50 $^\circ\text{C}$.

Entry	$[\mathbf{4.3}]_{\text{initial}}$ (mM)	V_{init} (mM/s)
1	2.16	8.01×10^{-4}
2	4.85	1.95×10^{-3}
3	9.15	3.73×10^{-3}
4	16.5	6.58×10^{-3}
5	24.2	9.72×10^{-3}
6	32.6	1.24×10^{-2}
7	39.7	1.40×10^{-2}
8	62.4	1.58×10^{-2}
9	132	1.92×10^{-2}
10	199	2.03×10^{-2}
11	276	2.18×10^{-2}
12	298	2.22×10^{-2}

Activation parameter measurements for the thermal cyclization of 4.3. A solution of **4.3** (500 μL , 48 mM in benzene- d_6 , 0.0240 mmol; containing 5 mol% hexamethylbenzene as an internal standard) and benzene- d_6 (100 μL) were combined in a standard or J-Young NMR tube. Kinetic analyses of the reactions monitored at 36.0 and 44.0 $^\circ\text{C}$ were carried out in the following fashion. The NMR tube was sealed under vacuum and completely submerged in a circulating oil bath equilibrated to the desired temperature; the tube was removed from the oil bath and cooled rapidly to room temperature under a stream of hexanes; the reaction was monitored for disappearance of **4.3** and appearance of **4.4** (via single scan ^1H NMR spectroscopy using an AVB-400 spectrometer) and the tube was replaced in the oil bath. Only time spent in the oil bath was included in the concentration versus time plots. Kinetic analyses of the reactions monitored at 50.4 and 52.4 $^\circ\text{C}$ were carried out in the following fashion: the NMR tube was sealed under vacuum and placed in an AV-500 NMR probe pre-equilibrated to the desired temperature, and

the reaction was monitored for disappearance of **4.3** and appearance of **4.4** (*via* single scan ^1H NMR spectroscopy). Kinetic analyses of the reactions monitored at 60.6, 68.7, and 76.8 °C were carried out in the following fashion: the J-Young NMR tube was sealed and placed in an AV-500 NMR probe pre-equilibrated to the desired temperature, and the reaction was monitored for disappearance of **4.3** and appearance of **4.4** (*via* single scan ^1H NMR spectroscopy). The first order rate constants and Eyring plot can be found in Table 5 and Figure 7, respectively.

Table 5. First order rate constants of the thermal electrocyclization of **4.3** at various temperatures.

Entry	Temperature (°C)	k_{obs} (s^{-1})
1	36.0	$8.8(1)\times 10^{-6}$
2	44.0	$2.26(6)\times 10^{-5}$
3	50.4	$4.75(4)\times 10^{-5}$
4	52.4	$5.05(5)\times 10^{-5}$
5	60.6	$1.54(1)\times 10^{-4}$
6	60.6	$1.51(1)\times 10^{-4}$
7	68.7	$3.17(5)\times 10^{-4}$
8	76.8	$6.61(2)\times 10^{-4}$

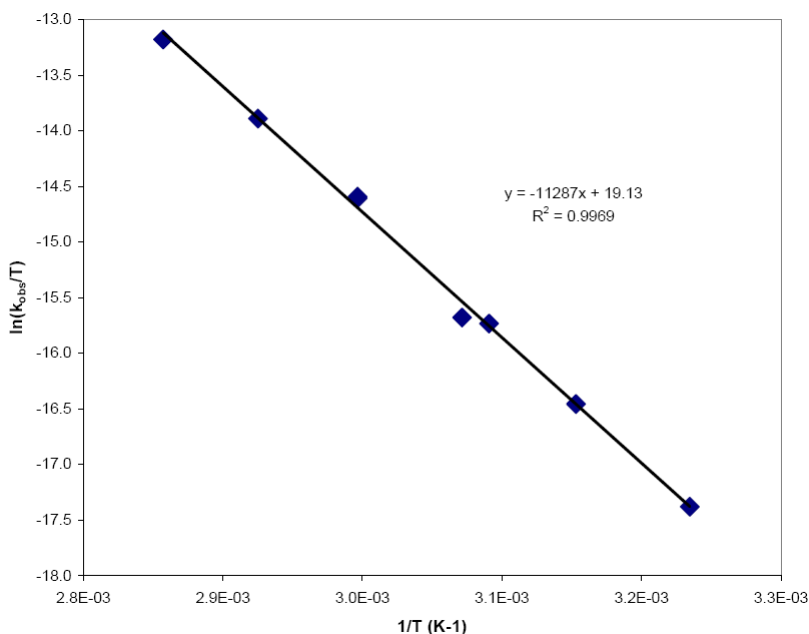


Figure 7. Eyring plot for the thermal electrocyclization of **4.3** in benzene- d_6 .

Activation parameter measurements for the catalyzed cyclization of 4.3. A solution of **4.3** (400 μL , 48 mM in benzene- d_6 , 0.0192 mmol; containing 5 mol% hexamethylbenzene as an internal standard) was combined in a J-Young NMR tube with a solution of Me_2AlCl (80 μL , 480 mM in benzene- d_6 , 0.0384 mmol). The J-Young tube was then sealed, the solution was agitated, the tube was placed in an AV-500 NMR probe pre-equilibrated to the desired temperature, and the reaction was monitored for disappearance of **4.3** and appearance of **4.4** (*via* single scan ^1H NMR spectroscopy). The concentration of Me_2AlCl was determined to be 80(2) mM in all experiments by integration against the internal standard. The NMR probe for the

above experiments was calibrated to 34.1, 42.3, 50.4, 58.5, 66.7, and 74.8 °C. The first order rate constants and the Eyring plot for these experiments are displayed in Table 6 and Figure 8, respectively.

Table 6. First order rate constants of the catalyzed electrocyclization of **4.3** at various temperatures.

Entry	Temperature (°C)	k_{obs} (s ⁻¹)
1	34.1	1.09(9)x10 ⁻⁴
2	42.3	2.6(1)x10 ⁻⁴
3	50.4	5.59(6)x10 ⁻⁴
4	58.5	1.27(1)x10 ⁻³
5	66.7	2.76(4)x10 ⁻³
6	74.8	5.6(4)x10 ⁻³

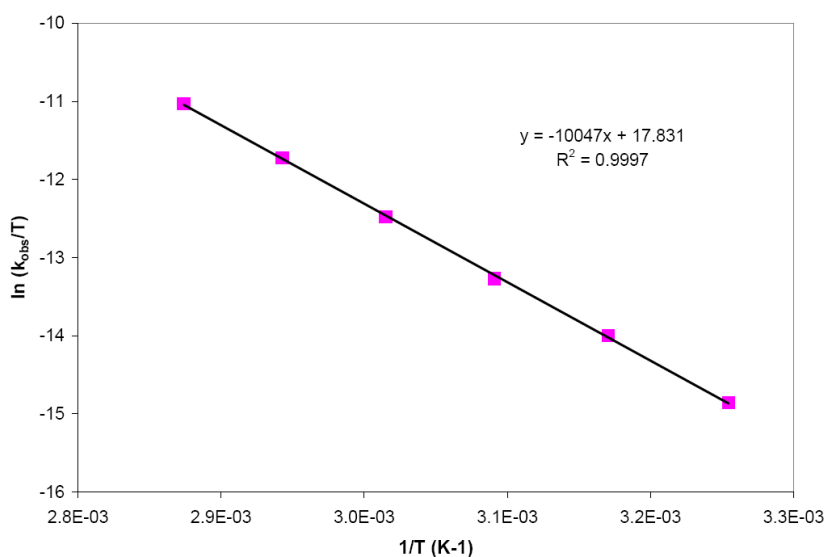


Figure 8. Eyring plot for the catalyzed electrocyclization of **4.3** in benzene-*d*₆.

Titration of 4.3 with Me₂AlCl. A solution of **4.3** (500 μL, 48 mM in benzene-*d*₆, 0.0240 mmol; containing 5 mol% hexamethylbenzene as an internal standard) was added to an NMR tube, which was subsequently sealed with a rubber septum. The NMR tube was placed in an AV-500 NMR spectrometer pre-equilibrated to 9.7 °C and the shift of the ¹H NMR spectrum of **4.3** was monitored as a function of added Me₂AlCl (240 mM in benzene-*d*₆). The Me₂AlCl solution was added by ejecting the sample from the NMR probe, injecting the solution through the septum, agitating the sample, and replacing it in the NMR probe. The concentration of Me₂AlCl was determined by integration against the internal standard. Stacked NMR spectra of three representative resonances are shown in Figure 3, and the graphical representations of the change in chemical shift of two representative resonances are shown in Figures 4 and 9.

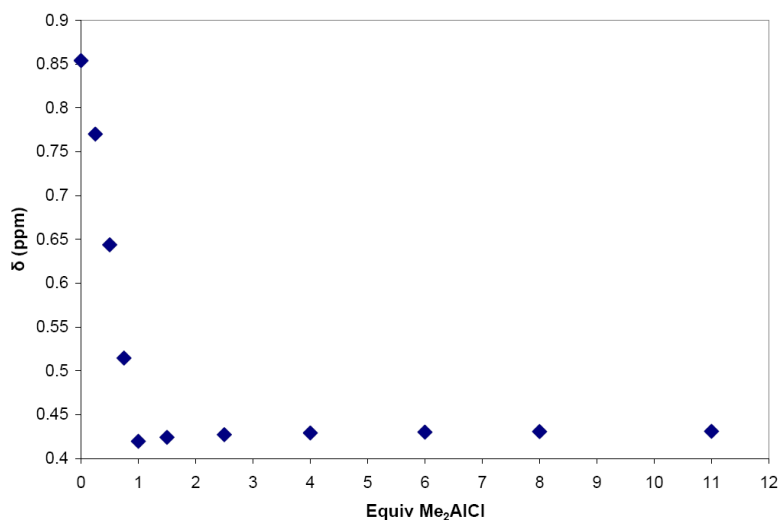


Figure 9. Chemical shift of a representative resonance of **4.3** versus added equivalents of Me₂AlCl in benzene-*d*₆ at 10 °C.

References

- (1) Bishop, L. M.; Barbarow, J. E.; Bergman, R. G.; Trauner, D. *Angew. Chem. Int. Ed.* **2008**, *47*, 8100.
- (2) Barbarow, J. E., The University of California, 2007.
- (3) Allred, G. D.; Liebeskind, L. S. *J. Am. Chem. Soc.* **1996**, *118*, 2748.
- (4) Fürstner, A.; Nevado, C.; Tremblay, M.; Chevrier, C.; Teplý, F.; Aïssa, C.; Waser, M. *Angew. Chem. Int. Ed.* **2006**, *45*, 5837.
- (5) Woodward, R. B.; Hoffmann, R. *J. Am. Chem. Soc.* **1965**, *87*, 395.
- (6) Woodward, R. B.; Hoffmann, R. *The Conservation of Orbital Symmetry*; Verlag Chemie: Weinheim, 1970.
- (7) Marvell, E. N. *Thermal Electrocyclic Reactions*; Academic Press: New York, 1980; Vol. 43.
- (8) Synergy Software: Reading, PA, 2003.
- (9) Alaimo, P. J.; Peters, D. W.; Arnold, J.; Bergman, R. G. *J. Chem. Ed.* **2001**, *78*, 64.
- (10) Roubelakis, M. M.; Vougioukalakis, G. C.; Angelis, Y. S.; Orfanopoulos, M. *Org. Lett.* **2006**, *8*, 39.
- (11) Appel, M.; Blaurock, S.; Berger, S. *Eur. J. Org. Chem.* **2002**, 1143.
- (12) Chen, J.; Wang, T.; Zhao, K. *Tetrahedron Lett.* **1994**, *35*, 2827.

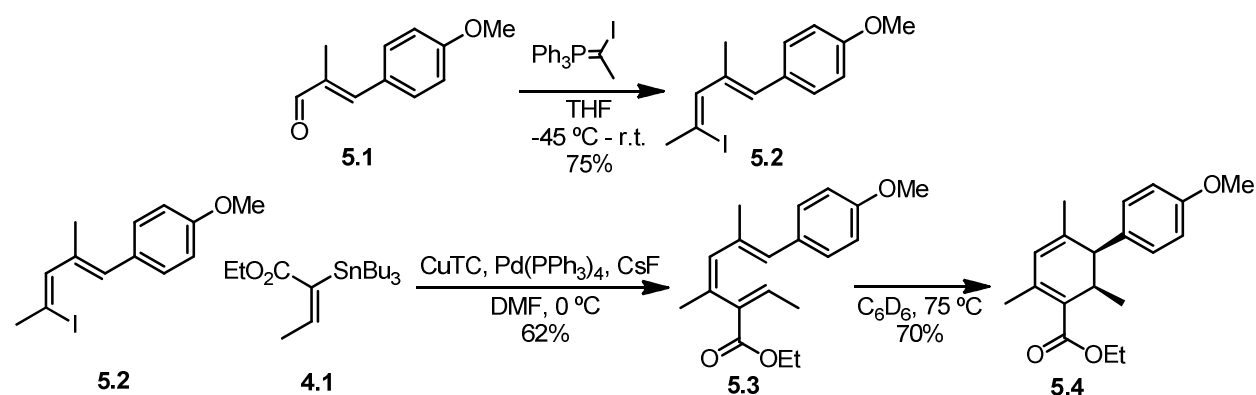
Part 1 - Chapter 5. Investigations into the Substrate Scope of Catalytic Carba-6 π Electrocyclizations

Introduction

Having established that catalysis of a carba-6 π electrocyclization was possible through binding of a Lewis acid to a Lewis basic ester moiety in the 2-position of a triene substrate, our next goal was to expand the substrate scope of this methodology. The first challenge to be overcome is the clean isolation of triene substrates—the main obstacle being the triene undergoing undesired reactions during isolation, including thermal electrocyclization. However, while substrates undergoing facile thermal electrocyclization may hamper efforts to showcase catalysis, they do highlight the powerful synthetic strategy of six-membered ring synthesis *via* facile thermal electrocyclization of trienes containing electron-withdrawing groups in the 2-position. Our substrate-scope explorations outlined in this chapter have included varying the substitution pattern around the triene as well as using different Lewis basic groups as catalyst docking sites. Parts of this work were published in *Angewandte Chemie* in 2008.¹

Results & Discussion

We began our investigation of the substrate scope of this reaction by synthesizing the *para*-methoxyphenyl analog of triene substrate **4.3** (Scheme 1). The synthesis and thermal cyclization of **5.3** proceeded in a fashion analogous to those of **4.3**. Furthermore, it was found that the rate of the electrocyclization of **5.3** increased in the presence of Me₂AlCl. Eyring analysis of the thermal and catalyzed reactions gave activation parameters similar to those for triene **4.3** (Figure 1 and Table 1).



Scheme 1. Synthesis and thermal electrocyclization of triene substrate **5.3**. CuTC = copper(I) thiophene-2-carboxylate.

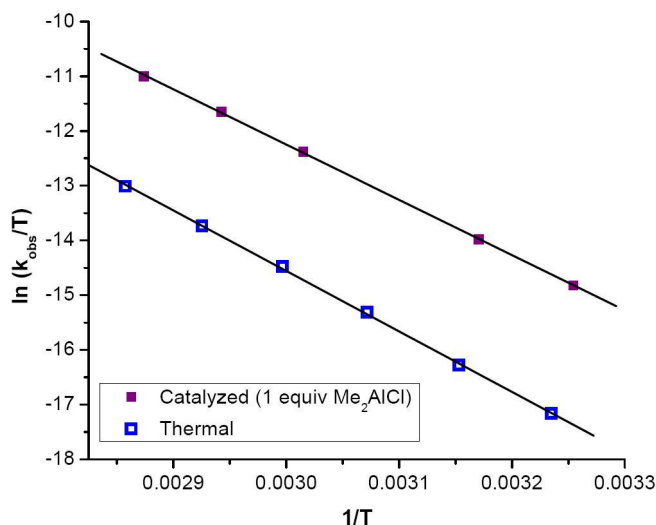


Figure 1. Eyring plots for the catalyzed and thermal cyclization of **5.3** in C_6D_6 .

Table 1. Activation parameters of the thermal and catalyzed (1 equiv Me_2AlCl) electrocyclization of **5.3**. Conditions: $[5.3] = 40$ mM in C_6D_6 .

	Thermal	Catalyzed
ΔH^\ddagger (kcal/mol)	22.0(2)	20.1(1)
ΔS^\ddagger (e.u.)	-10.3(2)	-11.4(1)
ΔG^\ddagger_{298} (kcal/mol)	25.0(2)	23.5(2)

A plot of the logarithm of the rate constant versus the logarithm of Me_2AlCl concentration at sub-stoichiometric catalyst loadings yielded a straight line with a slope of 0.71 (3), indicating the reaction is first order in catalyst (Figure 2). The reaction rate began to decrease with super-stoichiometric catalyst loadings, as opposed to the gradual taper observed in the catalyst saturation experiments using triene **4.3** (Chapter 4, Figure 2).

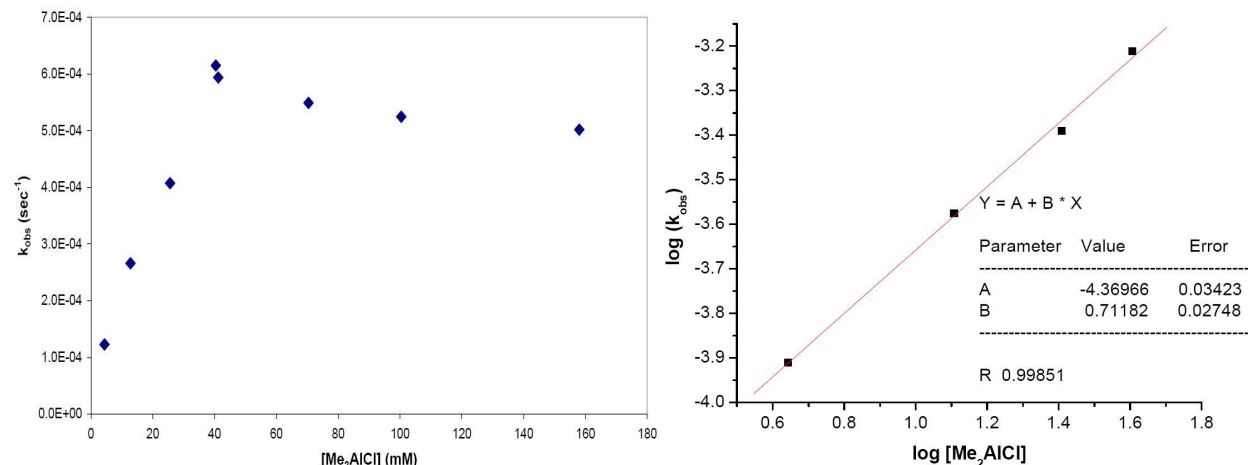


Figure 2. Saturation and kinetic order in Me_2AlCl . Conditions: $[5.3] = 40$ mM in C_6D_6 at $50^\circ C$.

A 1H NMR titration of triene **5.3** with Me_2AlCl revealed a possible mechanism for this reaction rate decrease at super-stoichiometric catalyst loadings (Figure 3). As in the titration of triene **4.3**, the 1H NMR resonances of **5.3** gradually shift in the presence of varying sub-

stoichiometric amounts of Me_2AlCl . However, the methyl resonance of the aryl methyl ether shifts dramatically from 1-2 equivalents Me_2AlCl . These experiments indicate that once the Me_2AlCl binds to the ester groups of all the triene molecules, Me_2AlCl begins to bind to the less Lewis basic sp^3 -hybridized oxygen atoms. The triene substrate bound to two catalyst molecules evidently undergoes electrocyclization more slowly, as indicated by the decrease in the rate constant of the reaction at super-stoichiometric catalyst loadings.

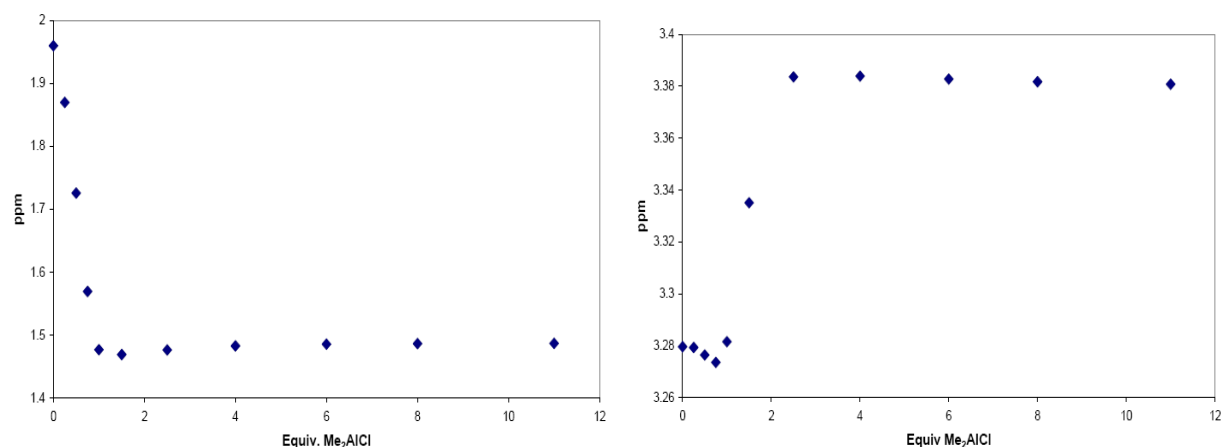
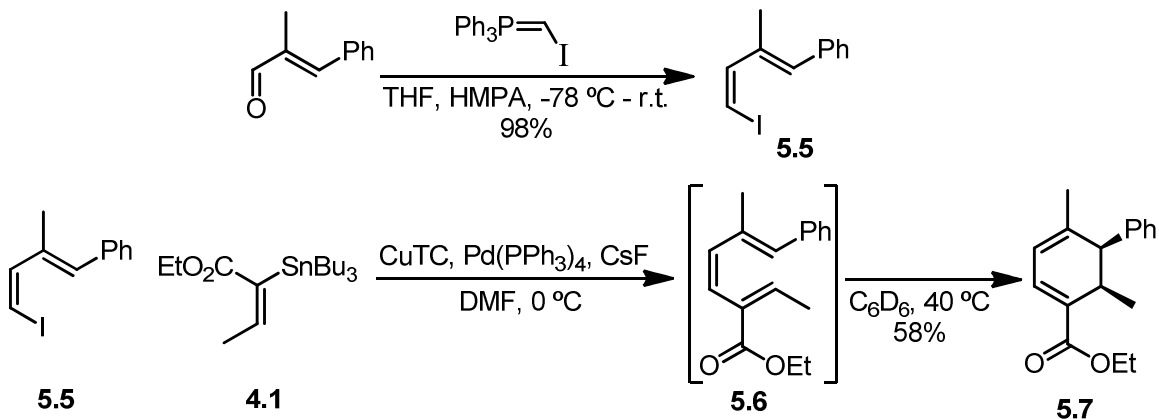


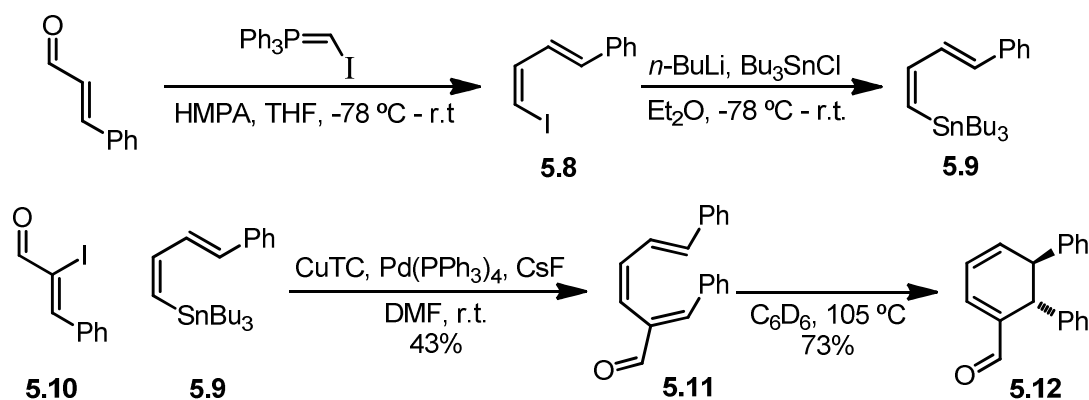
Figure 3. Chemical shifts of two representative ^1H NMR resonances of **5.3** versus number of added equivalents of Me_2AlCl in C_6D_6 at 10°C .

Our ability to cleanly isolate triene substrates is dictated in large part by their thermal electrocyclization rate. Triene **5.6** provides our first example of facile thermal electrocyclization prohibiting substrate isolation (Scheme 2). Stork-Zhao olefination of α -methyl-cinnamaldehyde gave vinyl iodide **5.5**, which was coupled with stannane **4.1** yielding triene **5.6**. The crude reaction mixture contained a mixture of triene **5.6** and cyclohexadiene **5.7**, the latter of which could be isolated cleanly after gentle heating. Triene substrate **5.6** could not be isolated with any less than 50% cyclohexadiene **5.7**. The increased thermal electrocyclization rate of **5.6** as compared to that of structurally related triene **4.3** is puzzling.



Scheme 2. Synthesis of cyclohexadiene **5.7** via triene intermediate **5.6**. CuTC = copper(I) thiophene-2-carboxylate.

We began our exploration of substrates possessing non-ester Lewis-basic groups by focusing on trienes with a formyl group at the 2-position. Our interest in aldehydes stemmed partially from our desire to explore the possibility of an aminocatalytic electrocyclization.² Accordingly, Stork-Zhao olefination of cinnamaldehyde gave vinyl iodide **5.8**, which was contaminated with triphenylphosphine oxide. Further purification of **5.8** *via* precipitation from hexanes was unsuccessful and *via* chromatography led to isomerization products. Impure **5.8** was treated with *n*-BuLi, and the resultant anion was quenched with tributyltin chloride yielding vinyl stannane **5.9** contaminated with 5-10% protodestannylated 1-phenyl-1,3-butadiene. Tin impurities were removed from the crude reaction mixture by basic alumina chromatography, after which stannane **5.9** was coupled with α -iodo-aldehyde **5.10**^{3,4} to give formyl triene **5.11** (Scheme 3). Significantly higher temperatures were required to affect the thermal electrocyclization of **5.11** than those employed for trienes **4.3**, **5.3**, and **5.6**. This is presumably due in part to the bulky phenyl ring beta to the formyl group, which during the electrocyclization transition state undergoes a steric clash with the vinyl proton on the opposite reacting terminus.⁵



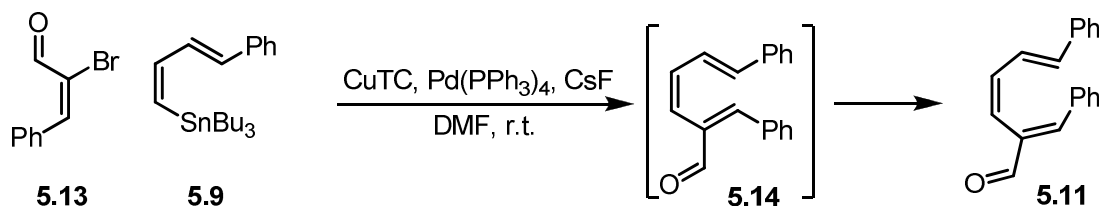
Scheme 3. Synthesis and thermal cyclization of triene **5.11**. CuTC = copper(I) thiophene-2-carboxylate.

Table 2. First order observed rate constants for the electrocyclization of **5.11** in various solvents at 100 °C.

Solvent	k_{obs} (sec^{-1})
CD_2Cl_2	$2.9(2) \times 10^{-5}$
CD_3NO_2	$3.0(1) \times 10^{-5}$
CD_3OD	$3.1(1) \times 10^{-5}$
Acetone- d_6	$2.9(1) \times 10^{-5}$

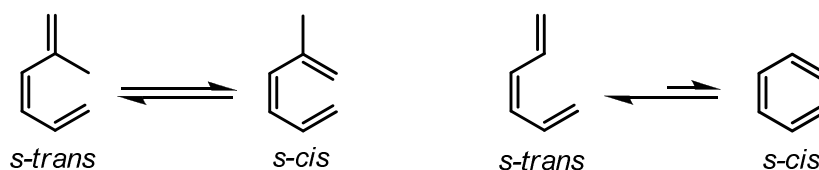
Submitting triene **5.11** to Me_2AlCl , as well as to other Lewis acids such as $\text{Sc}(\text{OTf})_3$ and $\text{Cu}(\text{OTf})_2$, resulted in substrate decomposition. Treatment of **5.11** with a variety of primary and secondary amines as well as Brønsted acids also resulted in substrate decomposition. The rates of electrocyclizations are known to be insensitive to solvent polarity,⁶⁻⁹ but in a search for mild reaction conditions to avoid substrate decomposition, the rate constants for the electrocyclization of **5.11** in solvents of varying polarity were measured (Table 2), with no observable solvent effect.

In an effort to lower the thermal electrocyclization energy barrier in order to favor electrocyclization over other competing decomposition pathways, we attempted to synthesize the *E, Z, Z* analogue of **5.11**. The rationale for this was based on the observation that “*cis*” terminal triene substituents undergo a steric clash at the electrocyclization transition state, raising the electrocyclization energy barriers of those substrates relative to their unsubstituted or “*trans*” substituted analogues.⁵ Accordingly, crude stannane **5.9** was coupled with vinyl bromide **5.13**,^{10,11} resulting in a complex mixture containing triene **5.11**, presumably the result of *in-situ* isomerization of triene **5.14**. Attempts to cleanly isolate **5.14** *via* silica or alumina gel chromatography yielded only triene isomer **5.11** (Scheme 4).



Scheme 4. Synthesis of triene **5.11** *via* isomerization of triene **5.14**. CuTC = copper(I) thiophene-2-carboxylate.

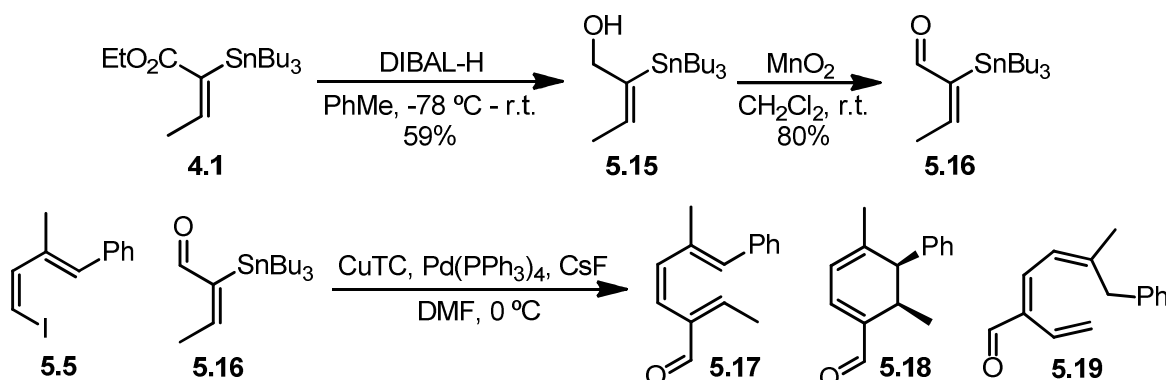
In an alternative strategy designed to lower the electrocyclization energy barrier and disfavor non-specific decomposition pathways, we next explored trienes possessing 2,5-methyl,formyl substitution patterns. A triene possessing a substituent in the 2-position is expected to more highly populate the *s-cis* conformation of the neighboring single bond, based on unfavorable steric interactions present between the methyl group and the triene terminus in the *s-trans* conformation (Scheme 5). Those interactions are not present in 2-unsubstituted trienes, whose neighboring single bonds therefore adopt primarily *s-trans* conformations. The *s-cis* triene conformer more closely resembles the electrocyclization transition state, and therefore, 2-substituted trienes are expected to be more entropically biased towards electrocyclization over other reaction pathways, relative to 2-unsubstituted trienes. Substitution in the 2-position is also expected to lower the electrocyclization enthalpy of activation due to ground-state destabilization of the substituted triene relative to the unsubstituted triene, caused by unfavorable steric interactions analogous to those discussed above. Finally, inclusion of an electron-donating methyl group in the 2-position along with the electron-withdrawing formyl group in the 5-position is expected to lower the electrocyclization energy barrier due to the “captodative substitution” effect outlined by Fu and Liu (Chapter 1).¹²



Scheme 5. Conformations of 2-substituted and 2-unsubstituted trienes.

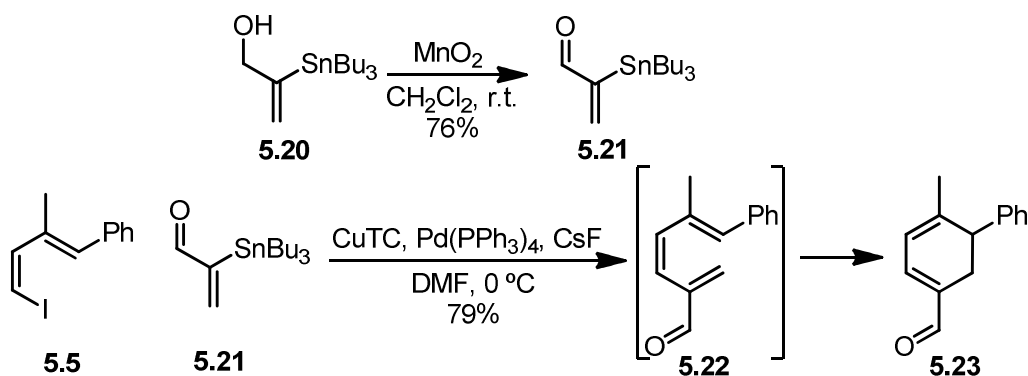
In designing our next 2-substituted triene substrate, a methyl group β to the formyl group was included in an effort to kinetically disfavor the isomerization of that alkene. Synthesis of triene **5.17** began with reduction and re-oxidation of vinyl stannane **4.1** to give α -stannyl aldehyde **5.16**, which was coupled with vinyl iodide **5.5** (Scheme 6). After aqueous workup the crude reaction mixture contained the triene product contaminated with approximately 25%

cyclohexadiene **5.18** and 35% triene isomer **5.19**, the latter formed by alkene isomerization and subsequent 1,7-hydride shift. Attempts to purify triene **5.17** resulted in further conversion to **5.18** and **5.19**.



Scheme 6. Synthesis of triene **5.17** and its electrocyclization and isomerization, hydride shift products. DIBAL-H = diisobutylaluminum hydride, CuTC = copper(I) thiophene-2-carboxylate.

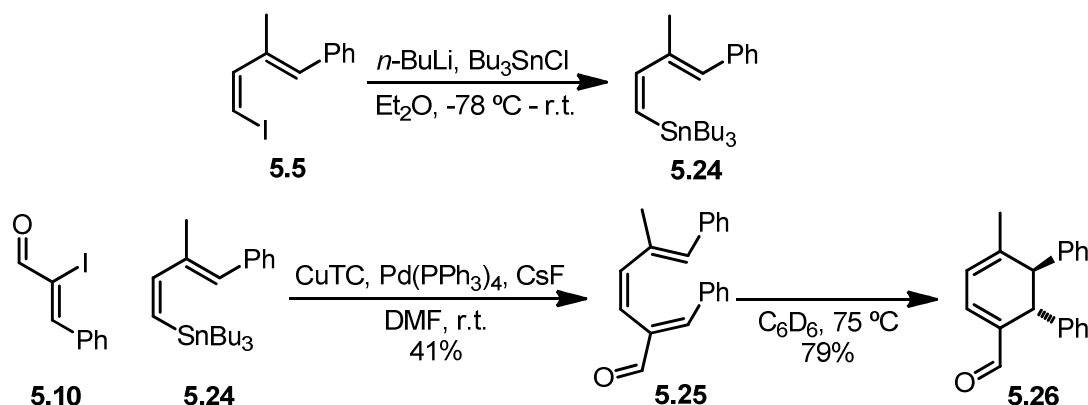
In order to completely avoid problems associated with the alkene isomerizations outlined above, we next targeted β -unsubstituted triene **5.22** (Scheme 7). However, the crude reaction mixture formed upon coupling of **5.5** and **5.21** (the MnO_2 oxidation product of **5.20**¹³) showed only cyclohexadiene **5.23**, the product of the *in-situ* electrocyclization of **5.22**. The facile nature of this electrocyclization can be attributed to a relative lack of unfavorable steric interactions between triene-termini in the electrocyclization transition state, as compared to those that would be expected for triene **5.17**, for example.



Scheme 7. Synthesis of cyclohexadiene **5.23** via triene intermediate **5.22**. CuTC = copper(I) thiophene-2-carboxylate.

Returning to β -phenyl-substitution, we next targeted triene **5.25** (Scheme 8), which possessed a δ -methyl substituent that we hoped would bias this substrate towards electrocyclization. Lithium-iodine exchange of vinyl iodide **5.5** followed by tributyltin chloride quench gave vinyl stannane **5.24** contaminated with 15-35% protodestannylated 1-phenyl-2-methyl-1,3-butadiene. As no conditions could be found not resulting in protodestannylation, and attempted purification simply resulted in complete protodestannylation, crude stannane **5.24** was coupled with iodide **5.10** to give triene **5.25** in low yield. The thermal electrocyclization of **5.25** was effected at only 75°C , as opposed to the 105°C needed for the cyclization of the des-methyl

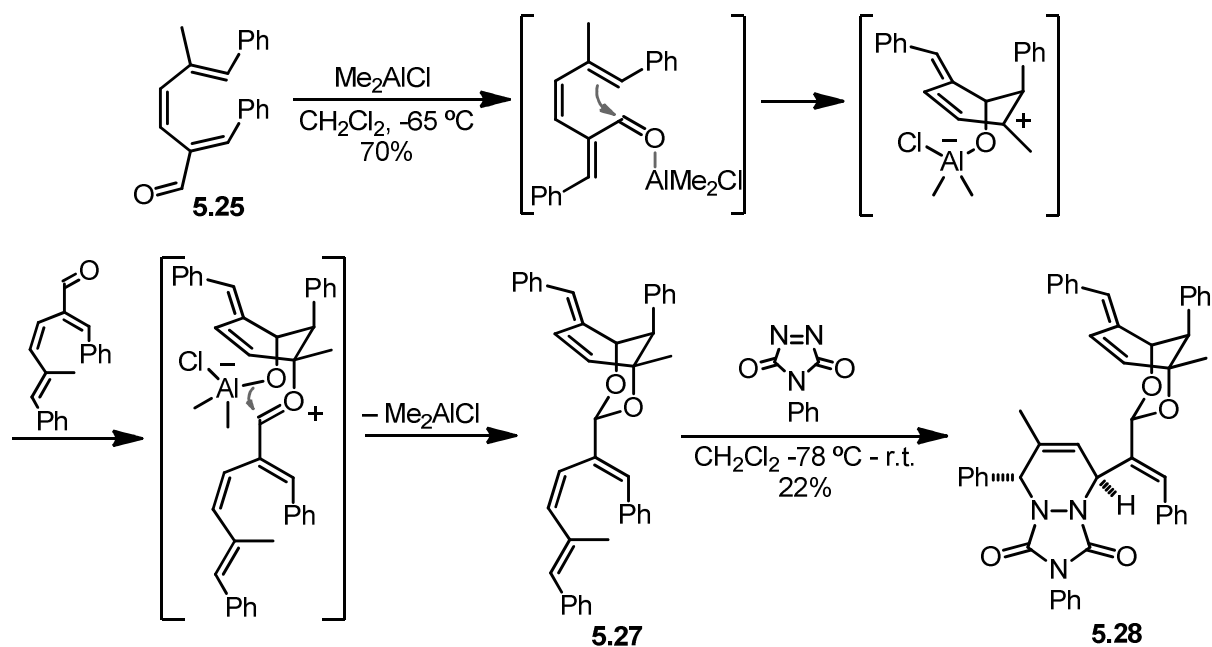
analogue **5.11** (Scheme 8). This difference can be attributed to the influence of the δ -methyl substituent, as discussed above (Scheme 5).



Scheme 8. Synthesis and thermal cyclization of triene **5.25**. CuTC = copper(I) thiophene-2-carboxylate.

In the presence of a variety of Lewis and Brønsted acids, decomposition of **5.25** was observed. However, at $-65\text{ }^\circ\text{C}$, catalytic amounts of Me_2AlCl effected the formation of acetal **5.27**. A reasonable mechanism for the formation of **5.27** is given in Scheme 9. The cation of a Prins-type cyclization of aldehyde **5.25** is intercepted by another equivalent of aldehyde to give an oxonium aluminate, which gives way to bicyclic acetal **5.27**. Though exo cyclization of **5.25** would give a benzylic carbocation, the endo cyclization observed in this case results in a doubly allylic carbocation. In addition, the *Z* alkene present in **5.25** provides a conformational bias towards endo cyclization. Though we believe these kinetic arguments are valid, it is likely that the entire reaction is reversible under conditions of Me_2AlCl catalysis and therefore the product outcome is under thermodynamic control. Low temperature acetal cleavage by Me_2AlCl is known.¹⁴ In addition, previous work by the Snider group suggests that the alkylaluminum halide induced nucleophilic attack of alkenes on carbonyl compounds to give zwitterionic species is a reversible process.¹⁵⁻²⁰ Indeed, non-specific decomposition of triene dimer **5.27** was observed at temperatures above $-65\text{ }^\circ\text{C}$ in the presence of Me_2AlCl .

Attempts to characterize **5.27** via one- and two-dimensional NMR techniques were unsuccessful due to the complexity of the spectra. In addition, single crystal X-ray analysis was not possible due to the liquid nature of **5.27**. Dimer **5.27** was therefore treated with the highly reactive dienophile *N*-phenyltriazolinedione in the hopes that the latter compound would react with the diene moiety proposed to be present in **5.27**, leading to a crystalline Diels-Alder adduct suitable for single crystal X-ray analysis. Indeed, this reaction yielded two crystalline products. The major product, **5.28**, was crystallographically analyzed and is shown in Scheme 8. The minor product is presumably the opposite Diels-Alder diastereomer. An ORTEP diagram derived from the X-ray crystal structure of **5.28** is shown in Figure 4.



Scheme 9. The Me_2AlCl -catalyzed dimerization of **5.25** and its Diels-Alder derivatization.

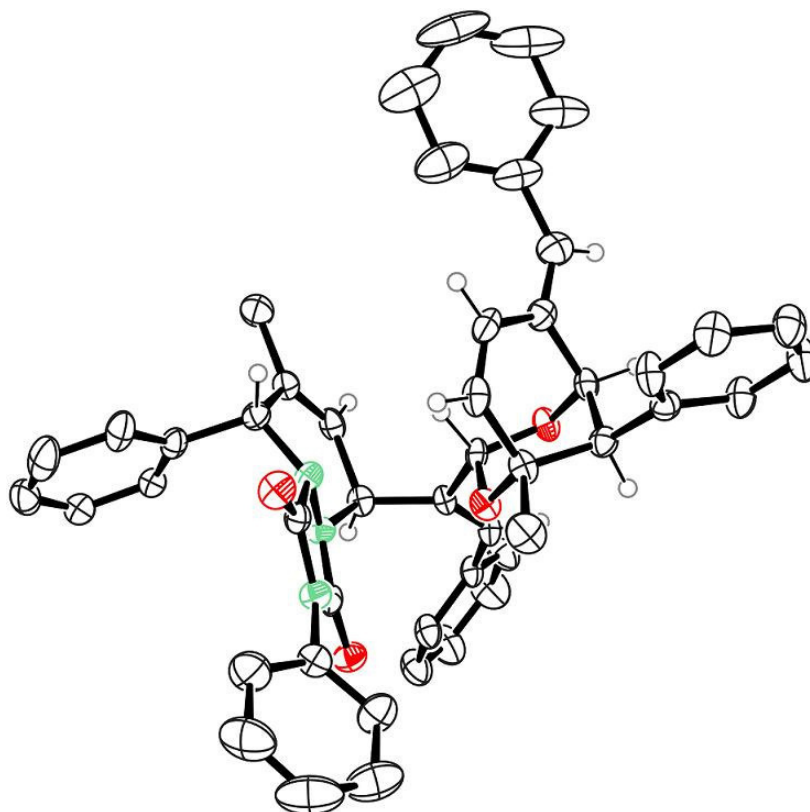
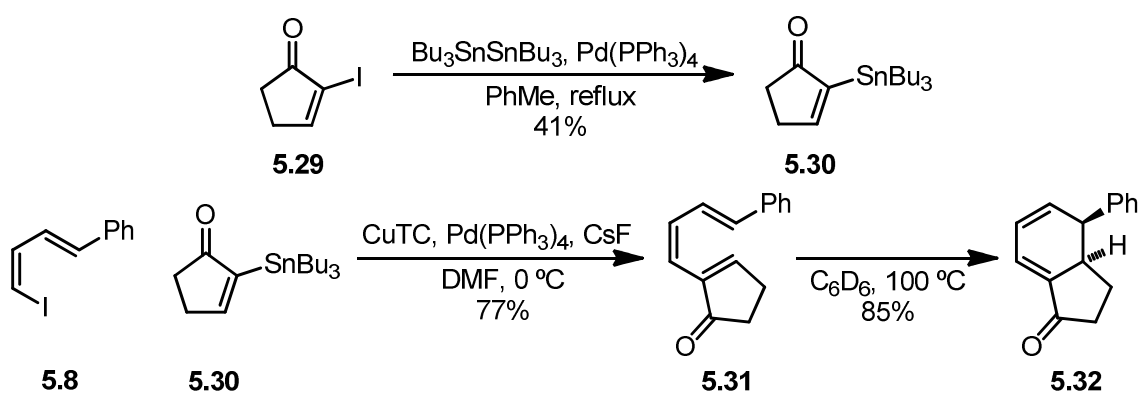


Figure 4. ORTEP diagram of **5.28** at the 50% probability level. Some hydrogen atoms have been removed for clarity.

The formation of triene dimer **5.27** and its decomposition at temperatures above $-65\text{ }^\circ\text{C}$ provide a possible explanation for the decomposition of triene **5.11** under conditions of Me_2AlCl

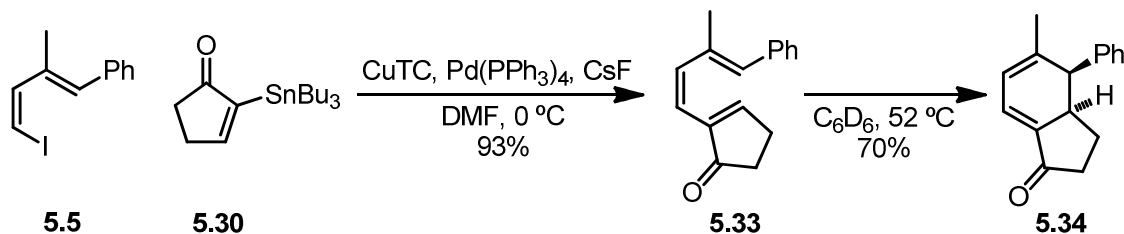
catalysis. It is possible that triene **5.11** was undergoing a similar dimerization/decomposition under the conditions we explored. This, in addition to the olefin isomerization issues outlined above, prompted us to turn our attention to substrates possessing ketones as Lewis basic groups, in the hopes that these substrates would be less prone to competitive intramolecular side reactions.

Accordingly, synthesis of **5.31** proceeded by palladium-catalyzed tin-iodine exchange of **5.29**^{21,22} to give vinyl stannane **5.30**, which was coupled with vinyl iodide **5.8**. Isolation of **5.31** was not hampered by facile electrocyclization, as heating to 100 °C was required to affect its electrocyclization to cyclohexadiene **5.32**. This is presumably due in part to the absence of a substituent in the position δ to the carbonyl carbon (*vide supra*). Attempts to catalyze the electrocyclization of **5.31** with Me₂AlCl resulted only in non-specific substrate decomposition.



Scheme 10. Synthesis and thermal electrocyclization of triene substrate **5.31**. CuTC = copper(I) thiophene-2-carboxylate.

We attributed the decomposition under catalytic conditions of triene **5.31** to the above-described absence of a δ -substituent, resulting in low population of the *s-cis* conformation of the neighboring single bond, entropically biasing the substrate towards decomposition over electrocyclization. To address this, triene **5.33** was synthesized *via* coupling of **5.5** and **5.30** (Scheme 11). Indeed, inclusion of the δ -methyl substituent allowed the cyclization of **5.33** to be efficiently carried out at only 52 °C, compared to the 100 °C necessary for the cyclization of the des-methyl analogue **5.31**. The relatively low electrocyclization energy barrier of **5.33** resulted in it being isolated along with ~10% cyclohexadiene **5.34**, the result of thermal electrocyclization during isolation.



Scheme 11. Synthesis and thermal electrocyclization of triene substrate **5.33**. CuTC = copper(I) thiophene-2-carboxylate.

It was found that inclusion of this methyl group indeed resulted in successful catalysis. The rate of the electrocyclization of **5.33** is substantially increased in the presence of catalytic or stoichiometric amounts of Me_2AlCl (Figure 5). Similar to that of triene **4.3**, the data in Figure 5 provide clear evidence in support of catalytic turnover—the rate of the reaction is increased at catalyst loadings as low as 6 mol% and all kinetic data fit a first order exponential process. A plot of the logarithm of the rate constant versus the logarithm of Me_2AlCl concentration at sub-stoichiometric catalyst loadings yields a straight line with a slope of 0.97(3), indicating the reaction is first order in catalyst, consistent with that for triene substrate **4.3**. A 55-fold rate acceleration is observed for this substrate in the presence of 1 equiv of Lewis acid at 28 °C. This rate acceleration is significantly larger than the 13-fold rate acceleration observed for triene **4.3**.

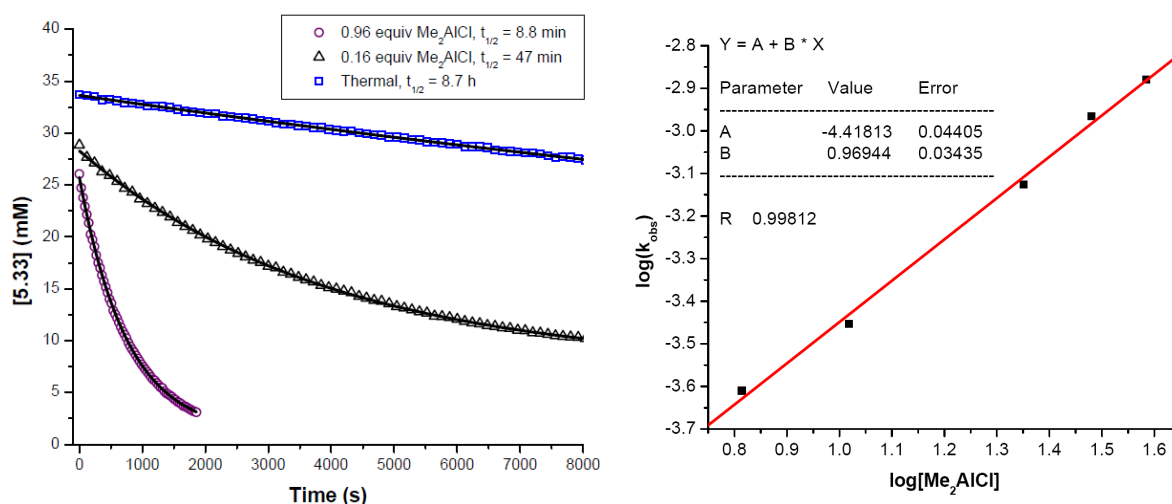


Figure 5. Kinetic plots (with first order exponential decay fits) and half-lives of the electrocyclization of **5.33** at 28 °C in the presence and absence of Me_2AlCl , and kinetic order in Me_2AlCl . Conditions: $[\mathbf{5.33}] = 40 \text{ mM}$ in C_6D_6 at 28 °C.

The results of a ^1H NMR titration of triene **5.33** are similar to those of triene **4.3**. A shift in all resonances of the ^1H NMR spectrum of **5.33** is observed (Figure 6). Again, this shift levels off at approximately one equivalent of Me_2AlCl for all resonances, which provides evidence for an energetically favorable 1:1 binding of Me_2AlCl to **5.33**. The observation of a time-averaged mixture of bound and unbound triene reveals that even though catalyst binding is exothermic, it is rapid and reversible for ketone substrates as well as ester substrates.

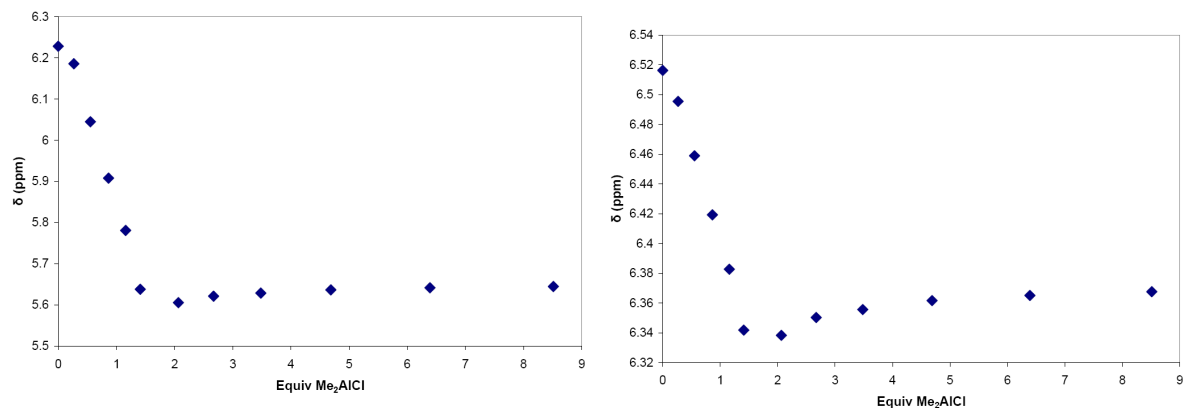


Figure 6. Chemical shifts of two representative ^1H NMR resonances of **5.33** versus added equivalents of Me_2AlCl in C_6D_6 at 10°C .

Eyring analysis revealed a 2.4 kcal/mol decrease in the Gibbs free energy of activation for the catalyzed process (Figure 7 and Table 3). Again, this catalysis is primarily enthalpic in nature, exhibiting a 2.2 kcal/mol decrease in the enthalpy of activation and a 0.2 kcal/mol increase in $T\Delta S^\ddagger$ (298 K). This result demonstrates that ketones as well as esters are suitable Lewis basic groups for catalytic 6π electrocyclizations, and is an indication of the broad synthetic potential of this reaction.

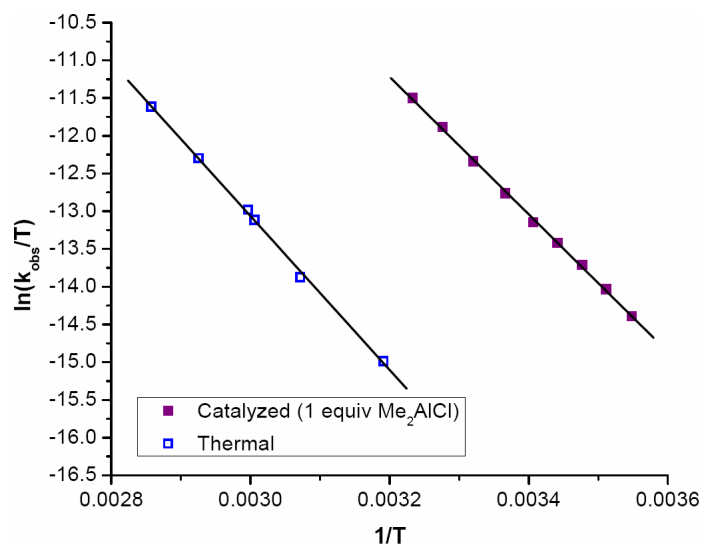


Figure 7. Eyring plots for the catalyzed and thermal cyclization of **5.33** in C_6D_6 .

Table 3. Activation parameters of the thermal and catalyzed (1 equiv. Me_2AlCl) electrocyclizations of **5.33**. Conditions: $[\mathbf{5.33}] = 40\text{ mM}$ in C_6D_6 .

	Thermal	Catalyzed
ΔH^\ddagger (kcal/mol)	20.3(4)	18.1(1)
ΔS^\ddagger (e.u.)	-12.4(5)	-11.6(1)
ΔG^\ddagger_{298} (kcal/mol)	24.0(5)	21.6(1)

With this new substrate in hand, we undertook another screen for catalysts of the electrocyclization of **5.33**. Comparison of the results of this catalyst screen (Table 4) to the

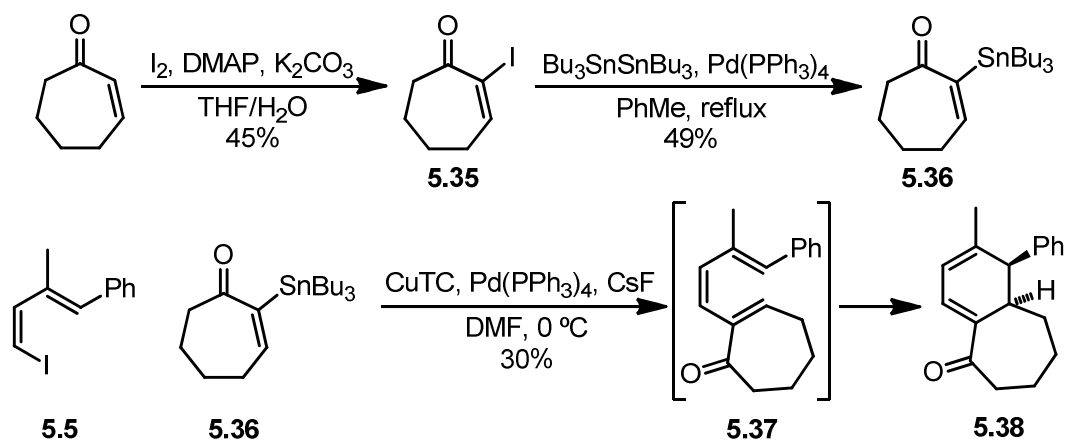
results of the catalyst screen using triene **4.3** (Chapter 4, Table 1) reveals a few differences between substrates **4.3** and **5.33**. Scandium(III) triflate appears to catalyze the electrocyclization of **5.33** more efficiently than for **4.3** (Chapter 4, Table 1, entry 2 versus present chapter, Table 4, entry 2). More notably, boron trifluoride diethyl etherate results in a 100-fold rate acceleration of the electrocyclization of **5.33**, while no catalysis of the electrocyclization of **4.3** was observed under identical conditions (Chapter 4, Table 1, entry 7 versus present chapter, Table 4, entry 4). In another example of catalysis with boron-based Lewis acids, tris-pentafluorophenylborane resulted in a significant 400-fold rate acceleration of the electrocyclization of **5.33** (Table 4, entry 3). Dimethylaluminum triflate catalyzes this reaction as efficiently as dimethylaluminum chloride (Table 4, entries 5 and 6). Alkylaluminum bis-halides appear to be the most efficient catalysts of the electrocyclization of **5.33**, with methylaluminum diiodide resulting in a 600-fold rate acceleration (Table 4, entries 7-9).

Table 4. Screen for catalysis of the electrocyclization of **5.33** in C₆D₆ in the presence of Lewis acids (1 equiv). OTf = trifluoromethanesulfonyl.

Entry	Lewis Acid	Approx t _{1/2} , temperature	Approx rate acceleration
1	Cu(OTf) ₂ *	20 min, 45 °C	4
2	Sc(OTf) ₃ *	20 min, r.t.	55
3	B(C ₆ F ₅) ₃	2.5 min, r.t.	400
4	BF ₃ ·OEt ₂ *	8 min, r.t.	100
5	Me ₂ AlCl	20 min, r.t.	55
6	Me ₂ AlOTf	15 min, r.t.	70
7	MeAlCl ₂	24 min, 9 °C	200
8	MeAlI ₂	7 min, 9 °C	600
9	PhAlCl ₂	4 min, r.t.	300

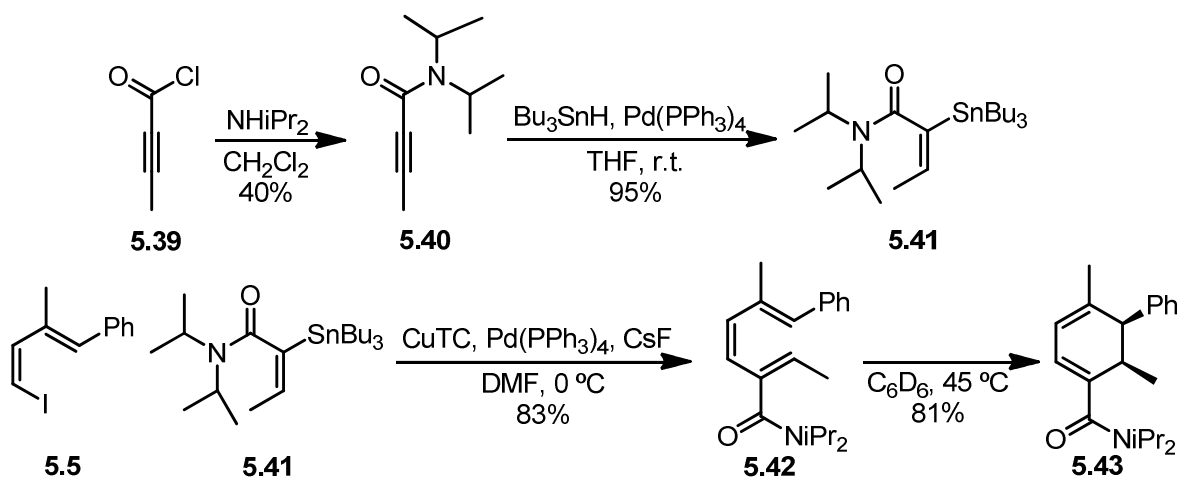
* 2,6-di-*t*-butyl-4-methylpyridine (1.2 equiv) added

One can envision targeting a variety of bicyclic systems by simply varying the ring size of stannyl enone **5.30**. To this end, iodination of cycloheptenone yielded iodide **5.35**,²¹ which after palladium-catalyzed lithium-iodine exchange gave stannane **5.36**. Analysis of the crude reaction mixture resulting from the coupling of **5.5** and **5.36** revealed only cyclohexadiene **5.38** (Scheme 12). The rapid electrocyclization of triene **5.37** is puzzling in light of the fact that cyclopentenone-derived triene **5.33** was isolated cleanly. Though we were not able to explore catalysis of the electrocyclization of triene **5.37**, its rapid thermal electrocyclization is an example of the power of this synthetic strategy for the synthesis of bicyclic systems.



Scheme 12. Synthesis of cyclohexadiene **5.38** via triene intermediate **5.37**. DMAP = 4-(dimethylamino)pyridine, CuTC = copper(I) thiophene-2-carboxylate.

The amide analogue of carboethoxy-substituted-triene **5.6** (Scheme 2) was next targeted. Treatment of butynoyl chloride **5.39**²³ with diisopropylamine yielded amide **5.40**, which after hydrostannylation cleanly yielded stannane **5.41** as a single regioisomer. Coupling of **5.41** and **5.5** yielded triene **5.42**, which undergoes thermal electrocyclic cyclization to cyclohexadiene **5.43** at 45 °C (Scheme 13). Interestingly, the ester analogue of triene **5.42** (Scheme 2) was not isolable due to the rapidity of its thermal electrocyclic cyclization at room temperature. The cause of this rate difference is not clear. Eyring analysis of the thermal electrocyclic cyclization of triene **5.42** reveals activation parameters typical of a carba-6 π electrocyclic cyclization (Table 5) and similar to those measured for triene substrates **4.3**, **5.3**, and **5.33** (Chapter 4, Table 2, and present chapter, Tables 1 and 3).⁵ The electrocyclic cyclization of triene **5.42** was catalyzed by Me₂AlCl, resulting in a 7-fold increase in the reaction rate in C₆D₆ in the presence of 0.58 equivalents catalyst.

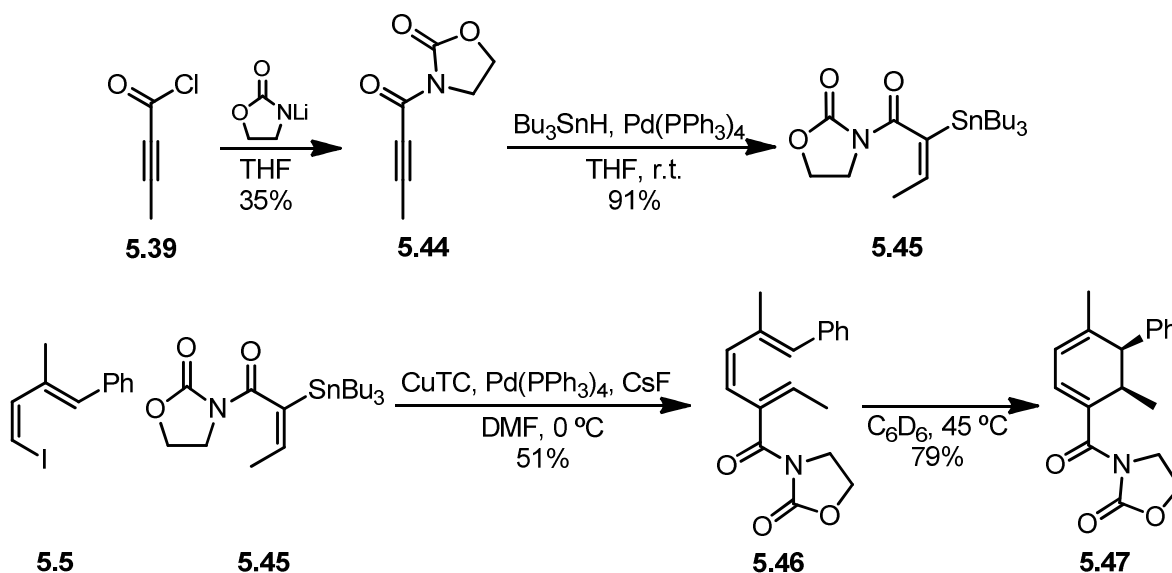


Scheme 13. Synthesis and thermal cyclization of triene **5.42**. CuTC = copper(I) thiophene-2-carboxylate.

Table 5. Activation parameters of the thermal electrocyclization of **5.42**. Conditions: [**5.42**] = 40 mM in C₆D₆.

ΔH^\ddagger (kcal/mol)	20.1 (2)
ΔS^\ddagger (e.u.)	-11.5 (2)
ΔG^\ddagger_{298} (kcal/mol)	23.6 (3)

The use of acyl oxazolidinones as Lewis basic catalyst-binding sites is well established in the catalytic asymmetric cycloaddition literature.²⁴⁻²⁸ We therefore targeted triene **5.46** (Scheme 14), and began its synthesis by addition of the lithium amide of oxazolidinone to butynoyl chloride. Hydrostannylation of the resultant acyl oxazolidinone gave stannane **5.45** as a single regioisomer. Coupling of this with **5.5** yielded triene **5.46**. The thermal cyclization of **5.46** was effected at 45 °C and cleanly yielded cyclohexadiene **5.47**. Though no attempts to catalyze this cyclization have yet been made, it would be interesting to discover if Lewis acids such as copper(II) triflate, known to catalyze reactions of substrates possessing acyl oxazolidinone binding motifs, is a more efficient catalyst of this reaction than it is for trienes **4.3** and **5.33**.



Scheme 14. Synthesis and thermal cyclization of triene **5.46**. CuTC = copper(I) thiophene-2-carboxylate.

Summary & Conclusions

We have demonstrated that ester, ketone, and amide functionalities are useful Lewis-basic docking groups for the catalysis of 6 π electrocyclizations. Catalysis using aldehyde moieties as docking groups was unsuccessful, most likely due to the high reactivity of the aldehyde functional group towards intramolecular nucleophilic attack, as demonstrated by the formation of a novel triene dimer. We have shown one clear example in which it is necessary for the substrate structure to be entropically biased towards electrocyclization in order for catalysis to be successful. We have further shown that boron-, copper-, scandium-, as well as aluminum-based Lewis acids are competent catalysts for this reaction, with methylaluminum diiodide resulting in the most significant rate accelerations. We have also found that expansion of this

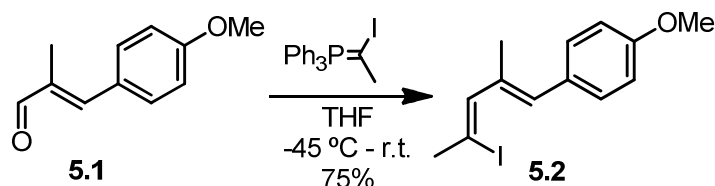
catalytic methodology may be hampered by facile thermal electrocyclozation of trienes with electron-withdrawing Lewis basic groups in the 2-position, but this facile thermal electrocyclozation does highlight the broad utility of the general synthetic strategy employed.

Experimental

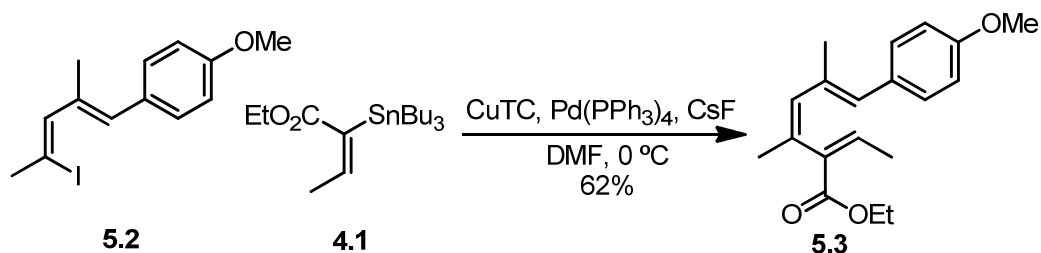
General Information. All reactions and manipulations, unless otherwise noted, were carried out in an inert atmosphere (N_2) glovebox or using standard Schlenk and high vacuum techniques. Sealed NMR tubes were prepared by attaching the NMR tube directly to a Kontes high-vacuum stopcock *via* a cajon ultra-torr reducing union, then flame-sealing on a vacuum line. All glassware was dried in an oven at 150 °C for at least 12 h prior to use or was flame-dried under reduced pressure. 1H NMR and ^{13}C NMR spectra were recorded on Bruker DRX-500 (500 MHz), AV-500 (500 MHz), AVB-400 (400 MHz), AVQ-400 (400 MHz), and AV-300 (300 MHz) spectrometers as indicated. 1H NMR chemical shifts (δ) are reported in parts per million relative to residual protiated solvent. Data are reported in the following format: (s = singlet, d = doublet, t = triplet, q = quartet, m = multiplet; coupling constant; integration). ^{13}C NMR chemical shifts (δ) are reported in parts per million relative to the carbon resonance of the deuterated solvent. Column chromatography was performed using a Biotage SP1 MPLC purification system and pre-packed silica gel columns. HPLC was performed using an Alltech Econosil C18 10u column (250mm x 22mm). IR spectra were obtained on neat samples on NaCl plates using a ThermoNicolet Avatar 370 FT-IR spectrometer. The temperatures of the kinetics experiments carried out in a circulating oil bath were measured using a calibrated mercury thermometer, and varied ± 0.1 °C. The temperatures of the kinetics and titration experiments carried out in an NMR probe were determined from the 1H NMR chemical shifts of ethylene glycol and MeOH samples, and varied ± 0.1 °C. The values for k_{obs} were determined by fitting the concentration versus time plots to the equation $C_t = C_\infty - (C_\infty - C_0)\exp(-k_{obs}t)$ using the program KaleidaGraph (where C_t , C_∞ , C_0 are the concentration at time t , time infinity, and time zero).²⁹ All well-resolved starting material and product 1H NMR resonances were integrated and fit separately; which 1H NMR resonances are well-resolved depended on the Me_2AlCl :Triene ratio (see 1H NMR titrations); the k_{obs} values shown are averages of those individual values. The reported errors in the k_{obs} values are one standard deviation of the k_{obs} values obtained from each integrated resonance.

Materials. Tetrahydrofuran, toluene, diethyl ether, and dichloromethane were dried and purified by passage through a column of activated alumina under N_2 pressure followed by sparging with N_2 .³⁰ Dry DMF was obtained from EMD and used without further purification. C_6D_6 , $CDCl_3$, CD_2Cl_2 , CD_3NO_2 , CD_3OD , and acetone- d_6 , were obtained from Cambridge Isotope Labs, Inc. C_6D_6 for use as a reaction solvent or for characterization of alkylaluminum species was sparged with N_2 and stored over activated 4 Å molecular sieve pellets overnight prior to use. $CDCl_3$ was stored over K_2CO_3 and used without further purification. CD_2Cl_2 was vacuum transferred from CaH_2 and degassed with three freeze-evacuation-thaw cycles. CD_3NO_2 and acetone- d_6 were distilled from anhydrous $MgSO_4$, sparged with N_2 , and stored over activated 4 Å molecular sieve pellets overnight. CD_3OD was distilled from activated Mg and sparged with N_2 . Activated 4 Å molecular sieve pellets were obtained from Sigma-Aldrich and heated at 150 °C under vacuum for 24 h. Hexamethylbenzene was obtained from Sigma-Aldrich and was sublimed prior to use.

HMPA was obtained from Sigma-Aldrich and distilled from CaH₂ prior to use. 1,1,2,2-tetrachloroethane, obtained from Sigma-Aldrich, was sparged with N₂ and stored over activated 4 Å molecular sieve pellets overnight prior to use. Diisopropylamine was obtained from Fisher Scientific and was distilled from KOH prior to use. Pd(PPh₃)₄ and B(C₆F₅)₃ were obtained from Strem Chemicals; Bu₃SnH, Bu₃SnCl, CsF, diisobutylaluminum hydride, *n*-BuLi, NaHMDS, *trans*-cinnamaldehyde, α -methyl-*trans*-cinnamaldehyde, 2,6-di-*tert*-butyl-4-methylpyridine, Cu(OTf)₂, Sc(OTf)₃, Me₃Al, Me₂AlCl, BF₃·OEt₂, AlI₃, and trifluoromethanesulfonic acid were obtained from Sigma-Aldrich; iodine was obtained from Fisher Scientific; oxazolidin-2-one was obtained from Fluka; these reagents were used without further purification. *Para*-methoxy- α -methyl-*trans*-cinnamaldehyde,^{31,32} (ethyl)triphenylphosphonium iodide,^{33,34} copper(I) thiophene-2-carboxylate,³⁵ (iodomethyl)triphenylphosphonium iodide,³⁶ α -bromo-cinnamaldehyde,^{10,11} manganese dioxide,³⁷ phenylaluminum dichloride,³⁸ 2-tributylstannylpropenol,¹³ and butynoyl chloride³⁹ were synthesized according to literature procedures. Characterization data for these compounds agree with literature values.

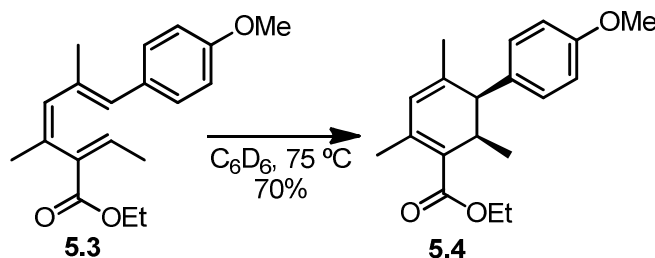


Synthesis of 2-iodo-4-methyl-5-(*p*-methoxyphenyl)-2,4-pentadiene (5.2). This material was synthesized in a fashion analogous to that employed for 2-iodo-4-methyl-5-phenyl-2,4-pentadiene (4.2), using ethyl(triphenyl)phosphonium iodide (2.6 g, 6.2 mmol), THF (60 mL), *n*-BuLi (3.85 mL, 1.6 M in hexanes, 6.2 mmol), iodine (1.6 g, 6.2 mmol), NaHMDS (10.3 mL, 0.6 M in toluene, 6.2 mmol), and *p*-methoxy- α -methyl-*trans*-cinnamaldehyde **5** (0.50 mL, 3.1 mmol). The crude product was purified by silica gel chromatography (0-2% EtOAc in hexanes), yielding 722 mg product as a yellow oil (75%). ¹H NMR (400 MHz, C₆D₆): δ 7.18 (d, *J* = 8.5 Hz, 2H), 6.75 (d, *J* = 8.8 Hz, 2H), 6.58 (s, 1H), 5.93 (s, 1H), 3.36 (s, 3H), 2.38 (s, 3H), 1.96 (s, 3H) ppm; ¹³C NMR (100 MHz, C₆D₆): δ 159.3, 139.5, 134.5, 132.1, 131.1, 130.6, 114.4, 97.5, 55.2, 35.8, 18.4 ppm; HRMS (EI⁺) Exact mass calcd for C₁₃H₁₅IO [M]⁺: 314.0168, found 314.0170.



Synthesis of triene 5.3. This material was synthesized in a fashion analogous to that employed for triene 4.3, using ethyl 2-tributylstannyl-2-butenoate (4.1) (749 mg, 1.9 mmol), 2-iodo-4-methyl-5-(*p*-methoxyphenyl)-2,4-pentadiene (5.2) (700 mg, 2.2 mmol), DMF (25 mL), Pd(PPh₃)₄ (107 mg, 0.1 mmol), copper(I) thiophene-2-carboxylate (390 mg, 2.0 mmol), CsF (565 mg, 3.7 mmol). The crude product was purified by silica gel chromatography (4-7% EtOAc in hexanes) followed by reverse-phase HPLC (67:33 MeCN:H₂O) yielding 349 mg product as a colorless oil (62%). ¹H NMR (400 MHz, C₆D₆): δ 7.23 (d, *J* = 8.4 Hz, 2H), 6.78 (d, *J* = 8.8 Hz,

2H), 6.56 (s, 1H), 6.06 (s, 1H), 5.86 (q, $J = 7.2$ Hz, 1H), 3.98 (q, $J = 7.1$ Hz, 2H), 3.33 (s, 3H), 2.02 (s, 3H), 1.98-1.93 (m, 6H), 0.93 (t, $J = 7.0$ Hz, 3H) ppm; ^{13}C NMR (100 MHz, C_6D_6): δ 167.3, 159.2, 137.2, 136.4, 134.6, 134.4, 134.2, 131.4, 131.3, 131.1, 114.3, 60.5, 55.1, 26.2, 18.8, 15.9, 14.6 ppm; IR 3034, 2935, 2836, 1716, 1606, 1509, 1252, 1178, 1035, 679 cm^{-1} ; HRMS (FAB $^+$) Exact mass calcd for $\text{C}_{19}\text{H}_{24}\text{O}_3$ [M] $^+$: 300.1725, found 300.1711.



Thermal synthesis of cyclohexadiene 5.4. This material was synthesized in a fashion analogous to that employed for cyclohexadiene 4.4, using triene 5.3 (0.40 mL, 48 mM in benzene- d_6 , 0.019 mmol; containing 5 mol% hexamethylbenzene as an internal standard), with the exception that the reaction mixture was heated for 1.5 h at 70 °C. The crude product was purified by silica gel chromatography (4-7% EtOAc in hexanes) yielding 3.6 mg product (70%). Quantitative conversion was observed by ^1H NMR. ^1H NMR (400 MHz, C_6D_6): δ 6.98 (d, $J = 8.5$ Hz, 2H), 6.73 (d, $J = 8.7$ Hz, 2H), 5.68 (s, 1H), 4.12-4.06 (m, 2H), 3.37 (d, $J = 7.6$ Hz, 1H), 3.33 (s, 3H), 3.18 (quintet, $J = 7.2$ Hz, 1H), 2.24 (s, 3H), 1.61 (s, 3H), 1.10 (d, $J = 7.0$ Hz, 3H), 0.99 (t, $J = 7.2$ Hz, 3H) ppm; ^{13}C NMR (100 MHz, C_6D_6): δ 168.1, 159.2, 143.7, 139.5, 131.4, 131.3, 127.6, 126.7, 113.9, 59.8, 54.8, 51.2, 36.0, 22.3, 20.7, 14.5, 13.9 ppm; IR 2975, 2935, 2908, 2835, 1699 cm^{-1} ; HRMS (FAB $^+$) Exact mass calcd for $\text{C}_{19}\text{H}_{24}\text{O}_3$ [M] $^+$: 300.1725, found 300.1716.

Activation parameter measurements for the thermal cyclization of 5.3. A solution of 5.3 (500 μL , 48 mM in benzene- d_6 , 0.0240 mmol; containing 5 mol% hexamethylbenzene as an internal standard) and benzene- d_6 (100 μL) were combined in a standard or J-Young NMR tube. Kinetic analyses of the reactions monitored at 36.0 and 44.0 °C were carried out in the following fashion. The NMR tube was sealed under vacuum and completely submerged in a circulating oil bath equilibrated to the desired temperature, the tube was removed from the oil bath and cooled rapidly to room temperature under a stream of hexanes, the reaction was monitored for disappearance of 5.3 and appearance of 5.4 (via single scan ^1H NMR spectroscopy using an AVB-400 spectrometer) and the tube was replaced in the oil bath. Only time spent in the oil bath was included in the concentration versus time plots. Kinetic analyses of the reactions monitored at 52.4, 60.6, 68.7, and 76.8 °C were carried out in the following fashion: the J-Young NMR tube was sealed and placed in an AV-500 NMR probe pre-equilibrated to the desired temperature, and the reaction was monitored for disappearance of 5.3 and appearance of 5.4 (via single scan ^1H NMR spectroscopy). The first order rate constants and Eyring plot can be found in Table 6 and Figure 8, respectively.

Table 6. First order rate constants of the thermal electrocyclization of 5.3 at various temperatures.

Entry	Temperature (°C)	k_{obs} (s^{-1})
1	36.0	$1.09(9) \times 10^{-5}$

2	44.0	$2.70(6)\times 10^{-5}$
3	52.4	$7.32(7)\times 10^{-5}$
4	60.6	$1.72(1)\times 10^{-4}$
5	68.7	$3.70(4)\times 10^{-4}$
6	76.8	$7.82(9)\times 10^{-4}$

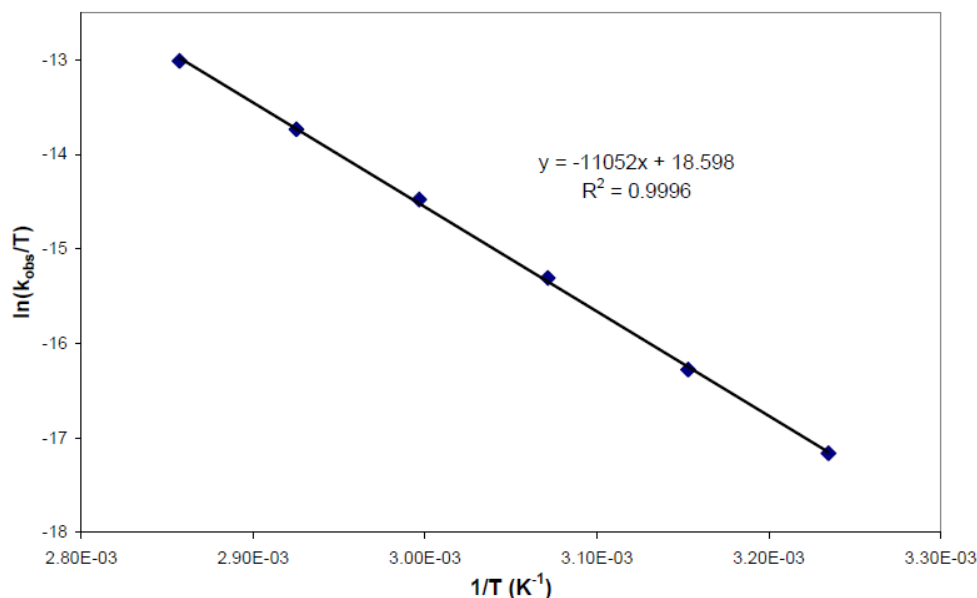


Figure 8. Eyring plot for the thermal electrocyclicization of **5.3** in C_6D_6 .

Activation parameter measurements for the catalyzed cyclization of 5.3. A solution of **5.3** (500 μ L, 48 mM in benzene- d_6 , 0.0240 mmol; containing 5 mol% hexamethylbenzene as an internal standard) was combined in a J-Young NMR tube with a solution of Me_2AlCl (100 μ L, 240 mM in benzene- d_6 , 0.0240 mmol). The J-Young tube was then sealed, the solution was agitated, the tube was placed in an AV-500 NMR probe pre-equilibrated to the desired temperature, and the reaction was monitored for disappearance of **5.3** and appearance of **5.4** (via single scan 1H NMR spectroscopy). The concentration of Me_2AlCl was determined to be 40(5) mM in all experiments by integration against the internal standard. The NMR probe for the above experiments was calibrated to 34.1, 42.3, 58.5, 66.7, and 74.8 $^{\circ}C$. The first order rate constants and the Eyring plot for these experiments are displayed in Table 7 and Figure 9, respectively.

Table 7. First order rate constants of the catalyzed electrocyclicization of **5.3** at various temperatures.

Entry	Temperature ($^{\circ}C$)	k_{obs} (s^{-1})
1	34.1	$1.1(1)\times 10^{-4}$
2	42.3	$2.67(6)\times 10^{-4}$
3	58.5	$1.39(5)\times 10^{-3}$
4	66.7	$3.0(1)\times 10^{-3}$
5	74.8	$5.8(3)\times 10^{-3}$

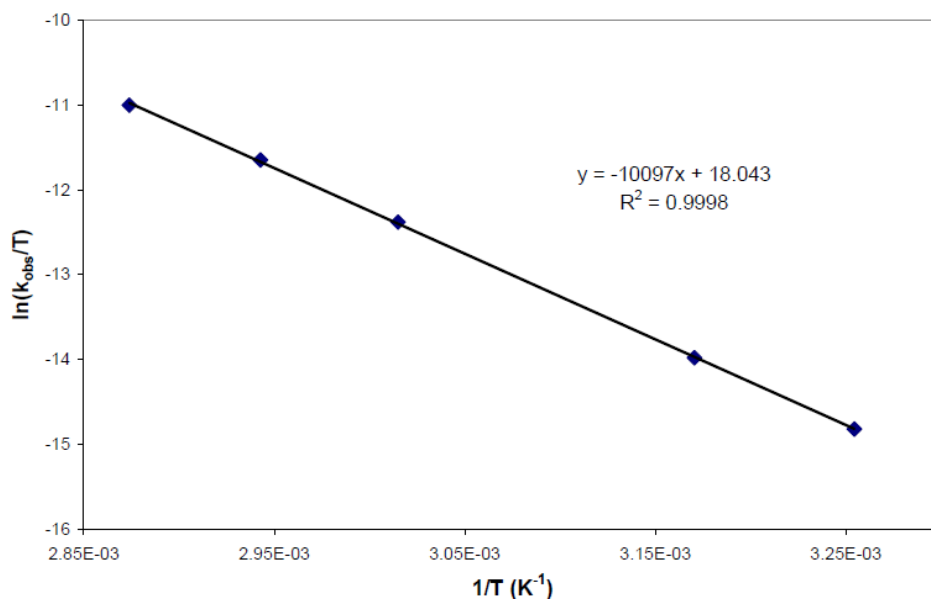


Figure 9. Eyring plot for the catalyzed electrocyclicization of **5.3** in C₆D₆.

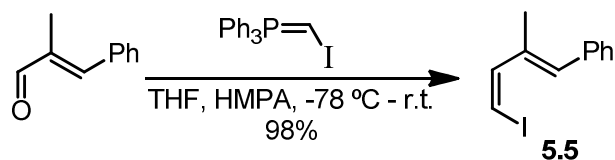
Saturation and kinetic order in Me₂AlCl for triene 5.3. A solution of triene **5.3** (500 μL, 48 mM in benzene-*d*₆, 0.0240 mmol; containing 5 mol% hexamethylbenzene as an internal standard) was combined in a J-Young NMR tube with varying amounts of a solution of Me₂AlCl in benzene-*d*₆. Benzene-*d*₆ was then added such that the total volume of the solution in the tube was 600 μL. A 240 mM Me₂AlCl solution was used for the kinetic runs with the five lowest Me₂AlCl concentrations, and a 1.44 M Me₂AlCl solution was used for the remaining runs. The J-Young tube was then sealed and the reaction mixture was frozen in ice-water until ready for kinetic analysis. Once ready for analysis, the solution was thawed and agitated, the tube was placed in an AV-500 NMR probe pre-equilibrated to 50.4 °C, and the reaction was monitored for disappearance of **5.3** and appearance of **5.4** (*via* single scan ¹H NMR spectroscopy). The concentration of Me₂AlCl was determined by integration against the internal standard. The first order rate constants and Me₂AlCl concentrations can be found numerically in Table 8 and graphically in Figure 2.

Table 8. First order rate constants of the electrocyclicization of **5.3** in the presence of varying concentrations of Me₂AlCl.

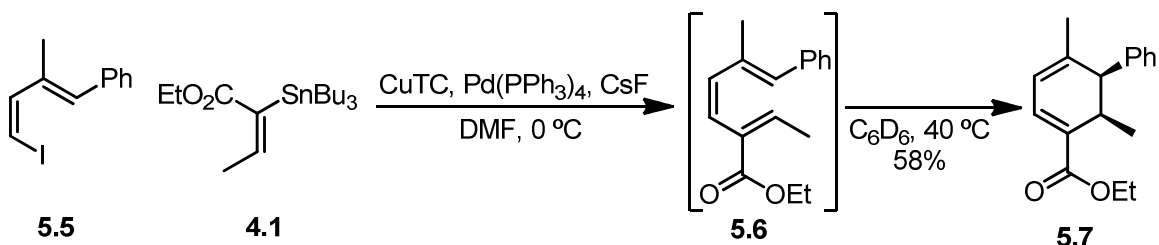
Entry	[Me ₂ AlCl] (mM)	k _{obs} (s ⁻¹)
1	4.4	1.22(5)x10 ⁻⁴
2	12.8	2.7(1)x10 ⁻⁴
3	25.6	4.07(9)x10 ⁻⁴
4	40.4	6.2(3)x10 ⁻⁴
5	41.2	5.9(2)x10 ⁻⁴
6	70.4	5.50(9)x10 ⁻⁴
7	100	5.2(1)x10 ⁻⁴
8	158	5.02(5)x10 ⁻⁴

Titration of 5.3 with Me₂AlCl. A solution of **5.3** (500 μL, 48 mM in benzene-*d*₆, 0.0240 mmol; containing 5 mol% hexamethylbenzene as an internal standard) was added to an NMR

tube, which was subsequently sealed with a rubber septum. The NMR tube was placed in an AV-500 NMR spectrometer pre-equilibrated to 9.7 °C and the shift of the ^1H NMR spectrum of **5.3** was monitored as a function of added Me_2AlCl (240 mM in benzene- d_6). The Me_2AlCl solution was added by ejecting the sample from the NMR probe, injecting the solution through the septum, agitating the sample, and replacing it in the NMR probe. The concentration of Me_2AlCl was determined by integration against the internal standard. Graphical representations of the change in chemical shift of two representative resonances are shown in Figure 3.

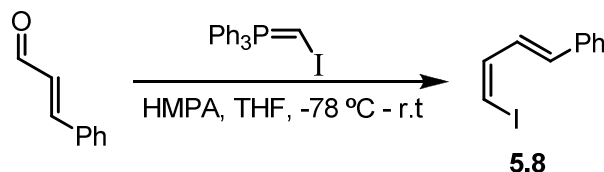


Synthesis of 4-iodo-2-methyl-1-phenyl-1,3-butadiene (5.5). This material was synthesized according to the procedure developed by Stork and Zhao.⁴⁰ A Schlenk flask was charged with THF (40 mL), (iodomethyl)triphenylphosphonium iodide (2.09 g, 3.9 mmol), and NaHMDS (4.30 mL, 1.0 M in THF, 4.30 mmol). This solution was stirred for 5 minutes at room temperature and cooled to -60 °C. HMPA was then added and the reaction mixture was cooled to -78 °C and stirred for a further 15 minutes. α -Methyl-*trans*-cinnamaldehyde (0.50 mL, 3.6 mmol) was added dropwise and the reaction mixture was allowed to warm to room temperature over 1.5 h, after which hexanes was added and the resultant suspension was filtered through Celite. The filtrate was concentrated *in vacuo*, hexanes was added, and the organic suspension was washed five times with water, once with brine, dried over MgSO_4 , filtered, and concentrated *in vacuo*. Hexanes was again added, the resultant suspension was filtered through Celite, and the filtrate was concentrated *in vacuo* yielding 0.95 g product as an orange oil (98%). ^1H NMR (400 MHz, CDCl_3): δ 7.45-7.21 (m, 5H), 6.96 (d, J = 8.6 Hz, 1H), 6.77 (s, 1H), 6.34 (d, J = 8.6 Hz, 1H) 2.21 (s, 3H) ppm; ^{13}C NMR (100 MHz, CDCl_3): δ 142.6, 137.1, 135.0, 133.3, 129.3, 128.4, 127.1, 77.0, 17.7 ppm; HRMS (EI^+) Exact mass calcd for $\text{C}_{11}\text{H}_{11}\text{I}$ [M] $^+$: 269.9903, found 269.9906.

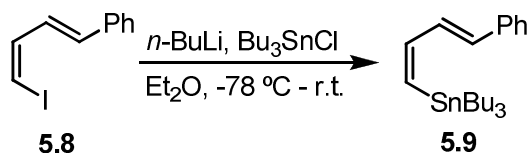


Synthesis of cyclohexadiene 5.7. Triene intermediate **5.6** was synthesized in a fashion analogous to that employed for triene **4.3**, using ethyl 2-tributylstannyl-2-butenoate (**4.1**) (211 mg, 0.52 mmol), 4-iodo-2-methyl-1-phenyl-1,3-butadiene (**5.5**) (134 mg, 0.50 mmol), DMF (5.5 mL), $\text{Pd}(\text{PPh}_3)_4$ (29 mg, 0.025 mmol), copper(I) thiophene-2-carboxylate (105 mg, 0.55 mmol), and CsF (152 mg, 1.0 mmol). The crude product was purified by silica gel chromatography (2-10% EtOAc in hexanes) yielding a 1:1 mixture of **5.6**:**5.7**. The diagnostic ^1H NMR resonances of **5.6** are the following: ^1H NMR (500 MHz, C_6D_6): δ 6.52 (s, 1H), 6.02 (d, J = 11.7 Hz, 1H), 5.96 (d, J = 11.7 Hz, 1H) ppm. This mixture of **5.6** and **5.7** was dissolved in C_6D_6 (1.0 mL), transferred to an NMR tube, and heated to 40 °C for 2 h. The crude product was purified by silica gel chromatography (1-7% EtOAc in hexanes) yielding 75 mg cyclohexadiene **5.7** as a

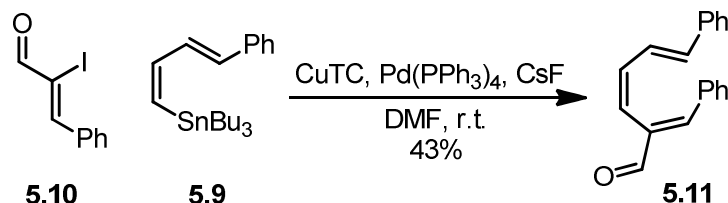
colorless oil (58% from **5.5**). $^1\text{H NMR}$ (500 MHz, CDCl_3): δ 7.38-7.26 (m, 3H), 7.16 (d, $J = 7.5$ Hz, 2H), 6.98 (d, $J = 6.0$ Hz, 1H), 6.00 (d, $J = 6.0$ Hz, 1H), 4.28-4.11 (m, 2H), 3.74 (d, $J = 7.5$ Hz, 1H), 2.86 (quintet, $J = 7.2$ Hz, 1H), 1.74 (s, 3H), 1.29 (t, $J = 7.1$ Hz, 3H), 0.83 (d, $J = 7.0$ Hz, 3H) ppm; $^{13}\text{C NMR}$ (125 MHz, CDCl_3): δ 167.4, 145.3, 139.4, 132.7, 131.4, 130.6, 128.1, 126.8, 121.6, 60.4, 52.2, 33.8, 22.9, 14.5, 13.0 ppm; IR 2976, 1703, 1577, 1265, 1233 cm^{-1} ; HRMS (EI^+) Exact mass calcd for $\text{C}_{17}\text{H}_{20}\text{O}_2$ [M] $^+$: 256.1463, found 256.1460.



Synthesis of 4-iodo-1-phenyl-1,3-butadiene (5.8). This material was synthesized in a fashion analogous to that employed for vinyl iodide **5.5**, using THF (110 mL), (iodomethyl)triphenylphosphonium iodide (6.3 g, 12 mmol), NaHMDS (13 mL, 1.0 M in THF, 13 mmol), HMPA (3.2 mL), and *trans*-cinnamaldehyde (1.4 mL, 11 mmol). The crude product was concentrated *in vacuo* yielding the vinyl iodide **5.8** as an orange oil containing ~15% triphenylphosphine oxide. $^1\text{H NMR}$ (400 MHz, CDCl_3): δ 7.55-7.28 (m, 5H), 7.09-6.90 (m, 2H), 6.87 (d, $J = 15.4$ Hz, 1H), 6.41 (d, $J = 7.3$ Hz, 1H) ppm; $^{13}\text{C NMR}$ (100 MHz, CDCl_3): δ 145.5, 138.6, 136.9, 136.8, 128.9, 128.6, 127.0, 83.0 ppm; HRMS (EI^+) Exact mass calcd for $\text{C}_{10}\text{H}_9\text{I}$ [M] $^+$: 255.9749, found 255.9750.

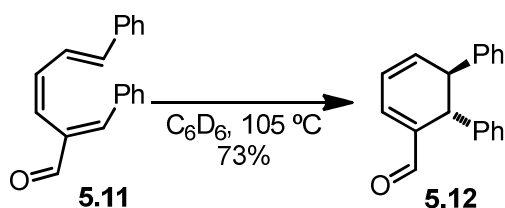


Synthesis of 4-tributylstannyl-1-phenyl-1,3-butadiene (5.9). A round-bottom flask was charged with 4-iodo-1-phenyl-1,3-butadiene (**5.8**) (4.0 g, ~16 mmol) and Et_2O (160 mL). The resultant solution was cooled to $-78\text{ }^\circ\text{C}$ and *n*-BuLi (7.8 mL, 2.2 M in hexanes, 17.2 mmol) was added dropwise. After stirring the reaction mixture for 10 min, Bu_3SnCl (4.7 mL, 17.2 mmol) was added dropwise and the reaction mixture was stirred a further 2 h at $-78\text{ }^\circ\text{C}$. The reaction mixture was warmed to $0\text{ }^\circ\text{C}$, after which water (10 mL) was added. The organic solution was then washed once with water and once with brine, dried over MgSO_4 , filtered, concentrated *in vacuo*, and purified by activity I basic alumina chromatography (0.5% EtOAc in hexanes) yielding stannane **5.9** as a yellow oil containing 15% 1-phenyl-1,3-butadiene. The diagnostic $^1\text{H NMR}$ resonances of **5.9** are as follows: $^1\text{H NMR}$ (500 MHz, CDCl_3): δ 6.71-6.62 (m, 2H), 6.55 (d, $J = 13.5$ Hz, 1H), 6.21 (d, $J = 12.5$ Hz, 1H) ppm. Spectral data for 1-phenyl-1,3-butadiene agree with literature values.⁴¹



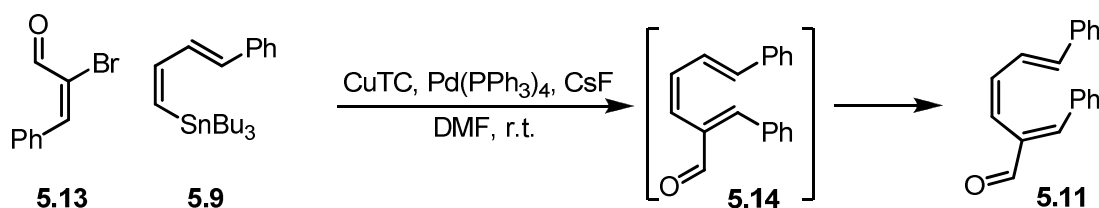
Synthesis of triene 5.11. Synthesized in a fashion analogous to that employed for triene **4.3**, using crude 4-tributylstannyl-1-phenyl-1,3-butadiene (**5.9**) (6.4 g, 15.3 mmol), α -iodo-

cinnamaldehyde (**5.10**) (2.6 g, 10.2 mmol), DMF (300 mL), Pd(PPh₃)₄ (590 mg, 0.51 mmol), copper(I) thiophene-2-carboxylate (2.9 g, 15.3 mmol), and CsF (3.1 g, 20.4 mmol). The reaction mixture was stirred for 1 h at room temperature instead of 1 h at 0 °C. The crude product was purified by silica gel chromatography (10-40% EtOAc in hexanes) yielding 1.14 g triene **5.11** as a yellow solid (43%). ¹H NMR (400 MHz, C₆D₆): δ 9.44 (s, 1H), 7.37 (d, *J* = 7.6 Hz, 2H), 7.10-6.91 (m, 8H), 6.82 (s, 1H), 6.70 (dd, *J* = 11.2, 15.6 Hz, 1H), 6.40 (d, *J* = 15.6 Hz, 1H), 6.30 (t, *J* = 11.2 Hz, 1H), 6.17 (d, *J* = 11.2 Hz, 1H) ppm; ¹³C NMR (100 MHz, CDCl₃): δ 193.9, 149.5, 137.5, 137.1, 135.5, 134.9, 134.5, 131.1, 130.6, 128.9, 128.7, 128.1, 126.9, 126.3, 121.8 ppm; IR 1667, 1161, 753, 688 cm⁻¹; HRMS (EI⁺) Exact mass calcd for C₁₉H₁₆O [M]⁺: 260.1201, found 260.1210.

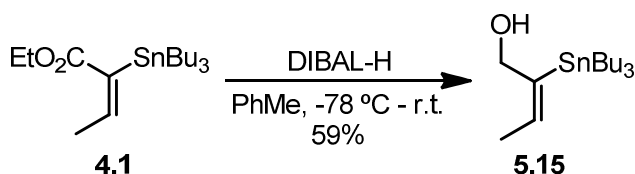


Synthesis of cyclohexadiene 5.12. This material was synthesized in a fashion analogous to that employed for cyclohexadiene **4.4**, using triene **5.11** (0.5 mL, 38 mM in benzene-*d*₆, 0.019 mmol; containing 5 mol% hexamethylbenzene as an internal standard), with the exception that the reaction mixture was heated for 12 h at 105 °C. The crude product was purified by silica gel chromatography (5-25% EtOAc in hexanes) yielding 3.6 mg cyclohexadiene **5.12** (73%). Quantitative conversion was observed by ¹H NMR. ¹H NMR (500 MHz, C₆D₆): δ 9.22 (s, 1H), 7.29 (d, *J* = 7.0 Hz, 2H), 7.15-6.98 (m, 8H), 6.17 (d, *J* = 5.5 Hz, 1H), 5.86-5.82 (m, 1H), 5.77-5.73 (m, 1H), 4.36 (s, 1H), 3.53 (d, *J* = 5.5 Hz, 1H) ppm; ¹³C NMR (100 MHz, C₆D₆): δ 192.6, 143.3, 142.3, 141.7, 138.3, 137.7, 129.1, 128.9, 127.42, 127.38, 127.26, 127.21, 123.4, 48.4, 43.0 ppm; IR 1670, 1569, 1161, 726, 697 cm⁻¹; HRMS (FAB⁺) Exact mass calcd for C₁₉H₁₆O [M]⁺: 260.1201, found 260.1206.

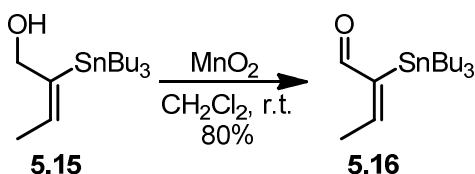
Screen of the sensitivity of the rate constant of the electrocyclicization of 5.11 to solvents of varying polarity. A solution of **5.11** (550 μL, 35 mM in desired solvent, 0.0192 mmol; containing 5 mol% hexamethylbenzene as an internal standard) was added to a standard NMR tube, which was sealed under vacuum. The NMR tube was completely submerged in a circulating oil bath equilibrated to 100 °C; the tube was removed from the oil bath and cooled rapidly to room temperature under a stream of hexanes; the reaction was monitored for disappearance of **5.11** and appearance of **5.12** (*via* single scan ¹H NMR spectroscopy using an AVB-400 spectrometer) and the tube was replaced in the oil bath. Only time spent in the oil bath was included in the concentration versus time plots. The first order rate constants can be found in Table 2.



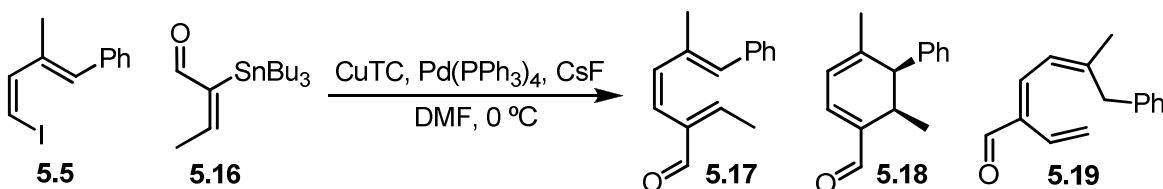
Synthesis of triene 5.11 via isomerization of triene 5.14. This material was synthesized in a fashion analogous to that employed for triene 4.3, using crude 4-tributylstannyl-1-phenyl-1,3-butadiene (5.9) (149 mg, 0.36 mmol), α -bromo-cinnamaldehyde (5.13) (50 mg, 0.24 mmol), DMF (6 mL), Pd(PPh₃)₄ (14 mg, 0.012 mmol), copper(I) thiophene-2-carboxylate (68 mg, 0.36 mmol), and CsF (72 mg, 0.47 mmol). The reaction mixture was stirred for 1 h at room temperature instead of 1 h at 0 °C. ¹H NMR analysis of the crude reaction mixture revealed a complex mixture of products, including triene 5.11. Any attempt to cleanly isolate 5.14 via silica or alumina gel chromatography yielded triene isomer 5.11.



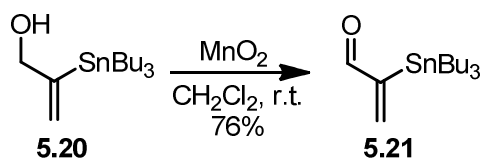
Synthesis of 2-tributylstannyl-but-2-enol (5.15). A round-bottom flask was charged with ethyl 2-tributylstannyl-2-butenoate (4.10) (122 mg, 0.30 mmol) and toluene (5 mL). The reaction mixture was cooled to -78 °C and diisobutylaluminum hydride (0.67 mL, 1.0 M in PhMe, 0.67 mmol) was added dropwise. The reaction mixture was warmed to room temperature, quenched with saturated aqueous potassium sodium tartrate, and extracted three times with ethyl acetate. The organic solution was then dried over MgSO₄, filtered, concentrated *in vacuo*, and purified by silica gel chromatography (20% EtOAc in hexanes) yielding 64 mg stannane 5.15 as a yellow oil (59%). ¹H NMR (400 MHz, CDCl₃): δ 5.64 (qt, $J_{\text{H-H}} = 2.0, 6.8$ Hz, $J_{\text{Sn-H}} = 34.2$ Hz, 1H), 4.36 (d, $J_{\text{H-H}} = 7.4$ Hz, $J_{\text{Sn-H}} = 25.2$ Hz, 15H), 1.67 (d, $J = 6.4$ Hz, 3H), 1.50-1.38 (m, 6H), 1.33-1.22 (m, 6H), 0.87 (t, $J_{\text{H-H}} = 2.0$ Hz, $J_{\text{Sn-H}} = 19.9$ Hz, 2H) ppm; ¹³C NMR (125 MHz, CDCl₃): δ 146.8, 134.3, 63.7 ($J_{\text{Sn-C}} = 11.0$ Hz), 29.4 ($J_{\text{Sn-C}} = 9.6$ Hz), 27.6 ($J_{\text{Sn-C}} = 28.5$ Hz), 15.4 ($J_{\text{Sn-C}} = 27.2$ Hz), 13.9, 10.2 ($J_{\text{Sn-C}} = 164$ Hz) ppm.



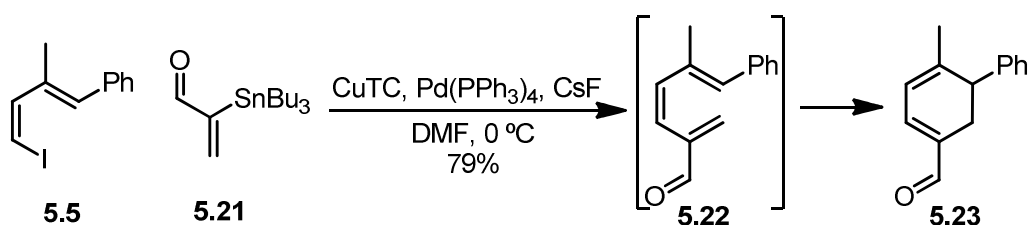
Synthesis of 2-tributylstannyl-but-2-enal (5.16). A round-bottom flask was charged with 2-tributylstannyl-but-2-enol (5.15) (264 mg, 0.73 mmol), MnO₂ (3.2 g, 36.5 mmol), and dichloromethane (8 mL). The reaction mixture was stirred at room temperature for 5 h, filtered through Celite, and concentrated *in vacuo* to yield 210 mg stannane 5.16 as a yellow oil (80%). ¹H NMR (400 MHz, CDCl₃): δ 10.34 (s, $J_{\text{Sn-H}} = 30.4$ Hz, 1H), 6.83 (q, $J_{\text{H-H}} = 7.1$ Hz, $J_{\text{Sn-H}} = 29.6$ Hz, 1H), 2.18 (d, $J = 7.2$ Hz, 3H), 1.50-1.37 (m, 6H), 1.32-1.18 (m, 6H), 0.93-0.79 (m, 15H) ppm; ¹³C NMR (100 MHz, CDCl₃): δ 194.9, 156.7, 147.4, 29.2 ($J_{\text{Sn-C}} = 9.8$ Hz), 27.5 ($J_{\text{Sn-C}} = 29.8$ Hz), 16.7, 13.9, 9.9 ($J_{\text{Sn-C}} = 167.4$ Hz) ppm.



Synthesis of trienes 5.17 and 5.19 and cyclohexadiene 5.18. This material was synthesized in a fashion analogous to that employed for triene 4.3, using 2-tributylstannyl-but-2-enal (5.16) (50 mg, 0.14 mmol), 4-iodo-2-methyl-1-phenyl-1,3-butadiene (5.5) (38 mg, 0.14 mmol), DMF (2 mL), Pd(PPh₃)₄ (8 mg, 0.007 mmol), copper(I) thiophene-2-carboxylate (29 mg, 0.15 mmol), and CsF (42 mg, 0.28 mmol). ¹H NMR analysis of the crude reaction mixture revealed resonances consistent with 5.17, 5.18, and 5.19 in a ratio of 60:25:35. Triene 5.17 and cyclohexadiene 5.18 could not be isolated cleanly. Triene 5.19 was isolated *via* silica gel chromatography (10-25% EtOAc in hexanes). The diagnostic ¹H NMR resonances of 5.17 are as follows: ¹H NMR (500 MHz, C₆D₆): δ 9.23 (s, 1H), 6.23 (d, *J* = 12.0 Hz, 1H), 5.84 (m, 2H) ppm. The diagnostic ¹H NMR resonances of 5.18 are as follows: ¹H NMR (400 MHz, C₆D₆): δ 9.42 (s, 1H), 6.10 (d, *J* = 5.6 Hz, 1H), 5.66 (d, *J* = 5.6 Hz, 1H), 3.23 (d, *J* = 8.0 Hz, 1H), 3.06 (quintet, *J* = 7.3 Hz, 1H) ppm. The complete ¹H NMR spectrum of 5.19 is as follows: ¹H NMR (500 MHz, C₆D₆): δ 9.39 (s, 1H), 7.16-6.98 (m, 5H), 6.92 (d, *J* = 7.0 Hz, 1H), 6.77 (d, *J* = 12.0 Hz, 1H), 6.58 (dd, *J* = 11.5, 17.5 Hz, 1H), 6.45 (dd, *J* = 2.0, 17.8 Hz, 1H), 6.37 (d, *J* = 12.0 Hz, 1H), 5.40 (d, *J* = 12.0 Hz, 1H), 3.20 (s, 2H), 1.49 (s, 3H) ppm.

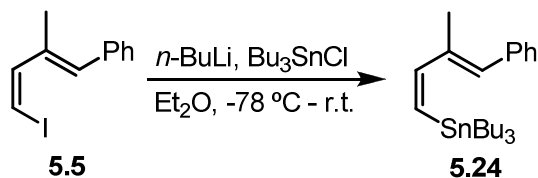


Synthesis of 2-tributylstannylacrolein (5.21). This material was synthesized in a fashion analogous to that employed for 5.16, using 2-tributylstannylpropenol (72 mg, 0.21 mmol), MnO₂ (274 mg, 3.2 mmol), and dichloromethane (8 mL), yielding 54 mg 5.21 as a yellow oil (76%). Decomposition of 5.21 was observed over the course of one hour at room temperature, so it was characterized *via* ¹H NMR and LRMS and employed in the subsequent reaction immediately. ¹H NMR (300 MHz, CDCl₃): δ 9.64 (s, *J*_{Sn-H} = 26.9 Hz, 1H), 6.84 (d, *J*_{H-H} = 2.1 Hz, 1H), 6.67 (d, *J*_{H-H} = 2.1 Hz, *J*_{Sn-H} = 23.8 Hz, 1H), 1.52-1.38 (m, 6H), 1.37-1.20 (m, 6H), 1.00-0.91 (m, 6H), 0.85 (t, *J* = 7.2 Hz, 9H) ppm. LRMS (EI⁺) Exact mass calcd for C₁₁H₂₁OSn [M-Bu]⁺: 289, found 289.

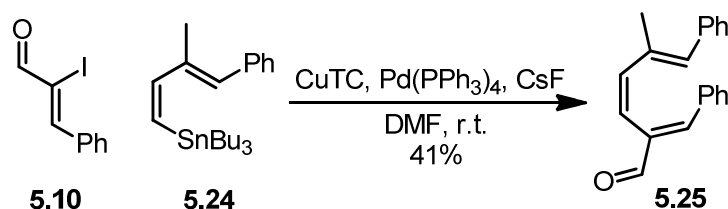


Synthesis of cyclohexadiene 5.23. This material was synthesized in a fashion analogous to that employed for triene 4.3, using 2-tributylstannylacrolein (5.21) (50 mg, 0.14 mmol), 4-iodo-2-methyl-1-phenyl-1,3-butadiene (5.5) (42 mg, 0.16 mmol), DMF (2 mL), Pd(PPh₃)₄ (9 mg, 0.008 mmol), copper(I) thiophene-2-carboxylate (34 mg, 0.18 mmol), and CsF (49 mg, 0.32 mmol). The crude product was purified by silica gel chromatography (2-18% EtOAc in hexanes) yielding 22 mg cyclohexadiene 5.23 as a yellow oil (79%). ¹H NMR (400 MHz, CDCl₃): δ 9.44 (s, 1H), 7.28-7.07 (m, 5H), 6.80 (d, *J* = 5.6 Hz, 1H), 6.20 (d, *J* = 6.0 Hz, 1H), 3.49 (t, *J* = 8.0 Hz, 1H), 2.76 (d, *J* = 7.2 Hz, 2H), 1.80 (s, 3H) ppm; ¹³C NMR (100 MHz, C₆D₆): δ 192.6, 150.1, 143.3, 142.1, 134.3, 128.8, 127.8, 127.1, 121.2, 44.5, 27.9, 23.2 ppm; IR 3025, 2918, 2849,

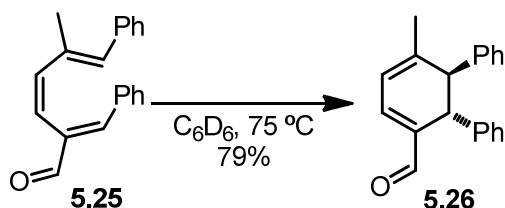
2809, 1668, 1642, 1578, 1211 cm^{-1} ; **HRMS** (ESI⁺) Exact mass calcd for $\text{C}_{14}\text{H}_{15}\text{O}$ $[\text{M}+\text{H}]^+$: 199.1117, found 199.1119.



Synthesis of 4-tributylstannyl-2-methyl-1-phenyl-1,3-butadiene (5.24). This material was synthesized in a fashion analogous to that employed for 4-tributylstannyl-1-phenyl-1,3-butadiene (**5.9**), using 4-iodo-2-methyl-1-phenyl-1,3-butadiene (**5.5**) (1.0 g, ~3.7 mmol), Et_2O (40 mL), *n*-BuLi (2.5 mL, 1.8 M in hexanes, 4.4 mmol), and Bu_3SnCl (1.1 mL, 4.1 mmol). The resultant crude yellow oil containing **5.24**, 2-methyl-1-phenyl-1,3-butadiene, and stannane impurities was not subjected to any chromatographic purification as with **5.9**, but was instead used directly in subsequent reactions. The diagnostic ^1H NMR resonances of **5.24** are as follows: ^1H NMR (400 MHz, CDCl_3): δ 7.33-7.15 (m, 5H), 7.13 (d, $J = 13.2$ Hz, 1H), 6.48 (s, 1H), 5.91 (d, $J = 13.6$ Hz, 1H) ppm. Spectral data for 2-methyl-1-phenyl-1,3-butadiene agree with literature values.⁴²

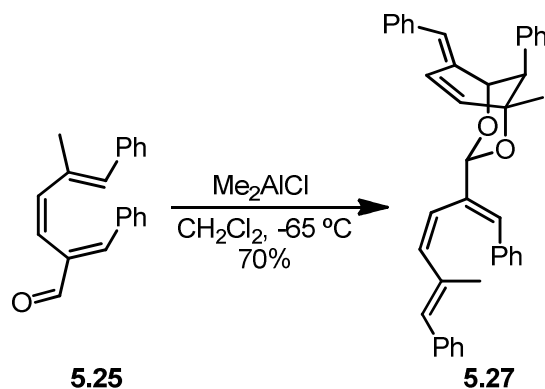


Synthesis of triene 5.25. This material was synthesized in a fashion analogous to that employed for triene **4.3**, using crude 4-tributylstannyl-2-methyl-1-phenyl-1,3-butadiene (**5.24**) (70 mg, ~0.16 mmol), α -iodo-cinnamaldehyde (**5.10**) (42 mg, 0.16 mmol), DMF (2 mL), $\text{Pd(PPh}_3)_4$ (9 mg, 0.008 mmol), copper(I) thiophene-2-carboxylate (34 mg, 0.18 mmol), and CsF (49 mg, 0.32 mmol). The reaction mixture was stirred for 1 h at room temperature instead of 1 h at 0°C . The crude product was purified by silica gel chromatography (5-35% EtOAc in hexanes) yielding 18.2 mg triene **5.25** as a yellow solid (41%). ^1H NMR (400 MHz, C_6D_6): δ 9.39, 7.46 (d, $J = 7.2$ Hz, 2H), 7.16-6.93 (m, 8H), 6.84 (s, 1H), 6.55 (s, 1H), 6.29 (d, $J = 11.6$ Hz, 1H), 6.00 (d, $J = 11.6$ Hz, 1H), 1.86 (s, 3H) ppm; ^1H NMR (500 MHz, CDCl_3): δ 9.56 (s, 1H), 7.71 (d, $J = 6.5$ Hz, 2H), 7.41-7.14 (m, 9H), 6.56-6.50 (m, 2H), 6.12 (d, $J = 12.0$ Hz, 1H), 1.89 (s, 3H) ppm; ^{13}C NMR (125 MHz, CDCl_3): δ 193.6, 147.0, 140.3, 138.7, 137.5, 136.4, 135.2, 132.2, 130.9, 130.5, 129.4, 129.0, 128.3, 127.0, 121.0, 17.4 ppm; IR 3022, 2923, 1684, 1142 cm^{-1} ; **HRMS** (EI⁺) Exact mass calcd for $\text{C}_{20}\text{H}_{18}\text{O}$ $[\text{M}]^+$: 274.1358, found 274.1352.

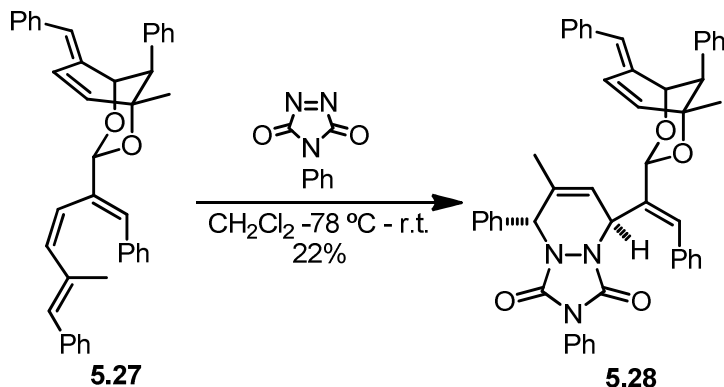


Synthesis of cyclohexadiene 5.26. This material was synthesized in a fashion analogous to that employed for cyclohexadiene **4.4**, using triene **5.25** (2.0 mL, 64 mM in benzene- d_6 , 0.13

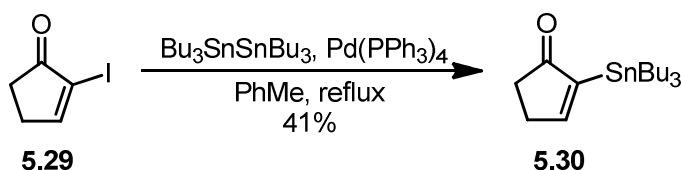
mmol; containing 5 mol% hexamethylbenzene as an internal standard), with the exception that the reaction mixture was heated for 14 h at 75 °C. The crude product was purified by silica gel chromatography (5-35% EtOAc in hexanes) yielding 28 mg cyclohexadiene **5.26** (79%). Quantitative conversion was observed by $^1\text{H NMR}$. $^1\text{H NMR}$ (400 MHz, C_6D_6): δ 9.27 (s, 1H), 7.32 (d, $J = 7.2$ Hz, 2H), 7.20-7.00 (m, 8H), 5.25 (d, $J = 6.0$ Hz, 1H), 5.74 (d, $J = 5.8$ Hz, 1H), 4.31 (s, 1H), 3.40 (s, 1H), 1.37 (s, 3H) ppm; $^1\text{H NMR}$ (500 MHz, CD_2Cl_2): δ 9.45 (s, 1H), 7.35-7.19 (m, 10H), 7.08 (d, $J = 5.5$ Hz, 1H), 6.36 (d, $J = 5.5$ Hz, 1H), 4.00 (s, 1H), 3.56 (s, 1H), 1.79 (s, 3H) ppm; $^{13}\text{C NMR}$ (125 MHz, CD_2Cl_2): δ 192.5, 148.8, 144.0, 143.8, 142.3, 136.6, 129.4, 129.2, 127.74, 127.71, 127.6, 127.4, 121.2, 54.2, 44.8, 23.6 ppm; **IR** 3059, 3025, 1672, 1579, 1493, 698 cm^{-1} ; **HRMS** (EI^+) Exact mass calcd for $\text{C}_{20}\text{H}_{18}\text{O}$ [M] $^+$: 274.1358, found 274.1361.



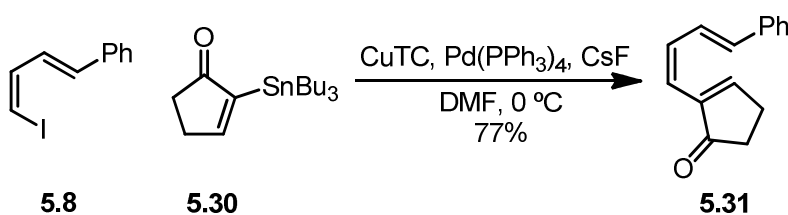
Synthesis of triene dimer 5.27. A Schlenk flask was charged with triene **5.25** (257 mg, 0.938 mmol) and dichloromethane (8 mL) and immersed in liquid nitrogen under positive nitrogen pressure until the reaction mixture was completely frozen. A solution of Me_2AlCl (2.6 mL, 91 mM in dichloromethane, 0.234 mmol) was added dropwise to the frozen reaction mixture, after which the Schlenk flask was sealed and placed in a $-65\text{ }^\circ\text{C}$ bath. After being stirred for 6 h at $-65\text{ }^\circ\text{C}$, the reaction mixture was quenched with water (2 mL) with vigorous stirring, extracted three times with EtOAc, dried over MgSO_4 , filtered, concentrated *in vacuo*, and purified by silica gel chromatography (4-15% EtOAc in hexanes) yielding 180 mg dimer **5.27** as a colorless oil (70%). $^1\text{H NMR}$ (500 MHz, C_6D_6): δ 7.61 (d, $J = 7.5$ Hz, 2H), 7.29 (d, $J = 10$ Hz, 1H), 7.26-7.20 (m, 3H), 7.16-6.93 (m, 15H), 6.71 (s, 1H), 6.51 (d, $J = 12.5$ Hz, 1H), 6.38 (s, 1H), 6.25 (d, $J = 12.5$ Hz, 1H), 6.11 (s, 1H), 5.45 (d, $J = 10$ Hz, 1H), 4.67 (d, $J = 2.5$ Hz, 1H), 3.82 (d, $J = 2.5$ Hz, 1H), 2.06 (s, 3H), 1.35 (s, 3H) ppm; $^1\text{H NMR}$ (500 MHz, CD_2Cl_2): δ 7.54 (d, $J = 7.8$ Hz, 2H), 7.37-7.19 (m, 15H), 7.18-7.14 (m, 1H), 7.14 (d, $J = 7.0$ Hz, 2H), 6.92 (s, 1H), 6.63 (s, 1H), 6.56 (s, 1H), 6.25 (app q, $J = 12.5$ Hz, 2H), 5.81 (s, 1H), 5.68 (d, $J = 10.0$ Hz, 1H), 4.62 (d, $J = 2.0$ Hz, 1H), 3.64 (d, $J = 2.5$ Hz, 1H), 1.87 (s, 3H), 1.29 (s, 3H) ppm; $^{13}\text{C NMR}$ (125 MHz, CD_2Cl_2): δ 137.8, 137.6, 137.2, 137.0, 136.2, 136.1, 136.0, 134.4, 131.7, 131.4, 130.9, 129.6, 129.5, 129.3, 129.1, 128.3, 128.1, 128.0, 127.9, 127.6, 127.2, 126.8, 126.4, 125.0, 93.6, 79.2, 73.6, 25.1, 17.1 ppm; **HRMS** (ESI^+) Exact mass calcd for $\text{C}_{40}\text{H}_{36}\text{O}_2\text{Na}$ [$\text{M}+\text{Na}$] $^+$: 571.2608, found 571.2596.



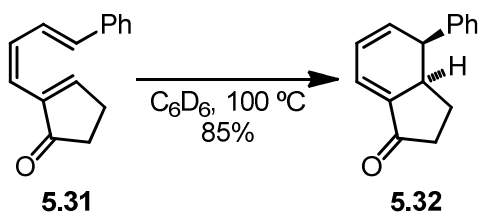
Synthesis of Diels-Alder adduct 5.28. A round-bottom flask was charged with triene dimer **5.27** (145 mg, 0.26 mmol) and dichloromethane (3 mL). After cooling the reaction mixture to -78 °C, a solution of 4-phenyl-1,2,4-triazoline-3,5-dione (1 mL, 0.32 M in dichloromethane, 0.32 mmol) was added dropwise. The reaction mixture was slowly warmed to 10 °C over the course of 6 h, after which it was concentrated *in vacuo* to a yellow oil. The crude product was purified by silica gel chromatography to yield a 2:1 mixture of diastereomers, which were separated *via* reverse-phase HPLC (85:15 MeCN:H₂O) to yield 43 mg major diastereomer **5.28** (22%) and 29 mg minor diastereomer (15%). Characterization data for the minor diastereomer are as follows: ¹H NMR (500 MHz, C₆D₆): δ 7.90 (s, 1H), 7.85 (d, *J* = 7.6 Hz, 2H), 7.65 (d, *J* = 7.5 Hz, 2H), 7.48 (d, *J* = 7.5 Hz, 2H), 7.38 (d, *J* = 10.0 Hz, 1H), 7.25-6.85 (m, 17H), 6.80 (t, *J* = 7.5 Hz, 1H), 6.69 (s, 1H), 5.98 (s, 2H), 5.46 (d, *J* = 10.0 Hz, 1H), 5.18 (s, 1H), 5.09 (s, 1H), 4.51 (s, 1H), 3.68 (s, 1H), 1.31 (s, 3H), 1.22 (s, 3H) ppm; ¹H NMR (500 MHz, CDCl₃): δ 7.62 (d, *J* = 8.0 Hz, 2H), 7.53-7.47 (m, 3H), 7.46-7.15 (m, 21H), 6.71 (s, 1H), 5.76-5.69 (m, 3H), 5.62 (s, 1H), 4.97 (s, 1H), 4.47 (s, 1H), 3.68 (s, 1H), 1.62 (s, 3H), 1.36 (s, 3H) ppm; ¹³C NMR (125 MHz, CDCl₃): δ 151.7, 150.9, 137.7, 136.6, 136.3, 135.9, 135.7, 133.8, 132.5, 132.3, 132.0, 131.8, 130.7, 130.1, 129.8, 129.12, 129.07, 129.0, 128.93, 128.85, 128.7, 128.6, 128.5, 128.4, 128.1, 127.8, 127.7, 127.3, 125.5, 119.4, 88.8, 79.2, 74.4, 60.2, 53.7, 52.4, 25.8, 20.5 ppm; HRMS (ESI⁺) Exact mass calcd for C₄₈H₄₁O₄N₃Na [M+Na]⁺: 746.2989, found 746.2980. Characterization data for the major diastereomer **5.28** are as follows: ¹H NMR (500 MHz, C₆D₆): δ 7.87 (d, *J* = 7.6 Hz, 2H), 7.78-7.73 (m, 3H), 7.42 (d, *J* = 10.0 Hz, 1H), 7.33-7.28 (m, 4H), 7.22 (t, *J* = 7.5 Hz, 2H), 7.15-7.00 (m, 10H), 6.94 (t, *J* = 7.7 Hz, 3H), 6.81 (t, *J* = 7.5 Hz, 1H), 6.32 (s, 1H), 6.04 (s, 1H), 5.97 (s, 1H), 5.78 (d, *J* = 10.0 Hz, 1H), 5.33 (s, 1H), 5.17 (d, *J* = 4.0 Hz, 1H), 4.61 (d, *J* = 2.5 Hz, 1H), 3.80 (d, *J* = 2.5 Hz, 1H), 1.26 (s, 3H), 1.12 (s, 3H) ppm; ¹H NMR (500 MHz, CDCl₃): δ 7.65 (d, *J* = 8.0 Hz, 2H), 7.50-7.14 (m, 24H), 6.60 (s, 1H), 5.80 (s, 2H), 5.73 (d, *J* = 10.0 Hz, 1H), 5.67 (d, *J* = 4.5 Hz, 1H), 5.29 (s, 1H), 4.55 (d, *J* = 2.5 Hz, 1H), 3.66 (d, *J* = 2.5 Hz, 1H), 1.68 (s, 3H), 1.19 (s, 3H) ppm; ¹³C NMR (125 MHz, CDCl₃): δ 151.7, 151.6, 137.7, 136.3, 135.9, 135.6, 135.2, 134.7, 133.0, 131.9, 131.8, 131.5, 131.4, 129.8, 129.54, 129.48, 129.08, 129.06, 128.9, 128.7, 128.63, 128.55, 128.5, 128.0, 127.8, 127.7, 127.2, 125.1, 119.9, 91.1, 79.7, 74.3, 60.6, 53.6, 52.2, 25.6, 20.5 ppm; HRMS (ESI⁺) Exact mass calcd for C₄₈H₄₁O₄N₃Na [M+Na]⁺: 746.2989, found 746.2980.



Synthesis of 2-tributylstannyl-2-cyclopentenone (5.30). A round bottom flask was charged with toluene (60 mL), 2-iodo-2-cyclopentenone (**5.29**) (1.44 g, 6.9 mmol), Pd(PPh₃)₄ (800 mg, 0.7 mmol), and Bu₃SnSnBu₃ (7.0 mL, 13.8 mmol). The flask was equipped with a reflux condenser and the reaction mixture was heated at reflux for 16 h. The cooled reaction mixture was diluted with hexanes and washed three times with water and once with brine. The organic solution was then dried over MgSO₄, filtered, concentrated *in vacuo*, and purified by silica gel chromatography (5% EtOAc in hexanes) yielding 1.06 g product as a colorless oil (41%). ¹H NMR (500 MHz, CDCl₃): δ 7.74 (t, *J*_{H-H} = 2.0 Hz, *J*_{Sn-H} = 13.5 Hz, 1H), 2.72-2.69 (m, 2H), 2.28-2.24 (m, 2H) 1.54-1.36 (m, 6H), 1.31-1.20 (m, 6H), 1.05-0.87 (t, *J*_{H-H} = 8.0 Hz, *J*_{Sn-H} = 26.5 Hz, 6H), 0.84 (t, *J* = 6.0 Hz, 9H) ppm; ¹³C NMR (125 MHz, CDCl₃): δ 215.4, 173.6, 149.0, 33.9, 32.2, 29.3 (*J*_{Sn-C} = 10.4 Hz), 27.4 (*J*_{Sn-C} = 29.8 Hz), 13.9, 9.5 (*J*_{Sn-C} = 174 Hz) ppm; IR 2956, 2923, 2870, 2852, 1691, 1278, 1164, 696 cm⁻¹; HRMS (EI⁺) Exact mass calcd for C₁₃H₂₃OSn [M-Bu]⁺: 315.0771, found 315.0775.

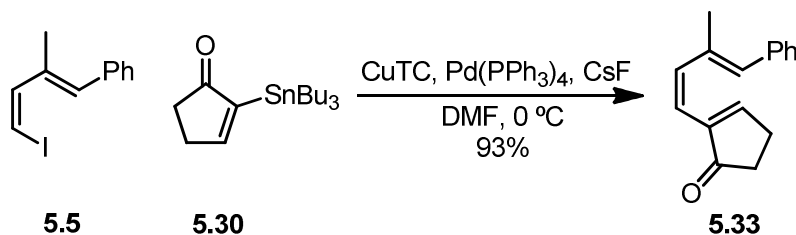


Synthesis of triene 5.31. This material was synthesized in a fashion analogous to that employed for triene **4.3**, using 4-iodo-1-phenyl-1,3-butadiene (**5.8**) (168 mg, 0.65 mmol), 2-tributylstannyl-2-cyclopentenone (**5.30**) (162 mg, 0.44 mmol), DMF (5 mL), Pd(PPh₃)₄ (25 mg, 0.022 mmol), copper(I) thiophene-2-carboxylate (92 mg, 0.48 mmol), and CsF (132 mg, 0.87 mmol). The crude product was purified by silica gel chromatography (23-25% EtOAc in hexanes) yielding 71 mg triene **5.31** as a yellow oil (77%). ¹H NMR (400 MHz, C₆D₆): δ 7.31 (d, *J* = 7.5 Hz, 2H), 7.27 (dd, *J* = 15.5, 10.5 Hz, 1H), 7.16-7.12 (m, 2H), 7.05 (t, *J* = 7.2 Hz, 1H), 6.97-6.95 (m, 1H), 6.50 (d, *J* = 15.5 Hz, 1H), 6.39-6.29 (m, 2H), 1.94-1.90 (m, 2H), 1.83-1.80 (m, 2H) ppm; ¹H NMR (400 MHz, CDCl₃): δ 7.75 (s, 1H), 7.46 (d, *J* = 7.2 Hz, 2H), 7.37 (t, *J* = 7.4 Hz, 2H), 7.31-7.18 (m, 1H), 6.75 (d, *J* = 15.6 Hz, 1H), 6.51 (t, *J* = 11.4 Hz, 1H), 6.12 (d, *J* = 11.2 Hz, 1H), 2.81-2.77 (m, 2H), 2.55-2.48 (m, 2H) ppm; ¹³C NMR (100 MHz, CDCl₃): δ 208.7, 159.4, 141.4, 137.1, 135.9, 133.6, 128.8, 128.2, 126.8, 125.3, 118.6, 34.3, 27.3 ppm; IR 2960, 2921, 2903, 1695, 1451, 993, 956, 751 cm⁻¹; HRMS (EI⁺) Exact mass calcd for C₁₅H₁₄O [M]⁺: 210.1045, found 210.1046.

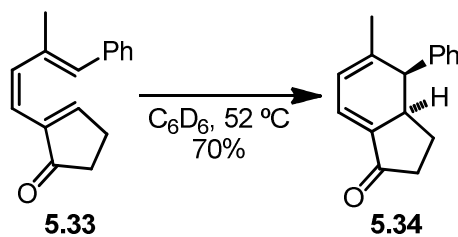


Synthesis of cyclohexadiene 5.32. This material was synthesized in a fashion analogous to that employed for cyclohexadiene **4.4**, using triene **5.31** (1.6 mL, 24 mM in benzene-*d*₆, 0.038 mmol; containing 5 mol% hexamethylbenzene as an internal standard), with the exception that the reaction mixture was heated for 20 h at 100 °C. The crude product was purified by silica gel chromatography (20-23% EtOAc in hexanes) yielding 6.8 mg cyclohexadiene **5.32** (85%). ¹H NMR (500 MHz, C₆D₆): δ 7.06-6.92 (m, 3H), 6.88 (d, *J* = 6.5 Hz, 2H), 6.73 (t, *J* = 4.5 Hz, 1H),

5.89 (dd, $J = 9.5, 5.5$ Hz, 1H), 5.72 (dd, $J = 9.3, 5.8$ Hz, 1H), 3.19 (dd, $J = 11.5, 5.5$ Hz, 1H), 2.91-2.80 (m, 1H), 1.89-1.71 (m, 2H), 1.38-1.29 (m, 1H), 0.95-0.85 (m, 1H) ppm; $^{13}\text{C NMR}$ (125 MHz, C_6D_6): δ 203.6, 137.8, 136.6, 135.8, 129.8, 129.0, 127.8, 124.9, 124.7, 43.1, 40.5, 38.8, 23.2 ppm; **IR** 3029, 2960, 1705, 1644, 1561, 1226, 764, 700 cm^{-1} ; **HRMS** (EI^+) Exact mass calcd for $\text{C}_{15}\text{H}_{14}\text{O}$ $[\text{M}]^+$: 210.1045, found 210.1048.



Synthesis of triene 5.33. This material was synthesized in a fashion analogous to that employed for triene **4.3**, using 4-iodo-2-methyl-1-phenyl-1,3-butadiene (**5.5**) (180 mg, 0.67 mmol), 2-tributylstannyl-2-cyclopentenone (**5.30**) (264 mg, 0.71 mmol), DMF (6.7 mL), $\text{Pd(PPh}_3)_4$ (39 mg, 0.03 mmol), copper(I) thiophene-2-carboxylate (140 mg, 0.73 mmol), and CsF (202 mg, 1.3 mmol). The crude product was purified by silica gel chromatography (17-20% EtOAc in hexanes) yielding 139 mg product as a yellow oil (93%). $^1\text{H NMR}$ (400 MHz, CDCl_3): δ 7.62 (m, 1H), 7.38-7.18 (m, 5H), 6.52 (s, 1H), 6.36 (d, $J = 12.2$ Hz, 1H), 5.98 (d, $J = 12.2$ Hz, 1H), 2.66-2.60 (m, 2H), 2.43-2.38 (m, 2H), 1.95 (s, 3H) ppm; $^{13}\text{C NMR}$ (100 MHz, CDCl_3): δ 208.5, 159.3, 142.1, 139.0, 137.6, 135.6, 131.6, 129.3, 128.4, 127.0, 117.6, 34.3, 27.1, 17.9 ppm; **IR** 2956, 2922, 1705, 1573, 1439, 737, 698 cm^{-1} ; **HRMS** (FAB^+) Exact mass calcd for $\text{C}_{16}\text{H}_{17}\text{O}$ $[\text{M}+\text{H}]^+$: 225.1285, found 225.1279.



Thermal synthesis of cyclohexadiene 5.34. This material was synthesized in a fashion analogous to that employed for cyclohexadiene **4.4**, using triene **5.33** (0.96 mL, 40 mM in benzene- d_6 , 0.038 mmol; containing 5 mol% hexamethylbenzene as an internal standard), with the exception that the reaction mixture was heated for 3 h at 52 °C. The crude product was purified by silica gel chromatography (16-19% EtOAc in hexanes) yielding 6 mg product (70%). Quantitative conversion was observed by $^1\text{H NMR}$. $^1\text{H NMR}$ (500 MHz, CDCl_3): δ 7.28-7.19 (m, 3H), 7.10-7.01 (m, 2H), 6.88-6.84 (m, 1H), 6.20 (d, $J = 5.5$ Hz, 1H) 3.50 (d, $J = 10.5$ Hz, 1H), 3.49-3.40 (m, 1H), 2.33-2.19 (m, 2H), 2.00-1.90 (m, 1H), 1.81 (s, 3H), 1.20-1.09 (m, 1H) ppm; $^{13}\text{C NMR}$ (125 MHz, CDCl_3): δ 205.4, 147.7, 137.0, 133.6, 129.2, 128.7, 127.5, 126.8, 121.5, 49.0, 41.0, 39.3, 23.2, 22.8 ppm; **IR** 2963, 1702, 1649, 1574, 1225, 699 cm^{-1} ; **LRMS** 224; **HRMS** (EI^+) Exact mass calcd for $\text{C}_{16}\text{H}_{14}\text{O}$ $[\text{M}-2\text{H}]^+$: 222.1045, found 222.1045.

Catalyzed synthesis of cyclohexadiene 5.34. A solution of triene **5.33** (450 μL , 48 mM in benzene- d_6 , 0.022 mmol; containing 25 mol% 1,1,2,2-tetrachloroethane as an internal standard) was combined in an NMR tube with a solution of Me_2AlCl (80 μL , 240 mM in benzene- d_6 , 0.019 mmol). The NMR tube was sealed and kept at room temperature for 1.75 h.

The reaction mixture was quenched with water and extracted three times with dichloromethane. The organic solution was then dried over MgSO₄, filtered, concentrated *in vacuo*, and purified by silica gel chromatography (17% EtOAc in hexanes) yielding 4.7 mg product (97%). Quantitative conversion was observed by ¹H NMR. Spectral data were identical to those listed above.

Kinetic order in Me₂AlCl for triene 5.33. A solution of triene **5.33** (400 μL, 48 mM in benzene-*d*₆, 0.0192 mmol; containing 25 mol% 1,1,2,2-tetrachloroethane as an internal standard) was combined in a J-Young NMR tube with varying amounts of a 240 mM solution of Me₂AlCl in benzene-*d*₆. Benzene-*d*₆ was then added such that the total volume of the solution in the tube was 480 μL. The J-Young tube was then sealed and the reaction mixture was frozen in ice-water until ready for kinetic analysis. Once ready for analysis, the solution was thawed and agitated, the tube was placed in an AV-500 NMR probe pre-equilibrated to 28.0 °C, and the reaction was monitored for disappearance of **5.33** and appearance of **5.34** (*via* single scan ¹H NMR spectroscopy). The concentration of Me₂AlCl was determined by integration against the internal standard. The first order rate constants and Me₂AlCl concentrations can be found numerically in Table 9 and graphically in Figure 5.

Table 9. First order rate constants of the electrocyclization of **5.33** in the presence of varying concentrations of Me₂AlCl.

Entry	[Me ₂ AlCl] (mM)	k _{obs} (s ⁻¹)
1	6.51	2.5(4)x10 ⁻⁴
2	10.4	3.5(6)x10 ⁻⁴
3	22.4	7.5(3)x10 ⁻⁴
4	30.2	1.1(1)x10 ⁻³
5	38.4	1.32(2)x10 ⁻³

Titration of 5.33 with Me₂AlCl. A solution of **5.33** (500 μL, 63 mM in toluene-*d*₈, 0.0315 mmol; containing 25 mol% 1,1,2,2-tetrachloroethane as an internal standard) was added to an NMR tube, which was subsequently sealed with a rubber septum. The NMR tube was placed in an AV-500 NMR spectrometer pre-equilibrated to -25 °C and the shift of the ¹H NMR spectrum of **5.33** was monitored as a function of added Me₂AlCl (317 mM in toluene-*d*₈). The Me₂AlCl solution was added by ejecting the sample from the NMR probe, injecting the solution through the septum, agitating the sample, and replacing it in the NMR probe. The concentration of Me₂AlCl was determined by integration against the internal standard. The graphical representations of the change in chemical shift of two representative resonances are shown in Figure 6.

Activation parameter measurements for the thermal cyclization of 5.33. A solution of **5.33** (400 μL, 48 mM in benzene-*d*₆, 0.0192 mmol; containing 25 mol% 1,1,2,2-tetrachloroethane as an internal standard) and benzene-*d*₆ (80 μL) were combined in a J-Young NMR tube. The J-Young tube was then sealed, the solution was agitated, the tube was placed in an AV-500 NMR probe pre-equilibrated to the desired temperature, and the reaction was monitored for disappearance of **5.33** and appearance of **5.34** (*via* single scan ¹H NMR spectroscopy). The NMR probe for the above experiments was calibrated to 40.2, 52.4, 59.5, 60.6, 68.7, and 76.8 °C. The first order rate constants and the Eyring plot for these experiments are displayed in Table 10 and Figure 10, respectively.

Table 10. First order rate constants of the thermal electrocyclization of **5.33** at various temperatures.

Entry	Temperature (°C)	k_{obs} (s ⁻¹)
1	40.2	$9.74(5) \times 10^{-5}$
2	52.4	$3.1(3) \times 10^{-4}$
3	59.5	$6.7(5) \times 10^{-4}$
4	60.6	$7.7(1) \times 10^{-4}$
5	68.7	$1.6(1) \times 10^{-3}$
6	76.8	$3.2(3) \times 10^{-3}$

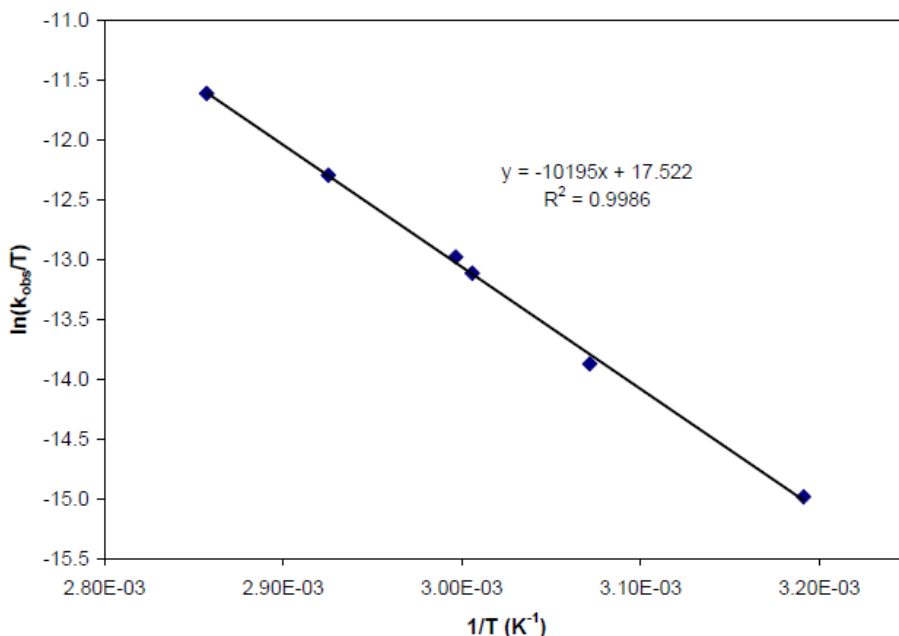


Figure 10. Eyring plot for the thermal electrocyclization of **5.33** in C₆D₆.

Activation parameter measurements for the catalyzed cyclization of 5.33. A solution of **5.33** (400 μ L, 48 mM in benzene-*d*₆, 0.0192 mmol; containing 25 mol% 1,1,2,2-tetrachloroethane as an internal standard) was combined in a J-Young NMR tube with a solution of Me₂AlCl (80 μ L, 240 mM in benzene-*d*₆, 0.0192 mmol). The J-Young tube was then sealed, the solution was agitated, the tube was placed in an AV-500 NMR probe pre-equilibrated to the desired temperature, and the reaction was monitored for disappearance of **5.33** and appearance of **5.34** (via single scan ¹H NMR spectroscopy). The concentration of Me₂AlCl was determined to be 40(5) mM in all experiments by integration against the internal standard. The NMR probe for the above experiments was calibrated to 8.7, 11.6, 14.5, 17.4, 20.4, 23.9, 28.0, 32.1, and 36.2 °C. The first order rate constants and the Eyring plot for these experiments are displayed in Table 11 and Figure 11, respectively.

Table 11. First order rate constants of the catalyzed electrocyclization of **5.33** at various temperatures.

Entry	Temperature (°C)	k_{obs} (s ⁻¹)
1	8.7	$1.59(3) \times 10^{-4}$
2	11.6	$2.3(1) \times 10^{-4}$

3	14.5	$3.2(1)\times 10^{-4}$
4	17.4	$4.32(5)\times 10^{-4}$
5	20.4	$5.72(8)\times 10^{-4}$
6	23.9	$8.5(2)\times 10^{-4}$
7	28.0	$1.32(2)\times 10^{-3}$
8	32.1	$2.11(6)\times 10^{-3}$
9	36.2	$3.13(8)\times 10^{-3}$

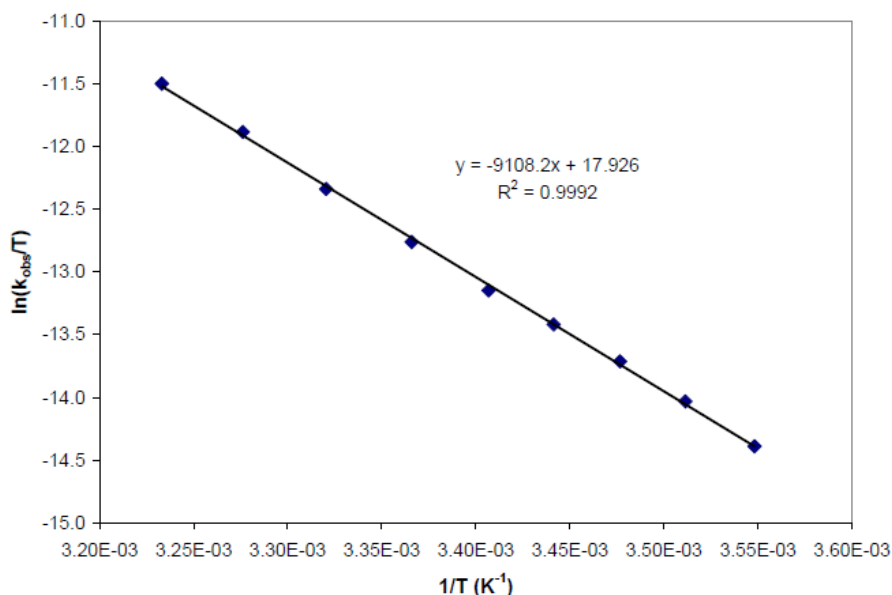
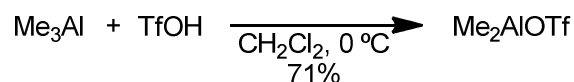


Figure 11. Eyring plot for the catalyzed electrocyclization of **5.33** in C_6D_6 .

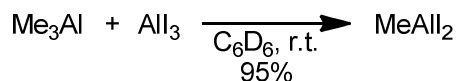
Screen for catalysis of the electrocyclization of triene 5.33—representative procedure. An NMR tube was charged with 2,6-di-*tert*-butyl-4-methylpyridine (3 mg, 0.0146 mmol; only added for reactions using $Cu(OTf)_2$, $Sc(OTf)_3$, and $BF_3\cdot OEt_2$), Lewis acid (0.0120 mmol), benzene- d_6 (230 μL), and triene **5.33** (250 μL , 48 mM in benzene- d_6 , 0.0120 mmol; containing 25 mol% 1,1,2,2-tetrachloroethane as an internal standard). The NMR tube was then sealed under vacuum and the reaction was monitored at regular intervals *via* 1H NMR. The reaction mixture was kept at room temperature initially, and heated in a circulating oil bath at increasing temperatures until significant conversion was observed.

Note: the rate acceleration of the methylaluminum diiodide-catalyzed reaction shown in Table 4 was obtained by assembling the reaction mixture as described above, after which the NMR tube was placed in an AV-500 NMR probe pre-equilibrated to 8.7 $^{\circ}C$, and the reaction was monitored for disappearance of **5.33** and appearance of **5.34** (*via* single scan 1H NMR spectroscopy). The first order rate constant for this reaction was $1.2(2)\times 10^{-3} s^{-1}$ which represents a 600-fold rate acceleration when compared to the first order rate constant of $2.1\times 10^{-6} s^{-1}$ at 8.7 $^{\circ}C$ obtained by extrapolation of the Eyring plot for the thermal cyclization of **5.33**.

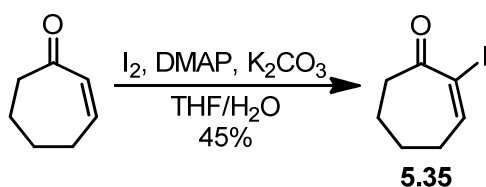


Synthesis of dimethylaluminum triflate. Adapted from the procedure developed by Yamamoto et al.⁴³ A solution of trimethylaluminum (10 mL, 113 mM in dichloromethane, 1.13

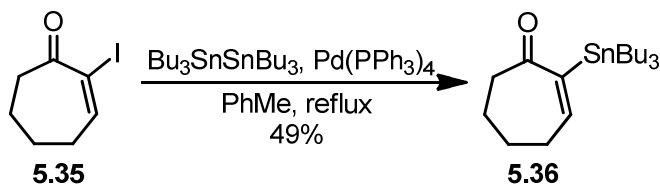
mmol) was cooled to 0 °C. To this solution was added trifluoromethanesulfonic acid (100 μL, 1.13 mmol) dropwise over the course of 5 minutes, which resulted in the evolution of a gas from the reaction mixture (*Caution*: care should be taken to perform this addition slowly). The reaction mixture was stirred at 0 °C for 10 minutes after which it was warmed to room temperature and stirred a further 10 minutes, after which the solution became cloudy. Concentration of the reaction mixture *in vacuo* yielded 161 mg product as a white solid (70 %). $^1\text{H NMR}$ (400 MHz, C_6D_6): δ -0.48 (s) ppm; $^{19}\text{F NMR}$ (376 MHz, C_6D_6): δ -76.0 (s) ppm. For reference, spectral data for trimethylaluminum are as follows: $^1\text{H NMR}$ (500 MHz, C_6D_6): δ -0.36 (s) ppm.



Synthesis of methylaluminum diiodide. A J-Young tube was charged with aluminum iodide (84.8 mg, 0.208 mmol), benzene- d_6 (565 μL), and trimethylaluminum (435 μL, 239 mM in benzene- d_6 , 0.104 mmol), yielding a heterogeneous mixture. The tube was sealed and stored at room temperature for 2 hours, during which time the reaction mixture became homogeneous. Concentration of the reaction mixture *in vacuo* yielded 87.3 mg product as a white solid (95%). $^1\text{H NMR}$ (500 MHz, C_6D_6): δ 0.28 (s) ppm; **LRMS** 296; For reference, spectral data for trimethylaluminum are as follows: $^1\text{H NMR}$ (500 MHz, C_6D_6): δ -0.36 (s) ppm.

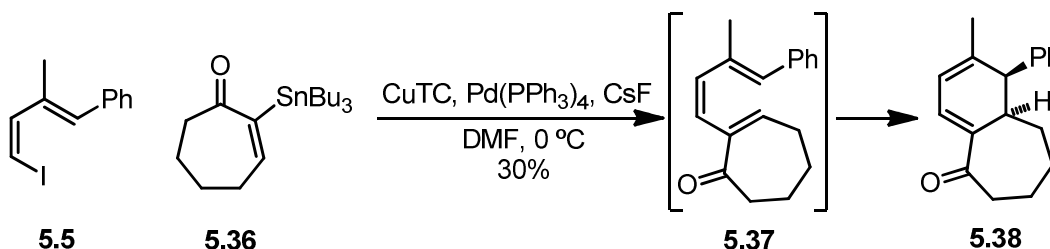


Synthesis of 2-iodocyclohept-2-enone (5.35). To a flame-dried round bottom flask was added cyclohept-2-enone (1.0 mL, 7.2 mmol), I_2 (3.42 g, 13.4 mmol), 4-dimethylaminopyridine (439 mg, 3.59 mmol), potassium carbonate (1.487 g, 10.8 mmol) and a solution of 1:1 THF- H_2O (100mL). The mixture was stirred at room temperature for 2 h, diluted with H_2O (100 mL), and extracted four times with Et_2O . The combined organic extracts were washed twice with $\frac{1}{2}$ -saturated aqueous $\text{Na}_2\text{S}_2\text{O}_3$, twice with 0.1N HCl, and once with brine. The organic solution was then dried over MgSO_4 , filtered, concentrated *in vacuo*, and purified by silica gel chromatography (2-18% EtOAc in hexanes) yielding 756 mg product as a yellow oil (45%). $^1\text{H NMR}$ (400 MHz, CDCl_3): δ 7.66 (t, $J = 6.6$ Hz, 1H), 2.70 (t, $J = 6.4$ Hz, 2H), 2.42-2.37 (m, 2H), 1.84-1.73 (m, 4H) ppm; $^{13}\text{C NMR}$ (100 MHz, CDCl_3): δ 198.3, 155.8, 106.8, 40.3, 31.6, 25.0, 21.6 ppm; **IR** 3054, 2945, 2869, 1679, 1265 cm^{-1} ; **HRMS** (EI^+) Exact mass calcd for $\text{C}_7\text{H}_9\text{IO}$ [$\text{M}]^+$: 235.9701, found 235.9698.

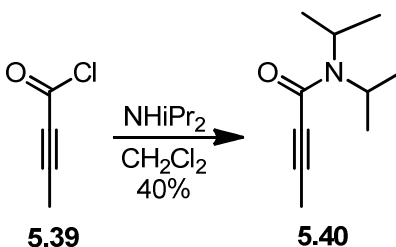


Synthesis of 2-(tributylstannyl)cyclohept-2-enone (5.36). This material was synthesized in a fashion analogous to that employed for stannane **5.30**, using toluene (10 mL), 2-iodo-2-cycloheptenone **5.35** (250 mg, 1.06 mmol), $\text{Pd}(\text{PPh}_3)_4$ (127 mg, 0.11 mmol), and

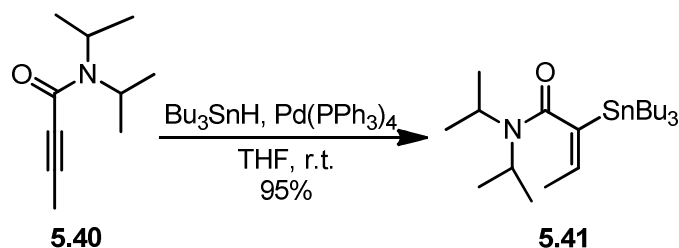
Bu₃SnSnBu₃ (1.06 mL, 2.12 mmol). The crude product was purified by silica gel chromatography (5% EtOAc in hexanes) yielding 208 mg product as a yellow oil (49%). ¹H NMR (500 MHz, CDCl₃): δ 6.58 (t, *J*_{H-H} = 5.5 Hz, *J*_{Sn-H} = 32.5 Hz, 1H), 2.55 (t, *J* = 6.8 Hz, 2H), 2.41 (q, *J* = 5.5 Hz, 2H), 1.79-1.68 (m, 4H), 1.53-1.36 (m, 6H), 1.31-1.23 (m, 6H), 0.92-0.82 (m, 15H) ppm; ¹³C NMR (125 MHz, CDCl₃): δ 209.5, 152.1, 149.8, 42.9, 32.2, 29.3 (*J*_{Sn-C} = 10.0 Hz), 27.5 (*J*_{Sn-C} = 29.6 Hz), 25.7, 22.7, 13.9, 10.5 (*J*_{Sn-C} = 164 Hz) ppm; IR 2955, 2926, 2870, 2854, 1652, 1456 cm⁻¹; HRMS (EI⁺) Exact mass calcd for C₁₅H₂₇OSn [M-Bu]⁺: 343.1084, found 343.1093.



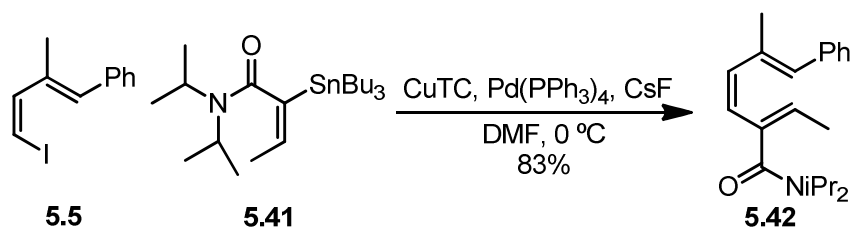
Synthesis of cyclohexadiene 5.38. This material was synthesized in a fashion analogous to that employed for triene 4.3, using 2-(tributylstannyl)cyclohept-2-enone (5.36) (207 mg, 0.52 mmol), 4-iodo-2-methyl-1-phenyl-1,3-butadiene (5.5) (132 mg, 0.49 mmol), DMF (5.2 mL), Pd(PPh₃)₄ (23 mg, 0.020 mmol), copper(I) thiophene-2-carboxylate (103 mg, 0.54 mmol), and CsF (149 mg, 0.98 mmol). The crude product was purified by silica gel chromatography (2-18% EtOAc in hexanes) yielding 39 mg cyclohexadiene 5.38 as a yellow oil (30%). ¹H NMR (500 MHz, CDCl₃): δ 7.31-7.15 (m, 5H), 6.69-6.65 (m, 1H), 5.96 (d, *J* = 5.0 Hz, 1H), 3.23 (d, *J* = 8.9 Hz, 1H), 3.11 (d, *J* = 10.0 Hz, 1H), 2.65-2.61 (m, 2H), 1.85-1.65 (m, 6H), 1.55-1.36 (m, 2H), 1.01 (q, *J* = 12.0 Hz, 1H) ppm; ¹³C NMR (100 MHz, CDCl₃): δ 205.2, 147.6, 139.2, 138.1, 131.1, 129.6, 128.3, 127.3, 119.9, 52.7, 43.3, 39.7, 30.0, 29.5, 23.6, 22.5 ppm; IR 3024, 2926, 2856, 1668, 1567 cm⁻¹; HRMS (ESI⁺) Exact mass calcd for C₁₈H₂₀O [M]⁺: 252.1514, found 252.1507.



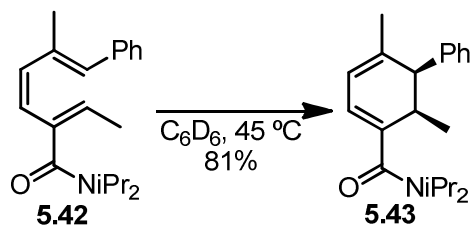
Synthesis of *N,N*-diisopropylbut-2-ynamide (5.40). A round-bottom flask was charged with butynoyl chloride (5.39) (1.22 g, 11.9 mmol) and dichloromethane (50 mL). Diisopropylamine (3.34 mL, 23.8 mmol) was then added dropwise to the resultant solution, which was subsequently stirred for 15 h at room temperature. The organic solution was then washed four times with 0.1N HCl and once with brine, after which it was dried over MgSO₄, filtered, concentrated *in vacuo*, and purified by silica gel chromatography (12-30% EtOAc in hexanes) yielding 803 mg product as a yellow oil (40%). ¹H NMR (300 MHz, CDCl₃): δ 4.46 (quintet, 6.7 Hz, 1H), 3.58-3.39 (m, 1H), 1.91 (s, 3H), 1.27 (d, *J* = 6.9 Hz, 6H), 1.14 (d, *J* = 6.6 Hz, 6H) ppm; ¹³C NMR (100 MHz, CDCl₃): δ 153.8, 87.0, 74.9, 50.4, 45.5, 21.0, 20.2, 4.1 ppm; IR 2999, 2976, 1625, 1437, 1332 cm⁻¹; HRMS (EI⁺) Exact mass calcd for C₁₀H₁₇NO [M]⁺: 167.1310, found 167.1310.



Synthesis of (E)-N,N-diisopropyl-2-(tributylstannyl)but-2-enamide (5.41). A round bottom flask was charged with Pd(PPh₃)₄ (52 mg, 0.045 mmol), THF (50 mL), and *N,N*-diisopropylbut-2-ynamide (**5.40**) (445 mg, 2.66 mmol). To this solution was added Bu₃SnH (2.0 mL, 1.33 M in THF, 2.66 mmol) dropwise over 2 h at room temperature. The reaction mixture was stirred for an additional 2 h, concentrated *in vacuo*, and purified by silica gel chromatography (5-30% EtOAc in hexanes) to yield 1.16 g product as a colorless oil (95%). ¹H NMR (CDCl₃, 500 MHz): δ 5.61 (q, *J*_{H-H} = 6.5 Hz, *J*_{Sn-H} = 31 Hz, 1H; vinyl CH, nOe to CH₂CH₃), 4.10 (septet, *J* = 6.6 Hz, 1H), 3.33 (septet, *J* = 6.6 Hz, 1H), 1.71 (d, *J* = 6.5 Hz, 3H), 1.51-1.36 (m, 12H), 1.27 (sextet, *J* = 7.3 Hz, 6H), 1.12 (d, *J* = 6.5 Hz, 3H), 1.05 (d, *J* = 6.5 Hz, 3H), 0.94-0.88 (m, 6H), 0.84 (t, *J* = 7.2 Hz, 9H; CH₂CH₃, nOe to vinyl CH) ppm; ¹³C NMR (CDCl₃, 125 MHz): δ 173.0, 143.0, 135.1, 50.0, 45.6, 29.0, (*J*_{Sn-C} = 9.8 Hz), 27.5 (*J*_{Sn-C} = 30 Hz), 21.4, 21.3, 21.2, 20.9, 18.1, 13.8, 10.3 (*J*_{Sn-C} = 165 Hz) ppm; IR 2958, 2929, 2871, 1615, 1432, 1295 cm⁻¹; HRMS (EI⁺) Exact mass calcd for C₂₂H₄₄NOSn [M-H]⁺: 458.2445, found 458.2452.



Synthesis of triene 5.42. This material was synthesized in a fashion analogous to that employed for triene **4.3**, using 4-iodo-2-methyl-1-phenyl-1,3-butadiene (**5.5**) (56 mg, 0.205 mmol), (*E*)-*N,N*-diisopropyl-2-(tributylstannyl)but-2-enamide (**5.41**) (94 mg, 0.205 mmol), DMF (3.0 mL), Pd(PPh₃)₄ (12 mg, 0.010 mmol), copper(I) thiophene-2-carboxylate (43 mg, 0.226 mmol), and CsF (62 mg, 0.41 mmol). The crude product was purified by silica gel chromatography (12-20% EtOAc in hexanes) yielding 53 mg product as a yellow oil (83%). ¹H NMR (500 MHz, CDCl₃): δ 7.37-7.14 (m, 5H), 6.62 (s, 1H), 6.07 (d, *J* = 12 Hz, 1H), 5.81 (d, *J* = 12 Hz, 1H), 5.68 (q, *J* = 7.2 Hz, 1H), 4.09 (septet, *J* = 6.6 Hz, 1H), 3.35 (septet, *J* = 6.9 Hz, 1H), 2.08 (s, 3H), 1.77 (d, *J* = 7.0 Hz, 3H), 1.38 (d, *J* = 6.8 Hz, 6H), 1.13 (d, *J* = 6.7 Hz, 6H) ppm; ¹³C NMR (125 MHz, CDCl₃): δ 169.2, 137.91, 137.88, 135.4, 134.3, 132.4, 129.5, 128.9, 128.2, 126.6, 125.9, 50.5, 45.8, 21.2, 20.9, 18.5, 15.3 ppm; IR 2965, 1630, 1439 cm⁻¹; HRMS (EI⁺) Exact mass calcd for C₂₁H₂₉NO [M]⁺: 311.2250, found 311.2249.



Thermal synthesis of cyclohexadiene 5.43. This material was synthesized in a fashion analogous to that employed for cyclohexadiene 4.4, using triene 5.42 (0.48 mL, 40 mM in benzene-*d*₆, 0.019 mmol; containing 5 mol% hexamethylbenzene as an internal standard), with the exception that the reaction mixture was heated for 13 h at 45 °C. The crude product was purified by silica gel chromatography (12-20% EtOAc in hexanes) yielding 29 mg product (81%). Quantitative conversion was observed by ¹H NMR. ¹H NMR (500 MHz, CDCl₃): δ 7.29-7.20 (m, 5H), 5.97 (d, *J* = 4.6 Hz, 1H), 5.84 (m, 1H), 4.04-3.87 (broad, 1H), 3.30 (m, 2H), 3.18 (d, *J* = 8.6 Hz, 1H), 1.74 (s, 3H), 1.46-1.29 (broad, 6H), 1.13-1.00 (broad, 3H), 0.89 (d, *J* = 7.4 Hz, 3H), 0.81-0.65 (broad, 3H) ppm; ¹³C NMR (125 MHz, CDCl₃): δ 170.8, 140.2, 137.7, 136.1, 129.8, 128.0, 127.1, 120.6, 120.0, 50.6, 50.1 (broad), 45.6 (broad), 35.5, 22.4, 20.6 (broad), 14.2 ppm; IR 2966, 2931, 1621, 1438, 1330 cm⁻¹; HRMS (EI⁺) Exact mass calcd for C₂₁H₂₉NO [M]⁺: 311.2249, found 311.2245.

Kinetic analysis of the catalyzed cyclization of triene 5.42. A solution of triene 5.42 (400 μL, 48 mM in benzene-*d*₆, 0.0192 mmol; containing 5 mol% hexamethylbenzene as an internal standard) was combined in a J-Young NMR tube with Me₂AlCl (80 μL, 144 mM in benzene-*d*₆, 0.0111 mmol). The J-Young tube was then sealed, the solution was agitated, the tube was placed in an AV-500 NMR probe pre-equilibrated to 45.3 °C, and the reaction was monitored for disappearance of 5.42 and appearance of 5.43 (*via* single scan ¹H NMR spectroscopy). The concentration of Me₂AlCl was determined by integration against the internal standard to be 23 mM (0.58 equiv). Under these conditions the first order rate constant for the cyclization was 2.1(4) × 10⁻³ s⁻¹, which represents a 7-fold rate acceleration when compared to the first order rate constant of 3.1 × 10⁻⁴ s⁻¹ at 45.3 °C obtained by extrapolation of the Eyring plot for the thermal cyclization of 5.42.

Activation parameter measurements for the thermal cyclization of 5.42. A solution of 5.42 (400 μL, 48 mM in benzene-*d*₆, 0.0192 mmol; containing 5 mol% hexamethylbenzene as an internal standard) and benzene-*d*₆ (80 μL) were combined in a J-Young NMR tube. The J-Young tube was then sealed, the solution was agitated, the tube was placed in an AV-500 NMR probe pre-equilibrated to the desired temperature, and the reaction was monitored for disappearance of 5.42 and appearance of 5.43 (*via* single scan ¹H NMR spectroscopy). The NMR probe for the above experiments was calibrated to 36.2, 44.3, 52.4, 60.6, and 68.7 °C. The first order rate constants and the Eyring plot for these experiments are displayed in Table 12 and Figure 12, respectively.

Table 12. First order rate constants of the thermal electrocyclization of 5.33 at various temperatures.

Entry	Temperature (°C)	k _{obs} (s ⁻¹)
1	36.2	1.1(1) × 10 ⁻⁴
2	44.3	2.8(2) × 10 ⁻⁴
3	52.4	6.1(1) × 10 ⁻⁴
4	60.6	1.34(1) × 10 ⁻³
5	68.7	2.94(9) × 10 ⁻³

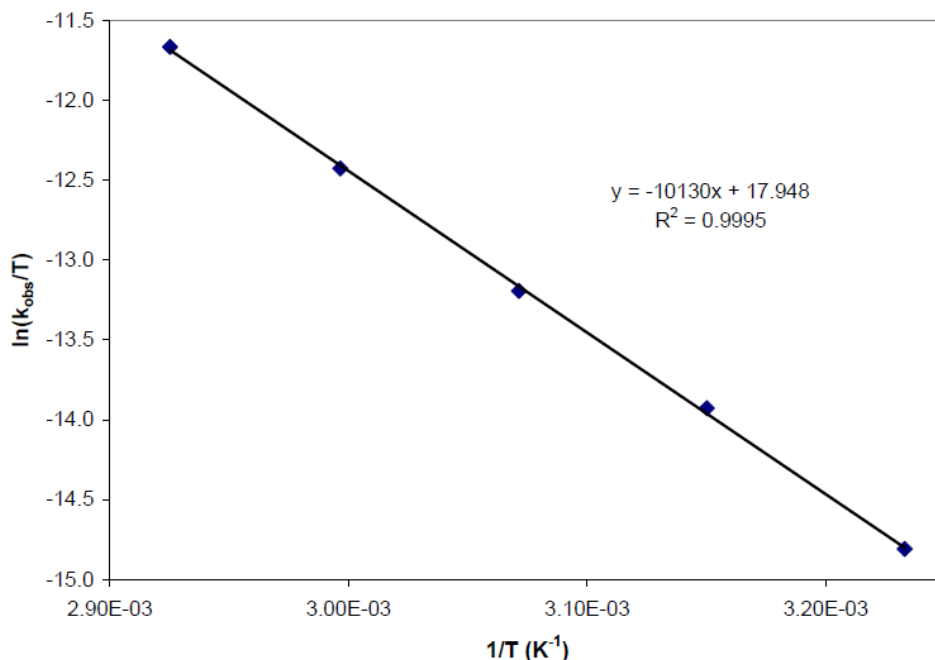
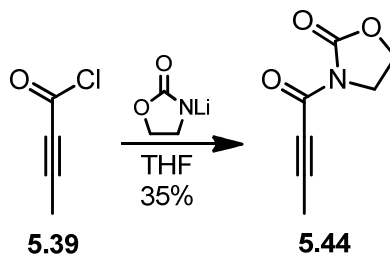
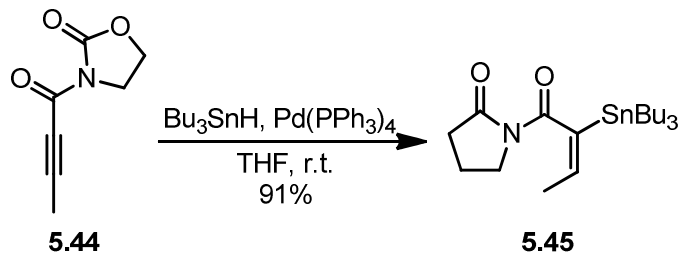


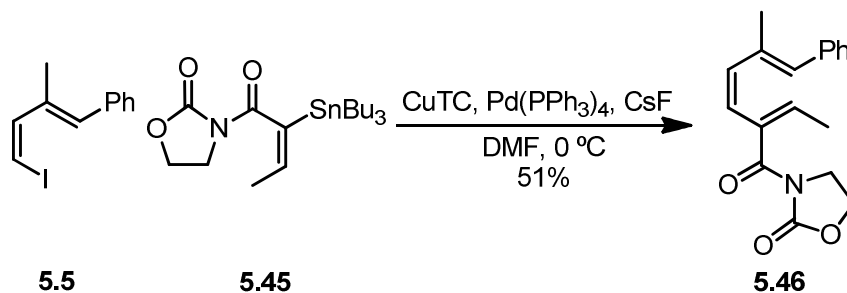
Figure 12. Eyring plot for the thermal electrocyclicization of **5.42** in C₆D₆.



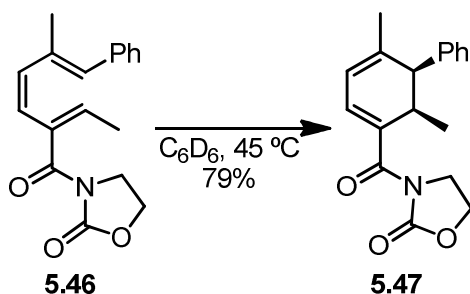
Synthesis of 3-(but-2-ynoyl)oxazolidin-2-one (5.44). A round-bottom flask was charged with oxazolidin-2-one (1.04 g, 11.9 mmol) and THF (150 mL), after which the resultant solution was cooled to -78 °C. To this solution was added *n*-BuLi (5.25 mL, 2.5 M in hexanes, 13.1 mmol) over the course of 5 minutes, after which the reaction mixture was warmed to 0 °C, stirred for 20 minutes at this temperature, and cooled to -78 °C. To this solution was added butynoyl chloride (**5.39**) (20 mL, 595 mM in THF, 11.9 mmol) dropwise, after which the reaction mixture was warmed to room temperature, stirred for 30 minutes, quenched with saturated aqueous NH₄Cl (50 mL), and extracted twice with diethyl ether. The combined organic extracts were washed twice with brine, dried over MgSO₄, filtered, concentrated *in vacuo*, and purified by silica gel chromatography (40-52% EtOAc in hexanes) yielding 633 mg product as a yellow oil (35%). ¹H NMR (400 MHz, CDCl₃): δ 4.38 (t, *J* = 8.0 Hz, 2H), 4.00 (t, *J* = 8.0 Hz, 2H), 2.07 (s, 3H) ppm; ¹³C NMR (100 MHz, CDCl₃): δ 152.3, 151.0, 95.1, 72.7, 62.1, 42.5, 4.7 ppm; IR 2994, 1787, 1658, 1334, 1220 cm⁻¹; HRMS (EI⁺) Exact mass calcd for C₇H₈NO₃ [M+H]⁺: 154.0504, found 154.0504.



Synthesis of (E)-3-(2-(tributylstannyl)but-2-enoyl)oxazolidin-2-one (5.45). A round bottom flask was charged with Pd(PPh₃)₄ (81 mg, 0.070 mmol), THF (50 mL), and 3-(but-2-ynoyl)oxazolidin-2-one (**5.44**) (633 mg, 4.13 mmol). To this solution was added Bu₃SnH (3.0 mL, 1.38 M in THF, 4.14 mmol) dropwise over 2 h at room temperature. The reaction mixture was stirred for an additional 1 h, concentrated *in vacuo*, and purified by silica gel chromatography (14-19% EtOAc in hexanes) to yield 1.68 g product as a colorless oil (91%). ¹H NMR (CDCl₃, 400 MHz): δ 5.86 (q, *J*_{H-H} = 6.6 Hz, *J*_{Sn-H} = 28 Hz, 1H; vinyl CH, nOe to CH₂CH₃), 4.38 (t, *J* = 8.1 Hz, 2H), 4.02 (t, *J* = 8.1 Hz, 2H), 1.73 (d, *J* = 6.6 Hz, 3H), 1.57-1.34 (m, 6H), 1.33-1.20 (m, 6H), 1.01-0.90 (m, 6H; CH₂CH₃, nOe to vinyl CH), 0.86 (t, *J* = 7.3 Hz, 9H) ppm; ¹³C NMR (CDCl₃, 125 MHz): δ 173.0, 153.1, 140.6, 139.1, 62.2, 42.6, 28.9 (*J*_{Sn-C} = 9.8 Hz), 27.5 (*J*_{Sn-C} = 30 Hz), 18.1, 13.9, 11.2 (*J*_{Sn-C} = 173 Hz) ppm; IR 2956, 2922, 2871, 2853, 1782, 1666 cm⁻¹; HRMS (EI⁺) Exact mass calcd for C₁₉H₃₆NO₃Sn [M+H]⁺: 446.1717, found 446.1709.



Synthesis of triene 5.46. This material was synthesized in a fashion analogous to that employed for triene **4.3**, using 4-iodo-2-methyl-1-phenyl-1,3-butadiene (**5.5**) (35 mg, 0.13 mmol), (E)-3-(2-(tributylstannyl)but-2-enoyl)oxazolidin-2-one (**5.45**) (58 mg, 0.13 mmol), DMF (2.0 mL), Pd(PPh₃)₄ (7.6 mg, 0.0065 mmol), copper(I) thiophene-2-carboxylate (27 mg, 0.14 mmol), and CsF (39 mg, 0.26 mmol). The crude product was purified by silica gel chromatography (20-25% EtOAc in hexanes) yielding 20 mg product as a yellow oil (51%). ¹H NMR (400 MHz, CDCl₃): δ 7.37-7.15 (m, 5H), 6.31 (s, 1H), 6.04-5.95 (m, 2H), 5.92 (d, *J* = 11.6 Hz, 1H), 3.75-3.61 (m, 4H), 1.94 (s, 3H), 1.70 (d, *J* = 7.6 Hz, 3H) ppm; ¹³C NMR (100 MHz, CDCl₃): δ 168.6, 152.0, 137.1, 136.6, 134.6, 133.8, 133.5, 129.3, 128.5, 128.4, 127.9, 127.1, 61.7, 42.4, 18.4, 15.0 ppm; IR 3003, 2916, 1784, 1683, 1382, 1358, 1287 cm⁻¹; HRMS (EI⁺) Exact mass calcd for C₁₈H₁₉NO₃ [M]⁺: 297.1365, found 297.1369.



Thermal synthesis of cyclohexadiene 5.47. This material was synthesized in a fashion analogous to that employed for cyclohexadiene **4.4**, using triene **5.46** (1.0 mL, 40 mM in benzene-*d*₆, 0.040 mmol; containing 25 mol% 1,1,2,2-tetrachloroethane as an internal standard), with the exception that the reaction mixture was heated for 8 h at 45 °C. The crude product was purified by silica gel chromatography (20-27% EtOAc in hexanes) yielding 9.5 mg product (79%). Quantitative conversion was observed by ¹H NMR. ¹H NMR (500 MHz, CDCl₃): δ 7.34-7.17 (m, 5H), 6.47 (d, *J* = 5.5 Hz, 1H), 5.97 (d, *J* = 5.5 Hz, 1H), 4.45-4.34 (m, 2H), 4.08 (q, *J* = 9.5 Hz, 1H), 3.96-3.89 (m, 1H), 3.44 (d, *J* = 8.5 Hz, 1H), 3.31 (quintet, *J* = 7.5 Hz, 1H), 1.76 (s, 3H), 0.88 (d, *J* = 7.0 Hz, 3H) ppm; ¹³C NMR (125 MHz, CDCl₃): δ 169.7, 153.5, 146.4, 138.5, 132.0, 131.9, 130.0, 128.2, 127.1, 119.6, 62.3, 51.9, 43.4, 34.2, 22.8, 14.1 ppm; IR 2965, 2924, 1784, 1668 cm⁻¹; HRMS (EI⁺) Exact mass calcd for C₁₈H₁₉LiNO₃ [M+Li]⁺: 304.1525, found 304.1529.

X-Ray Crystal Structure Determination of 5.28. A colorless block was mounted on a Cryoloop with Paratone oil. Data were collected in a nitrogen gas stream at using phi and omega scans. Crystal-to-detector distance was 60 mm and exposure time was 10 seconds per frame using a scan width of 0.5°. Data collection was 97.9% complete to 25.00° in θ. Indexing and unit cell refinement by CELL_NOW indicated a twinned crystal with two unique domains, both of which having the same primitive, triclinic lattice parameters. The twin law that relates the two domains is given by the 3 × 3 matrix [-1.002 -0.739 -0.003 0.005 1.002 0.005 0.005 -0.004 -1.000]. The space group was found to be P-1 (No. 2). The twinned data were integrated and separated into domains using the Bruker SAINT⁴⁴ software program and scaled using the TWINABS software program. Solution by direct methods (SHELXS-97)⁴⁵ produced a complete heavy-atom phasing model consistent with the proposed structure. All non-hydrogen atoms were refined anisotropically by full-matrix least-squares (SHELXL-97).⁴⁶ All hydrogen atoms were placed using a riding model. Their positions were constrained relative to their parent atom using the appropriate HFIX command in SHELXL-97.⁴⁶ Crystallographic data for **5.28** are summarized in Tables 13-18.

Table 13. Crystal data and structure refinement for **5.28**.

Empirical formula	C101 H94 N6 O8	
Formula weight	1519.82	
Temperature	139(2) K	
Wavelength	0.71073 Å	
Crystal system	Triclinic	
Space group	P-1	
Unit cell dimensions	a = 14.152(4) Å	α = 89.705(4)°
	b = 14.743(4) Å	β = 84.895(4)°

	$c = 21.851(6) \text{ \AA}$	$\gamma = 67.217(3)^\circ$.
Volume	$4184.8(19) \text{ \AA}^3$	
Z	2	
Density (calculated)	1.206 Mg/m^3	
Absorption coefficient	0.076 mm^{-1}	
F(000)	1612	
Crystal size	$0.20 \times 0.15 \times 0.15 \text{ mm}^3$	
Crystal color/habit	colorless block	
Theta range for data collection	$2.44 \text{ to } 25.69^\circ$.	
Index ranges	$-17 \leq h \leq 17, -16 \leq k \leq 17, -26 \leq l \leq 26$	
Reflections collected	33309	
Independent reflections	15908 [R(int) = 0.0706]	
Completeness to theta = 25.00°	97.9%	
Absorption correction	Semi-empirical from equivalents	
Max. and min. transmission	0.9886 and 0.9849	
Refinement method	Full-matrix least-squares on F^2	
Data / restraints / parameters	15908 / 5 / 1043	
Goodness-of-fit on F^2	1.022	
Final R indices [$I > 2\sigma(I)$]	R1 = 0.0663, wR2 = 0.1286	
R indices (all data)	R1 = 0.1771, wR2 = 0.1603	
Largest diff. peak and hole	0.533 and $-0.484 \text{ e.\AA}^{-3}$	

Table 14. Atomic coordinates ($\times 10^4$) and equivalent isotropic displacement parameters ($\text{\AA}^2 \times 10^3$) for **5.28**. U(eq) is defined as one third of the trace of the orthogonalized U_{ij} tensor.

	x	y	z	U(eq)
C(1)	12122(2)	766(2)	4009(1)	24(1)
C(2)	11613(2)	375(2)	4521(1)	27(1)
C(3)	11401(2)	706(2)	5100(1)	24(1)
C(4)	11651(2)	1556(2)	5303(1)	27(1)
C(5)	11974(2)	2940(2)	4792(1)	24(1)
C(6)	12961(2)	1984(2)	3963(1)	25(1)
C(7)	10934(2)	256(2)	5597(1)	39(1)
C(8)	12597(2)	1235(2)	5662(1)	27(1)
C(9)	12627(2)	1781(2)	6165(1)	39(1)
C(10)	13509(3)	1487(3)	6483(2)	50(1)
C(11)	14353(3)	653(3)	6292(2)	48(1)
C(12)	14338(2)	111(3)	5786(2)	42(1)
C(13)	13462(2)	401(2)	5472(1)	34(1)
C(14)	13079(2)	3614(2)	4140(2)	30(1)
C(15)	13430(2)	4013(3)	4592(2)	49(1)
C(16)	13829(3)	4721(3)	4445(2)	66(1)
C(17)	13902(3)	5004(3)	3855(2)	73(1)
C(18)	13548(3)	4603(3)	3404(2)	64(1)
C(19)	13118(2)	3910(2)	3541(2)	43(1)
C(20)	11400(2)	1177(2)	3508(1)	23(1)

C(21)	11541(2)	783(2)	2949(1)	27(1)
C(22)	12415(2)	-77(2)	2658(1)	27(1)
C(23)	13430(2)	-170(2)	2641(1)	31(1)
C(24)	14216(2)	-981(2)	2348(1)	43(1)
C(25)	14001(2)	-1704(3)	2071(2)	50(1)
C(26)	12992(3)	-1608(2)	2071(2)	53(1)
C(27)	12212(2)	-794(2)	2360(1)	41(1)
C(28)	10416(2)	2052(2)	3708(1)	26(1)
C(29)	8685(2)	2897(2)	3488(1)	25(1)
C(30)	8250(2)	2957(2)	4149(1)	29(1)
C(31)	8596(2)	3490(2)	4574(1)	32(1)
C(32)	9273(2)	3890(2)	4391(1)	31(1)
C(33)	9697(2)	3836(2)	3729(1)	27(1)
C(34)	8918(2)	3795(2)	3301(1)	27(1)
C(35)	10102(2)	4634(2)	3582(2)	42(1)
C(36)	7583(2)	2508(2)	4289(2)	37(1)
C(37)	7104(3)	2351(2)	4876(2)	46(1)
C(38)	6188(3)	2194(2)	4872(2)	64(1)
C(39)	5723(3)	1991(3)	5397(3)	86(2)
C(40)	6136(4)	1930(3)	5945(2)	83(2)
C(41)	7041(4)	2074(3)	5966(2)	75(1)
C(42)	7530(3)	2278(2)	5428(2)	64(1)
C(43)	7896(2)	4681(2)	3275(1)	27(1)
C(44)	7312(2)	4670(2)	2804(1)	35(1)
C(45)	6344(2)	5388(2)	2762(2)	42(1)
C(46)	5940(2)	6141(2)	3197(2)	40(1)
C(47)	6513(2)	6173(2)	3667(2)	40(1)
C(48)	7485(2)	5448(2)	3708(1)	35(1)
C(49)	7975(2)	2249(2)	971(1)	26(1)
C(50)	8395(2)	1493(2)	449(1)	29(1)
C(51)	8618(2)	1665(2)	-129(2)	29(1)
C(52)	8473(2)	2687(2)	-335(1)	26(1)
C(53)	8205(2)	4282(2)	172(1)	26(1)
C(54)	7208(2)	4097(2)	1013(2)	26(1)
C(55)	9017(2)	876(2)	-632(1)	42(1)
C(56)	7574(2)	3149(2)	-723(1)	31(1)
C(57)	7686(3)	3656(2)	-1237(2)	50(1)
C(58)	6863(4)	4125(3)	-1580(2)	80(2)
C(59)	5930(4)	4096(3)	-1397(2)	86(2)
C(60)	5795(3)	3603(3)	-886(2)	80(2)
C(61)	6633(2)	3108(3)	-547(2)	54(1)
C(62)	7144(2)	5795(2)	814(2)	31(1)
C(63)	6734(2)	6440(3)	363(2)	49(1)
C(64)	6368(3)	7440(3)	490(2)	76(2)
C(65)	6375(3)	7787(3)	1063(3)	77(2)
C(66)	6780(3)	7139(3)	1518(2)	63(1)

C(67)	7179(2)	6119(3)	1392(2)	46(1)
C(68)	8761(2)	2068(2)	1440(1)	23(1)
C(69)	8659(2)	1760(2)	2006(1)	29(1)
C(70)	7774(2)	1645(2)	2352(1)	26(1)
C(71)	6809(2)	2416(2)	2427(1)	29(1)
C(72)	6017(2)	2318(2)	2807(1)	32(1)
C(73)	6162(2)	1451(2)	3100(2)	41(1)
C(74)	7107(2)	683(2)	3031(1)	41(1)
C(75)	7909(2)	786(2)	2668(1)	34(1)
C(76)	9729(2)	2212(2)	1215(1)	26(1)
C(77)	11487(2)	1743(2)	1380(1)	26(1)
C(78)	11870(2)	1577(2)	705(1)	25(1)
C(79)	11455(2)	2424(2)	319(1)	30(1)
C(80)	10794(2)	3299(2)	550(1)	29(1)
C(81)	10439(2)	3470(2)	1226(1)	26(1)
C(82)	11272(2)	2786(2)	1614(1)	25(1)
C(83)	10044(2)	4542(2)	1426(1)	37(1)
C(84)	12554(2)	676(2)	506(1)	33(1)
C(85)	12955(2)	296(2)	-123(2)	36(1)
C(86)	13964(3)	-382(3)	-237(2)	63(1)
C(87)	14369(3)	-776(3)	-819(2)	85(2)
C(88)	13771(3)	-510(3)	-1300(2)	69(1)
C(89)	12772(3)	152(3)	-1206(2)	55(1)
C(90)	12371(3)	550(2)	-621(2)	44(1)
C(91)	12265(2)	2936(2)	1632(1)	24(1)
C(92)	12882(2)	2458(2)	2094(1)	31(1)
C(93)	13838(2)	2494(2)	2129(1)	37(1)
C(94)	14188(2)	3035(2)	1715(2)	35(1)
C(95)	13575(2)	3525(2)	1268(2)	39(1)
C(96)	12623(2)	3477(2)	1223(1)	32(1)
C(900)	10852(5)	2664(5)	-1802(5)	285(6)
C(901)	10297(9)	2177(7)	-2162(4)	508(18)
C(902)	10035(7)	3053(4)	-2589(5)	269(6)
C(903)	9749(9)	2440(9)	-3038(4)	410(14)
C(904)	8944(6)	3194(7)	-3389(6)	305(7)
N(1)	12467(2)	1473(2)	4283(1)	24(1)
N(2)	11765(2)	2097(2)	4753(1)	24(1)
N(3)	12679(2)	2880(2)	4291(1)	26(1)
N(4)	7662(2)	3215(2)	692(1)	24(1)
N(5)	8370(2)	3299(2)	217(1)	24(1)
N(6)	7519(2)	4758(2)	675(1)	26(1)
O(1)	11596(1)	3592(1)	5185(1)	34(1)
O(2)	13547(1)	1706(1)	3498(1)	32(1)
O(3)	9628(1)	2020(1)	3367(1)	27(1)
O(4)	10617(1)	2910(1)	3594(1)	28(1)
O(5)	8587(1)	4648(1)	-227(1)	33(1)

O(6)	6632(1)	4267(1)	1485(1)	33(1)
O(7)	10568(1)	1542(1)	1508(1)	27(1)
O(8)	9539(1)	3207(1)	1365(1)	27(1)

Table 15. Bond lengths (Å) for **5.28**.

C(1)-N(1)	1.462(3)	C(18)-H(18)	0.9500
C(1)-C(2)	1.509(4)	C(19)-H(19)	0.9500
C(1)-C(20)	1.523(4)	C(20)-C(21)	1.322(4)
C(1)-H(1)	1.0000	C(20)-C(28)	1.517(3)
C(2)-C(3)	1.323(4)	C(21)-C(22)	1.482(3)
C(2)-H(2)	0.9500	C(21)-H(21)	0.9500
C(3)-C(7)	1.504(4)	C(22)-C(27)	1.379(4)
C(3)-C(4)	1.506(4)	C(22)-C(23)	1.386(4)
C(4)-N(2)	1.470(3)	C(23)-C(24)	1.389(4)
C(4)-C(8)	1.526(4)	C(23)-H(23)	0.9500
C(4)-H(4)	1.0000	C(24)-C(25)	1.372(4)
C(5)-O(1)	1.214(3)	C(24)-H(24)	0.9500
C(5)-N(2)	1.388(3)	C(25)-C(26)	1.380(4)
C(5)-N(3)	1.393(3)	C(25)-H(25)	0.9500
C(6)-O(2)	1.216(3)	C(26)-C(27)	1.383(4)
C(6)-N(1)	1.365(3)	C(26)-H(26)	0.9500
C(6)-N(3)	1.403(3)	C(27)-H(27)	0.9500
C(7)-H(7A)	0.9800	C(28)-O(3)	1.411(3)
C(7)-H(7B)	0.9800	C(28)-O(4)	1.417(3)
C(7)-H(7C)	0.9800	C(28)-H(28)	1.0000
C(8)-C(9)	1.378(4)	C(29)-O(3)	1.458(3)
C(8)-C(13)	1.390(4)	C(29)-C(30)	1.508(4)
C(9)-C(10)	1.400(4)	C(29)-C(34)	1.529(4)
C(9)-H(9)	0.9500	C(29)-H(29)	1.0000
C(10)-C(11)	1.376(4)	C(30)-C(36)	1.361(4)
C(10)-H(10)	0.9500	C(30)-C(31)	1.452(4)
C(11)-C(12)	1.374(4)	C(31)-C(32)	1.340(4)
C(11)-H(11)	0.9500	C(31)-H(31)	0.9500
C(12)-C(13)	1.387(4)	C(32)-C(33)	1.507(4)
C(12)-H(12)	0.9500	C(32)-H(32)	0.9500
C(13)-H(13)	0.9500	C(33)-O(4)	1.485(3)
C(14)-C(15)	1.374(4)	C(33)-C(35)	1.516(4)
C(14)-C(19)	1.382(4)	C(33)-C(34)	1.527(4)
C(14)-N(3)	1.429(4)	C(34)-C(43)	1.534(3)
C(15)-C(16)	1.390(4)	C(34)-H(34)	1.0000
C(15)-H(15)	0.9500	C(35)-H(35A)	0.9800
C(16)-C(17)	1.361(5)	C(35)-H(35B)	0.9800
C(16)-H(16)	0.9500	C(35)-H(35C)	0.9800
C(17)-C(18)	1.376(5)	C(36)-C(37)	1.457(4)
C(17)-H(17)	0.9500	C(36)-H(36)	0.9500
C(18)-C(19)	1.397(4)	C(37)-C(42)	1.382(5)

C(37)-C(38)	1.402(4)	C(58)-H(58)	0.9500
C(38)-C(39)	1.361(5)	C(59)-C(60)	1.368(6)
C(38)-H(38)	0.9500	C(59)-H(59)	0.9500
C(39)-C(40)	1.368(6)	C(60)-C(61)	1.404(5)
C(39)-H(39)	0.9500	C(60)-H(60)	0.9500
C(40)-C(41)	1.381(6)	C(61)-H(61)	0.9500
C(40)-H(40)	0.9500	C(62)-C(67)	1.365(4)
C(41)-C(42)	1.400(5)	C(62)-C(63)	1.371(4)
C(41)-H(41)	0.9500	C(62)-N(6)	1.435(3)
C(42)-H(42)	0.9500	C(63)-C(64)	1.380(4)
C(43)-C(44)	1.380(4)	C(63)-H(63)	0.9500
C(43)-C(48)	1.384(4)	C(64)-C(65)	1.357(5)
C(44)-C(45)	1.380(3)	C(64)-H(64)	0.9500
C(44)-H(44)	0.9500	C(65)-C(66)	1.377(5)
C(45)-C(46)	1.372(4)	C(65)-H(65)	0.9500
C(45)-H(45)	0.9500	C(66)-C(67)	1.404(4)
C(46)-C(47)	1.376(4)	C(66)-H(66)	0.9500
C(46)-H(46)	0.9500	C(67)-H(67)	0.9500
C(47)-C(48)	1.388(3)	C(68)-C(69)	1.331(4)
C(47)-H(47)	0.9500	C(68)-C(76)	1.506(4)
C(48)-H(48)	0.9500	C(69)-C(70)	1.471(4)
C(49)-N(4)	1.465(3)	C(69)-H(69)	0.9500
C(49)-C(50)	1.508(4)	C(70)-C(75)	1.394(4)
C(49)-C(68)	1.526(4)	C(70)-C(71)	1.394(3)
C(49)-H(49)	1.0000	C(71)-C(72)	1.388(4)
C(50)-C(51)	1.322(4)	C(71)-H(71)	0.9500
C(50)-H(50)	0.9500	C(72)-C(73)	1.378(4)
C(51)-C(55)	1.507(4)	C(72)-H(72)	0.9500
C(51)-C(52)	1.511(4)	C(73)-C(74)	1.373(4)
C(52)-N(5)	1.474(3)	C(73)-H(73)	0.9500
C(52)-C(56)	1.521(4)	C(74)-C(75)	1.384(4)
C(52)-H(52)	1.0000	C(74)-H(74)	0.9500
C(53)-O(5)	1.217(3)	C(75)-H(75)	0.9500
C(53)-N(5)	1.380(3)	C(76)-O(7)	1.419(3)
C(53)-N(6)	1.390(3)	C(76)-O(8)	1.420(3)
C(54)-O(6)	1.220(3)	C(76)-H(76)	1.0000
C(54)-N(4)	1.370(3)	C(77)-O(7)	1.445(3)
C(54)-N(6)	1.398(3)	C(77)-C(78)	1.512(4)
C(55)-H(55A)	0.9800	C(77)-C(82)	1.529(4)
C(55)-H(55B)	0.9800	C(77)-H(77)	1.0000
C(55)-H(55C)	0.9800	C(78)-C(84)	1.352(4)
C(56)-C(61)	1.376(4)	C(78)-C(79)	1.458(4)
C(56)-C(57)	1.378(4)	C(79)-C(80)	1.335(3)
C(57)-C(58)	1.386(4)	C(79)-H(79)	0.9500
C(57)-H(57)	0.9500	C(80)-C(81)	1.506(4)
C(58)-C(59)	1.362(6)	C(80)-H(80)	0.9500

C(81)-O(8)	1.476(3)	C(93)-C(94)	1.384(4)
C(81)-C(83)	1.510(3)	C(93)-H(93)	0.9500
C(81)-C(82)	1.541(3)	C(94)-C(95)	1.373(4)
C(82)-C(91)	1.510(4)	C(94)-H(94)	0.9500
C(82)-H(82)	1.0000	C(95)-C(96)	1.389(4)
C(83)-H(83A)	0.9800	C(95)-H(95)	0.9500
C(83)-H(83B)	0.9800	C(96)-H(96)	0.9500
C(83)-H(83C)	0.9800	C(900)-C(901)	1.518(5)
C(84)-C(85)	1.466(4)	C(900)-H(90A)	0.9800
C(84)-H(84)	0.9500	C(900)-H(90B)	0.9800
C(85)-C(90)	1.387(4)	C(900)-H(90C)	0.9800
C(85)-C(86)	1.391(4)	C(901)-C(902)	1.535(5)
C(86)-C(87)	1.378(5)	C(901)-H(90D)	0.9900
C(86)-H(86)	0.9500	C(901)-H(90E)	0.9900
C(87)-C(88)	1.369(5)	C(902)-C(903)	1.520(5)
C(87)-H(87)	0.9500	C(902)-H(90F)	0.9900
C(88)-C(89)	1.370(4)	C(902)-H(90G)	0.9900
C(88)-H(88)	0.9500	C(903)-C(904)	1.512(5)
C(89)-C(90)	1.385(4)	C(903)-H(90H)	0.9900
C(89)-H(89)	0.9500	C(903)-H(90I)	0.9900
C(90)-H(90)	0.9500	C(904)-H(90J)	0.9800
C(91)-C(96)	1.385(4)	C(904)-H(90K)	0.9800
C(91)-C(92)	1.397(4)	C(904)-H(90L)	0.9800
C(92)-C(93)	1.383(4)	N(1)-N(2)	1.417(3)
C(92)-H(92)	0.9500	N(4)-N(5)	1.417(3)

Table 16. Bond angles (°) for **5.28**.

N(1)-C(1)-C(2)	107.6(2)	O(1)-C(5)-N(3)	128.1(3)
N(1)-C(1)-C(20)	114.5(2)	N(2)-C(5)-N(3)	106.0(3)
C(2)-C(1)-C(20)	110.5(2)	O(2)-C(6)-N(1)	126.8(3)
N(1)-C(1)-H(1)	108.0	O(2)-C(6)-N(3)	127.2(3)
C(2)-C(1)-H(1)	108.0	N(1)-C(6)-N(3)	105.9(2)
C(20)-C(1)-H(1)	108.0	C(3)-C(7)-H(7A)	109.5
C(3)-C(2)-C(1)	125.9(3)	C(3)-C(7)-H(7B)	109.5
C(3)-C(2)-H(2)	117.1	H(7A)-C(7)-H(7B)	109.5
C(1)-C(2)-H(2)	117.1	C(3)-C(7)-H(7C)	109.5
C(2)-C(3)-C(7)	123.4(3)	H(7A)-C(7)-H(7C)	109.5
C(2)-C(3)-C(4)	120.9(3)	H(7B)-C(7)-H(7C)	109.5
C(7)-C(3)-C(4)	115.7(3)	C(9)-C(8)-C(13)	118.8(3)
N(2)-C(4)-C(3)	107.7(2)	C(9)-C(8)-C(4)	121.0(3)
N(2)-C(4)-C(8)	112.1(2)	C(13)-C(8)-C(4)	120.1(3)
C(3)-C(4)-C(8)	113.0(2)	C(8)-C(9)-C(10)	120.3(3)
N(2)-C(4)-H(4)	107.9	C(8)-C(9)-H(9)	119.8
C(3)-C(4)-H(4)	107.9	C(10)-C(9)-H(9)	119.8
C(8)-C(4)-H(4)	107.9	C(11)-C(10)-C(9)	120.0(3)
O(1)-C(5)-N(2)	125.9(3)	C(11)-C(10)-H(10)	120.0

C(9)-C(10)-H(10)	120.0	C(25)-C(26)-C(27)	119.6(3)
C(12)-C(11)-C(10)	120.2(3)	C(25)-C(26)-H(26)	120.2
C(12)-C(11)-H(11)	119.9	C(27)-C(26)-H(26)	120.2
C(10)-C(11)-H(11)	119.9	C(22)-C(27)-C(26)	121.7(3)
C(11)-C(12)-C(13)	119.8(3)	C(22)-C(27)-H(27)	119.1
C(11)-C(12)-H(12)	120.1	C(26)-C(27)-H(27)	119.1
C(13)-C(12)-H(12)	120.1	O(3)-C(28)-O(4)	111.8(2)
C(12)-C(13)-C(8)	120.9(3)	O(3)-C(28)-C(20)	108.5(2)
C(12)-C(13)-H(13)	119.6	O(4)-C(28)-C(20)	107.0(2)
C(8)-C(13)-H(13)	119.6	O(3)-C(28)-H(28)	109.8
C(15)-C(14)-C(19)	120.8(3)	O(4)-C(28)-H(28)	109.8
C(15)-C(14)-N(3)	119.6(3)	C(20)-C(28)-H(28)	109.8
C(19)-C(14)-N(3)	119.7(3)	O(3)-C(29)-C(30)	110.9(2)
C(14)-C(15)-C(16)	119.6(4)	O(3)-C(29)-C(34)	108.3(2)
C(14)-C(15)-H(15)	120.2	C(30)-C(29)-C(34)	113.1(3)
C(16)-C(15)-H(15)	120.2	O(3)-C(29)-H(29)	108.1
C(17)-C(16)-C(15)	120.7(4)	C(30)-C(29)-H(29)	108.1
C(17)-C(16)-H(16)	119.6	C(34)-C(29)-H(29)	108.1
C(15)-C(16)-H(16)	119.6	C(36)-C(30)-C(31)	126.6(3)
C(16)-C(17)-C(18)	119.4(4)	C(36)-C(30)-C(29)	117.4(3)
C(16)-C(17)-H(17)	120.3	C(31)-C(30)-C(29)	116.0(3)
C(18)-C(17)-H(17)	120.3	C(32)-C(31)-C(30)	121.9(3)
C(17)-C(18)-C(19)	121.2(4)	C(32)-C(31)-H(31)	119.0
C(17)-C(18)-H(18)	119.4	C(30)-C(31)-H(31)	119.0
C(19)-C(18)-H(18)	119.4	C(31)-C(32)-C(33)	121.8(3)
C(14)-C(19)-C(18)	118.2(4)	C(31)-C(32)-H(32)	119.1
C(14)-C(19)-H(19)	120.9	C(33)-C(32)-H(32)	119.1
C(18)-C(19)-H(19)	120.9	O(4)-C(33)-C(32)	110.6(2)
C(21)-C(20)-C(28)	119.9(2)	O(4)-C(33)-C(35)	103.5(2)
C(21)-C(20)-C(1)	124.8(3)	C(32)-C(33)-C(35)	112.4(3)
C(28)-C(20)-C(1)	115.1(2)	O(4)-C(33)-C(34)	105.3(2)
C(20)-C(21)-C(22)	129.6(3)	C(32)-C(33)-C(34)	110.6(2)
C(20)-C(21)-H(21)	115.2	C(35)-C(33)-C(34)	113.9(2)
C(22)-C(21)-H(21)	115.2	C(33)-C(34)-C(29)	105.7(2)
C(27)-C(22)-C(23)	118.1(3)	C(33)-C(34)-C(43)	119.9(2)
C(27)-C(22)-C(21)	118.8(3)	C(29)-C(34)-C(43)	108.6(2)
C(23)-C(22)-C(21)	123.0(3)	C(33)-C(34)-H(34)	107.4
C(22)-C(23)-C(24)	120.4(3)	C(29)-C(34)-H(34)	107.4
C(22)-C(23)-H(23)	119.8	C(43)-C(34)-H(34)	107.4
C(24)-C(23)-H(23)	119.8	C(33)-C(35)-H(35A)	109.5
C(25)-C(24)-C(23)	120.6(3)	C(33)-C(35)-H(35B)	109.5
C(25)-C(24)-H(24)	119.7	H(35A)-C(35)-H(35B)	109.5
C(23)-C(24)-H(24)	119.7	C(33)-C(35)-H(35C)	109.5
C(24)-C(25)-C(26)	119.5(3)	H(35A)-C(35)-H(35C)	109.5
C(24)-C(25)-H(25)	120.3	H(35B)-C(35)-H(35C)	109.5
C(26)-C(25)-H(25)	120.3	C(30)-C(36)-C(37)	131.4(3)

C(30)-C(36)-H(36)	114.3	C(49)-C(50)-H(50)	116.9
C(37)-C(36)-H(36)	114.3	C(50)-C(51)-C(55)	123.4(3)
C(42)-C(37)-C(38)	117.8(4)	C(50)-C(51)-C(52)	121.7(3)
C(42)-C(37)-C(36)	124.3(4)	C(55)-C(51)-C(52)	114.9(3)
C(38)-C(37)-C(36)	117.7(4)	N(5)-C(52)-C(51)	107.8(2)
C(39)-C(38)-C(37)	121.3(4)	N(5)-C(52)-C(56)	111.7(2)
C(39)-C(38)-H(38)	119.4	C(51)-C(52)-C(56)	113.9(3)
C(37)-C(38)-H(38)	119.4	N(5)-C(52)-H(52)	107.7
C(38)-C(39)-C(40)	121.0(5)	C(51)-C(52)-H(52)	107.7
C(38)-C(39)-H(39)	119.5	C(56)-C(52)-H(52)	107.7
C(40)-C(39)-H(39)	119.5	O(5)-C(53)-N(5)	126.6(3)
C(39)-C(40)-C(41)	119.4(5)	O(5)-C(53)-N(6)	127.6(3)
C(39)-C(40)-H(40)	120.3	N(5)-C(53)-N(6)	105.8(3)
C(41)-C(40)-H(40)	120.3	O(6)-C(54)-N(4)	126.7(3)
C(40)-C(41)-C(42)	120.2(5)	O(6)-C(54)-N(6)	127.7(3)
C(40)-C(41)-H(41)	119.9	N(4)-C(54)-N(6)	105.6(3)
C(42)-C(41)-H(41)	119.9	C(51)-C(55)-H(55A)	109.5
C(37)-C(42)-C(41)	120.4(4)	C(51)-C(55)-H(55B)	109.5
C(37)-C(42)-H(42)	119.8	H(55A)-C(55)-H(55B)	109.5
C(41)-C(42)-H(42)	119.8	C(51)-C(55)-H(55C)	109.5
C(44)-C(43)-C(48)	117.8(3)	H(55A)-C(55)-H(55C)	109.5
C(44)-C(43)-C(34)	116.8(3)	H(55B)-C(55)-H(55C)	109.5
C(48)-C(43)-C(34)	125.2(3)	C(61)-C(56)-C(57)	119.6(3)
C(45)-C(44)-C(43)	121.8(3)	C(61)-C(56)-C(52)	120.6(3)
C(45)-C(44)-H(44)	119.1	C(57)-C(56)-C(52)	119.8(3)
C(43)-C(44)-H(44)	119.1	C(56)-C(57)-C(58)	120.8(4)
C(46)-C(45)-C(44)	119.8(3)	C(56)-C(57)-H(57)	119.6
C(46)-C(45)-H(45)	120.1	C(58)-C(57)-H(57)	119.6
C(44)-C(45)-H(45)	120.1	C(59)-C(58)-C(57)	119.3(5)
C(45)-C(46)-C(47)	119.4(3)	C(59)-C(58)-H(58)	120.4
C(45)-C(46)-H(46)	120.3	C(57)-C(58)-H(58)	120.4
C(47)-C(46)-H(46)	120.3	C(58)-C(59)-C(60)	121.2(4)
C(46)-C(47)-C(48)	120.6(3)	C(58)-C(59)-H(59)	119.4
C(46)-C(47)-H(47)	119.7	C(60)-C(59)-H(59)	119.4
C(48)-C(47)-H(47)	119.7	C(59)-C(60)-C(61)	119.6(4)
C(43)-C(48)-C(47)	120.5(3)	C(59)-C(60)-H(60)	120.2
C(43)-C(48)-H(48)	119.7	C(61)-C(60)-H(60)	120.2
C(47)-C(48)-H(48)	119.7	C(56)-C(61)-C(60)	119.5(4)
N(4)-C(49)-C(50)	106.5(2)	C(56)-C(61)-H(61)	120.2
N(4)-C(49)-C(68)	114.6(2)	C(60)-C(61)-H(61)	120.2
C(50)-C(49)-C(68)	110.8(2)	C(67)-C(62)-C(63)	121.4(3)
N(4)-C(49)-H(49)	108.3	C(67)-C(62)-N(6)	119.8(3)
C(50)-C(49)-H(49)	108.3	C(63)-C(62)-N(6)	118.9(3)
C(68)-C(49)-H(49)	108.3	C(62)-C(63)-C(64)	119.5(4)
C(51)-C(50)-C(49)	126.1(3)	C(62)-C(63)-H(63)	120.2
C(51)-C(50)-H(50)	116.9	C(64)-C(63)-H(63)	120.2

C(65)-C(64)-C(63)	120.5(4)	C(78)-C(77)-H(77)	107.8
C(65)-C(64)-H(64)	119.7	C(82)-C(77)-H(77)	107.8
C(63)-C(64)-H(64)	119.7	C(84)-C(78)-C(79)	125.2(3)
C(64)-C(65)-C(66)	119.9(4)	C(84)-C(78)-C(77)	118.7(3)
C(64)-C(65)-H(65)	120.0	C(79)-C(78)-C(77)	116.1(3)
C(66)-C(65)-H(65)	120.0	C(80)-C(79)-C(78)	121.9(3)
C(65)-C(66)-C(67)	120.2(4)	C(80)-C(79)-H(79)	119.1
C(65)-C(66)-H(66)	119.9	C(78)-C(79)-H(79)	119.1
C(67)-C(66)-H(66)	119.9	C(79)-C(80)-C(81)	121.9(3)
C(62)-C(67)-C(66)	118.4(4)	C(79)-C(80)-H(80)	119.0
C(62)-C(67)-H(67)	120.8	C(81)-C(80)-H(80)	119.0
C(66)-C(67)-H(67)	120.8	O(8)-C(81)-C(80)	110.0(2)
C(69)-C(68)-C(76)	119.7(3)	O(8)-C(81)-C(83)	103.6(2)
C(69)-C(68)-C(49)	124.6(3)	C(80)-C(81)-C(83)	112.8(2)
C(76)-C(68)-C(49)	115.6(2)	O(8)-C(81)-C(82)	105.3(2)
C(68)-C(69)-C(70)	130.6(3)	C(80)-C(81)-C(82)	110.9(2)
C(68)-C(69)-H(69)	114.7	C(83)-C(81)-C(82)	113.7(2)
C(70)-C(69)-H(69)	114.7	C(91)-C(82)-C(77)	110.5(2)
C(75)-C(70)-C(71)	118.0(3)	C(91)-C(82)-C(81)	119.1(2)
C(75)-C(70)-C(69)	120.2(3)	C(77)-C(82)-C(81)	105.2(2)
C(71)-C(70)-C(69)	121.5(3)	C(91)-C(82)-H(82)	107.2
C(72)-C(71)-C(70)	120.2(3)	C(77)-C(82)-H(82)	107.2
C(72)-C(71)-H(71)	119.9	C(81)-C(82)-H(82)	107.2
C(70)-C(71)-H(71)	119.9	C(81)-C(83)-H(83A)	109.5
C(73)-C(72)-C(71)	120.6(3)	C(81)-C(83)-H(83B)	109.5
C(73)-C(72)-H(72)	119.7	H(83A)-C(83)-H(83B)	109.5
C(71)-C(72)-H(72)	119.7	C(81)-C(83)-H(83C)	109.5
C(74)-C(73)-C(72)	120.0(3)	H(83A)-C(83)-H(83C)	109.5
C(74)-C(73)-H(73)	120.0	H(83B)-C(83)-H(83C)	109.5
C(72)-C(73)-H(73)	120.0	C(78)-C(84)-C(85)	129.5(3)
C(73)-C(74)-C(75)	119.6(3)	C(78)-C(84)-H(84)	115.2
C(73)-C(74)-H(74)	120.2	C(85)-C(84)-H(84)	115.2
C(75)-C(74)-H(74)	120.2	C(90)-C(85)-C(86)	116.9(3)
C(74)-C(75)-C(70)	121.5(3)	C(90)-C(85)-C(84)	123.6(3)
C(74)-C(75)-H(75)	119.3	C(86)-C(85)-C(84)	119.5(3)
C(70)-C(75)-H(75)	119.3	C(87)-C(86)-C(85)	121.6(4)
O(7)-C(76)-O(8)	112.2(2)	C(87)-C(86)-H(86)	119.2
O(7)-C(76)-C(68)	109.3(2)	C(85)-C(86)-H(86)	119.2
O(8)-C(76)-C(68)	105.9(2)	C(88)-C(87)-C(86)	120.0(4)
O(7)-C(76)-H(76)	109.8	C(88)-C(87)-H(87)	120.0
O(8)-C(76)-H(76)	109.8	C(86)-C(87)-H(87)	120.0
C(68)-C(76)-H(76)	109.8	C(87)-C(88)-C(89)	120.1(4)
O(7)-C(77)-C(78)	111.4(2)	C(87)-C(88)-H(88)	119.9
O(7)-C(77)-C(82)	109.1(2)	C(89)-C(88)-H(88)	119.9
C(78)-C(77)-C(82)	112.7(2)	C(88)-C(89)-C(90)	119.6(4)
O(7)-C(77)-H(77)	107.8	C(88)-C(89)-H(89)	120.2

C(90)-C(89)-H(89)	120.2	C(903)-C(902)-H(90G)	114.2
C(89)-C(90)-C(85)	121.7(3)	C(901)-C(902)-H(90G)	114.1
C(89)-C(90)-H(90)	119.1	H(90F)-C(902)-H(90G)	111.3
C(85)-C(90)-H(90)	119.1	C(904)-C(903)-C(902)	104.0(12)
C(96)-C(91)-C(92)	118.0(3)	C(904)-C(903)-H(90H)	110.9
C(96)-C(91)-C(82)	125.7(3)	C(902)-C(903)-H(90H)	110.9
C(92)-C(91)-C(82)	116.3(3)	C(904)-C(903)-H(90I)	111.1
C(93)-C(92)-C(91)	121.1(3)	C(902)-C(903)-H(90I)	111.0
C(93)-C(92)-H(92)	119.5	H(90H)-C(903)-H(90I)	108.9
C(91)-C(92)-H(92)	119.5	C(903)-C(904)-H(90J)	109.6
C(92)-C(93)-C(94)	120.3(3)	C(903)-C(904)-H(90K)	109.3
C(92)-C(93)-H(93)	119.9	H(90J)-C(904)-H(90K)	109.5
C(94)-C(93)-H(93)	119.9	C(903)-C(904)-H(90L)	109.6
C(95)-C(94)-C(93)	119.0(3)	H(90J)-C(904)-H(90L)	109.5
C(95)-C(94)-H(94)	120.5	H(90K)-C(904)-H(90L)	109.5
C(93)-C(94)-H(94)	120.5	C(6)-N(1)-N(2)	109.1(2)
C(94)-C(95)-C(96)	121.1(3)	C(6)-N(1)-C(1)	124.8(2)
C(94)-C(95)-H(95)	119.5	N(2)-N(1)-C(1)	114.7(2)
C(96)-C(95)-H(95)	119.5	C(5)-N(2)-N(1)	107.5(2)
C(91)-C(96)-C(95)	120.6(3)	C(5)-N(2)-C(4)	121.6(2)
C(91)-C(96)-H(96)	119.7	N(1)-N(2)-C(4)	112.3(2)
C(95)-C(96)-H(96)	119.7	C(5)-N(3)-C(6)	110.4(3)
C(901)-C(900)-H(90A)	109.4	C(5)-N(3)-C(14)	125.0(3)
C(901)-C(900)-H(90B)	109.5	C(6)-N(3)-C(14)	124.6(3)
H(90A)-C(900)-H(90B)	109.5	C(54)-N(4)-N(5)	108.6(2)
C(901)-C(900)-H(90C)	109.5	C(54)-N(4)-C(49)	124.7(2)
H(90A)-C(900)-H(90C)	109.5	N(5)-N(4)-C(49)	114.9(2)
H(90B)-C(900)-H(90C)	109.5	C(53)-N(5)-N(4)	108.0(2)
C(900)-C(901)-C(902)	87.4(8)	C(53)-N(5)-C(52)	120.9(2)
C(900)-C(901)-H(90D)	114.2	N(4)-N(5)-C(52)	113.3(2)
C(902)-C(901)-H(90D)	114.1	C(53)-N(6)-C(54)	110.9(3)
C(900)-C(901)-H(90E)	114.0	C(53)-N(6)-C(62)	124.6(3)
C(902)-C(901)-H(90E)	114.0	C(54)-N(6)-C(62)	124.4(2)
H(90D)-C(901)-H(90E)	111.3	C(28)-O(3)-C(29)	111.5(2)
C(903)-C(902)-C(901)	87.3(4)	C(28)-O(4)-C(33)	113.3(2)
C(903)-C(902)-H(90F)	114.1	C(76)-O(7)-C(77)	111.7(2)
C(901)-C(902)-H(90F)	114.1	C(76)-O(8)-C(81)	113.94(19)

Table 17. Anisotropic displacement parameters ($\text{\AA}^2 \times 10^3$) for **5.28**. The anisotropic displacement factor exponent takes the form: $-2\pi^2 [h^2 a^{*2} U^{11} + \dots + 2 h k a^* b^* U^{12}]$

	U11	U22	U33	U23	U13	U12
C(1)	26(2)	19(2)	24(2)	-6(2)	-4(1)	-6(2)
C(2)	29(2)	21(2)	35(2)	3(2)	-13(2)	-13(2)
C(3)	26(2)	21(2)	28(2)	2(2)	-6(2)	-11(2)
C(4)	27(2)	30(2)	21(2)	-2(2)	0(1)	-9(2)
C(5)	29(2)	25(2)	22(2)	0(2)	-6(2)	-12(2)

C(6)	26(2)	27(2)	19(2)	5(2)	-9(2)	-7(2)
C(7)	39(2)	43(2)	40(2)	6(2)	-6(2)	-23(2)
C(8)	37(2)	28(2)	24(2)	6(2)	-9(2)	-19(2)
C(9)	54(2)	40(2)	29(2)	4(2)	-14(2)	-22(2)
C(10)	82(3)	55(3)	38(2)	12(2)	-26(2)	-50(2)
C(11)	46(2)	65(3)	50(3)	30(2)	-23(2)	-35(2)
C(12)	36(2)	58(3)	35(2)	13(2)	-7(2)	-22(2)
C(13)	31(2)	47(2)	28(2)	11(2)	-7(2)	-17(2)
C(14)	32(2)	25(2)	34(2)	-3(2)	-2(2)	-12(2)
C(15)	56(2)	50(3)	51(3)	0(2)	-6(2)	-32(2)
C(16)	69(3)	66(3)	82(4)	-15(3)	3(2)	-47(2)
C(17)	84(3)	50(3)	95(4)	-12(3)	28(3)	-46(2)
C(18)	82(3)	42(3)	70(3)	9(2)	15(2)	-31(2)
C(19)	58(2)	34(2)	39(3)	3(2)	-5(2)	-22(2)
C(20)	21(2)	21(2)	26(2)	1(2)	-8(1)	-7(1)
C(21)	27(2)	26(2)	25(2)	1(2)	-11(1)	-6(2)
C(22)	28(2)	29(2)	23(2)	-1(2)	-10(1)	-10(2)
C(23)	31(2)	32(2)	27(2)	-8(2)	-7(2)	-7(2)
C(24)	34(2)	51(2)	39(2)	-11(2)	-5(2)	-11(2)
C(25)	34(2)	51(3)	54(3)	-25(2)	0(2)	-3(2)
C(26)	50(2)	46(2)	57(3)	-29(2)	0(2)	-13(2)
C(27)	32(2)	43(2)	47(2)	-13(2)	-7(2)	-13(2)
C(28)	31(2)	30(2)	17(2)	-2(2)	-10(1)	-12(2)
C(29)	23(2)	22(2)	27(2)	1(2)	-8(1)	-3(2)
C(30)	30(2)	23(2)	28(2)	2(2)	-3(2)	-5(2)
C(31)	35(2)	29(2)	20(2)	3(2)	-2(2)	-1(2)
C(32)	37(2)	23(2)	28(2)	-5(2)	-11(2)	-4(2)
C(33)	25(2)	22(2)	32(2)	-5(2)	-7(2)	-5(2)
C(34)	29(2)	27(2)	23(2)	-1(2)	-2(1)	-9(2)
C(35)	43(2)	26(2)	59(3)	5(2)	-9(2)	-14(2)
C(36)	36(2)	30(2)	38(2)	-2(2)	3(2)	-7(2)
C(37)	51(2)	25(2)	52(3)	0(2)	21(2)	-10(2)
C(38)	59(3)	43(3)	84(3)	-3(2)	32(2)	-22(2)
C(39)	85(3)	54(3)	108(4)	-21(3)	63(3)	-32(3)
C(40)	115(4)	30(3)	79(4)	-9(3)	69(4)	-16(3)
C(41)	102(4)	32(3)	68(4)	-1(2)	29(3)	-8(3)
C(42)	81(3)	39(3)	60(3)	7(2)	19(3)	-16(2)
C(43)	28(2)	25(2)	27(2)	3(2)	-2(2)	-10(2)
C(44)	40(2)	30(2)	28(2)	-6(2)	-9(2)	-4(2)
C(45)	38(2)	40(2)	39(2)	-4(2)	-16(2)	-2(2)
C(46)	37(2)	33(2)	38(2)	0(2)	-8(2)	1(2)
C(47)	45(2)	29(2)	36(2)	-8(2)	-5(2)	-3(2)
C(48)	38(2)	26(2)	36(2)	-2(2)	-17(2)	-4(2)
C(49)	30(2)	28(2)	24(2)	6(2)	-5(2)	-16(2)
C(50)	37(2)	25(2)	32(2)	0(2)	-8(2)	-18(2)
C(51)	30(2)	27(2)	32(2)	-3(2)	-5(2)	-13(2)

C(52)	29(2)	29(2)	19(2)	-5(2)	0(1)	-11(2)
C(53)	24(2)	31(2)	22(2)	5(2)	-9(2)	-11(2)
C(54)	26(2)	27(2)	25(2)	5(2)	-12(2)	-10(2)
C(55)	56(2)	34(2)	37(2)	-2(2)	-5(2)	-19(2)
C(56)	31(2)	31(2)	23(2)	-6(2)	-5(2)	-2(2)
C(57)	68(2)	40(2)	40(3)	8(2)	-27(2)	-16(2)
C(58)	118(4)	46(3)	73(3)	8(2)	-60(3)	-17(3)
C(59)	79(4)	59(3)	93(4)	-38(3)	-61(4)	15(3)
C(60)	43(3)	108(4)	71(3)	-43(3)	-17(3)	-8(3)
C(61)	35(2)	75(3)	42(2)	-18(2)	-9(2)	-10(2)
C(62)	25(2)	27(2)	40(2)	2(2)	2(2)	-10(2)
C(63)	51(2)	33(2)	53(3)	18(2)	6(2)	-7(2)
C(64)	74(3)	38(3)	90(4)	19(3)	37(3)	-2(2)
C(65)	71(3)	29(3)	122(5)	-14(3)	50(3)	-21(2)
C(66)	57(3)	56(3)	79(3)	-32(3)	17(2)	-30(2)
C(67)	42(2)	39(3)	55(3)	-8(2)	-2(2)	-15(2)
C(68)	26(2)	23(2)	22(2)	2(2)	-5(1)	-11(1)
C(69)	23(2)	29(2)	35(2)	4(2)	-8(2)	-11(2)
C(70)	27(2)	35(2)	23(2)	6(2)	-10(1)	-18(2)
C(71)	33(2)	34(2)	24(2)	8(2)	-11(2)	-16(2)
C(72)	23(2)	45(2)	31(2)	6(2)	-11(2)	-14(2)
C(73)	37(2)	56(3)	37(2)	21(2)	-7(2)	-26(2)
C(74)	44(2)	43(2)	42(2)	22(2)	-8(2)	-22(2)
C(75)	32(2)	36(2)	35(2)	11(2)	-4(2)	-14(2)
C(76)	28(2)	25(2)	27(2)	8(2)	-8(2)	-10(2)
C(77)	23(2)	27(2)	32(2)	2(2)	-9(1)	-14(2)
C(78)	23(2)	28(2)	28(2)	4(2)	-4(2)	-13(2)
C(79)	34(2)	32(2)	26(2)	5(2)	-6(2)	-17(2)
C(80)	25(2)	29(2)	35(2)	7(2)	-7(2)	-12(2)
C(81)	26(2)	26(2)	30(2)	2(2)	-2(2)	-13(2)
C(82)	29(2)	29(2)	24(2)	3(2)	-5(1)	-17(2)
C(83)	36(2)	27(2)	48(2)	0(2)	-8(2)	-11(2)
C(84)	30(2)	37(2)	34(2)	4(2)	-4(2)	-14(2)
C(85)	40(2)	31(2)	39(2)	-5(2)	-2(2)	-15(2)
C(86)	59(3)	57(3)	51(3)	-20(2)	-1(2)	1(2)
C(87)	73(3)	72(3)	75(4)	-29(3)	0(3)	7(3)
C(88)	93(3)	52(3)	56(3)	-20(2)	19(3)	-30(3)
C(89)	79(3)	54(3)	43(3)	-9(2)	2(2)	-38(2)
C(90)	56(2)	41(2)	42(3)	-7(2)	4(2)	-27(2)
C(91)	28(2)	21(2)	25(2)	-2(2)	-2(2)	-12(2)
C(92)	37(2)	39(2)	24(2)	7(2)	-7(2)	-22(2)
C(93)	35(2)	51(2)	29(2)	3(2)	-12(2)	-19(2)
C(94)	35(2)	39(2)	37(2)	-1(2)	-6(2)	-20(2)
C(95)	40(2)	46(2)	41(2)	7(2)	-7(2)	-26(2)
C(96)	33(2)	35(2)	32(2)	7(2)	-9(2)	-17(2)
C(900)	141(6)	102(6)	651(19)	100(10)	-205(9)	-56(5)

C(901)	450(20)	98(8)	850(40)	-39(16)	360(30)	-57(10)
C(902)	376(14)	83(6)	263(11)	-15(7)	194(10)	-43(8)
C(903)	450(20)	350(20)	420(30)	-260(20)	300(20)	-213(19)
C(904)	156(7)	204(10)	526(18)	-11(10)	-115(10)	-19(6)
N(1)	26(1)	23(2)	22(2)	-5(1)	2(1)	-10(1)
N(2)	30(1)	21(2)	20(2)	-4(1)	-1(1)	-9(1)
N(3)	31(1)	24(2)	26(2)	-3(1)	-1(1)	-15(1)
N(4)	28(1)	24(2)	22(2)	4(1)	-2(1)	-14(1)
N(5)	30(1)	23(2)	24(2)	1(1)	-2(1)	-15(1)
N(6)	35(2)	17(2)	28(2)	6(1)	-4(1)	-9(1)
O(1)	43(1)	25(1)	31(1)	-11(1)	0(1)	-13(1)
O(2)	35(1)	33(1)	27(1)	-2(1)	3(1)	-14(1)
O(3)	24(1)	20(1)	34(1)	-3(1)	-9(1)	-5(1)
O(4)	26(1)	21(1)	36(1)	1(1)	-5(1)	-8(1)
O(5)	36(1)	28(1)	37(2)	10(1)	-2(1)	-14(1)
O(6)	36(1)	33(1)	26(1)	3(1)	1(1)	-11(1)
O(7)	25(1)	27(1)	31(1)	9(1)	-7(1)	-11(1)
O(8)	26(1)	23(1)	33(1)	2(1)	-2(1)	-11(1)

Table 18. Hydrogen coordinates ($\times 10^4$) and isotropic displacement parameters ($\text{\AA}^2 \times 10^3$)
For 5.28.

	x	y	z	U(eq)
H(1)	12744	204	3824	29
H(2)	11427	-156	4420	32
H(4)	11049	2006	5577	32
H(7A)	10264	743	5762	58
H(7B)	11392	46	5927	58
H(7C)	10844	-315	5426	58
H(9)	12047	2360	6296	47
H(10)	13525	1864	6831	60
H(11)	14947	450	6511	58
H(12)	14925	-459	5651	50
H(13)	13453	24	5123	41
H(15)	13400	3806	5004	58
H(16)	14054	5010	4759	80
H(17)	14195	5473	3755	87
H(18)	13597	4802	2992	77
H(19)	12858	3648	3229	51
H(21)	11001	1098	2695	32
H(23)	13589	325	2832	37
H(24)	14909	-1036	2338	51
H(25)	14544	-2266	1881	60
H(26)	12833	-2098	1874	63
H(27)	11518	-727	2352	49
H(28)	10223	2022	4157	31
H(29)	8166	2850	3221	30

H(31)	8334	3557	4995	38
H(32)	9492	4218	4687	37
H(34)	9272	3658	2875	32
H(35A)	10667	4556	3832	63
H(35B)	9547	5281	3672	63
H(35C)	10352	4579	3145	63
H(36)	7398	2251	3942	44
H(38)	5887	2230	4497	77
H(39)	5101	1891	5382	103
H(40)	5805	1789	6309	100
H(41)	7333	2034	6345	91
H(42)	8157	2367	5444	76
H(44)	7584	4154	2499	42
H(45)	5958	5362	2434	51
H(46)	5272	6635	3173	48
H(47)	6240	6697	3967	48
H(48)	7872	5478	4035	42
H(49)	7348	2185	1181	31
H(50)	8509	832	544	35
H(52)	9114	2637	-591	31
H(55A)	9090	241	-459	63
H(55B)	9688	840	-817	63
H(55C)	8531	1036	-948	63
H(57)	8335	3686	-1358	60
H(58)	6950	4462	-1939	96
H(59)	5363	4424	-1628	103
H(60)	5137	3596	-762	96
H(61)	6552	2748	-198	65
H(63)	6702	6202	-35	59
H(64)	6108	7889	174	91
H(65)	6102	8476	1150	93
H(66)	6790	7382	1918	76
H(67)	7466	5667	1702	55
H(69)	9255	1587	2222	34
H(71)	6694	3009	2216	35
H(72)	5368	2855	2866	39
H(73)	5609	1384	3349	49
H(74)	7209	84	3232	50
H(75)	8567	260	2633	41
H(76)	9865	2096	760	32
H(77)	12035	1273	1616	31
H(79)	11661	2352	-110	35
H(80)	10540	3830	281	35
H(82)	10952	2851	2047	30
H(83A)	9475	4925	1187	56
H(83B)	10600	4780	1357	56

H(83C)	9799	4614	1864	56
H(84)	12812	222	819	40
H(86)	14384	-578	94	76
H(87)	15064	-1232	-885	102
H(88)	14049	-786	-1700	82
H(89)	12356	337	-1540	66
H(90)	11677	1010	-560	53
H(92)	12642	2103	2389	37
H(93)	14257	2146	2438	45
H(94)	14841	3067	1740	42
H(95)	13807	3903	985	47
H(96)	12214	3818	908	38
H(90A)	10356	3293	-1621	427
H(90B)	11376	2780	-2078	427
H(90C)	11184	2234	-1474	427
H(90D)	9690	2124	-1927	610
H(90E)	10754	1539	-2364	610
H(90F)	9449	3651	-2422	323
H(90G)	10634	3208	-2742	323
H(90H)	10356	2037	-3319	492
H(90I)	9465	1999	-2818	492
H(90J)	8609	3803	-3137	458
H(90K)	8428	2938	-3484	458
H(90L)	9273	3331	-3772	458

References

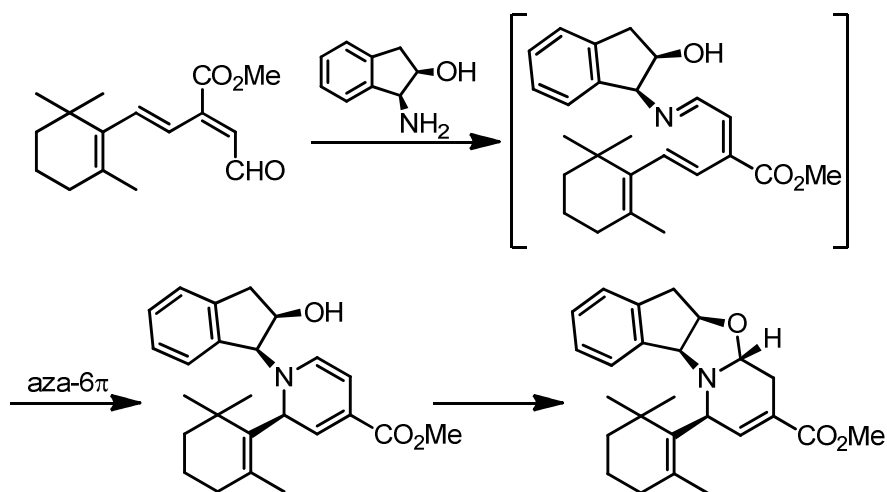
- (1) Bishop, L. M.; Barbarow, J. E.; Bergman, R. G.; Trauner, D. *Angew. Chem. Int. Ed.* **2008**, *47*, 8100.
- (2) Erkkilä, A.; Majander, I.; Pihko, P. M. *Chem. Rev.* **2007**, *107*, 5416.
- (3) Allen, C. F. H.; Edens, C. O. J. *Org. Syn.* **1945**, *25*, 92.
- (4) Bowman, W. R.; Bridge, C. F.; Brookes, P.; Cloonan, M. O.; Leach, D. C. *J. Chem. Soc. Perkin Trans. I* **2002**, 58.
- (5) Marvell, E. N. *Thermal Electrocyclic Reactions*; Academic Press: New York, 1980; Vol. 43.
- (6) Desimoni, G.; Faita, G.; Guidetti, S.; Righetti, P. P. *Eur. J. Org. Chem.* **1999**, 1921.
- (7) Huisgen, R.; Dahmen, A.; Huber, h. *Tetrahedron Lett.* **1969**, *10*, 1461.
- (8) Mayr, H.; Huisgen, R. *J. Chem. Soc. Chem. Commun.* **1976**, 57.
- (9) Jorgensen, W. L.; Blake, J. F.; Lim, D.; Severance, D. L. *J. Chem. Soc. Faraday Trans.* **1994**, *90*, 1727.
- (10) Marsura, A.; Luu-Duc, C.; Gellon, G. *Synthesis* **1985**, 537.
- (11) Nowak, I.; Robins, M. J. *J. Org. Chem.* **2007**, *72*, 2678.
- (12) Yu, T.-Q.; Fu, Y.; Liu, L.; Guo, Q.-X. *J. Org. Chem.* **2006**, *71*, 6157.
- (13) Betzer, J.-F.; Delalogue, F.; Muller, B.; Pancrazi, A.; Prunet, J. *J. Org. Chem.* **1997**, *62*, 7768.
- (14) Ogawa, Y.; Shibasaki, M. *Tetrahedron Lett.* **1984**, *25*, 663.

- (15) Snider, B. B.; Rodini, D. J.; van Straten, J. *J. Am. Chem. Soc.* **1980**, *102*, 5872.
- (16) Snider, B. B.; Karras, M. *J. Am. Chem. Soc.* **1980**, *102*, 7951.
- (17) Snider, B. B.; Karras, M.; Price, R. T.; Rodini, D. J. *J. Org. Chem.* **1982**, *47*, 4538.
- (18) Snider, B. B.; Kirk, T. C. *J. Am. Chem. Soc.* **1983**, *105*, 2364.
- (19) Snider, B. B.; Cartaya-Marin, C. P. *J. Org. Chem.* **1984**, *49*, 153.
- (20) Snider, B. B.; Lobera, M.; Marien, T. P. *J. Org. Chem.* **2003**, *68*, 6451.
- (21) Krafft, M. E.; Cran, J. W. *Synlett* **2005**, 1263.
- (22) Smith, A. B., III; Kürti, L.; Davulcu, A. H. *Org. Lett.* **2006**, *8*, 2167.
- (23) Parnes, H.; Huang, G. T. *J. Labelled Compd. Radiopharm.* **1995**, *36*, 51.
- (24) Kagan, H. B.; Riant, O. *Chem. Rev.* **1992**, *92*, 1007.
- (25) Gothelf, K. V.; Jørgensen, K. A. *Chem. Rev.* **1998**, *98*, 863.
- (26) Jørgensen, K. A. *Angew. Chem. Int. Ed.* **2000**, *39*, 3558.
- (27) Corey, E. J. *Angew. Chem. Int. Ed.* **2002**, *41*, 1650.
- (28) Kobayashi, S.; Jørgensen, K. A. *Cycloaddition Reactions in Organic Synthesis*; Wiley-VCH: Weinheim, 2002.
- (29) *KaleidaGraph*, Synergy Software: Reading, PA, **2003**.
- (30) Alaimo, P. J.; Peters, D. W.; Arnold, J.; Bergman, R. G. *J. Chem. Ed.* **2001**, *78*, 64.
- (31) Nongkhilaw, R. L.; Nongrum, R.; Myrboh, B. *J. Chem. Soc. Perkin Trans. I* **2001**, 1300.
- (32) Lahmar, N.; Aatar, J.; Ayed, T. B.; Amri, H.; Bellassoued, M. *J. Organomet. Chem.* **2006**, *691*, 3018.
- (33) Roubelakis, M. M.; Vougioukalakis, G. C.; Angelis, Y. S.; Orfanopoulos, M. *Org. Lett.* **2006**, *8*, 39.
- (34) Appel, M.; Blaurock, S.; Berger, S. *Eur. J. Org. Chem.* **2002**, 1143.
- (35) Allred, G. D.; Liebeskind, L. S. *J. Am. Chem. Soc.* **1996**, *118*, 2748.
- (36) Conway, J. C.; Quayle, P.; Regan, A. C.; Urch, C. J. *Tetrahedron* **2005**, *61*, 11910.
- (37) Attenburrow, J.; Cameron, A. F. B.; Chapman, J. H.; Evans, R. M.; Hems, B. A.; Jansen, A. B. A.; Walker, T. *J. Chem. Soc.* **1952**, 1094.
- (38) Olah, G. A.; Török, B.; Joschek, J. P.; Bucsi, I.; Esteves, P. M.; Rasul, G.; Prakash, G. K. S. *J. Am. Chem. Soc.* **2002**, *124*, 11379.
- (39) White, J. D.; Sheldon, B. G. *J. Org. Chem.* **1981**, *46*, 2273.
- (40) Stork, G.; Zhao, K. *Tetrahedron Lett.* **1989**, *30*, 2173.
- (41) Wuts, P. G. M.; Jung, Y. W. *J. Org. Chem.* **1991**, *56*, 365.
- (42) Wang, K. K.; Liu, C.; Gu, Y. G.; Burnett, F. N.; Sattsangi, P. D. *J. Org. Chem.* **1991**, *56*, 1914.
- (43) Sakane, S.; Fujiwara, J.; Maruoka, K.; Yamamoto, H. *Tetrahedron* **1986**, *42*, 2193.
- (44) *SAINT v. 6.40: SAX Area-Detector Integration Program*, Bruker Analytical X-ray Systems, Inc.: Madison, WI, **2003**.
- (45) *XS: Program for the solution of X-ray crystal structures, part of the SHELXTL Crystal Structure Determination Package*, Bruker Analytical X-Ray Systems, Inc.: Madison, WI, **1995-1999**.
- (46) *XL: Program for the solution of X-ray crystal structures, part of the SHELXTL Crystal Structure Determination Package*, Bruker Analytical X-Ray Systems, Inc.: Madison, WI, **1995-1999**.

Part 1 – Chapter 6. *Development of a Catalytic Asymmetric Carba-6 π Electrocyclization and Discovery of a Catalytic Photochemical Electrocyclic Ring-Opening.*

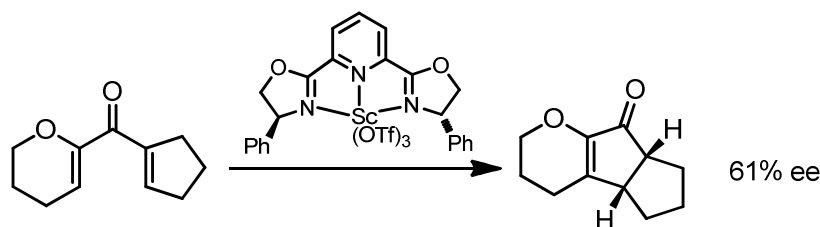
Introduction

The search for methods to achieve asymmetric induction at the stereocenters formed during 6π electrocyclizations began with torquoselective approaches based upon chiral auxiliaries.¹⁻⁶ Although the Katsumura group achieved an early example of this in the stereoselective tetrahydropyridine synthesis from trienals and chiral *cis*-1-amino-2-indanols, the utility of these reactions are limited by the stoichiometry requirement of auxiliary-based asymmetric processes.¹ In this instance, tetrahydropyridine formation is hypothesized to proceed by *in-situ* formation of an imine, diastereoselective aza- 6π electrocyclization, followed by aminoacetal formation (Scheme 1).



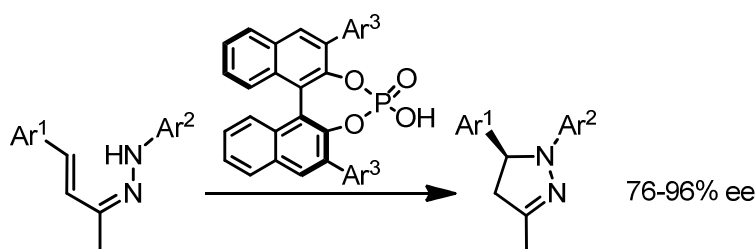
Scheme 1. Auxiliary-based asymmetric electrocyclization.¹

The first example of a catalytic asymmetric electrocyclization was published by the Trauner group in 2003. In this study, the Nazarov cyclization of a 2-alkoxy-1,4-pentadien-3-one was catalyzed by a scandium pyridine-bis-oxazoline (pybox) catalyst to yield the tricyclic product in 61% e.e. (Scheme 2).⁷ In the same year, the Aggarwal group published a copper bis-oxazoline catalyzed electrocyclization of a related system.⁸ While the Trauner system was later improved to achieve highly enantioselective Nazarov cyclizations through asymmetric proton transfer,⁹ the Rueping group employed chiral phosphoric acids and *N*-triflyl phosphoramides in the Nazarov cyclization of substrates like those shown in Scheme 2.¹⁰



Scheme 2. Catalytic asymmetric Nazarov cyclization.⁷

More recently, the Smith and List groups have reported catalytic asymmetric aza-6 π electrocyclizations under phase-transfer and chiral Brønsted acid conditions, respectively (Scheme 3).¹¹⁻¹³ To our knowledge there are currently no published examples of catalytic asymmetric carba-6 π electrocyclizations.



Scheme 3. Catalytic asymmetric aza-6 π electrocyclization.¹²

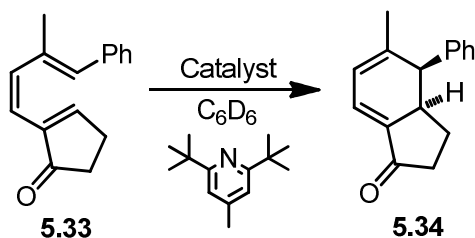
This chapter describes development of conditions to affect a catalytic asymmetric carba-6 π electrocyclization as well as the discovery of a catalytic photochemical electrocyclic ring-opening.

Results & Discussion

Development of a Catalytic Asymmetric Carba-6 π Electrocyclization

We conducted our screen of asymmetric catalysts using ketone-based triene **5.33** (for synthesis and achiral catalytic studies see Chapter 5). Reaction progress was monitored by ¹H NMR analysis, and enantioenrichment of products was analyzed by chiral HPLC. In most cases a full equivalent of catalyst and 1.2 equivalents of the hindered-base 2,6-di-*tert*-butyl-4-methylpyridine were employed to prevent Brønsted-acid catalyzed decomposition of the triene substrate (Scheme 4). As different batches of isolated substrate **5.33** contain varying amounts of thermally-produced, racemic cyclohexadiene **5.34** (typically between 8-20%), the enantioenrichment values shown are corrected to include only the cyclohexadiene formed under the catalytic conditions so that comparisons between runs are meaningful. For the full development of the catalytically enantioselective reaction, this obstacle of competitive thermal electrocyclization will certainly have to be overcome. The trials shown below were conducted on milligram quantities of substrate, causing isolated yields to be unreliable. Yield determination by ¹H NMR analysis was complicated by the shifting of substrate resonances and poor quality spectra due presumably to colloid formation (*vide infra*). Therefore, only enantioselectivities are shown for these trials. Approximate rate accelerations were obtained in

each case by measuring a half-life for the reaction *via* periodic ^1H NMR analysis and comparison to that of the thermal reaction.

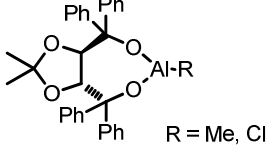
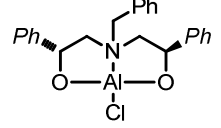
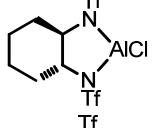
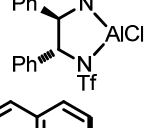
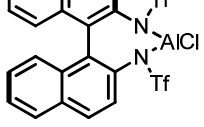
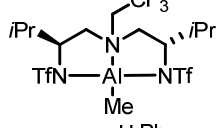
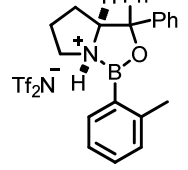
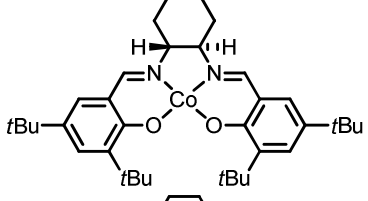
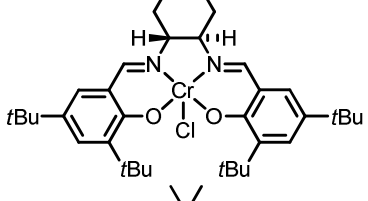
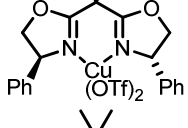
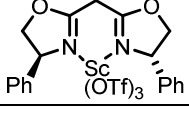


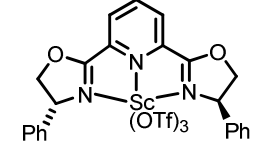
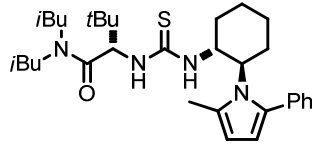
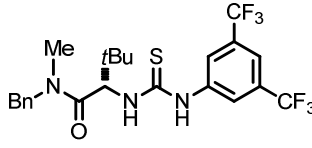
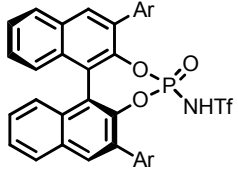
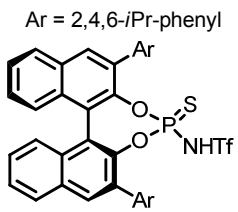
Scheme 4. Substrate and general conditions employed for asymmetric catalyst screen.

We began our screen of asymmetric catalysts by employing chiral alkoxyaluminum catalysts (Table 1, entries 1-3).¹⁴⁻²⁰ No rate acceleration or enantioenrichment was observed with these catalysts, and we attributed this to lone pair donation from oxygen into the empty p orbital of the aluminum center, weakening the Lewis acidity of the catalyst. We therefore turned our attention to chiral aluminum bis-triflamide catalysts,²¹⁻²³ in the hopes that the triflate groups would be sufficiently electron withdrawing to minimize the donation of the nitrogen lone pairs to the aluminum p orbital. Low levels of enantioselectivity as well as decomposition were observed using aluminum bis-triflamide catalysts (Table 1, entries 4-7). Though the level of enantioselectivity is low in these cases, they did serve as an initial indication that highly efficient catalytic asymmetric electrocyclizations might be possible. Corey's oxazaborolidinium catalyst (Table 1, entry 8) resulted in significant product enantioenrichment. One limitation to the use of this catalyst is its decomposition above 25 °C, precluding its use with substrates whose thermal electrocyclization barriers are too great, unless larger rate accelerations are achieved or long reaction times employed.^{24,25} The chiral cobalt and chromium-salen complexes shown (Table 1, entries 9, 10) did not catalyze the reaction,²⁶⁻²⁹ and neither did the *in situ* formed copper bis-oxazoline catalyst (Table 1, entry 11).³⁰ We were pleased to find that scandium bis-oxazoline and the well-established scandium pybox catalysts resulted in significant enantioenrichment (Table 1, entries 12, 13).^{7,9,31-33} Thioureas did not catalyze the reaction, presumably due to the relatively high thiourea pKa (Table 1, entries 14, 15).^{34,35} The stronger *N*-triflyl phosphoramidate Brønsted acid catalysts, which were generously donated by the group of Prof. Hisashi Yamamoto, were met with more success. The phosphoramidate catalyst (Table 1, entry 16) resulted in a low level of enantioselectivity, but the thiophosphoramidate catalyst (Table 1, entry 17) gave no apparent rate acceleration and no enantioenrichment.

Table 1. Trials of catalysts for the electrocyclization of **5.33** in the presence of catalyst (1 equiv) and 2,6-di-*tert*-butyl-4-methylpyridine (1.2 equiv). Tf = trifluoromethanesulfonyl; Decomp. = complete substrate decomposition observed.

Entry	Catalyst	Conditions	e.e. (%)*
1	 R = Me, Cl	C ₆ D ₆ ; 1 h, r.t., then 6 h, 45 °C	0

2	 R = Me, Cl	C ₆ D ₆ ; 1 h, r.t., then 6 h, 45 °C	0
3		C ₆ D ₆ ; 2 h, r.t., then 2 h, 55 °C	0
4		C ₆ D ₆ ; 3 h, r.t.	4
5		C ₆ D ₆ ; 2 h, r.t., then 1.5 h, 55 °C	8
6		C ₆ D ₆ ; 1 h, r.t.	decomp.
7		C ₆ D ₆ ; 2 h, r.t., then 1 h, 45 °C †	decomp.
8		C ₆ D ₆ ; 2 h, r.t.	17
9		C ₆ D ₆ ; 1 h, r.t., then 3 h, 45 °C †	0
10		C ₆ D ₆ ; 1 h, r.t., then 3 h, 45 °C †	0
11		THF- <i>d</i> ₈ ; 1 h, r.t., then 3 h, 45 °C	0
12		THF- <i>d</i> ₈ ; 3 h, r.t.	15

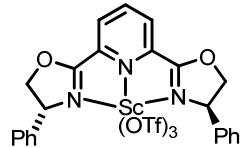
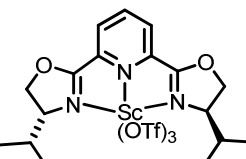
13		THF- <i>d</i> ₈ ; 1 h, r.t., then 1 h, 35 °C	32
14		C ₆ D ₆ ; 2 h, r.t., then 2 h, 45 °C	0
15		C ₆ D ₆ ; 2 h, r.t., then 2 h, 45 °C	0
16	 Ar = 2,4,6- <i>i</i> Pr-phenyl	C ₆ D ₆ ; 1 h, r.t., then 5 h, 45 °C †	13
17	 Ar = 2,4,6- <i>i</i> Pr-phenyl	C ₆ D ₆ ; 1 h, r.t., then 5 h, 45 °C †	0

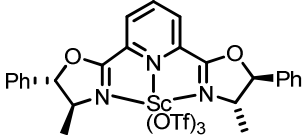
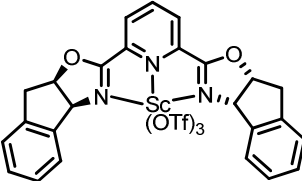
* e.e. values are corrected to account for initial thermal conversion of starting material using the formula %e.e. = (100 * e.e._{measured}) / (100 - % initial conversion)

† no 2,6-di-*tert*-butyl-4-methylpyridine added

As the scandium pybox catalysts from the above screen provided the most promising lead, we next screened a series of pybox ligands. This screen was conducted in methylene chloride, and phenyl and indenyl pybox ligands proved optimal for this reaction (Table 2). Of note also is the switch in the sense of enantioinduction using phenyl- and isopropyl-substituted pybox ligands of the same enantiomeric series.

Table 2. Pybox ligand screen for the electrocyclization of **5.33** in the presence of catalyst (1 equiv) and 2,6-di-*tert*-butyl-4-methylpyridine (0.7 equiv) in CD₂Cl₂ for 5 h at room temperature.

Entry	Catalyst	e.e. (%) [*]
1		42
2		-27

3		-13
4		42

* e.e. values are corrected to account for initial thermal conversion of starting material using the formula %e.e. = (100 * e.e._{measured}) / (100 - % initial conversion)

We next undertook a screen of solvents using the phenyl-substituted pybox ligand, allowing each reaction 5 h at room temperature to go to completion. Carrying out the reaction in THF-*d*₈ at room temperature (Table 3, entry 1) showed a drop in enantioselectivity as compared to that observed conducting the reaction for 1 h at room temperature followed by 1 h at 35 °C (Table 1, entry 13). We carried out the reaction under the former conditions in duplicate, with similar results. No further increase in enantioinduction was observed using benzene, nitromethane, or acetonitrile (Table 3, entries 2-4). The highest levels of enantioselectivity were observed using methylene chloride as solvent. Reproducibility was an issue with this catalyst system, as a number of trials carried out in methylene chloride gave enantioselectivities ranging from 32-42% (Table 3, entry 5). We hypothesized that the reproducibility issues were due to the presence of varying amounts of adventitious water, as performing the reaction with scandium(III) trifluoromethanesulfonate that had not been dried under vacuum at 150 °C resulted in no catalysis or enantioinduction (Table 3, entry 6). This prompted us to include dimethyl zirconocene in our reaction mixtures to serve as a desiccant. This compound reacts rapidly and quantitatively with water, and so observation of its upfield methyl signals verifies the dryness of our reaction mixtures. However, while the addition of dimethyl zirconocene increased the level of enantioinduction, it did not improve the reproducibility (Table 3, entry 7). Furthermore, ¹H NMR analyses of completely dry reaction mixtures containing scandium pybox catalyst were difficult due to extreme broadening of the NMR signals. We hypothesized that, though the reaction mixtures appeared homogenous, a colloidal mixture was being formed under these anhydrous conditions. The NMR signal resolution was improved, though not completely, when carrying out the reaction in a sealed NMR tube and centrifuging the tube immediately after assembly of the reaction, but the enantioselectivities were unaffected by this centrifugation step (Table 3, entry 8). The enantioselectivities improved significantly using 1,1,2,2-tetrachloroethane-*d*₂ as solvent, though reproducibility was not improved (Table 3, entry 9).

Table 3. Solvent screen for the electrocyclization of **5.33** in the presence of scandium phenyl-pybox catalyst (1 equiv) and 2,6-di-*tert*-butyl-4-methylpyridine (0.7 equiv). Conditions: 5 h, r.t.

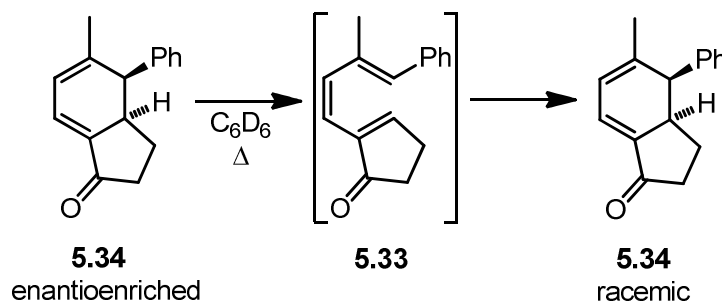
Entry	Solvent	Notes	e.e. (%) [*]
1	THF- <i>d</i> ₈		13, 18
2	C ₆ D ₆		35
3	CD ₃ NO ₂		35
4	CD ₃ CN		21
5	CD ₂ Cl ₂		32-42

6	CD ₂ Cl ₂	Sc(OTf) ₃ not dried prior to use	0
7	CD ₂ Cl ₂	Cp ₂ ZrMe ₂ (0.5 equiv) added	47-66
8	CD ₂ Cl ₂	Cp ₂ ZrMe ₂ (0.5 equiv) added Centrifuged sealed NMR tube	47, 56
9	(CDCl ₂) ₂	Cp ₂ ZrMe ₂ (0.5 equiv) added	57-77

* e.e. values are corrected to account for initial thermal conversion of starting material using the formula %e.e. = (100 * e.e.-measured) / (100 - % initial conversion)

Discovery of a Photochemical Electrocyclic Ring-Opening

In the context of our investigations into enantioselective electrocyclizations, we were interested in the reversibility of the electrocyclization of triene substrate **5.33**. Thermal electrocyclic ring-opening was detected by monitoring the e.e. of a heated enantioenriched solution of cyclohexadiene **5.34** in C₆D₆ (Scheme 5 and Table 4). No degradation of enantioenrichment was observed until the solution was heated to 150 °C, at which point the e.e. slowly degraded over the course of days. No decomposition of cyclohexadiene was observed by ¹H NMR analysis of the same reaction mixture. These observations are consistent with thermal electrocyclic ring-opening followed by cyclization to racemic cyclohexadiene. The elevated temperatures required for this process lead us to conclude that this pathway is not active in the catalytic studies outlined above.



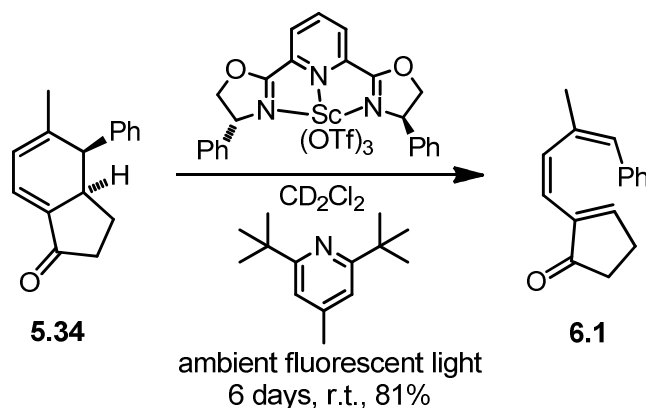
Scheme 5. Detection of the thermal electrocyclic ring-opening of **5.34**.

Table 4. Enantiomeric excess of an enantioenriched solution of **5.34** after heating for extended periods.

Entry	Conditions	e.e. (%)
1	Initial	40
2	21 h, 100 °C	40
3	17 h, 150 °C	37
4	34 h, 150 °C	32

When monitoring an enantioenriched solution of cyclohexadiene **5.34** under conditions of scandium pybox catalysis, a new product whose ¹H and ¹³C NMR resonances are similar to that of triene **5.33** was observed to grow in over the course of days. Based on this as well as a NOESY cross-peak between the vinyl and methyl singlets, we have assigned the structure as triene **6.1**, the product of a photochemical electrocyclic ring-opening (Scheme 6). Interestingly, the presence of both scandium triflate and ambient light are required for formation of **6.1**, the absence of either results in no reaction. In addition, density functional theory calculations

indicate that the ring-opening of **5.34** to **6.1** is energetically unfavorable by 12 kcal/mol (B3LYP/6-31G**). Based on these observations and calculations, we believe this is an example of a catalytic photochemical electrocyclic ring-opening.



Scheme 6. Catalytic photochemical electrocyclic ring-opening of cyclohexadiene **5.34**.

When the enantioenrichment of **5.34** is monitored under the conditions above at intermediate conversions to product, the e.e. of the starting material remaining is observed to increase (Table 5). The pybox ligand enantiomer used to produce the enantioenriched cyclohexadiene **5.34** was the same as that used in the photochemical reaction described above. In view of that, it is interesting to note that the enantiomer of **5.34** that is formed preferentially in the catalytic electrocyclization is *not* the enantiomer that preferentially undergoes electrocyclic ring-opening. This photochemical kinetic resolution process takes place with an irreproducible rate over the course of 6-21 days. As the cyclization reactions of triene **5.33** in the presence of chiral catalysts take place over the course of 6 hours at maximum, we are confident the enantioselectivities produced therein are the result of enantioselective electrocyclizations and not cyclization to racemic product followed by kinetic resolution.

Table 5. The e.e. of remaining cyclohexadiene **5.34** under ambient light and scandium-pybox catalysis as a function of conversion to **6.1**.

Entry	Conversion to 6.1 (%)	e.e. of unreacted 5.34 (%)
1	0	23
2	32	36
3	51	46
4	73	52

Summary & Conclusion

In conclusion, we have demonstrated moderate levels of enantioselectivity in catalytic 6π electrocyclizations using scandium pybox catalyst systems. For the future, it may be possible to achieve higher levels of enantioinduction by varying the steric bulk or electronic properties of aryl-substituted scandium-pybox catalyst systems. Also, as the most significant rate accelerations were observed using methylaluminum diiodide (Chapter 5, Table 4, entry 8), alkylaluminum diiodide catalysts with chiral alkyl moieties may exhibit improved

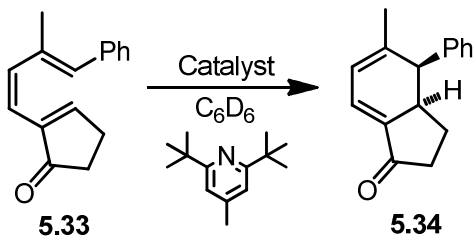
enantioselectivities. We have also discovered a catalytic photochemical electrocyclic ring-opening and kinetic resolution of a cyclohexadiene.

Experimental

General Information. All reactions and manipulations, unless otherwise noted, were carried out in an inert atmosphere (N_2) glovebox. Sealed NMR tubes were prepared by attaching the NMR tube directly to a Kontes high-vacuum stopcock via a cajon ultra-torr reducing union, then flame-sealing on a vacuum line. All glassware was dried in an oven at 150 °C for at least 12 h prior to use. 1H NMR and ^{13}C NMR spectra were recorded on Bruker DRX-500 (500 MHz), AV-500 (500 MHz), AVB-400 (400 MHz), AVQ-400 (400 MHz), and AV-300 (300 MHz) spectrometers as indicated. 1H NMR chemical shifts (δ) are reported in parts per million relative to residual protiated solvent. Data are reported in the following format: (s = singlet, d = doublet, t = triplet, q = quartet, m = multiplet; coupling constant; integration). ^{13}C NMR chemical shifts (δ) are reported in parts per million relative to the carbon resonance of the deuterated solvent. Column chromatography was performed using a Biotage SP1 MPLC purification system and pre-packed silica gel columns. IR spectra were obtained on neat samples on NaCl plates using a ThermoNicolet Avatar 370 FT-IR spectrometer. Enantiomeric excess was determined using a Shimadzu 10A VP Series Chiral HPLC with detection at 230, 254, and 280 nm.

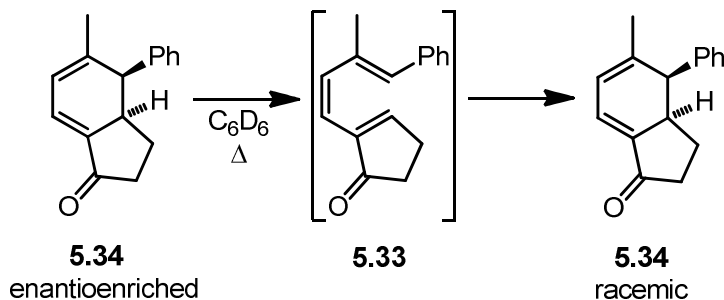
Materials. Benzene was dried and purified by passage through a column of activated alumina under N_2 pressure followed by sparging with N_2 .³⁶ $CDCl_3$, C_6D_6 , tetrahydrofuran- d_8 , CD_2Cl_2 , CD_3NO_2 , CD_3CN , and $(CDCl_2)_2$ were obtained from Cambridge Isotope Labs, Inc. $CDCl_3$ was stored over K_2CO_3 and used without further purification. C_6D_6 was sparged with N_2 and stored over activated 4 Å molecular sieve pellets overnight. Tetrahydrofuran- d_8 was vacuum transferred from purple sodium benzophenone/ketyl, degassed with three freeze-evacuation-thaw cycles, and stored over activated 4 Å molecular sieve pellets. CD_2Cl_2 was vacuum transferred from CaH_2 and degassed with three freeze-evacuation-thaw cycles. CD_3NO_2 was distilled from anhydrous $MgSO_4$, sparged with N_2 , and stored over activated 4 Å molecular sieve pellets overnight. CD_3CN and $(CDCl_2)_2$ were distilled from CaH_2 , degassed with three freeze-evacuation-thaw cycles, and stored over activated 4 Å molecular sieve pellets overnight. Activated 4 Å molecular sieve pellets were obtained from Sigma-Aldrich and heated at 150 °C under vacuum for 24 h. 1,1,2,2-tetrachloroethane, obtained from Sigma-Aldrich, was sparged with N_2 and stored over activated 4 Å molecular sieve pellets overnight prior to use. $Sc(OTf)_3$ was obtained from Sigma-Aldrich and was dried under vacuum at 150 °C for 12 h. $Cu(OTf)_2$, Me_3Al , Me_2AlCl , (R,R) - N,N' -bis(3,5-di-*tert*-butylsalicylidene)-1,2-cyclohexanediaminocobalt(II), (R,R) - N,N' -bis(3,5-di-*tert*-butylsalicylidene)-1,2-cyclohexanediaminochromium(III) chloride, 2,2'-isopropylidenebis[(4*S*)-4-phenyl-2-oxazoline], 2,6-bis[(4*R*)-4-phenyl-2-oxazoliny]pyridine, 2,6-bis[(4*R*)-4-isopropyl-2-oxazoliny]pyridine, 2,6-bis[(4*S*,5*S*)-4-methyl-5-phenyl-2-oxazoliny]pyridine, 2,6-bis[(3*aS*,8*aR*)-3*a*,8*a*-dihydro-8*H*-indeno(1,2-*d*)oxazoliny]pyridine, (2*S*)-3,3-dimethyl-2-[[1*R*,2*R*]-2-(2-methyl-5-phenyl-1-pyrrolyl)cyclohexyl]thioureido]-*N,N*-bis(2-isobutyl)butanamide, (S)-2-[[3,5-bis(trifluoromethyl)phenyl]thioureido]-*N*-benzyl-*N*,3,3-trimethylbutanamide, and 2,6-di-*tert*-butyl-4-methylpyridine were obtained from Sigma-Aldrich; (S)-1,1'-bi(2-naphthol) was obtained from Fluka; (4*R*,5*R*)-2,2-Dimethyl- α,α',α' -tetraphenyldioxolane-4,5-dimethanol was obtained

from Acros Organics; *N*-triflyl phosphoramidate and *N*-triflyl thiophosphoramidate catalysts were obtained from Prof. Hisashi Yamamoto at the University of Chicago; these reagents were used without further purification. *N,N'*-((2*S*,2'*S*)-((2,2,2-trifluoroethyl)azanediyl)bis(3-methylbutane-2,1-diyl))bis(1,1,1-trifluoromethanesulfonamide),³⁷ (1*R*,1'*R*)-2,2'-(benzylazanediyl)bis(1-phenylethanol),³⁸ (1*R*,2*R*)-1,2-*N,N'*-bis(trifluoromethanesulfonylamino)cyclohexane,^{39,40} (1*R*,2*R*)-1,2-*N,N'*-bis(trifluoromethanesulfonylamino)-1,2-diphenylethane,^{39,41} (*R*)-2,2'-bis(trifluoromethanesulfonylamino)-1,1'-binaphthyl,^{39,42} and (*S*)-3,3-diphenyl-1-*o*-tolyltetrahydropyrrolo[1,2-*c*][1,3,2]oxazaborolidinium triflimide,²⁴ were synthesized according to literature procedures. Characterization data for these compounds agree with literature values.

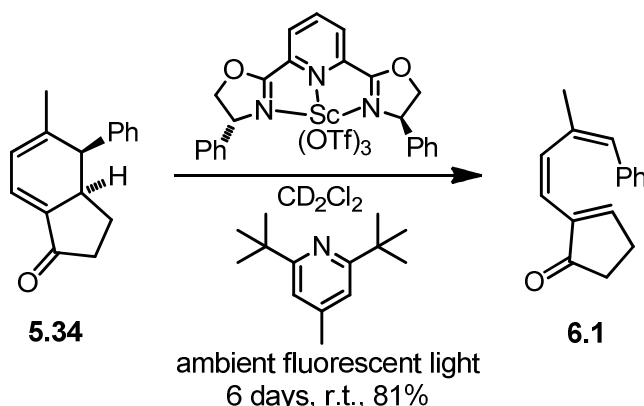


Screen for asymmetric catalysis of the electrocyclic cyclization of triene 5.33—representative procedure. An NMR tube was charged with 2,6-di-*tert*-butyl-4-methylpyridine (3 mg, 0.0146 mmol), chiral catalyst (0.0120 mmol), solvent of interest (230 μ L), and triene **5.33** (250 μ L, 48 mM in solvent of interest, 0.0120 mmol; containing 25 mol% 1,1,2,2-tetrachloroethane as an internal standard). The NMR tube was then sealed under vacuum and the reaction was monitored at regular intervals *via* ^1H NMR. The reaction mixture was kept at room temperature initially and heated in a circulating oil bath at increasing temperatures until significant conversion was observed. Upon reaction completion the NMR tube was opened and the reaction mixture was quenched with H_2O and extracted three times with dichloromethane. The combined organic extracts were dried over MgSO_4 , filtered, concentrated *in vacuo*, redissolved in dichloromethane, and passed through a small plug of silica gel (20% EtOAc in hexanes). The eluent was concentrated *in vacuo* and dissolved in *i*PrOH for chiral HPLC analysis (Chiralcel OD, flow rate 0.5 mL/min, 98:2 hexanes:*i*PrOH, Tr = 20.4, 23.1 min).

Synthesis of chiral aluminum catalysts (Table 1, entries 1-7). A five dram scintillation vial was charged with the diol or bis-triflamide of interest (1 equiv) and benzene such that the solution was 0.1 M in diol or bis-triflamide. To this solution was added trimethylaluminum or dimethylaluminum chloride (1 equiv, 240 mM in benzene) dropwise at room temperature. After stirring the reaction mixture for 5 min, the vial was capped. After a further 2 h, the reaction mixture was concentrated *in vacuo* and dissolved in the deuterated solvent of interest for use in the catalyst screen.



Observation of thermal electrocyclic ring-opening of cyclohexadiene 5.34. A solution of enantioenriched cyclohexadiene **5.34** (1.8 mL, 12.4 mM in benzene-*d*₆, 0.022 mmol; containing 25 mol% 1,1,2,2-tetrachloroethane as an internal standard), obtained from the asymmetric catalyst trials described above, was heated in a sealed J-Young NMR tube in a circulating oil bath. The reaction mixture was monitored for decomposition by ¹H NMR analysis. The enantiomeric excess of the cyclohexadiene was monitored by opening the tube under an inert atmosphere, removing a 50 μL aliquot of the reaction mixture, and re-sealing the tube. The aliquot was passed through a small plug of silica gel (20% EtOAc in hexanes). The eluent was concentrated *in vacuo* and dissolved in *i*PrOH for chiral HPLC analysis (Chiralcel OD, flow rate 0.5 mL/min, 98:2 hexanes:*i*PrOH, Tr = 20.4, 23.1 min). The results of this experiment can be found in Table 4.



Synthesis of triene 6.1. A J-Young NMR tube was charged with Sc(OTf)₃ (45 mg, 0.093 mmol), 2,2'-isopropylidenebis[(4*S*)-4-phenyl-2-oxazoline] (82 mg, 0.22 mmol), 2,6-di-*tert*-butyl-4-methylpyridine (23 mg, 0.11 mmol), dichloromethane-*d*₂ (600 μL), and cyclohexadiene **5.34** (1.2 mL, 77 mM in dichloromethane-*d*₂, 0.093 mmol). The NMR tube was then sealed and kept at room temperature under ambient fluorescent light for 6 days, after which time complete consumption of the starting materials was observed by ¹H NMR analysis. The reaction mixture was concentrated *in vacuo* and purified by silica gel chromatography (15-18% EtOAc in hexanes) yielding 17 mg triene **6.1** as a yellow oil (81%). ¹H NMR (500 MHz, CDCl₃): δ 7.61-7.58 (m, 1H), 7.34 (d, *J* = 7.6 Hz, 2H), 7.29-7.24 (m, 2H), 7.18 (t, *J* = 7.3 Hz, 1H), 6.46 (d, *J* = 12.2 Hz, 1H), 6.37 (s, 1H; vinyl CH, *n*Øe to CH₃), 6.13 (d, *J* = 12.2 Hz, 1H), 2.60-2.55 (m, 2H), 2.37-2.34 (m, 2H), 1.97 (s, 3H; CH₃, *n*Øe to vinyl CH) ppm; ¹³C NMR (125 MHz, CDCl₃): δ 208.6, 159.6, 141.2, 137.8, 135.0, 134.4, 129.4, 128.7, 128.3, 127.0, 119.1, 34.1, 27.3, 23.5 ppm; IR 2922, 1700, 1440, 696 cm⁻¹; HRMS (EI⁺) Exact mass calcd for C₁₆H₁₆O [M]⁺: 224.1201, found 224.1200.

Observation of kinetic resolution of cyclohexadiene 5.34 during formation of triene 6.1. A J-Young NMR tube was charged with Sc(OTf)₃ (15 mg, 0.031 mmol), 2,6-bis[(4*R*)-4-phenyl-2-oxazolynil]pyridine (23 mg, 0.062 mmol), 2,6-di-*tert*-butyl-4-methylpyridine (8 mg, 0.039 mmol), dichloromethane-*d*₂ (500 μL), and enantioenriched cyclohexadiene **5.34** (800 μL, 39 mM in dichloromethane-*d*₂, 0.031 mmol; containing 25 mol% 1,1,2,2-tetrachloroethane as an internal standard), obtained from the asymmetric catalyst trials described above. The reaction mixture was kept at room temperature under ambient fluorescent light and monitored over the course of 30 days. Conversion to triene **6.1** was measured by ¹H NMR analysis. The

enantiomeric excess of the cyclohexadiene was monitored by opening the J-Young NMR tube under an inert atmosphere, removing a 50 μ L aliquot of the reaction mixture, and re-sealing the J-Young NMR tube. The aliquot was passed through a small plug of silica gel (20% EtOAc in hexanes). The eluent was concentrated *in vacuo* and dissolved in *i*PrOH for chiral HPLC analysis (Chiralcel OD, flow rate 0.5 mL/min, 98:2 hexanes:*i*PrOH, Tr [cyclohexadiene **5.34**] = 20.4, 23.1 min, Tr [triene **6.1**] = 25.9 min). The results of this experiment can be found in Table 5.

References

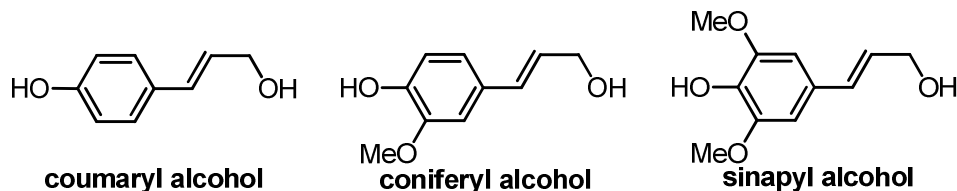
- (1) Tanaka, K.; Katsumura, S. *J. Am. Chem. Soc.* **2002**, *124*, 9660.
- (2) Sklenicka, H. M.; Hsung, R. P.; McLaughlin, M. J.; Wei, L.-L.; Gerasyuto, A. I.; Brennessel, W. B. *J. Am. Chem. Soc.* **2002**, *124*, 10435.
- (3) Tanaka, K.; Kobayashi, T.; Mori, H.; Katsumura, S. *J. Org. Chem.* **2004**, *69*, 5906.
- (4) Sydorenko, N.; Hsung, R. P.; Vera, E. L. *Org. Lett.* **2006**, *8*, 2611.
- (5) Parker, K. A.; Wang, Z. *Org. Lett.* **2006**, *8*, 3553.
- (6) Okamura, W. H.; De Lera, A. R. In *Comprehensive Organic Synthesis*; Trost, B. M., Fleming, I., Paquette, L. A., Eds.; Pergamon Press: New York, 1991; Vol. 5, p 699.
- (7) Liang, G.; Gradl, S. N.; Trauner, D. *Org. Lett.* **2003**, *5*, 4931.
- (8) Aggarwal, V. K.; Belfield, A. J. *Org. Lett.* **2003**, *5*, 5075.
- (9) Liang, G.; Trauner, D. *J. Am. Chem. Soc.* **2004**, *126*, 9544.
- (10) Rueping, M.; Ieawsuwan, W.; Antonchick, A. P.; Nachtsheim, B. J. *Angew. Chem. Int. Ed.* **2007**, *46*, 2097.
- (11) Maciver, E. E.; Thompson, S.; Smith, M. D. *Angew. Chem. Int. Ed.* **2009**, *48*, 9979.
- (12) Müller, S.; List, B. *Angew. Chem. Int. Ed.* **2009**, *48*, 9975.
- (13) Vicario, J. L.; Badia, D. *ChemCatChem* **2010**, *2*, 375.
- (14) Chapuis, C.; Jurczak, J. *Helv. Chim. Acta* **1987**, *70*, 436.
- (15) Maruoka, K.; Itoh, T.; Shirasaka, T.; Yamamoto, H. *J. Am. Chem. Soc.* **1988**, *110*, 310.
- (16) Graven, A.; Johannsen, M.; Jørgensen, K. A. *Chem. Commun.* **1996**, 2373.
- (17) Fhal, A.-R.; Renaud, P. *Tetrahedron Lett.* **1997**, *38*, 2661.
- (18) Soki, F.; Neudörfl, J.-M.; Goldfuss, B. *J. Organomet. Chem.* **2008**, *693*, 2139.
- (19) Whitesell, J. K. *Chem. Rev.* **1989**, *89*, 1581.
- (20) Brunel, J. M. *Chem. Rev.* **2005**, *105*, 857.
- (21) Corey, E. J.; Imwinkelried, R.; Pikul, S.; Xiang, Y. B. *J. Am. Chem. Soc.* **1989**, *111*, 5493.
- (22) Pikul, S.; Corey, E. J. *Org. Syn.* **1993**, *71*, 30.
- (23) Imai, N.; Takahashi, H.; Kobayashi, S. *Chem. Lett.* **1994**, 177.
- (24) Ryu, D. H.; Corey, E. J. *J. Am. Chem. Soc.* **2003**, *125*, 6388.
- (25) Corey, E. J.; Shibata, T.; Lee, T. W. *J. Am. Chem. Soc.* **2002**, *124*, 3808.
- (26) Leung, W.-H.; Chan, E. Y.; Chow, E. K. F.; Williams, I. D.; Peng, S.-M. *J. Chem. Soc. Dalton Trans.* **1996**, 1229.
- (27) Jacobsen, E. N.; Kakiuchi, F.; Konsler, R. G.; Larrow, J. F.; Tokunaga, M. *Tetrahedron Lett.* **1997**, *38*, 773.
- (28) Hu, Y.-J.; Huang, X.-D.; Yao, Z.-J.; Wu, Y.-L. *J. Org. Chem.* **1998**, *63*, 2456.
- (29) Martinez, L. E.; Leighton, J. L.; Carsten, D. H.; Jacobsen, E. N. *J. Am. Chem. Soc.* **1995**, *117*, 5897.

- (30) Evans, D. A.; Rovis, T.; Johnson, J. S. *Pure and Applied Chemistry* **1999**, *71*, 1407.
- (31) Fukuzawa, S.-i.; Matsuzawa, H.; Metoki, K. *Synlett* **2001**, 709.
- (32) Evans, D. A.; Masse, C. E.; Wu, J. *Org. Lett.* **2002**, *4*, 3375.
- (33) Evans, D. A.; Wu, J. *J. Am. Chem. Soc.* **2003**, *125*, 10162.
- (34) Taylor, M. S.; Tokunaga, N.; Jacobsen, E. N. *Angew. Chem. Int. Ed.* **2005**, *44*, 6700.
- (35) Reisman, S. E.; Doyle, A. G.; Jacobsen, E. N. *J. Am. Chem. Soc.* **2008**, *130*, 7198.
- (36) Alaimo, P. J.; Peters, D. W.; Arnold, J.; Bergman, R. G. *J. Chem. Ed.* **2001**, *78*, 64.
- (37) Nelson, S. G.; Zhu, C.; Shen, X. *J. Am. Chem. Soc.* **2004**, *126*, 14.
- (38) Trost, B. M.; Van Vranken, D. L.; Bingel, C. *J. Am. Chem. Soc.* **1992**, *114*, 9327.
- (39) Ostwald, R.; Chavant, P.-Y.; Stadtmüller, H.; Knochel, P. *J. Org. Chem.* **1994**, *59*, 4143.
- (40) Takahashi, H.; Kawakita, T.; Ohno, M.; Yoshioka, M.; Kobayashi, S. *Tetrahedron* **1992**, *48*, 5691.
- (41) Hilgraf, R.; Pfaltz, A. *Adv. Synth. Catal.* **2005**, *347*, 61.
- (42) Mikami, K.; Kakuno, H.; Aikawa, K. *Angew. Chem. Int. Ed.* **2005**, *44*, 7257.

Part 2 - Chapter 1. *Introduction to the Catalytic Disproportionation of Lignin Model Compounds.*

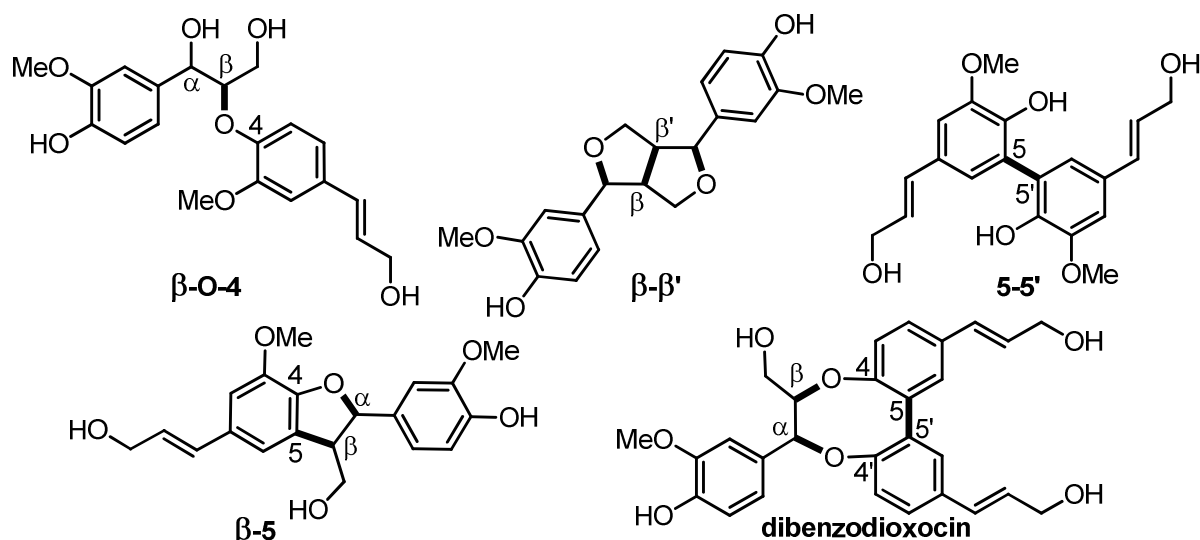
Petroleum, natural gas, and coal represent 86% of the total global energy consumed in 2006.¹ The chemical energy stored in these fossil fuels traces its origins to the photosynthetic biomass production of ancient plant life. Over tens to hundreds of millions of years of geological sequestration and heating, this biomass was transformed to the hydrocarbon-rich fossil fuels we use today.² Rapidly increasing global energy demand¹ and concern over the environmental consequences of the atmospheric release of this sequestered fossil carbon³ both highlight the need for the development of renewable energy technologies. Fuels produced directly from plant biomass, bypassing the exceedingly slow geological transformation process, represents an underutilized renewable energy platform. Biomass was the source for 1% of the total global energy consumed in 2006,¹ while recent analysis estimates the total sustainable global biomass energy production potential to be 25% of the 2006 global energy consumption.^{1,4} It should be noted that the production of fuels from biomass raises a variety of environmental and societal concerns,⁵ and has drawbacks as compared to other renewable energy technologies.⁶

Lignocellulose is the planet's most abundant form of biomass, and is composed primarily of C₅ and C₆ sugars in the form of cellulose (poly-β(1,4)-glucose) and hemicellulose (a heteropolymer of xylose, mannose, and glucose).^{7,8} Numerous methods have been developed for the chemical and biological transformation of these saccharide components into liquid fuels.⁹⁻¹² However there are comparatively fewer processes for the production of liquid fuels from lignin,^{10,13-15} which is the third primary constituent of lignocellulosic biomass (up to 30% by weight).¹⁰ Lignin is also of interest for the production of materials and commodity chemicals from biomass.¹⁵⁻¹⁹ Lignin is found primarily in and between the cell walls of vascular plants, and is thought to lend structural support, aid in water and nutrient transport, and provide resistance to microbial degradation.²⁰ Lignin is an amorphous polymer composed of the three 4-hydroxyphenylpropanoid monomers (monolignols) shown in Scheme 1.



Scheme 1. The three 4-hydroxyphenylpropanoids that are the building blocks of lignin.

The exact monomeric composition and structure of lignin differs from plant to plant. Softwood lignin is composed of >90% coniferyl alcohol subunits, while hardwood and grass lignin is composed of coniferyl and sinapyl alcohol subunits in varying ratios, with the remainder in both cases being comprised of coumaryl alcohol.²⁰ Lignin is biosynthesized by an enzymatically-initiated free-radical polymerization of the monolignols,^{21,22} which results in a heterogeneous structure.²³ However, a number of repeating linkages are found throughout this highly polydisperse biopolymer. The most common linkages are shown in Scheme 2, with chemical bonds connecting the monolignols in bold. In addition to variations in monomeric composition, the relative abundances of these linkages are also species specific (Table 1).



Scheme 2. Common linkages connecting the hydroxyphenylpropanoid subunits in lignin.

Table 1. Approximate abundance of the common linkages connecting the monolignols in lignin (number of linkages per 100 C₉ units).^{13,20,24-26} n.d. = not determined.

Linkage	Softwoods	Hardwoods	Grasses
β -O-4	45-51	60-65	65-93
β - β'	2-6	3-12	0-22
5-5'	19-27	2-9	n.d.
β -5	9-15	3-11	0-37
dibenzodioxocin	5-7	1-2	n.d.

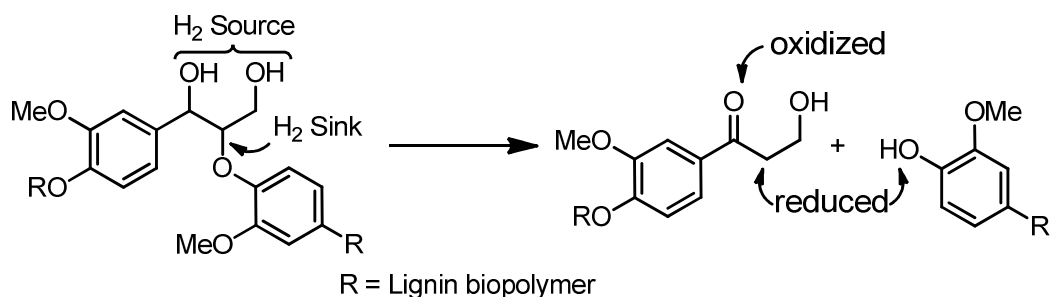
The structure of lignin is highly dependent not only on the source plant, but also on the isolation method employed. There are a wide variety of processes for the isolation (or removal) of lignin from lignocellulosic biomass. The most widely employed is the Kraft process, which typically involves adding the biomass input to an aqueous solution of sodium hydroxide and sodium sulfide and heating the resultant suspension at 150-180 °C for around 2 h, during which time lignin is cleaved into smaller, water-soluble fragments. This process results in considerable structural changes to lignin, including the introduction of styrene and stilbene moieties as well as competitive repolymerization.^{13,14} Another common lignin isolation process is the lignosulfonate process, whereby the biomass input is treated with aqueous calcium or magnesium sulfite. This process results in less depolymerization than does the Kraft process, and lignin is rendered water-soluble by the introduction of numerous sulfonate groups.¹³ Finally, the organosolv process extracts lignin using organic solvents and small amounts of acid catalysts at 90-220 °C for 25-100 min. While this process does not require the use of sulfides, sulfites, or alkali hydroxides, it does suffer from the high energy cost of solvent recovery.^{13,27}

In devising a lignin depolymerization strategy, we first looked to nature for inspiration. Lignin is degraded in the environment by a variety of fungi and bacteria,^{28,29} and the only known organisms capable of completely mineralizing the biopolymer are white-rot fungi.^{30,31} Environmental lignin degradation is mediated primarily by the enzymes lignin peroxidase, manganese peroxidase, and laccase.^{15,31} The reactions mediated by these enzymes are thought to proceed *via* radical mechanisms,³¹ which in the absence of complete oxidative lignin degradation

can result in re-polymerization yielding polymers of increased molecular weight.^{15,32} This is a concern from the standpoint of developing a biomimetic process for the production of liquid fuels from lignin, where low molecular weight C₇-C₁₈ molecules are ideal. In addition, the oxidative nature of these environmental degradation pathways is unproductive with respect to the energetic efficiency of a fuel production process.

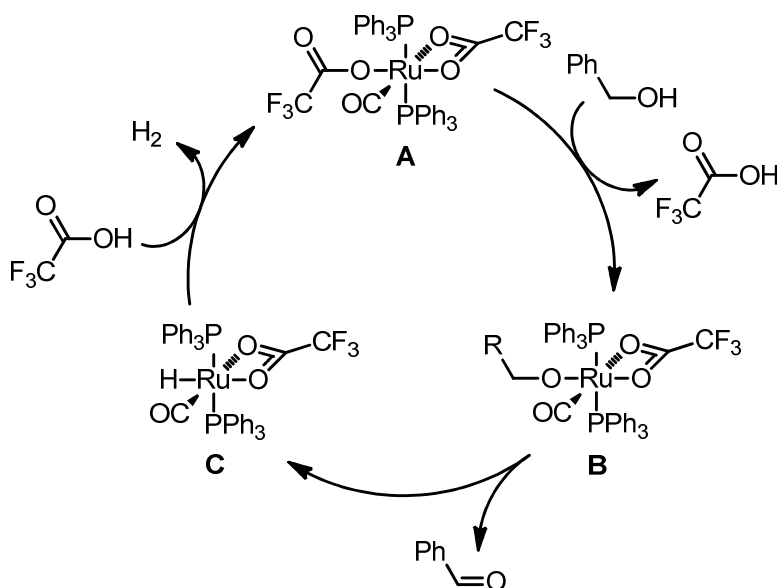
Current industrial lignin fragmentation processes can be divided into three categories—namely catalytic and thermochemical cracking and hydrolysis reactions, catalytic reductions, and catalytic oxidations.¹³ The high-temperature catalytic and thermochemical cracking and hydrolysis of lignin yields a variety of products, including gaseous hydrocarbons together with carbon dioxide and carbon monoxide, an aqueous fraction containing water and water-soluble hydrocarbons, as well as an organic fraction containing phenols and polysubstituted phenolic compounds. The primary drawbacks to these processes are the production of significant amounts of char and uncontrolled re-polymerization of the degradation products.^{13,33,34} Research into the catalytic reduction of lignin has focused primarily on hydrogenation using solid-supported metal catalysts such as Co-Mo, Ni-Mo, and Pt. While a 70% conversion of organosolv lignin to alkanols such as methanol and 4-*n*-propylcyclohexanol using a Cu-CrO hydrogenation catalyst system has been reported,³⁵ many of these systems suffer from poor conversions and all of them require an external hydrogen source.¹³ Finally, the development of processes for the catalytic oxidation of lignin has focused primarily on the production of fine chemicals and the delignification of biomass for the pulp and paper industry. Catalytic oxidation is of less interest with respect to biofuels production due to the increased oxygenation and decreased energy content of the resulting products, relative to those formed *via* reductive processes.¹³

A combination of the reductive and oxidative processes described above, a redox-neutral catalytic disproportionation of lignin, would represent a novel fragmentation strategy. The diverse array of functionality present in lignin here represents an opportunity to use one type of moiety present in the biopolymer as a source of molecular hydrogen and another type of moiety as a molecular hydrogen sink. Production of a liquid fuel from lignin first requires cleavage of the bonds holding the biopolymer together (Scheme 2). We targeted the most common type of linkage present in lignin, the β-O-4 (glycerol-β-aryl ether) moiety, to investigate the possibility of using this disproportionation strategy. This strategy requires a catalyst capable of both oxidizing carbinol moieties (the hydrogen source) and effecting reductive cleavage of sp³ carbon-oxygen single bonds (the hydrogen sink) (Scheme 3).



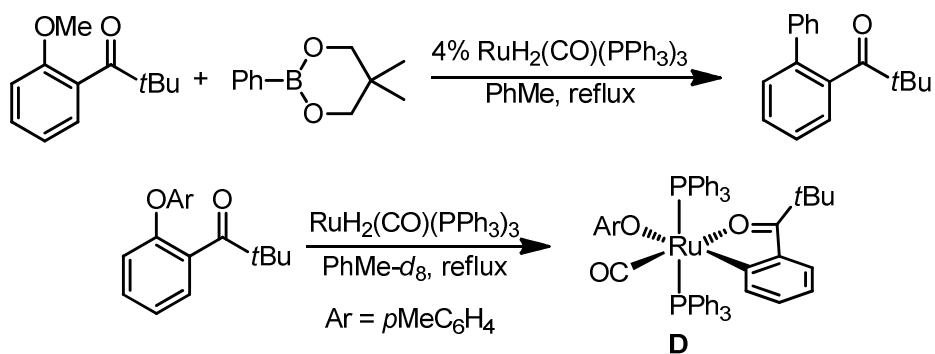
Scheme 3. Disproportionation strategy for the cleavage of the glycerol β-aryl ether linkage of lignin.

The use of primary and secondary alcohols as hydrogen sources is well preceded in the literature. This reaction is typically coupled with the hydrogenation of carbonyl or olefin moieties in a process known as transfer hydrogenation,³⁶⁻³⁸ but alcohol dehydrogenation with concomitant evolution of molecular hydrogen is also known. One of the most efficient examples of this is the Ru(O₂CCF₃)₂(CO)(PPh₃)₂-catalyzed dehydrogenation of benzyl alcohol shown in Scheme 4. This catalyst system is also capable of efficiently dehydrogenating a variety of primary and secondary alcohols. The reaction is thought to proceed through protonolysis of a trifluoroacetate ligand of **A** to yield ruthenium alkoxide **B**, which undergoes β-hydride elimination to liberate the dehydrogenated product (benzaldehyde in this case) and yield hydrido ruthenium trifluoroacetate species **C**. The catalytic cycle is completed by protonolysis with trifluoroacetic acid to regenerate bis-trifluoroacetato ruthenium species **A**.³⁹⁻⁴¹



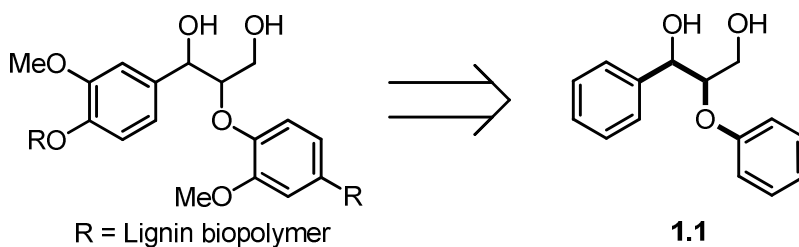
Scheme 4. Ruthenium-catalyzed dehydrogenation of alcohols.³⁹⁻⁴¹

While there are numerous examples of transfer hydrogenation using alcohol reductants, there are no examples that have coupled carbinol oxidation with the reductive cleavage of carbon-oxygen single bonds. There are, however, a few published examples of the transition metal-catalyzed cleavage of carbon-oxygen single bonds.⁴²⁻⁵³ Most relevant to our work is the chelation-assisted cleavage of an sp² carbon-oxygen bond by ruthenium, as is shown in Scheme 5.^{48,49} This transformation was discovered in the context of the ruthenium-catalyzed phenylation of methoxy-substituted pivalophenone derivatives using phenyl boronate (Scheme 5, top), which is thought to proceed by initial oxidative-addition of the carbon-oxygen single bond to the ruthenium catalyst.⁴⁸ Evidence for this mechanism was later provided in the form of the isolation of ruthenium-aryloxy complex **D** (Scheme 5, bottom).⁴⁹



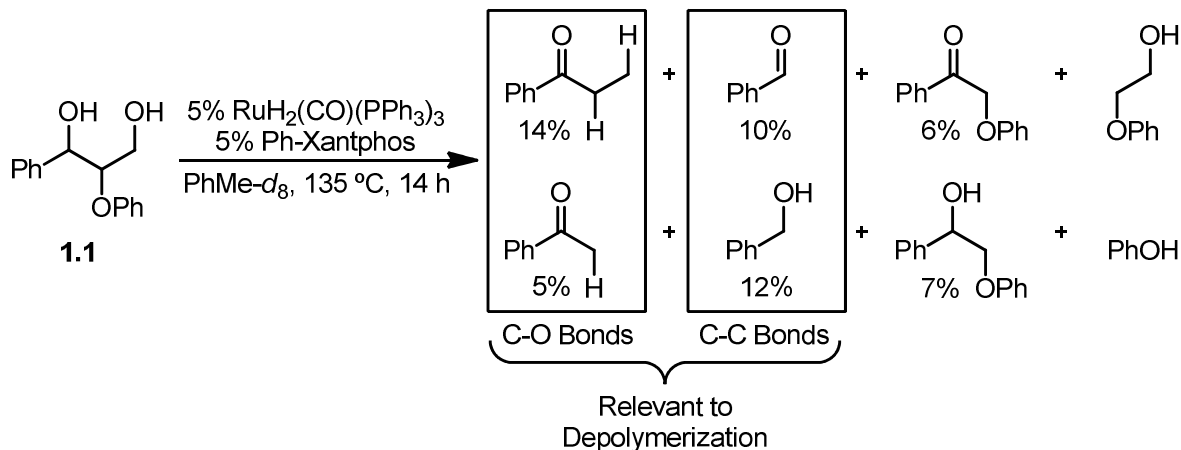
Scheme 5. Chelation-assisted carbon-oxygen bond cleavage and ruthenium-catalyzed phenylation of 2'-methoxypivalophenone.^{48,49}

The development of a catalytic reaction for the lignin depolymerization using lignin itself poses a number of analytical challenges. A common strategy employed in this context is the use of small molecules as mimics of the functionality present in lignin.¹³ As the glycerol- β -aryl ether linkage was our target, we employed model compounds such as that shown in Scheme 6. The bonds of model compound **1.1** relevant to the depolymerization of lignin are highlighted.



Scheme 6. Compound **1.1**, a small molecule model for the glycerol- β -aryl ether linkage of lignin. Bonds relevant to the depolymerization of lignin are highlighted.

Given the literature precedents for the use of $\text{RuH}_2(\text{CO})(\text{PPh}_3)_3$ in the catalytic cleavage of carbon-oxygen bonds, as well as this complex's application in transfer hydrogenation reactions,⁵⁴⁻⁶⁰ this was one of the first catalysts employed in the disproportionation of lignin model compound **1.1** by postdoctoral researcher Dr. Jason Nichols. ^1H NMR analysis of the reaction mixture formed upon treatment of **1.1** with 5 mol% of $\text{RuH}_2(\text{CO})(\text{PPh}_3)_3$ and 5 mol% of 4,5-bis(diphenylphosphino)-9,9-dimethylxanthene (Ph-xantphos) at 135 °C revealed the presence of a variety of products, the result of the cleavage of both carbon-oxygen and carbon-carbon bonds (Scheme 6). Importantly, products that are the result of the cleavage of bonds relevant to the depolymerization of lignin are observed, amounting to an overall 4% “depolymerization”. It should be noted that little to no conversion to products was observed in the absence of the wide-bite angle bis-phosphine ligand Ph-xantphos. The ruthenium complex presumably formed *in situ*, $\text{RuH}_2(\text{CO})(\text{PPh}_3)(\text{Ph-Xantphos})$, has been shown to be an active transfer hydrogenation catalyst.^{56,58,60}



Scheme 6. Ruthenium-catalyzed disproportionation of lignin model compound **1.1**. Ph-Xantphos = 4,5-Bis(diphenylphosphino)-9,9-dimethylxanthene.

The complex reaction outcome observed in the disproportionation of **1.1** underscored the need to develop model compounds that would result in simpler product distributions, in order to facilitate reaction optimization and the development of an understanding of the reaction mechanism. Toward this end, model compounds were synthesized that isolate both the carbon-oxygen and carbon-carbon bond cleavage reactions. Based on experiments carried out with these model compounds, our current understanding of how the products of the disproportionation of **1.1** arise is represented below in Scheme 7. We propose that carbon-carbon bonds are cleaved by oxidation of a carbinol moiety of **1.1** followed by retro-aldol cleavage. Our mechanistic proposal for the cleavage of carbon-oxygen bonds involves α -phenoxyacetophenone, α -phenoxypropiophenone, or 2-phenoxy-1-phenylpropenone as the immediate precursors to the chelation-assisted carbon-oxygen bond cleavage step. A detailed explanation of our investigations into the carbon-carbon and carbon-oxygen bond cleavage reactions is given in Chapters 2 and 3, respectively.

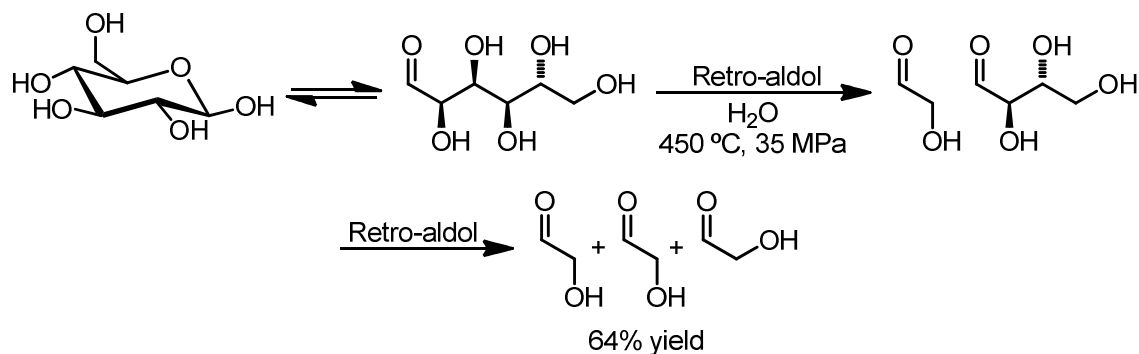
- (13) Zakzeski, J.; Bruijninx, P. C. A.; Jongerius, A. L.; Weckhuysen, B. M. *Chem. Rev.* **2010**, *110*, in press.
- (14) Chakar, F. S.; Ragauskas, A. J. *Ind. Crop. Prod.* **2004**, *20*, 131.
- (15) Sena-Martins, G.; Almeida-Vara, E.; Duarte, J. C. *Ind. Crop. Prod.* **2008**, *27*, 189.
- (16) Lora, J. H.; Glasser, W. G. *J. Polym. Environ.* **2002**, *10*, 39.
- (17) Nitz, H.; Semke, H.; Mülhaupt, R. *Macromol. Mater. Eng.* **2001**, *286*, 737.
- (18) Kadla, J. F.; Kubo, S.; Venditti, R. A.; Gilbert, R. D. C., A. L.; Griffith, W. *Carbon* **2002**, *40*, 2913.
- (19) Boudet, A. M.; Kajita, S.; Grima-Pettenati, J.; Goffner, D. *Trends Plant Sci.* **2003**, *8*, 576.
- (20) Lebo, S. E. J.; Gargulak, J. D.; McNally, T. J. Lignin. In *Kirk-Othmer Encyclopedia of Chemical Technology*; John Wiley & Sons, Inc.: Hoboken, 2001; Vol. 15.
- (21) Ralph, J.; Lundquist, K.; Brunow, G.; Lu, F.; Kim, H.; Schatz, P. F.; Marita, J. M.; Hatfield, R. D.; Ralph, S. A.; Christensen, J. H.; Boerjan, W. *Phytochem. Rev.* **2004**, *3*, 29.
- (22) Boerjan, W.; Ralph, J.; Baucher, M. *Annu. Rev. Plant Biol.* **2003**, *54*, 519.
- (23) Brunow, G.; Lundquist, K.; Gellerstedt, G. Lignin. In *Analytical Methods in Wood Chemistry, Pulping, and Papermaking*; Sjöström, E., Alén, R., Eds.; Springer-Verlag: Berlin, 1999, p 77.
- (24) Martínez, A. T.; Rencoret, J.; Marques, G.; Gutiérrez, A.; Ibarra, D.; Jiménez-Barbere, J.; del Río, J. C. *Phytochemistry* **2008**, *69*, 2831.
- (25) del Río, J. C.; Rencoret, J.; Marques, G.; Gutiérrez, A.; Ibarra, D.; Santos, J. I.; Jiménez-Barbere, J.; Zhang, L.; Martínez, A. T. *J. Agric. Food Chem.* **2008**, *56*, 9525.
- (26) del Río, J. C.; Rencoret, J.; Marques, G.; Li, J.; Gellerstedt, G.; Jiménez-Barbere, J.; Martínez, A. T.; Gutiérrez, A. *J. Agric. Food Chem.* **2009**, *57*, 10271.
- (27) da Costa Sousa, L.; Chundawat, S. P.; Balan, V.; Dale, B. E. *Curr. Opin. Biotechnol.* **2009**, *20*, 339.
- (28) Tuomela, M.; Vikman, M.; Hatakka, A.; Itävaara, M. *Bioresour. Technol.* **2000**, *72*, 169.
- (29) Martínez, A. T.; Speranza, M.; Ruiz-Dueñas, F. J.; Ferreira, P.; Camarero, S.; Guillén, F.; Martínez, M. J.; Gutiérrez, A.; del Río, J. C. *Int. Microbiol.* **2005**, *8*, 195.
- (30) Kirk, T. K.; Farrell, R. L. *Annu. Rev. Microbiol.* **1987**, *41*, 465.
- (31) ten Have, R.; Teunissen, P. J. M. *Chem. Rev.* **2001**, *101*, 3397.
- (32) Haemmerli, S. D.; Leisola, M. S. A.; Fiechter, A. *FEMS Microbiol. Lett.* **1986**, *35*, 33.
- (33) Dorrestijn, E.; Laarhoven, L. J. J.; Arends, I. W. C. E.; Mulder, P. *J. Anal. Appl. Pyrolysis* **2000**, *54*, 153.
- (34) Mohan, D.; Pittman, C. U. J.; Steele, P. H. *Energy Fuels* **2006**, *20*, 848.
- (35) Harris, E. E.; D'Ianni, J.; Adkins, H. *J. Am. Chem. Soc.* **1938**, *60*, 1467.
- (36) Brieger, G.; Nestrick, T. J. *Chem. Rev.* **1974**, *74*, 567.
- (37) Samec, J. S. M.; Bäckvall, J. E.; Andersson, P. G.; Brandt, P. *Chem. Soc. Rev.* **2006**, *35*, 237.
- (38) Zassinovich, G.; Mestroni, G.; Gladdiali, S. *Chem. Rev.* **1992**, *92*, 1051.
- (39) Dobson, A.; Robinson, S. D. *J. Organomet. Chem.* **1975**, *87*, C52.
- (40) Dobson, A.; Robinson, S. D. *Inorg. Chem.* **1977**, *16*, 137.
- (41) Dobson, A.; Robinson, S. D. *Inorg. Chem.* **1977**, *16*, 1321.
- (42) Wenkert, E.; Michelotti, E. L.; Swindell, C. S. *J. Am. Chem. Soc.* **1979**, *101*, 2246.

- (43) Wenkert, E.; Michelotti, E. L.; Swindell, C. S.; Tingoli, M. *J. Org. Chem.* **1984**, *49*, 4894.
- (44) Bryndza, H. E.; Tam, W. *Chem. Rev.* **1988**, *88*, 1163.
- (45) van der Boom, M. E.; Liou, S.-Y.; Ben-David, Y.; Vigalok, A.; Milstein, D. *Angew. Chem. Int. Ed.* **1997**, *36*, 625.
- (46) van der Boom, M. E.; Liou, S.-Y.; Ben-David, Y.; Shimon, L. J. W.; Milstein, D. *J. Am. Chem. Soc.* **1998**, *120*, 6531.
- (47) Dankwardt, J. W. *Angew. Chem. Int. Ed.* **2004**, *43*, 2428.
- (48) Kakiuchi, F.; Usui, M.; Ueno, S.; Chatani, N.; Murai, S. *J. Am. Chem. Soc.* **2004**, *126*, 2706.
- (49) Ueno, S.; Mizushima, E.; Chatani, N.; Kakiuchi, F. *J. Am. Chem. Soc.* **2006**, *128*, 16516.
- (50) Guan, B.-T.; Xiang, S.-K.; Wang, B.-Q.; Sun, Z.-P.; Wang, Y.; Zhao, K.-Q.; Shi, Z.-J. *J. Am. Chem. Soc.* **2008**, *130*, 3268.
- (51) Guan, B.-T.; Xiang, S.-K.; Wu, T.; Sun, Z.-P.; Wang, B.-Q.; Zhao, K.-Q.; Shi, Z.-J. *Chem. Commun.* **2008**, 1437.
- (52) Tobisu, M.; Shimasaki, T.; Chatani, N. *Angew. Chem. Int. Ed.* **2008**, *47*, 4866.
- (53) Choi, J.; Choliy, Y.; Zhang, X.; Emge, T. J.; Krogh-Jespersen, K.; Goldman, A. S. *J. Am. Chem. Soc.* **2009**, *131*, 15627.
- (54) Graser, B.; Steigerwald, H. *J. Organomet. Chem.* **1980**, *193*, C67.
- (55) Murahashi, S.-I.; Naota, T.; Ito, K.; Maeda, Y.; Taki, H. *J. Org. Chem.* **1987**, *52*, 4319.
- (56) Ledger, A. E. W.; Slatford, P. A.; Lowe, J. P.; Mahon, M. F.; Whittlesey, M. K.; Williams, J. M. J. *J. Chem. Soc. Dalton Trans.* **2009**, 716.
- (57) Shibahara, F.; Bower, J. F.; Krische, M. J. *J. Am. Chem. Soc.* **2008**, *130*, 14120.
- (58) Owston, N. A.; Parker, A. J.; Williams, J. M. J. *Chem. Commun.* **2008**, 624.
- (59) Maytum, H. C.; Tavassoli, B.; Williams, J. M. J. *Org. Lett.* **2007**, *9*, 4387.
- (60) Hall, M. I.; Pridmore, S. J.; Williams, J. M. J. *Adv. Synth. Catal.* **2008**, *350*, 1975.

Part 2 - Chapter 2. *Retro-aldol cleavage of a 1-phenylpropane-1,3-diol lignin model compound via β -hydroxypropiophenone*

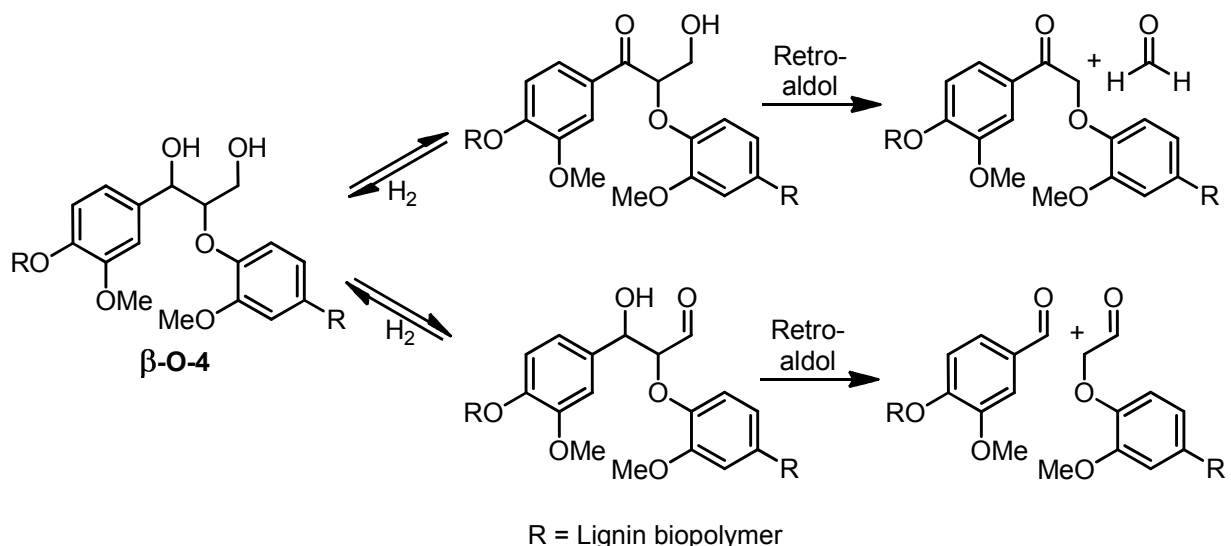
Introduction

Given the highly oxygenated nature of the components of lignocellulosic biomass, the development of molecular transformations aimed at depolymerizing and reducing the molecular complexity of this heterogeneous biopolymer have focused on reactions involving oxygenated moieties.¹ One such reaction is the retro-aldol cleavage of β -hydroxy carbonyl compounds. As this functionality is present in the open-chain form of monosaccharides, retro-aldol cleavage reactions have been observed in a variety of transformations of these biomass components.²⁻⁸ An example of this is a recent report of the retro-aldol cleavage of glucose to hydroxyacetaldehyde in supercritical water (Scheme 1).³ While hydroxyacetaldehyde is of interest as a commodity chemical it has less relevance as a liquid fuel due to its low molecular weight and high oxygen content. Furthermore, this reaction suffers from modest yields and requires harsh reaction conditions. To the best of our knowledge there have been only two reports of retro-aldol cleavage of saccharides in a catalytic system.^{5,6}



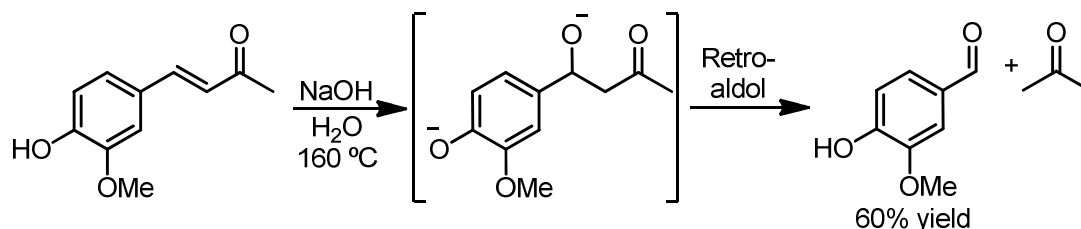
Scheme 1. Retro-aldol cleavage of glucose to yield glycolaldehyde.³

Compared to the number of retro-aldol cleavage studies on saccharides, there are far fewer reports on the analogous reaction of lignin model compounds.^{9,10} This is likely due in part to the lack of β -hydroxy carbonyl moieties in the structure of lignin itself. However, one of the most prevalent linkages in lignin, the β -O-4 (glycerol- β -aryl ether) linkage, contains a 1,3-diol, which upon oxidation would yield a β -hydroxy carbonyl moiety capable of undergoing either a thermal or catalyzed retro-aldol cleavage reaction (Scheme 2).



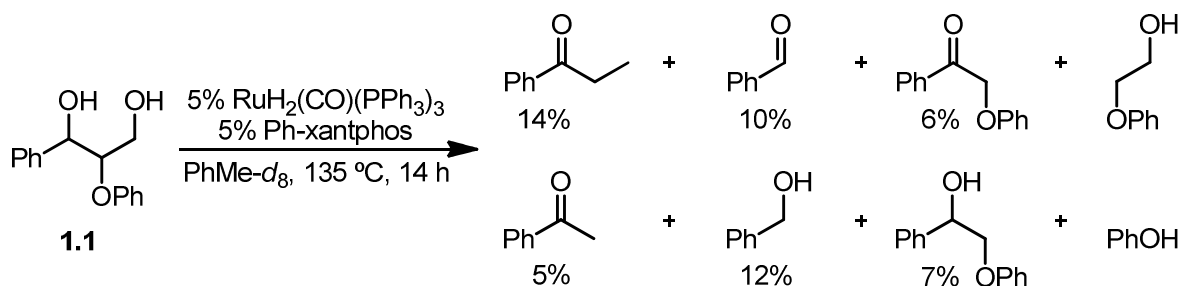
Scheme 2. Oxidative retro-aldol cleavage of the β -O-4 linkage of lignin.

The retro-aldol cleavage of a lignin model compound that was intended to mimic the glycerol- β -aryl ether linkage was the subject of a recent report. In this, the authors described the retro-aldol cleavage of 4-(4-hydroxy-3-methoxyphenyl)-3-buten-2-one under basic conditions, which resulted in a 60% yield of vanillin (Scheme 3).⁹ This model compound differs from the glycerol- β -aryl ether linkage in that it contains olefin and ketone moieties as well as a phenylbutanoid (as opposed to phenylpropanoid) skeleton and lacks an aryl ether linkage. While this study also suffers from moderate yields and the need for superstoichiometric amounts of NaOH, it serves as an indication that the oxidative retro-aldol cleavage of lignin, as outlined in Scheme 2, is possible.



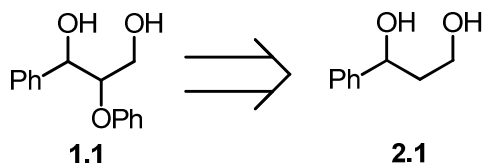
Scheme 3. Retro-aldol cleavage of a lignin model compound under basic conditions.⁹

Chapter 1 described the results of a ruthenium-catalyzed disproportionation of glycerol- β -aryl ether model compound **1.1** that was developed by Dr. Jason Nichols. While this reaction yielded a variety of products, the compounds 2-phenoxyacetophenone, 2-phenoxy-1-phenylethanol, benzaldehyde, benzyl alcohol, acetophenone, and 2-phenoxyethanol are all the result of a carbon-carbon bond cleavage. We hypothesized that these products are formed *via* an oxidative retro-aldol cleavage mechanism as outlined in Scheme 2. In addition, the compounds propiophenone, acetophenone, and phenol all occur through a carbon-oxygen bond cleavage process.



Scheme 4. Ruthenium-catalyzed disproportionation of lignin model compound **1.1**. Ph-xantphos = 4,5-bis(diphenylphosphino)-9,9-dimethylxanthene.

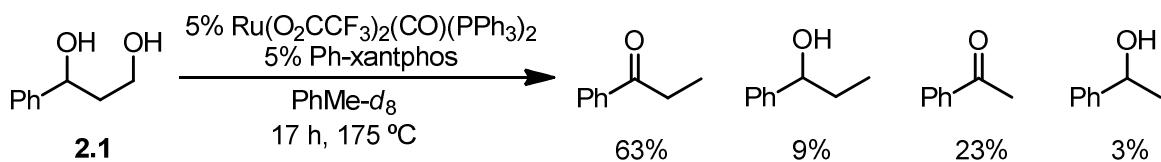
The present chapter will describe our investigations into the carbon-carbon bond cleavage reaction observed with **1.1**. Our studies were carried out using 1-phenylpropane-1,3-diol (**2.1**), a simplified version of **1.1** that lacks an aryl ether linkage (Scheme 5). This facilitated reaction optimization as well as mechanistic analysis of the carbon-carbon bond cleavage reaction in isolation from the carbon-oxygen bond cleavage reaction.



Scheme 5. Lignin model compound **2.1**, designed to carbon-carbon bond cleavage in isolation from carbon-oxygen bond cleavage.

Results & Discussion

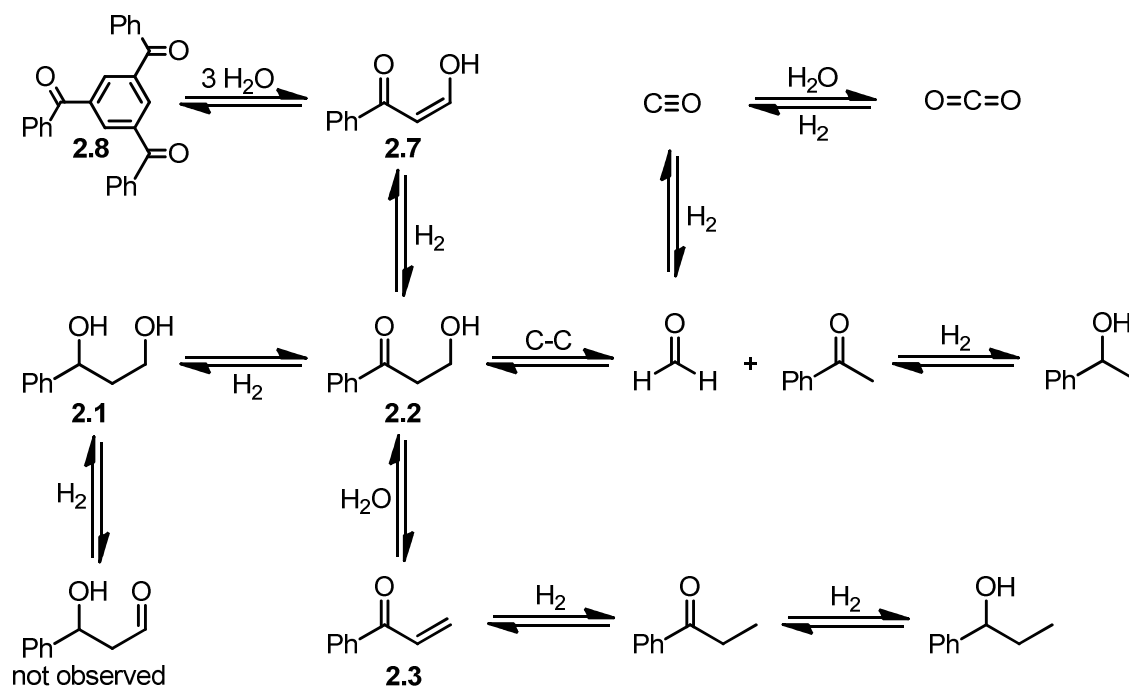
We began our investigation by subjecting lignin model compound **2.1** to the conditions developed for the ruthenium-catalyzed disproportionation of **1.1**. No conversion of **2.1** was observed at 135 °C. However, when the temperature was elevated to 175 °C, complete consumption of **2.1** was observed after 17 h (Scheme 6). In this case and all further studies in this chapter $\text{Ru}(\text{O}_2\text{CCF}_3)_2(\text{CO})(\text{PPh}_3)_2$ was used as the ruthenium source, as it was thought to be less prone to decomposition than $\text{RuH}_2(\text{CO})(\text{PPh}_3)_3$ at these elevated temperatures. However, the use of $\text{RuH}_2(\text{CO})(\text{PPh}_3)_3$ in the disproportionation of **2.1** resulted in a similar yield, product ratio, and reaction rate. A thermal control reaction in the absence of catalyst resulted primarily in non-specific decomposition of **2.1** (see experimental section).



Scheme 6. Disproportionation of lignin model compound **2.1**. Ph-xantphos = 4,5-bis(diphenylphosphino)-9,9-dimethylxanthene.

The complete proposed mechanism for the formation of products in the disproportionation of **2.1** is shown below in Scheme 7, in which β -hydroxypropiophenone (**2.2**)

is central to the formation of the observed products. Elimination of water from **2.2** yields phenyl vinyl ketone (**2.3**), which after hydrogenation yields propiophenone and 1-phenylpropanol. Retro-aldol cleavage of **2.2** yields formaldehyde (not observed) and acetophenone, the latter of which yields 1-phenylethanol after hydrogenation. Upon reaction completion, CO₂ is observed in the reaction mixture. We propose this is formed *via* dehydrogenation of formaldehyde followed by water-gas-shift reaction. When starting from **2.2** the vinylogous acid **2.7** and its aldol condensation trimer, **2.8** are observed in the reaction mixture. We propose that the rate of the overall reaction is controlled by the rate of the retro-aldol cleavage of **2.2**. However, we were not able to obtain kinetic data for this reaction, including *in situ* characterization of the catalyst resting state due to the high temperatures required and the physical limitations of our NMR and IR spectroscopic equipment.

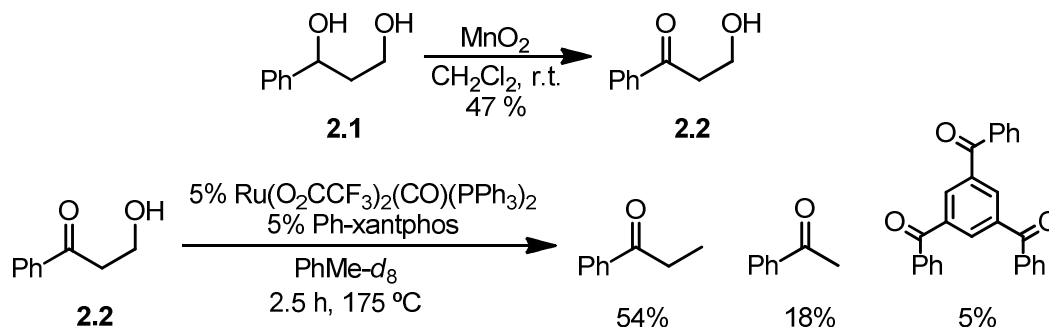


Scheme 7. Outline of the various reactions thought to be active in the ruthenium-catalyzed disproportionation of **2.1**. C-C = carbon-carbon bond cleavage.

It should be noted that this reaction differs from the oxidative process outlined in Scheme 2 in that the hydrogen produced to form the β -hydroxy carbonyl compound in this reaction is consumed in the olefin and carbonyl hydrogenation steps. This retro-aldol cleavage reaction and all subsequent reactions like it will therefore be referred to as disproportionations.

The centrality of **2.2** to the disproportionation of **2.1** is supported by the results of studies wherein **2.2** was subjected to disproportionation conditions. The synthesis of **2.2** proceeded by manganese dioxide oxidation of **2.1** (Scheme 8). The poor yield of **2.2** is presumably due to adsorption of **2.1** to the manganese dioxide surface. When subjecting **2.2** to the disproportionation conditions, complete consumption of **2.2** with concomitant formation of propiophenone, acetophenone, and 1,3,5-tribenzoylbenzene was observed after 2.5 h. Consumption of **2.2** was much more rapid than was consumption of **2.1** under identical conditions. This provides support for our proposed reaction mechanism, where **2.2** is an

intermediate in the formation of all observed products. The rate difference is therefore presumably due to the higher absolute concentration of **2.2** when employing this molecule directly as the starting material as compared to the lower absolute concentration achieved when producing **2.2** *in situ* from the dehydrogenation of **2.1**.



Scheme 8. Synthesis of **2.2** and its reactivity under disproportionation conditions. Ph-xantphos = 4,5-bis(diphenylphosphino)-9,9-dimethylxanthene.

The experimental support behind each step in the mechanism proposed in Scheme 7 will be outlined in detail below. This will begin with a discussion of the dehydrogenation/hydrogenation pre-equilibrium between **2.1** to **2.2**. Experiments related to the fate of the C1 formaldehyde fragment and the formation of 1,3,5-tribenzoylbenzene will be outlined in the context of the hydrogen sources for the reduction of **2.2** to propiophenone. This will be followed by a discussion of the dehydration/hydration equilibrium between **2.2** and **2.3** and the subsequent hydrogenation of **2.3**. Finally, our detailed examination of the retro-aldol cleavage step will be described. The formation of 1-phenylethanol and 1-phenylpropanol is a result of the well-precedented ruthenium-catalyzed hydrogenation of acetophenone and propiophenone, and will not be discussed further.¹¹⁻¹³

Dehydrogenation/Hydrogenation Pre-Equilibrium between 2.1 and 2.2

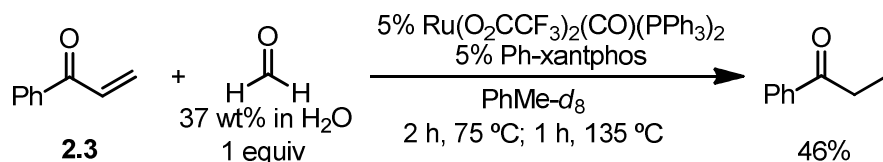
During the course of the disproportionation of **2.1**, β -hydroxypropiophenone (**2.2**), the result of dehydrogenation of the benzylic carbinol of **2.1**, is observed in up to 45% yield *via* ¹H NMR at intermediate conversions. It is interesting that 3-hydroxy-3-phenylpropanal, the result of dehydrogenation of the primary carbinol of **2.1**, is not observed in this reaction, nor are any products that result from it. We hypothesize that the product outcome is controlled by the relative thermodynamic stability of 3-hydroxy-3-phenylpropanal and **2.2**, with **2.2** being more stable due to π -system conjugation of the carbonyl and phenyl moieties. In addition, the fact that **2.2** is observed as an intermediate in the reaction mixture suggests the dehydrogenation equilibrium is rapid compared to the rate-limiting step in the disproportionation of **2.1**. This is consistent with ruthenium-catalyzed transfer hydrogenation rates found in the literature.¹⁴⁻²⁰

While the production of propiophenone and acetophenone from **2.1** is consistent with the results obtained with lignin model compound **1.1**, the absence of products arising from 3-hydroxy-3-phenylpropanal is inconsistent with those results, where benzaldehyde and benzyl alcohol are observed in significant amounts (Scheme 4). This difference is presumably the result of the aryl ether moiety, the presence or absence of which possibly alters the relative

thermodynamic stability of the β -hydroxy carbonyl species or alters the relative energies of the retro-aldol transition states.

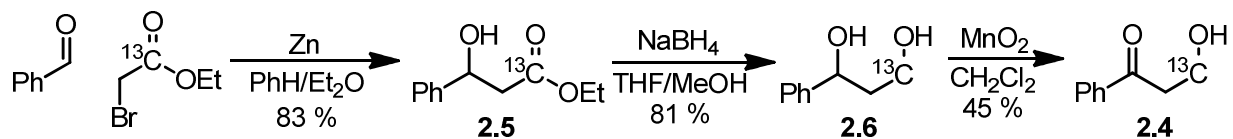
Hydrogen Budget 1: fate of the C1 formaldehyde fragment

The fact that a 54% yield of propiophenone is achieved in the disproportionation of **2.2** (Scheme 8) raises the question of the source of the hydrogen needed to reduce phenyl vinyl ketone (**2.3**) to propiophenone. When starting from **2.1**, the hydrogen arises from the dehydrogenation of the benzylic carbinol to yield **2.2**. However, this source of hydrogen is not available when starting from **2.2** itself. One potential hydrogen source is the C1 fragment whose formation we infer from the formation of acetophenone. However, neither formaldehyde nor its reduction product, methanol, were observed *via* ^1H NMR or GC/MS analysis of any of the above reaction mixtures. To test whether the formaldehyde C1 fragment was acting as a source of hydrogen, the ruthenium-catalyzed hydrogenation of **2.3** was carried out in the presence of aqueous formaldehyde, which resulted in a 46% yield of propiophenone (Scheme 9). The missing mass balance is presumably the result of oligomerization and polymerization of **2.3**. While this appears to be the first example of transfer hydrogenation using formaldehyde as the reductant, there is a precedent for the stoichiometric dehydrogenation of formaldehyde using $\text{RuH}_2(\text{PPh}_3)_3$, which in the presence of aqueous formaldehyde forms $\text{RuH}_2(\text{CO})(\text{PPh}_3)_3$.²¹



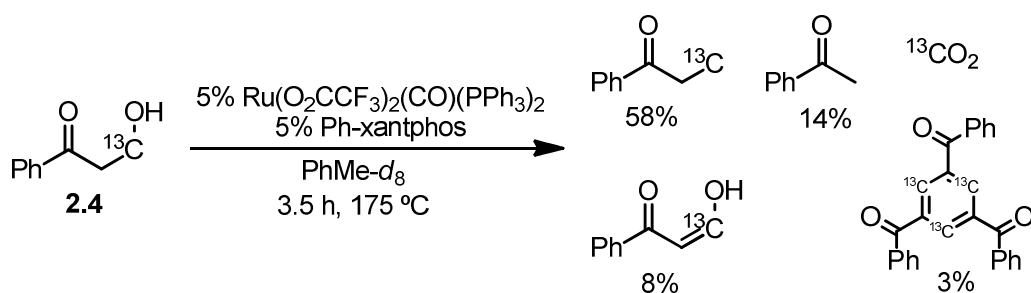
Scheme 9. Hydrogenation of **2.3** with aqueous formaldehyde. Ph-xantphos = 4,5-bis(diphenylphosphino)-9,9-dimethylxanthene.

The disproportionation of **2.2** results in an 18% yield of acetophenone from retro-aldol cleavage (Scheme 8), which implies that the other cleavage partner, formaldehyde, was also produced in 18% yield. The fact that this formaldehyde C1 fragment can serve as a hydrogen source accounts for the production of 18 mol% of the hydrogen needed to reduce **2.3** to propiophenone in 54% yield. This still leaves the source of 36 mol% of the hydrogen unaccounted for. In order to determine this source we sought to determine the fate of the C1 fragment of **2.2** under disproportionation conditions. In order to do this we synthesized β -hydroxypropiophenone with the primary carbinol carbon labeled with ^{13}C (**2.4**). Synthesis of **2.4** proceeded by addition of the ^{13}C -labeled Reformatsky enolate of ethyl bromoacetate to benzaldehyde to yield **2.5**. The IR carbonyl band of **2.5** is shifted by 42 cm^{-1} to 1684 cm^{-1} , compared to the 1726 cm^{-1} measured for its unlabeled analogue. Sodium borohydride reduction of **2.5** yielded **2.6**, which after manganese dioxide oxidation gave **2.4** (Scheme 10).



Scheme 10. Synthesis of β -hydroxypropiophenone- ^{13}C (**2.4**).

When ^{13}C -labeled compound **2.4** was subjected to the ruthenium-catalyzed disproportionation conditions, yields of propiophenone and acetophenone were comparable to those observed in the disproportionation of the unlabeled analogue **2.2** (Scheme 11). Analysis of the reaction mixture *via* ^{13}C NMR spectroscopy revealed a resonance consistent with that of ^{13}C -labeled carbon dioxide at 125.2 ppm. No resonances were observed at reaction completion or at intermediate conversions that were consistent with formaldehyde, carbon monoxide, or any C1 fragment other than carbon dioxide. The presence of carbon dioxide was verified by vacuum transferring the volatile contents of the reaction mixture at reaction completion to an NMR tube containing toluene- d_8 . ^{13}C NMR analysis of the contents of this new NMR tube revealed the only volatile compound transferred was carbon dioxide. Our assignment of this peak was further verified by adding additional ^{13}C -labeled carbon dioxide obtained from a commercial source to this NMR tube, which resulted in an increase in the intensity of the resonance at 125.2 ppm.



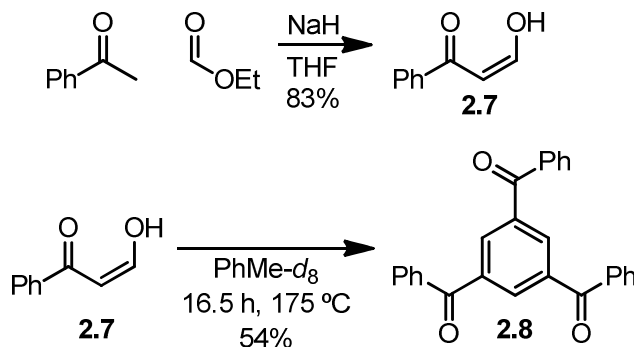
Scheme 11. Disproportionation of β -hydroxypropiophenone- ^{13}C **2.4**. Ph-xantphos = 4,5-bis(diphenylphosphino)-9,9-dimethylxanthene.

The production of carbon dioxide is presumably the result of formaldehyde dehydrogenation to yield carbon monoxide, which along with the water produced from the elimination of β -hydroxypropiophenone undergoes a water-gas-shift reaction to produce carbon dioxide and one further equivalent of hydrogen.²² Various ruthenium carbonyl sources have been shown to catalyze the water-gas-shift reaction.²³⁻²⁷ The fact that no formaldehyde, carbon monoxide, nor any other C1 fragment other than carbon dioxide was observed during intermediate conversions of the disproportionation of **2.4** leads us to conclude that ruthenium-catalyzed formaldehyde dehydrogenation and water-gas-shift reactions are rapid compared to the rate-limiting step in this process. This water-gas-shift process accounts for a further 18 mol% of the hydrogen needed to reduce **2.3** to propiophenone, which still leaves another 18 mol% hydrogen unaccounted for.

Hydrogen Budget 2: formation of 1,3,5-tribenzoylbenzene

Also produced in the disproportionation of **2.4** were 3-hydroxy-1-phenylpropanone and 1,3,5-tribenzoylbenzene (Scheme 11). The former product is the result of dehydrogenation of the primary hydroxy group of **2.4** followed by tautomerization. The latter product is a trimer of 3-hydroxy-1-phenylpropanone formed presumably *via* three aldol condensations. The formation of 1,3,5-tribenzoylbenzene (**2.8**) from 3-hydroxy-1-phenylpropanone (**2.7**) was verified by independent synthesis of **2.7** and its thermal transformation into **2.8** in toluene- d_8 solvent at 175 $^\circ\text{C}$ (Scheme 12). It should be noted that decomposition of **2.7** was a major reaction pathway observed in the formation of **2.8**, which provides one possible explanation for the incomplete

mass balance observed in the disproportionation of **2.2**. The independent syntheses of **2.7** and **2.8** also allowed verification of their presence in the reactions shown in Schemes 8 and 11.



Scheme 12. Synthesis of **2.7** and its thermal conversion to **2.8**.

The production of **2.8** in 5% yield in the disproportionation of **2.2** (Scheme 8) requires the consumption of 15 mol% of **2.7**. As **2.7** is formed by the dehydrogenation of **2.2**, a 15% yield of **2.8** would liberate a further 15 mol% hydrogen, which along with the hydrogen produced from formaldehyde dehydrogenation and water-gas-shift reactions, accounts for 51 mol% of the hydrogen necessary to reduce **2.3** to propiophenone. This leaves only 3 mol% of the hydrogen unaccounted for, which is possibly within experimental error of the acetophenone and propiophenone yield determination. Alternatively, the remaining hydrogen could arise from dehydrogenation of **2.2** to **2.7**, followed by decomposition of **2.7**.

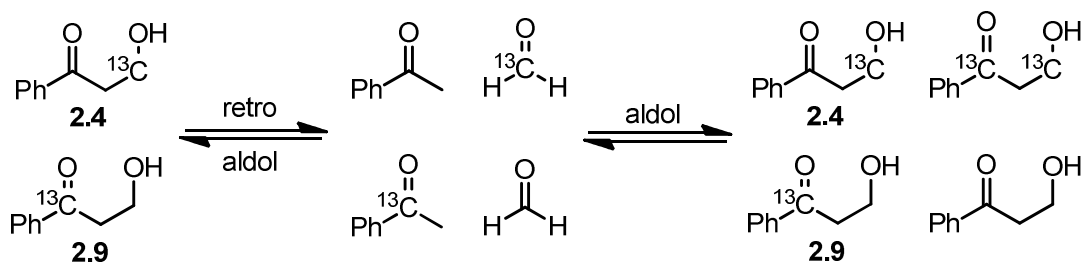
The disproportionation reactions carried out with **2.2** did not yield detectable amounts of **2.7**, while the disproportionation of its ¹³C-labeled analogue **2.4** resulted in an 8% yield of **2.7**. This difference is presumably due to the higher substrate concentration used in the disproportionation of **2.2** as compared to that used for **2.4**. Disproportionation of **2.4** was carried out at 125 mM substrate concentration due to the precious nature of **2.4**, while disproportionation of **2.2** was carried out at 500 mM substrate concentration. The resulting lower concentration of **2.7** would disfavor formation of its aldol condensation trimer **2.8**, allowing for the observation of **2.7** at reaction completion.

Dehydration of 2.2 to 2.3 and Hydrogenation of 2.3

We propose that **2.2** and **2.3** are in rapid equilibrium with one another during the disproportionation of **2.2**, as **2.3** is observed in up to 12% yield at intermediate conversions. During the disproportionation of **2.1** however, **2.3** is not observed. This is presumably due to the higher partial pressure of hydrogen produced from dehydrogenation of **2.1**, causing **2.3** to be hydrogenated rapidly upon its formation. This rapid dehydration/hydration equilibrium achieved during the disproportionation of **2.2** allows for the decomposition of **2.3**, which along with the decomposition of **2.7**, provides an explanation for the incomplete mass balance observed during this reaction. The significant amounts of decomposition observed in thermal control reactions with **2.2** and **2.7** provide further support for this hypothesis (see experimental section and Scheme 12, respectively)

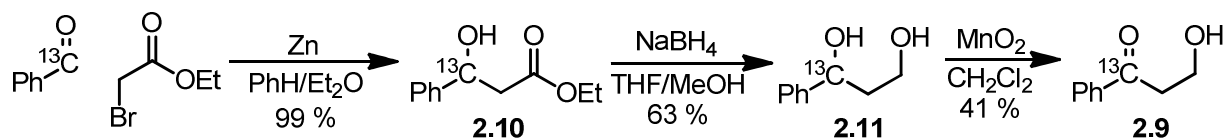
transfer hydrogenation literature, which suggests that olefin and carbonyl hydrogenation and dehydrogenation are rapid at 175 °C.^{14-20,28} Finally, we have provided evidence that formaldehyde dehydrogenation, the water-gas-shift reaction, and the dehydration equilibrium between **2.2** and **2.3** are all rapid compared to this rate-limiting retro-aldol step.

There is literature precedent for the reversibility of the aldol reaction of acetophenone and formaldehyde, which led us to denote the reaction accordingly in Scheme 7.²⁹⁻³¹ However, due to the comparatively rapid nature of the formaldehyde dehydrogenation and water-gas-shift reactions, it is possible that under disproportionation conditions the retro-aldol cleavage of **2.2** is essentially irreversible. Evidence for this can be obtained through a crossover experiment using differentially-¹³C-labeled samples of **2.2**. The retro-aldol cleavage of **2.4** and **2.9** would yield a mixture of ¹³C-labeled and non-¹³C-labeled acetophenone and formaldehyde, which upon aldol reaction would yield a mixture of **2.4**, **2.9**, as well as bis-¹³C-labeled and non-¹³C-labeled β-hydroxypropiophenone if the retro-aldol cleavage is indeed reversible (Scheme 15).



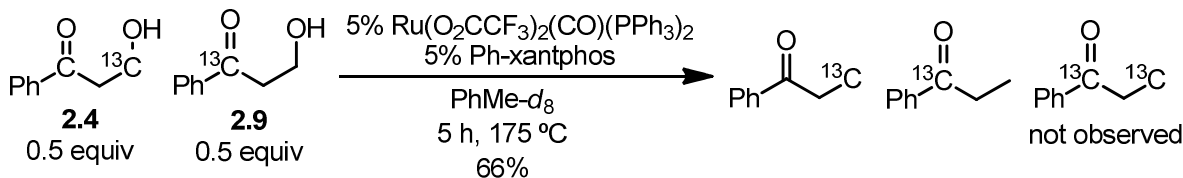
Scheme 15. Proposed crossover experiment to detect reversibility of retro-aldol cleavage of **2.4** and **2.9** under disproportionation conditions.

With methylene-¹³C-labeled **2.4** already in hand, synthesis of carbonyl-¹³C-labeled **2.9** proceeded in an analogous fashion (Scheme 16). The IR carbonyl band of **2.9** is shifted by 39 cm⁻¹ to 1641 cm⁻¹, compared to the 1680 cm⁻¹ measured for its unlabeled analogue.



Scheme 16. Synthesis of β-hydroxypropiophenone-¹³C (**2.9**).

The crossover experiment was conducted by subjecting a 1:1 mixture of **2.4**:**2.9** to disproportionation conditions and analyzing the isotopic distribution of the molecular ion of the propiophenone product by mass spectrometry in order to detect the bis-¹³C-labeled propiophenone crossover product (Scheme 17). Control experiments were conducted using reaction mixtures obtained from the disproportionations of **2.4** and **2.9** separately. Comparison of the isotopic distributions of the molecular ions of the propiophenone products obtained from the control experiments with that of the crossover experiment revealed no detectable differences, as the above-described isotopic distributions are within (or only slightly outside of) experimental error of one another (Table 1). Though literature precedent suggests that this retro-aldol reaction is reversible, these results suggest that under disproportionation conditions formaldehyde is consumed so rapidly as to not reach concentrations at which the back reaction becomes active.

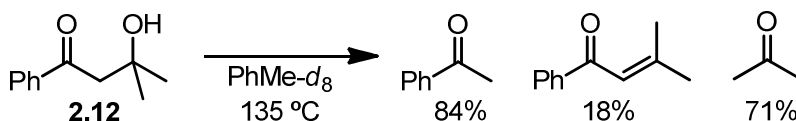


Scheme 17. Crossover experiment to detect the reversibility of the retro-aldol cleavage under disproportionation conditions. Ph-xantphos = 4,5-bis(diphenylphosphino)-9,9-dimethyl xanthene.

Table 1. Isotopic distributions of the molecular ions of propiophenone obtained by disproportionation of **2.4**, **2.9**, and a 1:1 mixture of **2.4:2.9**. n.d. = not detected.

m/z	Propiophenone from 2.4	Propiophenone from 2.9	Propiophenone from 2.4:2.9 (1:1)
135	100(0)	100(0)	100(0)
136	8.8(3)	8.7(2)	9.1(3)
137	0.4(1)	0.27(7)	0.57(7)
138	n.d.	n.d.	n.d.

Given that ruthenium carbonyl complexes are known to catalyze these transfer-hydrogenation steps, but are not known to catalyze retro-aldol reactions, it is possible that the ruthenium catalyst simply serves as a hydrogen shuttle in this reaction. In this scenario, the ruthenium catalyst would simply produce **2.2** and consume its retro-aldol and elimination products, with the retro-aldol cleavage occurring thermally. In order to determine whether this was the case, model compound **2.12** was targeted. The *gem*-dimethyl substituents of **2.12** prohibit C1 oxidation pathways following retro-aldol cleavage, allowing clear observation of the rate of a retro-aldol cleavage. Accordingly, retro-aldol cleavage of **2.12** leads to an 84% yield of acetophenone (Scheme 18). This reaction proceeds with $t_{1/2}$ of 11 h at 135 °C, based on the disappearance of **2.12** (Table 2).



Scheme 18. Retro-aldol cleavage of model compound **2.12**.

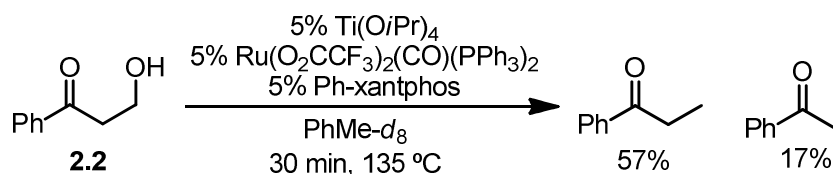
The effects of a variety of additives on the rate of the retro-aldol cleavage of **2.12** were investigated (Table 2). The trifluoroacetato ruthenium catalyst, with or without Ph-xantphos ligand, resulted in an approximately two-fold rate acceleration (entries 2 and 3). Trifluoroacetic acid resulted in an even more significant rate acceleration (entry 4). As liberation of trifluoroacetic acid from the trifluoroacetato ruthenium complex in the presence of **2.12** is expected due to ligand exchange processes, the rate acceleration observed in the presence of this complex could be a result of trifluoroacetic acid catalysis. However, late metal catalysis of retro-aldol cleavage is preceded in the literature.^{32,33} The most significant rate accelerations reported in the literature for retro-aldol cleavage employ early-metal and aluminum alkoxides and aryloxides.³⁴⁻⁴⁰ Indeed, addition of these catalysts to solutions of **2.12** resulted in extremely rapid retro-aldol cleavage (entries 5, 6, 8-10). Intrigued by these results, we also investigated

heterogeneous catalysis of the retro-aldol cleavage of **2.12** using acidic alumina, which resulted in a three-fold rate acceleration (entry 7).

Table 2. Catalyst screen for the retro-aldol cleavage of **2.12** (Scheme 18). Ph-xantphos = 4,5-bis(diphenyl phosphino)-9,9-dimethylxanthene.

Entry	Catalyst (5 mol%)	Approx $t_{1/2}$
1	None	11 h
2	Ru(O ₂ CCF ₃) ₂ (CO)(PPh ₃) ₂ , Ph-xantphos	3 h
3	Ru(O ₂ CCF ₃) ₂ (CO)(PPh ₃) ₂	3 h
4	CF ₃ COOH	40 min
5	Al(OiPr) ₃	< 5 min
6	Al(OPh) ₃	< 5 min
7	Acidic Alumina	1 h
8	Ti(OiPr) ₄	< 5 min
9	Ti(OtBu) ₄	< 5 min
10	Zr(OtBu) ₄	45 min (at r.t.)

Having proposed that the disproportionation of **2.2** proceeds through rate-limiting retro-aldol cleavage and established that a number of metal alkoxides were capable of catalyzing a retro-aldol cleavage reaction, we next set out to employ one of these catalysts in the disproportionation of **2.2**. Indeed, addition of 5% Ti(OiPr)₄ to the ruthenium-catalyzed disproportionation reaction mixture resulted in a much more rapid conversion to products compared to the same reaction in the absence of Ti(OiPr)₄ (Scheme 8 vs Scheme 19). The yield and ratio of propiophenone and acetophenone were not appreciably different in either case. This observation is interesting in that the amount of the retro-aldol cleavage product, acetophenone, is not appreciably increased in the presence of a retro-aldol cleavage catalyst. However, a larger concentration of the dehydration product of **2.2**, phenyl vinyl ketone (**2.3**), was observed at intermediate conversions in the presence of Ti(OiPr)₄, indicating that this additive facilitates elimination as well as retro-aldol cleavage. The fact that the ruthenium-catalyzed disproportionation of **2.2** in the presence of a retro-aldol catalyst can be carried out under much milder conditions compared to those necessary in the absence of a retro-aldol catalyst provides further support for retro-aldol cleavage being the rate-limiting step in this reaction.



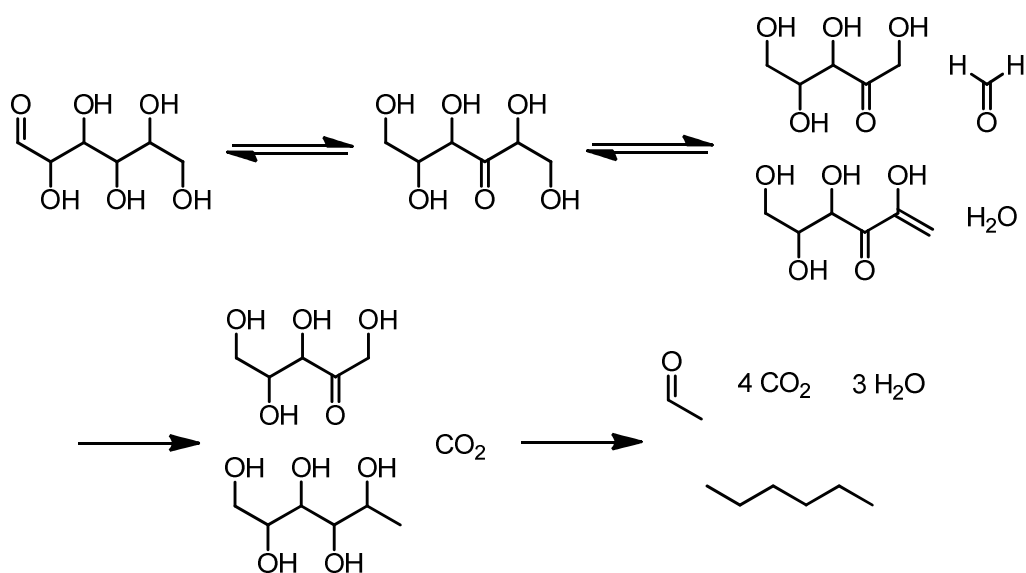
Scheme 19. Disproportionation of **2.2** in the presence of Ti(OiPr)₄ additive. Ph-xantphos = 4,5-bis(diphenylphosphino)-9,9-dimethylxanthene.

Summary & Conclusion

We have designed 1,3-diol model compound **2.1** in order to investigate and optimize the retro-aldol cleavage process observed in the disproportionation of lignin model dimer **1.1**. We propose that the disproportionation of **2.1** proceeds through rate-limiting retro-aldol cleavage,

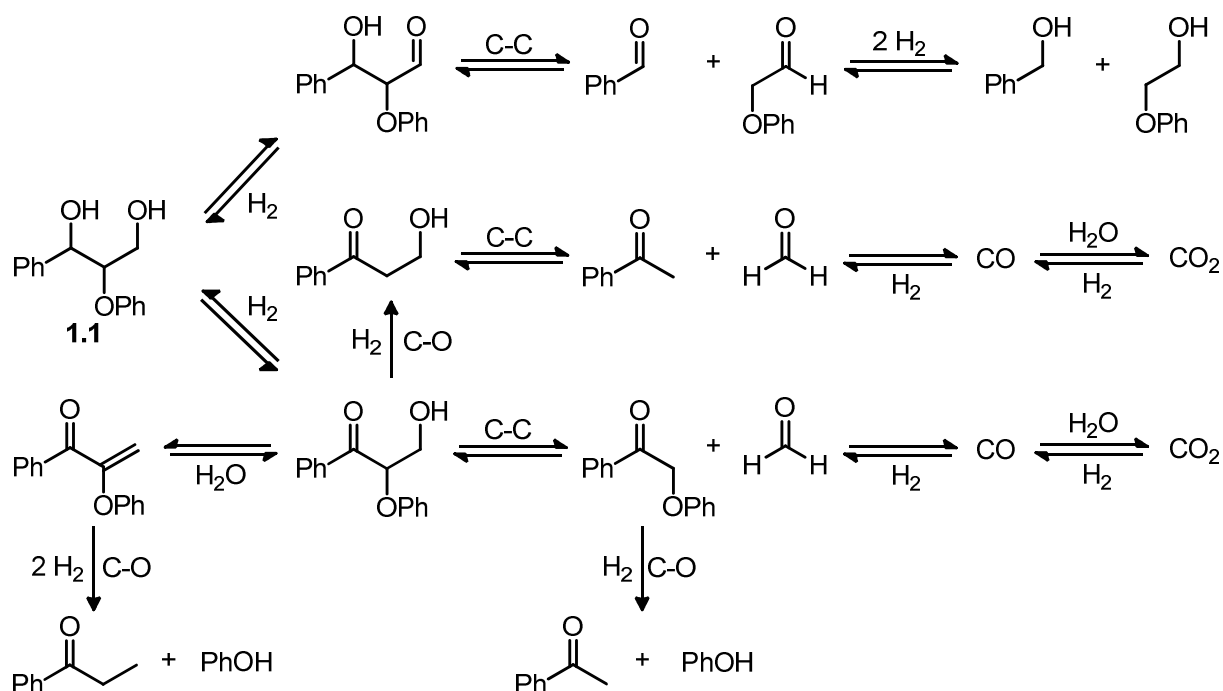
but dehydration, carbonyl and olefin hydrogenation, dehydrogenation of formaldehyde, and a water-gas-shift reaction are also active processes. Through the use of a more simplified retro-aldol model system we have shown that early metal and aluminum alkoxides and aryloxides are potent retro-aldol catalysts, one of which was applied to the disproportionation of β -hydroxypropiophenone (**2.2**).

Given that this disproportionation can be carried out in the presence of water, one could envision the development of a water-soluble ruthenium catalyst for the reduction of the molecular complexity of saccharides *via* this retro-aldol disproportionation strategy (Scheme 20). Achieving the selectivity depicted in Scheme 20 would be unlikely, but the efficient deoxygenation and liquification of saccharides to give a mixture of products in the absence of an external reductant *via* this methodology would represent a significant achievement.



Scheme 20. A hypothetical reaction outcome for the application of the retro-aldol disproportionation strategy to saccharides.

The insights gained into the mechanism of the disproportionation of **2.1** provide a foundation from which an understanding of the numerous reaction pathways active in the disproportionation of lignin model compound **1.1** is possible. Acetophenone, phenoxyacetophenone, and 2-phenoxy-1-phenylethanol are all likely produced through retro-aldol cleavage of β -hydroxypropiophenone molecules (Scheme 21). A byproduct of all these reactions is formaldehyde. In this chapter we have provided evidence that formaldehyde is converted to carbon dioxide under the reaction conditions, releasing two equivalents of hydrogen. The disproportionation of **2.1** results in no formation of benzaldehyde or benzyl alcohol as does the disproportionation of **1.1**, a difference which can be attributed to the aryl ether substituent, though the exact reason for this difference is not clear. Significant amounts of propiophenone are formed in the disproportionation of **2.1** *via* hydrogenation of phenyl vinyl ketone. However, our studies on the carbon-oxygen bond cleavage mechanism described in Chapter 3 provide evidence that phenyl vinyl ketone hydrogenation is not the dominant pathway for formation of propiophenone in the disproportionation of **1.1**.



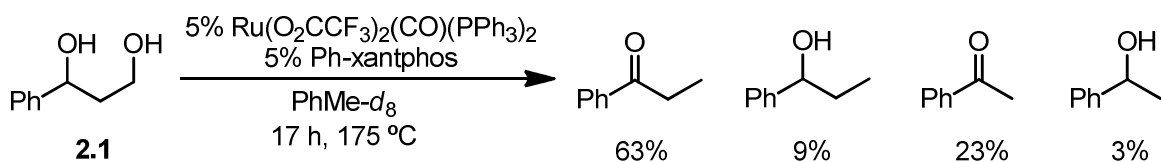
Scheme 21. Outline of the various reactions thought to be active in the ruthenium-catalyzed disproportionation of **1.1**. C-C = carbon-carbon bond cleavage. C-O = carbon-oxygen bond cleavage.

Experimental

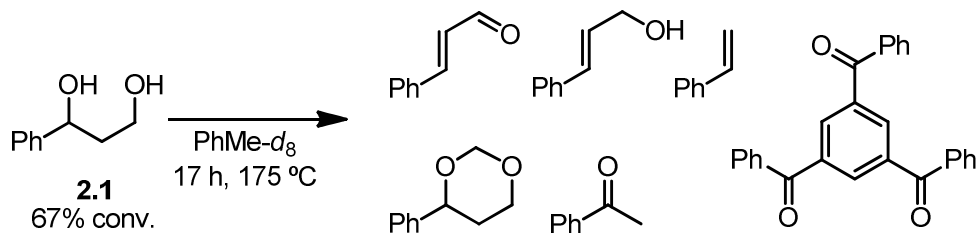
General Information. All reactions and manipulations, unless otherwise noted, were carried out in an inert atmosphere (N₂) glovebox or using standard Schlenk and high vacuum techniques. Sealed NMR tubes were prepared by attaching the NMR tube directly to a Kontes high-vacuum stopcock *via* a cajon ultra-torr reducing union, then flame-sealing on a vacuum line. All glassware was dried in an oven at 150 °C for at least 12 h prior to use or was flame-dried under reduced pressure. ¹H NMR and ¹³C NMR spectra were recorded on Bruker DRX-500 (500 MHz), AV-500 (500 MHz), AVB-400 (400 MHz), AVQ-400 (400 MHz), and AV-300 (300 MHz) spectrometers as indicated. ¹H NMR chemical shifts (δ) are reported in parts per million relative to residual protiated solvent. Data are reported in the following format: (s = singlet, d = doublet, t = triplet, q = quartet, m = multiplet; coupling constant; integration). ¹³C NMR chemical shifts (δ) are reported in parts per million relative to the carbon resonance of the deuterated solvent. Column chromatography was performed using a Biotage SP1 MPLC purification system and pre-packed silica gel columns. IR spectra were obtained on neat samples on NaCl plates using a ThermoNicolet Avatar 370 FT-IR spectrometer. GC/MS analysis was carried out using an Agilent Technologies 6890 network GC system coupled with an Agilent technologies 5973 network mass selective detector.

Materials. Dichloromethane, benzene, diethyl ether, and tetrahydrofuran were dried and purified by passage through a column of activated alumina under N₂ pressure followed by sparging with N₂.⁴¹ CDCl₃ and PhMe-*d*₈ were obtained from Cambridge Isotope Labs, Inc.

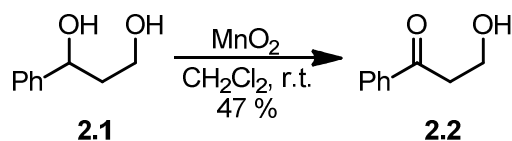
CDCl_3 was stored over K_2CO_3 . $\text{PhMe-}d_8$ was sparged with N_2 and stored over activated 4 Å molecular sieve pellets overnight. The 4 Å molecular sieve pellets were obtained from Sigma-Aldrich and activated by heating at 150 °C under vacuum for 24 h. Water was distilled and deionized on a Barnstead Nanopure Diamond deionization system. Benzaldehyde was obtained from Sigma-Aldrich and distilled from MgSO_4 . Acetophenone was obtained from Eastman Chemical Company and distilled. Trifluoroacetic acid was obtained from Sigma-Aldrich and distilled from P_2O_5 . $\text{Ru}(\text{O}_2\text{CCF}_3)_2(\text{CO})(\text{PPh}_3)_2$, $\text{RuH}_2(\text{CO})(\text{PPh}_3)_3$, 4,5-bis(diphenylphosphino)-9,9-dimethylxanthene, zinc dust, titanium *iso*-propoxide, titanium *tert*-butoxide, and zirconium *tert*-butoxide were obtained from Strem Chemicals; 4-trifluoromethylpyridine was obtained from Alfa Aesar; aqueous formaldehyde, methanol, and acidic alumina were obtained from Fisher Scientific; ethyl bromoacetate- ^{13}C , $^{13}\text{CO}_2$, ^{13}CO , benzaldehyde- ^{13}C were obtained from Cambridge Isotope Labs, Inc.; ethyl formate, sodium borohydride, sodium hydride, ethyl bromoacetate, aluminum *iso*-propoxide, and aluminum phenoxide were obtained from Sigma-Aldrich; these reagents were used without further purification. 1-phenylpropane-1,3-diol,⁴² phenyl vinyl ketone,^{43,44} manganese dioxide,⁴⁵ and 3-hydroxy-3-methyl-1-phenylbutanone³⁹ were synthesized according to literature procedures. Characterization data for these compounds agree with literature values.



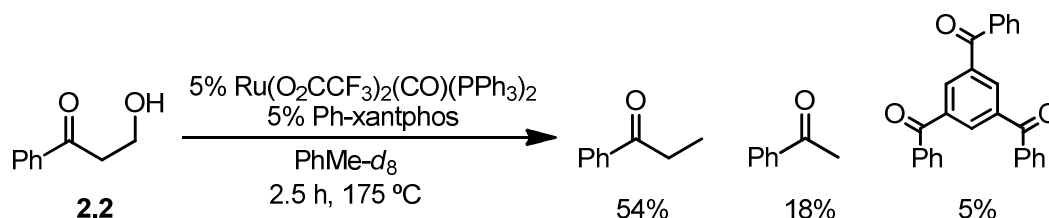
Disproportionation of 1-phenylpropane-1,3-diol (2.1). A solution of **2.1** (450 μL , 500 mM in toluene- d_8 , 0.225 mmol) was combined in an NMR tube with $\text{Ru}(\text{O}_2\text{CCF}_3)_2(\text{CO})(\text{PPh}_3)_2$ (10.3 mg, 0.0112 mmol), 4,5-bis(diphenylphosphino)-9,9-dimethylxanthene (6.5 mg, 0.011 mmol), and a glass capillary containing 4-trifluoromethylpyridine. The NMR tube was sealed under vacuum and heated at 135 °C for 1 h, after which no conversion of **2.1** was observed by ^1H NMR. The NMR tube was then heated at 175 °C and monitored periodically *via* ^1H NMR, which after 17 h of heating indicated complete consumption of **2.1**. The diagnostic resonances used to determine yields by comparison to the external standard are as follows: ^1H NMR (400 MHz, $\text{PhMe-}d_8$): propiophenone – δ 2.44 (q, $J = 7.2$ Hz, 2H), 1.06 (t, $J = 7.2$ Hz, 3H) ppm; 1-phenylpropanol – δ 4.27 (t, $J = 6.4$ Hz, 1H), 1.72-1.49 (m, 2H), 0.81 (t, $J = 7.2$ Hz, 3H) ppm; acetophenone – δ 2.14 (s, 3H) ppm; 1-phenylethanol – δ 4.56 (q, $J = 4.0$ Hz, 1H), 1.28 (d, $J = 6.4$ Hz, 3H) ppm; β -hydroxypropiophenone – δ 3.78 (t, $J = 5.6$ Hz, 2H), 2.64 (t, $J = 5.6$ Hz, 2H) ppm. The presence of these species was confirmed by GC/MS analysis of the reaction mixture. The diagnostic resonance of the 4-trifluoromethylpyridine external standard is as follows: ^1H NMR (400 MHz, neat): δ 8.82 (d, $J = 4.8$ Hz, 2H) ppm.



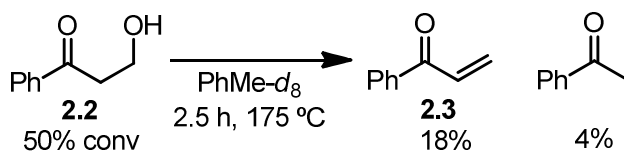
Thermal decomposition of 1-phenylpropane-1,3-diol (2.1). An NMR tube was charged with a solution of **2.1** (450 μ L, 500 mM in toluene- d_8 , 0.225 mmol) and a glass capillary containing 4-trifluoromethylpyridine. The NMR tube was sealed under vacuum and heated at 135 $^{\circ}$ C for 1 h, after which no conversion of **2.1** was observed by 1 H NMR. The NMR tube was then heated at 175 $^{\circ}$ C for 17 h and monitored periodically *via* 1 H NMR, which after 17 h of heating indicated consumption of 67% of **2.1**. The 1 H NMR spectrum was very complex, and no significant amount of any one product was observed at any point during the reaction. GC/MS analysis of the reaction mixture revealed the presence of small amounts of the products shown above, which were identified by comparison to the National Institute of Standards and Technology 2008 Mass Spectral Library and whose amounts were not quantified.



Synthesis of β -hydroxypropiophenone (2.2). A round bottom flask was charged with 1-phenylpropane-1,3-diol (1.90 g, 12.5 mmol), dichloromethane (125 mL), and MnO_2 (16.3 g, 187 mmol). After stirring the reaction mixture for 12 h at room temperature, it was filtered through a pad of Celite. The filtrate was concentrated *in vacuo* and purified by silica gel chromatography (50-90% EtOAc in hexanes) yielding 883 mg **2.2** as a clear oil (47%). Characterization data for this compound agree with literature values.⁴⁶

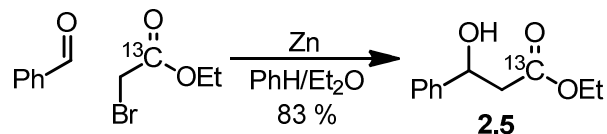


Disproportionation of β -hydroxypropiophenone (2.2). A solution of **2.2** (450 μ L, 500 mM in toluene- d_8 , 0.225 mmol) was combined in an NMR tube with $\text{Ru}(\text{O}_2\text{CCF}_3)_2(\text{CO})(\text{PPh}_3)_2$ (10.3 mg, 0.0112 mmol), 4,5-bis(diphenylphosphino)-9,9-dimethylxanthene (6.5 mg, 0.011 mmol), and a glass capillary containing 4-trifluoromethylpyridine. The NMR tube was sealed under vacuum, heated at 175 $^{\circ}$ C, and monitored periodically *via* 1 H NMR, which after 2.5 h of heating indicated complete consumption of **2.2**. The diagnostic resonances used to determine yields by comparison to the external standard are as listed above for the disproportionation of **2.1**. Those for other compounds are as follows: 1 H NMR (500 MHz, $\text{PhMe-}d_8$): 1,3,5-tribenzoylbenzene – δ 8.22 (s, 3H) ppm; phenyl vinyl ketone – δ 6.33 (d, $J = 17.2$ Hz, 1H), 5.44 (d, $J = 10.4$ Hz, 1H) ppm. The presence of these species was confirmed by GC/MS analysis of the reaction mixture.

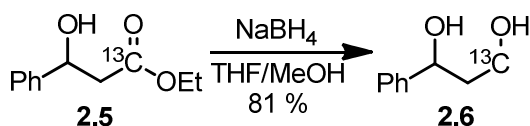


Thermal decomposition of β -hydroxypropiophenone (2.2). An NMR tube was charged with a solution of **2.2** (450 μ L, 500 mM in toluene- d_8 , 0.225 mmol) and a glass capillary

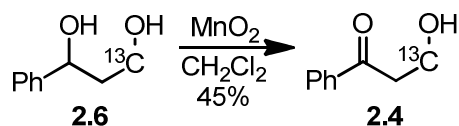
2.3 was observed by ^1H NMR. The diagnostic resonances used to determine yields by comparison to the external standard are as listed above for the disproportionations of **2.1** and **2.2**.



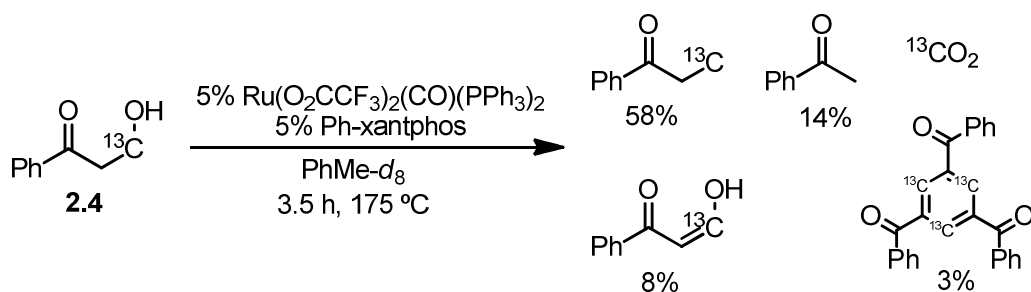
Synthesis of ethyl 3-hydroxy-3-phenylpropanoate- ^{13}C (2.5). This material was synthesized according to the procedure developed for the synthesis its non- ^{13}C -labeled analogue,⁴⁷ using benzaldehyde (0.40 mL, 3.95 mmol), ethyl bromoacetate- ^{13}C (0.35 mL, 3.16 mmol), zinc dust, (258 mg, 3.95 mmol), benzene (0.8 mL), and diethyl ether (0.2 mL), yielding 515 mg **2.5** as a yellow oil (83%). ^1H NMR (400 MHz, CDCl_3): δ 7.38-7.22 (m, 5H), 5.10 (dt, $J = 3.7, 8.8$ Hz, 1H), 4.15 (qd, $J = 3.1, 7.1$ Hz, 2H), 3.28 (broad, 1H), 2.79-2.61 (m, 2H), 1.24 (t, $J = 7.1$ Hz, 3H) ppm; ^{13}C NMR (100 MHz, CDCl_3): δ 172.8 (^{13}C enriched), 142.7 ($J_{\text{C-C}} = 4.4$ Hz), 128.7, 127.9, 125.8, 70.4 ($J_{\text{C-C}} = 1.4$ Hz), 61.0 ($J_{\text{C-C}} = 2.9$ Hz), 43.5 ($J_{\text{C-C}} = 56.4$ Hz), 14.3 ($J_{\text{C-C}} = 2.2$ Hz) ppm; IR 3461 (broad), 2982, 1684, 1455, 1150, 701 cm^{-1} ; HRMS (EI^+) Exact mass calcd for $^{12}\text{C}_{10}^{13}\text{CH}_{14}\text{O}_3$ [M] $^+$: 195.0976, found 195.0979.



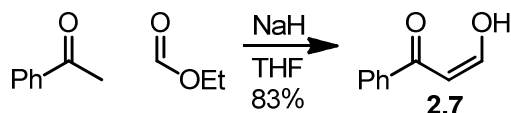
Synthesis of 1-phenylpropane-1,3-diol- ^{13}C (2.6). This material was synthesized in analogy to the procedure developed for the reduction of ethyl benzoylacetate to 1-phenylpropane-1,3-diol,⁴² using **2.5** (196 mg, 1.00 mmol), NaBH_4 (76 mg, 2.00 mmol), tetrahydrofuran (9 mL), and methanol (3 mL), yielding 124 mg **2.6** as a yellow oil (81%). ^1H NMR (400 MHz, CDCl_3): δ 7.38-7.22 (m, 5H), 4.89 (dt, $J = 3.9, 8.7$ Hz, 1H), 3.80 (dm, $J_{\text{C-H}} = 142.8$ Hz, 2H), 3.06 (broad, 2H), 2.02-1.82 (m, 2H) ppm; ^{13}C NMR (100 MHz, CDCl_3): δ 144.5 ($J_{\text{C-C}} = 3.0$ Hz), 128.6, 127.7, 125.8, 74.2, 61.4 (^{13}C enriched), 40.6 ($J_{\text{C-C}} = 36.7$ Hz) ppm; HRMS (EI^+) Exact mass calcd for $^{12}\text{C}_8^{13}\text{CH}_{12}\text{O}_2$ [M] $^+$: 153.0871, found 153.0868.



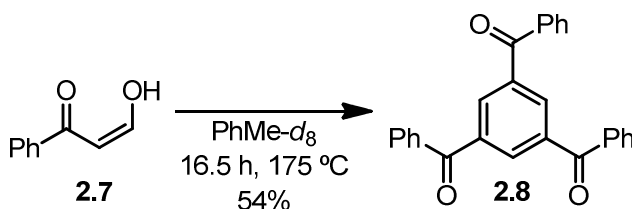
Synthesis of β -hydroxypropiophenone- ^{13}C (2.4). This material was synthesized in a fashion analogous to **2.2**, using **2.6** (146 mg, 0.952 mmol), dichloromethane (20 mL), and MnO_2 (2.5 g, 28.6 mmol) yielding 64 mg **2.4** as a clear oil (45%). ^1H NMR (400 MHz, CDCl_3): δ 7.92 (d, $J = 7.6$ Hz, 2H), 7.54 (t, $J = 7.3$ Hz, 1H), 7.43 (t, $J = 7.7$ Hz, 2H), 3.99 (dt, $J = 5.3$ Hz, $J_{\text{C-H}} = 144.2$ Hz, 2H), 3.19 (q, $J = 4.9$ Hz, 2H), 2.93 (broad, 1H) ppm; ^{13}C NMR (100 MHz, CDCl_3): δ 200.7, 136.8, 133.7, 128.9, 128.2, 58.2 (^{13}C enriched), 40.6 ($J_{\text{C-C}} = 38.3$ Hz) ppm; IR 3406 (broad), 2880, 1680, 1597, 1449, 1022, 690 cm^{-1} ; HRMS (EI^+) Exact mass calcd for $^{12}\text{C}_8^{13}\text{CH}_{10}\text{O}_2$ [M] $^+$: 151.0714, found 151.0711.



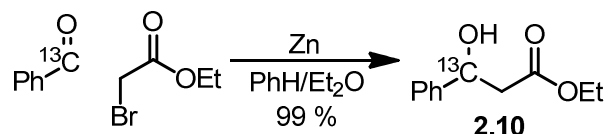
Disproportionation of β -hydroxypropiophenone- ^{13}C (2.4**).** A solution of **2.4** (200 μL , 250 mM in toluene- d_8 , 0.050 mmol) was combined in an NMR tube with $\text{Ru}(\text{O}_2\text{CCF}_3)_2(\text{CO})(\text{PPh}_3)_2$ (2.3 mg, 0.0025 mmol), 4,5-bis(diphenylphosphino)-9,9-dimethylxanthene (1.4 mg, 0.0025 mmol), toluene- d_8 (200 μL), and a glass capillary containing 4-trifluoromethylpyridine. The NMR tube was sealed under vacuum, heated at 175 °C, and monitored periodically *via* ^1H NMR, which after 3.5 h of heating indicated complete consumption of **2.4**. The diagnostic ^1H NMR resonances used to determine yields by comparison to the external standard are as listed above for the disproportionations of **2.1** and **2.2**. Those for 3-hydroxy-1-phenylpropenone are as follows: ^1H NMR (500 MHz, $\text{PhMe-}d_8$): δ 5.64 (s, 1H) ppm. The diagnostic ^{13}C NMR resonances used to identify products are as follows: ^{13}C NMR (125 MHz, $\text{PhMe-}d_8$): propiophenone – δ 8.6 ppm; 3-hydroxy-1-phenylpropenone – δ 178.8 ppm; 1,3,5-tribenzoylbenzene – δ 134.4 ppm; carbon dioxide – δ 125.2 ppm. The presence of the non-volatile species was confirmed by GC/MS analysis of the reaction mixture.



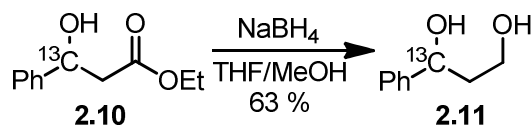
Synthesis of 3-hydroxy-1-phenylpropenone (2.7**).** A round bottom flask was charged with tetrahydrofuran (95 mL), ethyl formate (5.52 mL, 68.6 mmol), and sodium hydride (1.45 g, 60 wt% in mineral oil, 36.2 mmol). The reaction mixture was cooled to 0 °C and acetophenone (7.00 mL, 2.45 M in tetrahydrofuran, 17.1 mmol) was added dropwise. The reaction mixture was warmed to room temperature and stirred for 8 h, after which half-saturated aqueous brine (100 mL) and diethyl ether (50 mL) were added slowly. The aqueous layer was separated. The remaining organic layer was extracted twice with 10% aqueous NaOH. The combined aqueous layers were acidified with 6N HCl and extracted thrice with dichloromethane. The organic extracts were then dried over MgSO_4 , filtered, and concentrated *in vacuo* to yield 2.10 g **2.7** (83%). ^1H NMR (500 MHz, CDCl_3): δ 8.27 (d, J = 4.1 Hz, 1H), 7.91-7.87 (m, 2H), 7.54 (t, J = 7.4 Hz, 1H), 7.45 (t, J = 7.7 Hz, 2H), 6.21 (d, J = 4.2 Hz, 1H) ppm; ^{13}C NMR (125 MHz, CDCl_3): δ 188.1, 178.9, 135.2, 133.1, 128.9, 127.6, 98.5 ppm; IR 3431 (broad), 3063, 1600 (broad) cm^{-1} ; HRMS (EI^+) Exact mass calcd for $\text{C}_9\text{H}_8\text{O}_2$ [M] $^+$: 148.0524, found 148.0522.



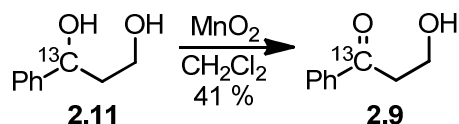
Synthesis of 1,3,5-tribenzoylbenzene (2.8). An NMR tube was charged with **2.7** (450 μL , 500 mM in toluene- d_8 , 0.225 mmol) and a glass capillary containing 4-trifluoromethylpyridine. The NMR tube was sealed under vacuum, heated at 175 $^\circ\text{C}$, and monitored periodically *via* ^1H NMR, which after 16.5 h of heating indicated complete consumption of starting material. A 62% yield of 1,3,5-tribenzoylbenzene was measured by comparison to the external standard. The reaction mixture was concentrated *in vacuo* and purified by silica gel chromatography (14-35% EtOAc in hexanes) yielding 18 mg **2.8** as a white solid (54%). Characterization data for this compound agree with literature values.⁴⁸



Synthesis of ethyl 3-hydroxy-3-phenylpropanoate- ^{13}C (2.10). This material was synthesized according to the procedure developed for the synthesis its non- ^{13}C -labeled analogue,⁴⁷ using benzaldehyde- ^{13}C (0.47 mL, 4.67 mmol), ethyl bromoacetate (0.52 mL, 4.67 mmol), zinc dust, (381 mg, 5.84 mmol), benzene (0.8 mL), and diethyl ether (0.2 mL), yielding 904 mg **2.10** as a yellow oil (99%). ^1H NMR (400 MHz, CDCl_3): δ 7.38-7.18 (m, 5H), 5.10 (ddd, $J = 4.0, 8.8$ Hz, $J_{\text{C-H}} = 145.9$ Hz, 1H), 4.14 (q, $J = 7.2$ Hz, 2H), 3.37 (broad, 1H), 2.78-2.61 (m, 2H), 1.23 (t, $J = 7.2$ Hz, 3H) ppm; ^{13}C NMR (100 MHz, CDCl_3): δ 172.4, 142.7 ($J_{\text{C-C}} = 49.0$ Hz), 128.6 ($J_{\text{C-C}} = 3.7$ Hz), 127.9, 125.8 ($J_{\text{C-C}} = 3.1$ Hz), 70.4 (^{13}C enriched), 61.0, 43.5 ($J_{\text{C-C}} = 37.5$ Hz), 14.3 ppm; IR 3466 (broad), 2982, 1726, 1452, 1192, 700 cm^{-1} ; HRMS (EI^+) Exact mass calcd for $^{12}\text{C}_{10}^{13}\text{C}_1\text{H}_{14}\text{O}_3$ [M] $^+$: 195.0976, found 195.0978.

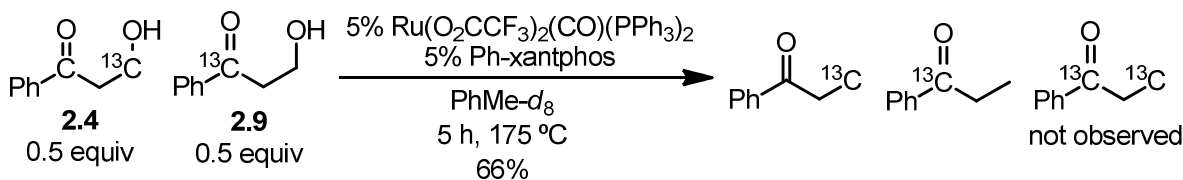


Synthesis of 1-phenylpropane-1,3-diol- ^{13}C (2.11). This material was synthesized in analogy to the procedure developed for the reduction of ethyl benzoylacetate to 1-phenylpropane-1,3-diol,⁴² using **2.10** (238 mg, 1.22 mmol), NaBH_4 (92 mg, 2.44 mmol), tetrahydrofuran (9 mL), and methanol (3 mL), yielding 118 mg **2.11** as a yellow oil (63%). ^1H NMR (400 MHz, CDCl_3): δ 7.34-7.20 (m, 5H), 4.89 (dm, $J_{\text{C-H}} = 143.1$ Hz, 1H), 3.81-3.70 (m, 2H), 3.32 (broad, 1H), 2.98 (broad, 1H), 2.01-1.80 (m, 2H) ppm; ^{13}C NMR (100 MHz, CDCl_3): δ 144.5 ($J_{\text{C-C}} = 48.1$ Hz), 128.7, 127.7, 125.8, 74.3 (^{13}C enriched), 61.5 ($J_{\text{C-C}} = 15.2$ Hz), 40.5 ($J_{\text{C-C}} = 37.5$ Hz) ppm; HRMS (EI^+) Exact mass calcd for $^{12}\text{C}_8^{13}\text{C}_1\text{H}_{12}\text{O}_2$ [M] $^+$: 153.0871, found 153.0869.

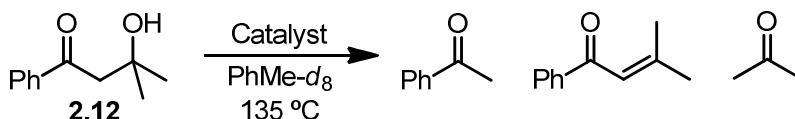


Synthesis of β -hydroxypropiophenone- ^{13}C (2.9). This material was synthesized in a fashion analogous to **2.2**, using **2.11** (227 mg, 1.48 mmol), dichloromethane (25 mL), and MnO_2 (3.86 g, 44.4 mmol) yielding 92 mg **2.9** as a clear oil (41%). ^1H NMR (500 MHz, CDCl_3): δ 7.92-7.85 (m, 2H), 7.56-7.48 (m, 1H), 7.44-7.32 (m, 2H), 4.00-3.91 (m, 2H), 3.19-3.12 (m, 2H), 3.11-2.91 (broad, 1H) ppm; ^{13}C NMR (125 MHz, CDCl_3): δ 200.4 (^{13}C enriched), 136.7 ($J_{\text{C-C}} = 53.3$ Hz), 133.6, 128.7 ($J_{\text{C-C}} = 4.0$ Hz), 128.2 ($J_{\text{C-C}} = 2.9$ Hz), 58.1, 40.6 ($J_{\text{C-C}} = 41.4$ Hz) ppm;

IR 3415 (broad), 2917, 1641, 1596, 1580, 1448, 1206 cm^{-1} ; HRMS (EI^+) Exact mass calcd for $^{12}\text{C}_8^{13}\text{CH}_{10}\text{O}_2$ [$\text{M}]^+$: 151.0714, found 151.0712.



Disproportionation crossover experiment using 2.4 and 2.9. Solutions of **2.4** (200 μL , 250 mM in toluene- d_8 , 0.050 mmol) and **2.9** (200 μL , 250 mM in toluene- d_8 , 0.050 mmol) were combined in an NMR tube with $\text{Ru}(\text{O}_2\text{CCF}_3)_2(\text{CO})(\text{PPh}_3)_2$ (4.6 mg, 0.0050 mmol), 4,5-bis(diphenylphosphino)-9,9-dimethylxanthene (2.9 mg, 0.0050 mmol), and a glass capillary containing 4-trifluoromethylpyridine. The NMR tube was sealed under vacuum, heated at 175 $^\circ\text{C}$, and monitored periodically *via* ^1H NMR, which after 5 h of heating indicated complete consumption of **2.4** and **2.9**. The diagnostic ^1H NMR resonances used to determine yields of propiophenone by comparison to the external standard are as listed above for the disproportionation of **2.1**. The isotopic distributions of the molecular ion of propiophenone obtained from this experiment were measured *via* GC/MS analysis of the crude reaction mixture and integration of the mass spectral signals at m/z values of 135, 136, 137, and 138 in the region ± 1 minutes of the propiophenone retention time. Control experiments using **2.4** and **2.9** separately were carried out as above, substituting the solution containing either **2.4** or **2.9** for toluene- d_8 , as appropriate. The results of these experiments can be found in Table 1.



Retro-aldol cleavage of 3-hydroxy-3-methyl-1-phenylbutanone (2.12). A solution of **2.12** (400 μL , 500 mM in toluene- d_8 , 0.200 mmol) was combined in an NMR tube with the appropriate catalyst (0.010 mmol) and a glass capillary containing 4-trifluoromethylpyridine. The NMR tube was sealed under vacuum, heated at 135 $^\circ\text{C}$, and monitored periodically *via* ^1H NMR. The diagnostic resonances used to determine yields of acetophenone by comparison to the external standard are as listed above for the disproportionation of **2.1**. Those for other compounds are as follows: ^1H NMR (400 MHz, $\text{PhMe-}d_8$): 3-hydroxy-3-methyl-1-phenylbutanone – δ 2.78 (s, 2H), 1.29 (s, 6H) ppm; 3-methyl-1-phenylbutenone – δ 6.57 (s, 1H), 2.15 (s, 3H), 1.67 (s, 3H) ppm; acetone – δ 1.67 (s, 6H) ppm. The presence of these species was confirmed by GC/MS analysis of the reaction mixture. All reactions were taken to full conversion of **2.12**, and yields were $\pm 5\%$ of those shown in Scheme 18.

References

- (1) Huber, G. W.; Iborra, S.; Corma, A. *Chem. Rev.* **2006**, *106*, 4044.
- (2) Sasaki, M.; Fukukawa, M.; Minami, K.; Adschiri, T.; Arai, K. *Ind. Eng. Chem. Res.* **2002**, *41*, 6642.
- (3) Sasaki, M.; Goto, K.; Tajima, K.; Adschiri, T.; Arai, K. *Green Chem.* **2002**, *4*, 285.
- (4) Huyghues-Despointes, A.; Yaylayan, V. A. *J. Agric. Food Chem.* **1996**, *44*, 672.

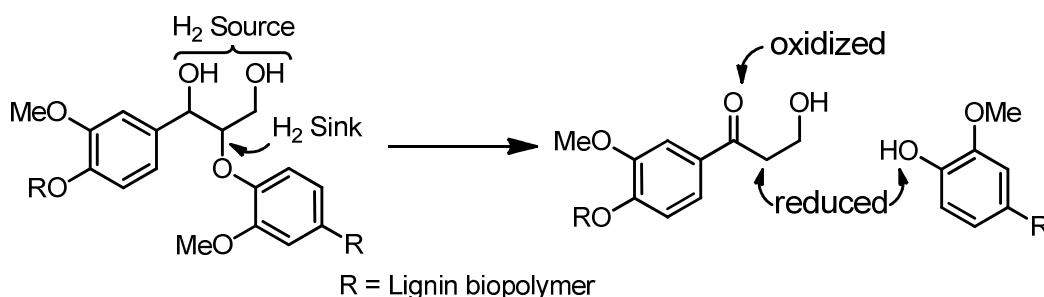
- (5) Carlson, T. R.; Jae, J.; Lin, Y.-C.; Tompsett, G. A.; Huber, G. W. *J. Catal.* **2010**, *270*, 110.
- (6) Zeng, W.; Cheng, D.-g.; Chen, F.; Zhan, X. *Catal. Lett.* **2009**, *133*, 221.
- (7) Paine, J. B. I.; Pithawalla, Y. B.; Naworal, J. D. *J. Anal. Appl. Pyrolysis* **2008**, *82*, 10.
- (8) Paine, J. B. I.; Pithawalla, Y. B.; Naworal, J. D. *J. Anal. Appl. Pyrolysis* **2008**, *82*, 42.
- (9) Tarabanko, V. E.; Hendogina, Y. V.; Petuhov, D. V.; Pervishina, E. P. *React. Kinet. Catal. Lett.* **2000**, *69*, 361.
- (10) Ralph, J.; Ede, R. M.; Robinson, N. P.; Main, L. *J. Wood Chem. Technol.* **1987**, *7*, 133.
- (11) Brieger, G.; Nestricks, T. J. *Chem. Rev.* **1974**, *74*, 567.
- (12) Graser, B.; Steigerwald, H. *J. Organomet. Chem.* **1980**, *193*, C67.
- (13) Mizushima, E.; Yamaguchi, M.; Yamagishi, T. *J. Mol. Catal. A: Chem.* **1999**, *148*, 69.
- (14) Dobson, A.; Robinson, S. D. *J. Organomet. Chem.* **1975**, *87*, C52.
- (15) Dobson, A.; Robinson, S. D. *Inorg. Chem.* **1977**, *16*, 137.
- (16) Maytum, H. C.; Tavassoli, B.; Williams, J. M. J. *Org. Lett.* **2007**, *9*, 4387.
- (17) Owston, N. A.; Parker, A. J.; Williams, J. M. J. *Chem. Commun.* **2008**, 624.
- (18) Hall, M. I.; Pridmore, S. J.; Williams, J. M. J. *Adv. Synth. Catal.* **2008**, *350*, 1975.
- (19) Ledger, A. E. W.; Slatford, P. A.; Lowe, J. P.; Mahon, M. F.; Whittlesey, M. K.; Williams, J. M. J. *J. Chem. Soc. Dalton Trans.* **2009**, 716.
- (20) Shibahara, F.; Bower, J. F.; Krische, M. J. *J. Am. Chem. Soc.* **2008**, *130*, 14120.
- (21) Levison, J. J.; Robinson, S. D. *J. Chem. Soc. A* **1970**, 2947.
- (22) Newsome, D. S. *Catal. Rev.* **1980**, *21*, 275.
- (23) Laine, R. M.; Rinker, R. G.; Ford, P. C. *J. Am. Chem. Soc.* **1977**, *99*, 252.
- (24) Kang, H.; Mauldin, C. H.; Slegeir, T. C. W.; Cann, K.; Pettit, R. *J. Am. Chem. Soc.* **1977**, *99*, 8323.
- (25) Ungermann, C.; Landis, V.; Moya, S. A.; Cohen, H.; Walker, H.; Pearson, R. G.; Rinker, R. G.; Ford, P. C. *J. Am. Chem. Soc.* **1979**, *101*, 5922.
- (26) Venäläinen, T.; Pakkanen, T. A.; Pakkanen, T. T.; Iiskola, E. *J. Organomet. Chem.* **1986**, *314*, C49.
- (27) Haukka, M.; Venäläinen, T.; Kallinen, M.; Pakkanen, T. A. *J. Mol. Catal. A: Chem.* **1998**, *136*, 127.
- (28) Doi, T.; Fukuyama, T.; Horiguchi, J.; Okamura, T.; Ryu, I. *Synlett* **2006**, *5*, 721.
- (29) Cravatto, G.; Demetri, A.; Nano, G. M.; Palmisano, G.; Penoni, A.; Tagliapietra, S. *Eur. J. Org. Chem.* **2003**, 4438.
- (30) Guthrie, J. P. *Can. J. Chem.* **1978**, *56*, 962.
- (31) Guthrie, J. P. *J. Am. Chem. Soc.* **1991**, *113*, 7249.
- (32) Tencer, Y.; Michman, M.; Goldenfeld, I. *J. Organomet. Chem.* **1991**, *412*, 203.
- (33) Murakami, K.; Ohmiya, H.; Yorimitsu, H.; Oshima, K. *Tetrahedron Lett.* **2008**, *49*, 2388.
- (34) Yang, W.; Digits, C. A.; Hatada, M.; Narula, S.; Rozamus, L. W.; Huestis, C. M.; Wong, J.; Dalgarno, D.; Holt, D. A. *Org. Lett.* **1999**, *1*, 2033.
- (35) Simpura, I.; Nevalainen, V. *Angew. Chem. Int. Ed.* **2000**, *39*, 3422.
- (36) Schneider, C.; Hansch, M. *Chem. Commun.* **2001**, 1218.
- (37) Schneider, C.; Hansch, M. *Synlett* **2003**, *6*, 837.
- (38) Simpura, I.; Nevalainen, V. *Tetrahedron* **2003**, *59*, 7535.
- (39) Schneider, C.; Hansch, M.; Weide, T. *Chem. Eur. J.* **2005**, *11*, 3010.
- (40) Xi, B.; Nevalainen, V. *Tetrahedron Lett.* **2006**, *47*, 2561.
- (41) Alaimo, P. J.; Peters, D. W.; Arnold, J.; Bergman, R. G. *J. Chem. Ed.* **2001**, *78*, 64.

- (42) De Castro, K. A.; Rhee, H. *Synthesis* **2008**, 1841.
- (43) Kano, K.; Scarpetti, D.; Warner, J. C.; Anselme, J.-P.; Springer, J. P.; Arison, B. H. *Can. J. Chem.* **1986**, *64*, 2211.
- (44) Imagawa, H.; Asai, Y.; Takano, H.; Hamagaki, H.; Nishizawa, M. *Org. Lett.* **2006**, *8*, 447.
- (45) Attenburrow, J.; Cameron, A. F. B.; Chapman, J. H.; Evans, R. M.; Hems, B. A.; Jansen, A. B. A.; Walker, T. *J. Chem. Soc.* **1952**, 1094.
- (46) Kawakami, T.; Shibata, I.; Baba, A. *J. Org. Chem.* **1996**, *61*, 82.
- (47) Hauser, C. R.; Breslow, D. S.; Shriner, R. L.; Hoehn, W. M.; Patterson, V. A. *Org. Syn.* **1941**, *3*, 408.
- (48) Elghamry, I. *Synthesis* **2003**, 2301.

Part 2 - Chapter 3. Reductive ether cleavage of 1-aryl-2-aryloxyalkanol lignin model compounds via α -aryloxy ketones

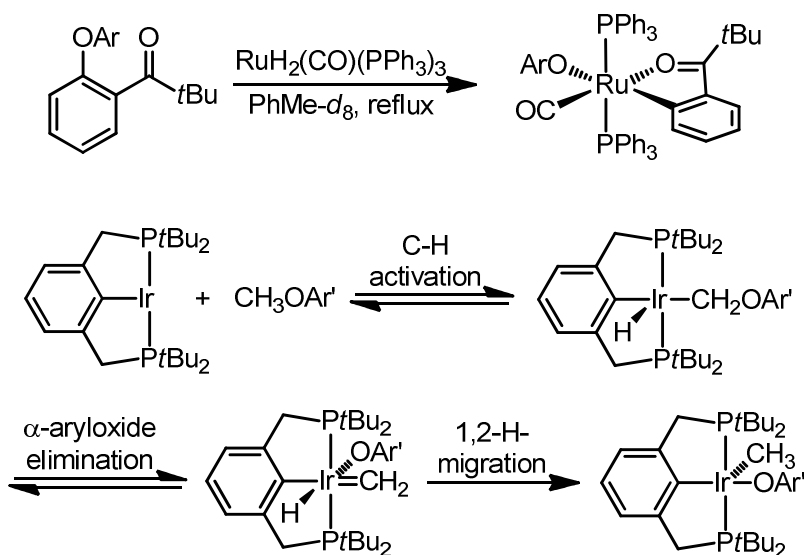
Introduction

Production of a liquid fuel from lignin requires cleavage of the bonds comprising the biopolymer skeleton. Chapter 1 described a disproportionation strategy for the depolymerization of lignin, wherein the hydrogen produced in the oxidation of carbinol moieties would be used to reductively cleave carbon-oxygen (C-O) bonds. We targeted the most common type of linkage present in lignin, the β -O-4 (glycerol- β -aryl ether) moiety, to investigate the possibility of using this disproportionative depolymerization strategy (Scheme 1).



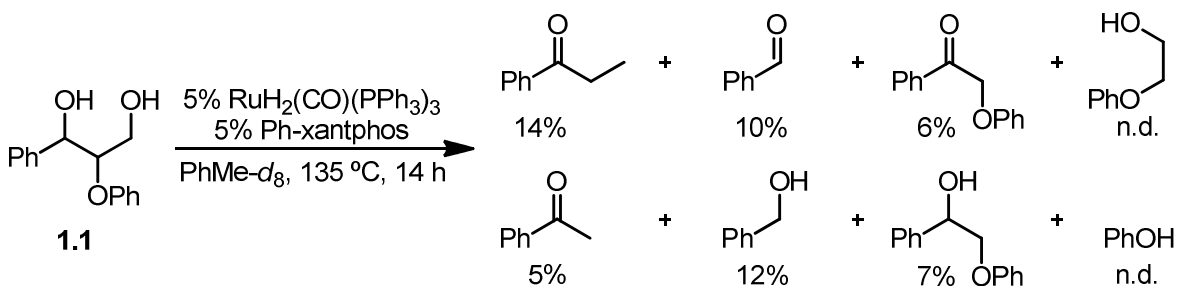
Scheme 1. Disproportionation strategy for the cleavage of the glycerol- β -aryl ether linkage of lignin.

This strategy requires a catalyst capable of carrying out both the oxidative and the reductive transformations described above. While there are numerous examples of the use of primary and secondary alcohols as hydrogen sources,¹⁻⁶ there are no examples that have coupled this reaction with the reductive cleavage of C-O single bonds. There are, however, a few reports on the transition metal-catalyzed cleavage of C-O single bonds.⁷⁻¹⁸ The complex $\text{RuH}_2(\text{CO})(\text{PPh}_3)_3$ has been shown to catalytically cleave sp^2 C-O bonds, a reaction whose mechanism has been proposed to proceed through oxidative addition of a C-O single bond to the metal (Scheme 2, top).¹⁴ Another example of C-O bond cleavage with relevance to the studies presented in this chapter is the iridium-mediated cleavage of the sp^3 C-O bond of anisole derivatives. The authors of this study provide experimental and computational evidence for a reaction mechanism that proceeds through an iridium methylidene complex *via* oxidative addition of a methyl carbon-hydrogen bond to the metal center followed by α -aryloxy elimination and subsequent 1,2-migration of a hydrogen atom (Scheme 2, bottom).¹⁸



Scheme 2. C-O bond cleavage *via* chelation-assisted oxidative addition (top),¹⁴ and C-O bond cleavage *via* carbon-hydrogen bond activation followed by α -aryloxide elimination and 1,2-H-migration (bottom).¹⁸

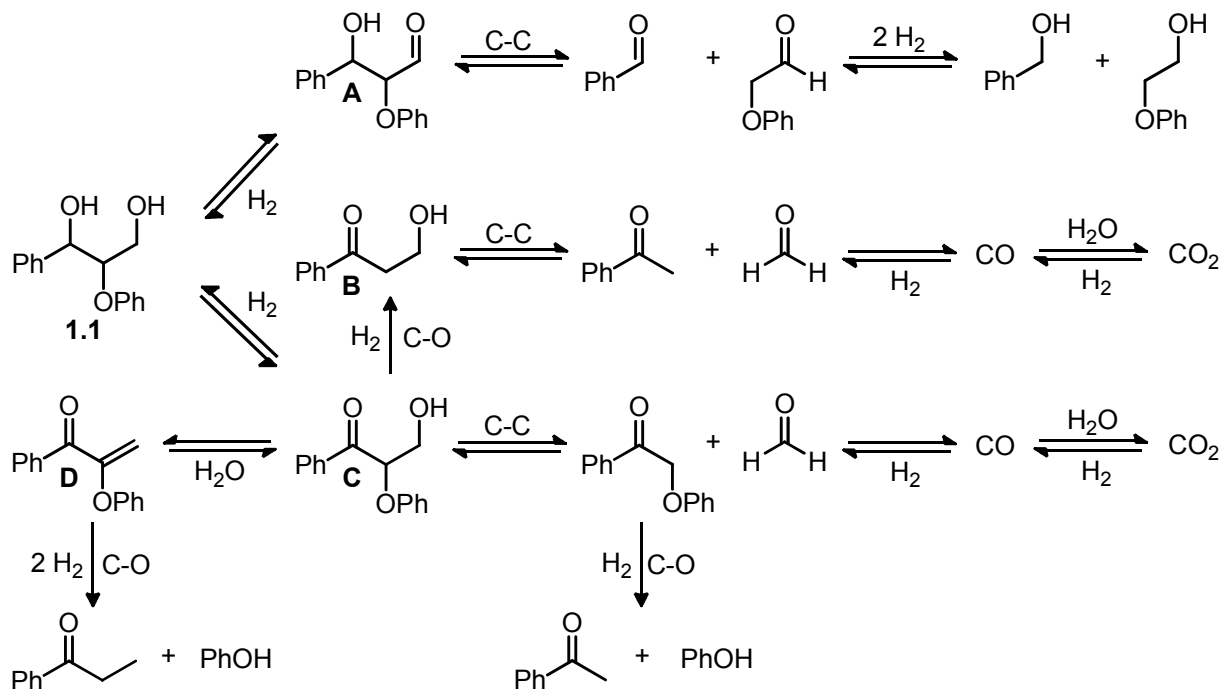
Chapter 1 introduced the ruthenium-catalyzed disproportionation of glycerol- β -aryl ether lignin model compound **1.1** using a method developed by postdoctoral researcher Dr. Jason Nichols. ^1H NMR analysis of the reaction mixture formed upon treatment of **1.1** with 5 mol% of $\text{RuH}_2(\text{CO})(\text{PPh}_3)_3$ and 5 mol% of 4,5-bis(diphenylphosphino)-9,9-dimethylxanthene (Ph-xantphos) at 135 °C revealed the presence of multiple products, resulting from the cleavage of both carbon-oxygen and carbon-carbon bonds (Scheme 3). Importantly, some of the products observed are formed through cleavage of bonds relevant to lignin depolymerization. The yield of those products (specifically, propiophenone, acetophenone, benzaldehyde, and benzyl alcohol) can be translated into a 41% degree of depolymerization. It should be noted that <5% conversion to products was observed when the reaction was performed in the absence of the wide-bite angle bis-phosphine ligand Ph-xantphos.



Scheme 3. Ruthenium-catalyzed disproportionation of lignin model compound **1.1**. Yields were calculated by ^1H NMR using an external standard. Ph-xantphos = 4,5-bis(diphenylphosphino)-9,9-dimethylxanthene. n.d. = yield not determined.

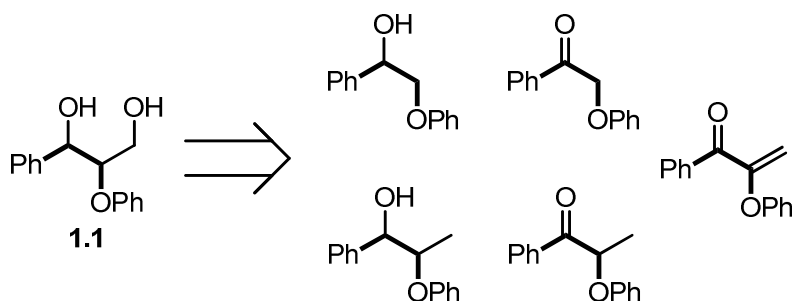
Our investigations into the carbon-carbon bond cleavage process observed in the disproportionation reaction of **1.1** are described in Chapter 2. Based on these studies as well as the results presented in this chapter, we propose the mechanism shown in Scheme 4 that explains

the formation of the observed products. In this mechanism, acetophenone and α -phenoxyacetophenone are generated through retro-aldol cleavage of β -hydroxypropiophenone (**B**) and β -hydroxy- α -phenoxypropiophenone (**C**). A byproduct of these reactions is formaldehyde, which was shown to be converted to carbon dioxide under the reaction conditions, releasing two equivalents of hydrogen. Additionally, we propose that benzaldehyde and benzyl alcohol are generated through the retro-aldol cleavage of β -hydroxy- β -phenylpropanal (**A**). While a reasonable pathway for the formation of propiophenone is the reduction of phenyl vinyl ketone, the results described in this chapter suggest that the dominant pathway for this transformation proceeds through 2-phenoxy-1-phenylprop-2-en-1-one (**D**).



Scheme 4. Proposed reaction pathways in the ruthenium-catalyzed disproportionation of **1.1**. C-C = carbon-carbon bond cleavage. C-O = carbon-oxygen bond cleavage.

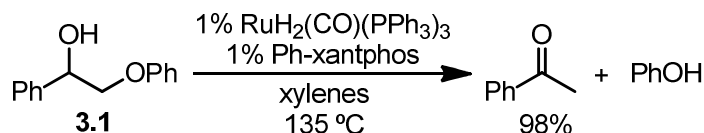
The present chapter describes mechanistic studies on the C-O bond cleavage reaction observed with **1.1**. Our studies were carried out using model compounds such as the mono-alcohol and ketone substrates shown in Scheme 5. These models do not contain the 1,3-diol motif present in **1.1** that was responsible for the carbon-carbon bond cleavage reactions. This simplification facilitated mechanistic analysis of the carbon-oxygen bond cleavage reaction in the absence of the carbon-carbon bond cleavage reaction.



Scheme 5. Lignin model compounds designed to study C-O bond cleavage in the absence of the carbon-carbon bond cleavage. Bonds that are common to all model compounds are drawn in bold.

Results & Discussion

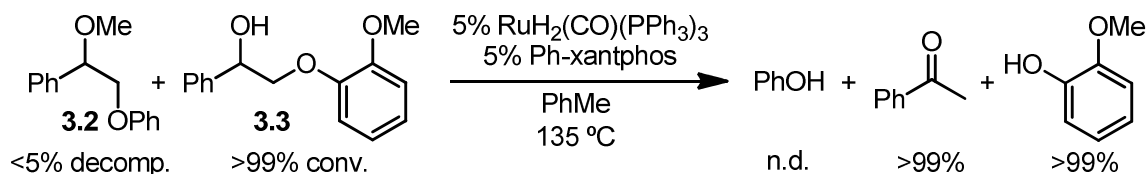
The disproportionation of lignin model compound **3.1**¹⁹ was effected by 1% RuH₂(CO)(PPh₃)₃ and 1% Ph-xantphos at 135 °C to produce phenol and acetophenone, the latter of which was isolated in 98% yield (Scheme 6). As this model compound showed reactivity analogous to that proposed for the disproportionation of **1.1** and no competitive side reactions, we proceeded to investigate the mechanism of this C-O bond cleavage reaction using 2-aryloxy-1-phenylethanol substrates such as **3.1**.



Scheme 6. Ruthenium-catalyzed disproportionation of lignin model compound **3.1**, performed by Dr. Jason Nichols, and yield of isolated product.

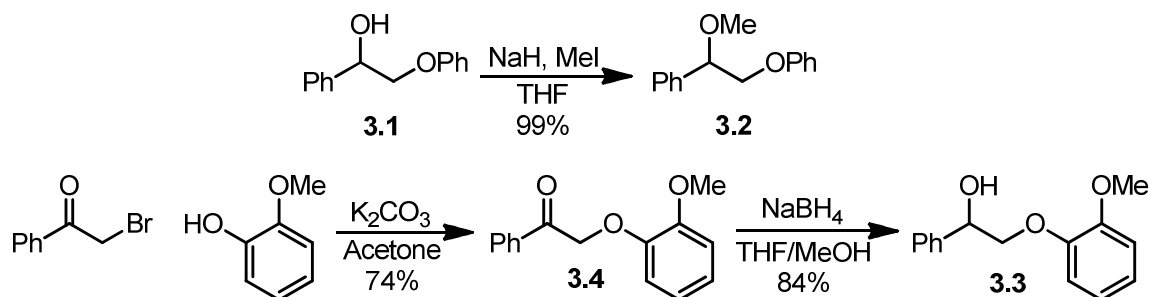
Requirement of a Free Hydroxyl Group for the Disproportionation Reaction

To determine whether the disproportionation reaction requires the free hydroxyl group of **3.1**, methyl ether **3.2** was subjected to the disproportionation conditions in the presence of 2-guaiacoxy-1-phenylethanol (**3.3**). Complete conversion of **3.3** was observed under these conditions, establishing that the active catalyst was present and capable of performing the disproportionation. However, conversion of **3.2** was not observed, which establishes that the presence of a free hydroxyl group is necessary for the disproportionation to occur (Scheme 7).



Scheme 7. Control reaction showing the necessity of a free hydroxyl group for successful disproportionation. Yields were calculated by ¹H NMR using an external standard. Decomp. = decomposition. Conv. = conversion.

Model compounds **3.2** and **3.3** were synthesized as shown in Scheme 8. Williamson etherification of **3.1**¹⁹ provided **3.2**, while **3.3** was synthesized by Williamson etherification of guaiacol with 2-bromoacetophenone followed by reduction with sodium borohydride.



Scheme 8. Synthesis of model compounds **3.2** and **3.3**.

Investigations into the Intermediacy of α -Aryloxyacetophenones

In the conversion of **3.3** to products during the reaction depicted in Scheme 7, small amounts (~10%) of 2-guaiaoxyacetophenone were observed *via* ¹H NMR analysis of the reaction mixture. This observation along with the fact that methyl ether **3.2** was not converted to products suggests a two-step mechanism that proceeds by oxidation of the benzylic carbinol followed by reductive cleavage of the sp³ C-O bond. In order to further investigate this hypothesis, the complete kinetic timecourse for the conversion of **3.3** to guaiacol and acetophenone was obtained (Figure 1). Indeed, the appearance and disappearance of **3.4** was observed during the course of the disproportionation, providing evidence for the intermediacy of **3.4** in this reaction.

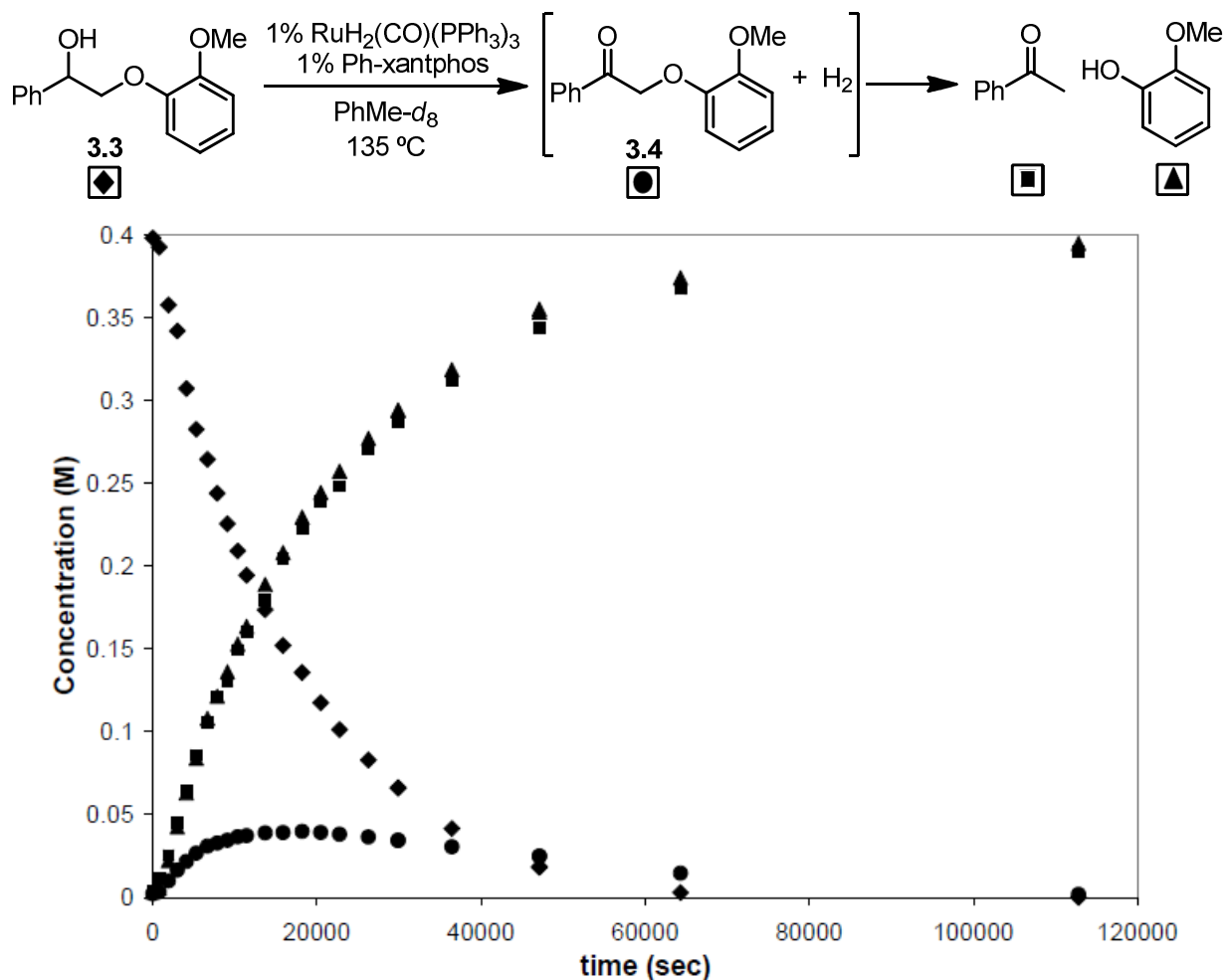


Figure 1. Experimental timecourse for the disproportionation of **3.3**. Appearance and disappearance of **3.4** is observed.

The kinetic profile shown in Figure 1 was modeled computationally to a number of different scenarios for the formation of products from **3.3** using the kinetic modeling program Copasi.^{20,21} As we did not have spectroscopic evidence of the presence or concentrations of any catalytic intermediates, simplified kinetic models were used in these simulations. In addition, the concentrations of acetophenone and guaiacol were averaged and used as the concentration of a hypothetical product in order to simplify computational analyses. A model whereby the catalytic dehydrogenation of **3.3** to give **3.4** was followed by catalytic cleavage of **3.4** to give product did not fit the kinetic data (Figure 2, A). This model exhibited a much more rapid growth of **3.4** and an induction period for product formation. We also modeled a scenario whereby **3.3** and catalyst interacted in the first step to produce a complex between the catalyst and **3.3**, which could either reversibly dissociate **3.4** or irreversibly form product (Figure 2, B). This model successfully fit the kinetic data. Models of these two scenarios including the interconversion between the various catalytic species and considering hydrogen explicitly showed no difference in their fit to the kinetic data. While these simulations suggest that the two-step oxidation-reduction model is incorrect, further experimental support for this could be obtained by carrying out the disproportionation reaction under varying concentrations of hydrogen and at varying initial

substrate concentrations. In addition, spectroscopic data on any catalytic intermediates would significantly improve these models.

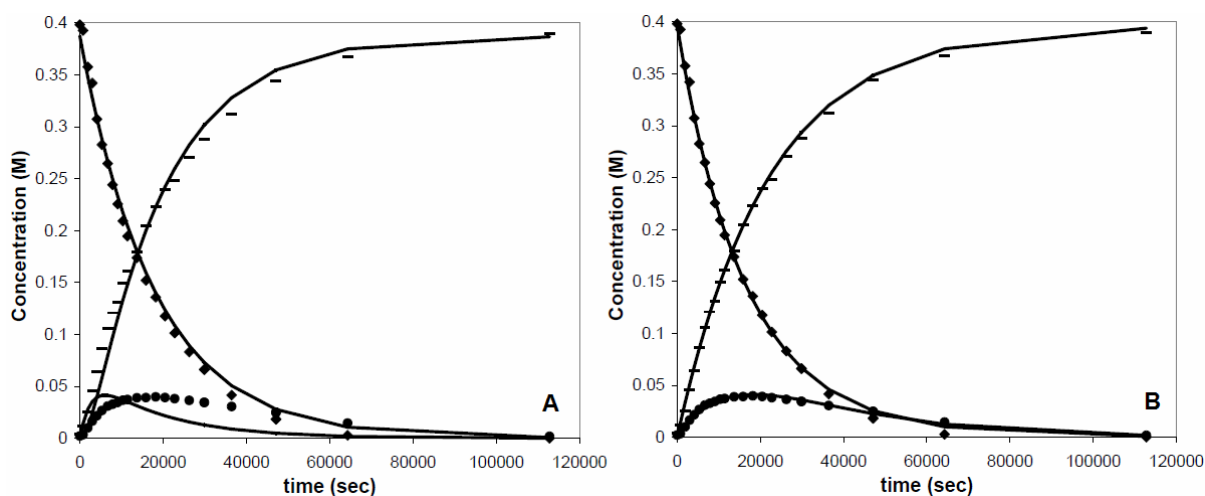
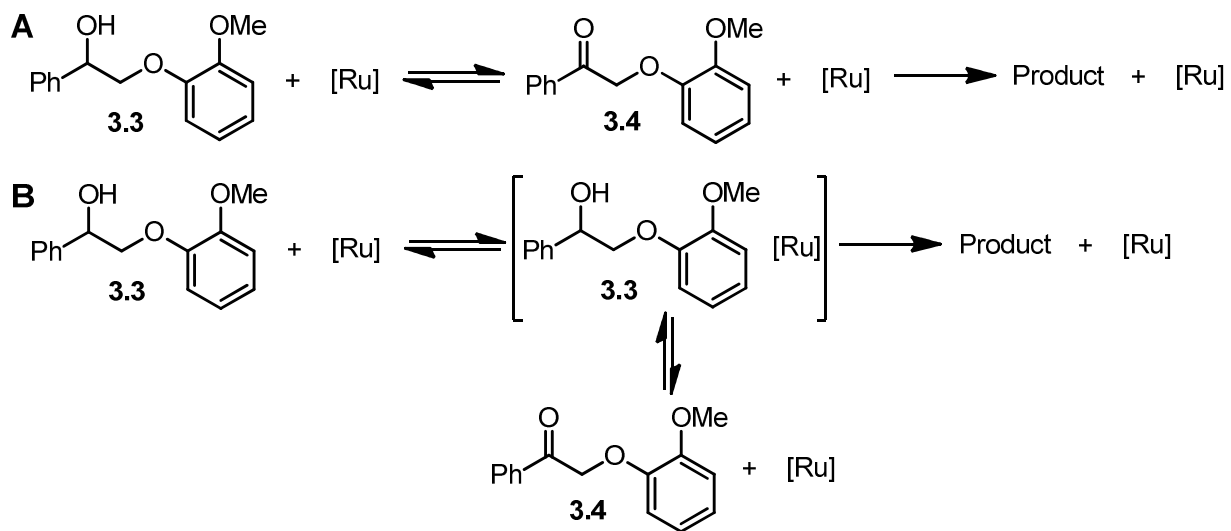
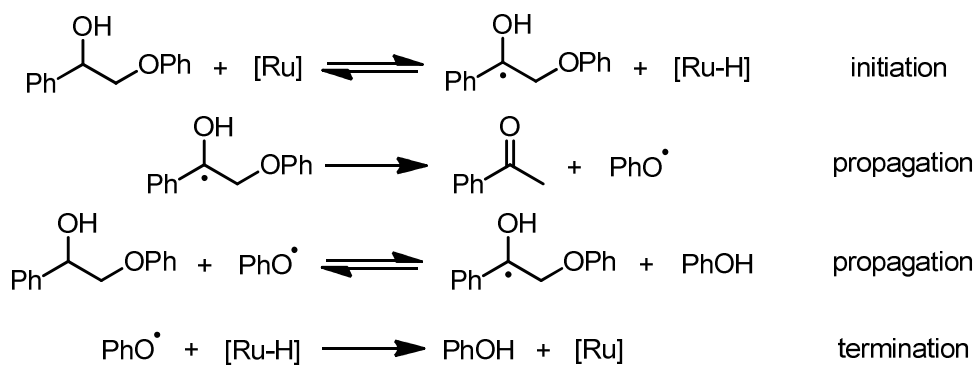


Figure 2. Top: kinetic models used for simulated timecourse. Bottom: experimental (data points) and simulated (lines) timecourses for the disproportionation of **3.3**. \blacklozenge = **3.3**; \bullet = **3.4**; $-$ = average concentration of acetophenone and guaiacol.

Radical Mechanism

As ruthenium has been employed in a number of reactions that proceed through radical intermediates,^{22,23} we set out to determine whether this was also the case in the disproportionative C-O bond cleavage process. A possible mechanism for the catalytic radical disproportionation of **3.1** is shown in Scheme 9. Computation modeling was performed using this radical mechanism along with a ruthenium-catalyzed carbinol dehydrogenation/hydrogenation step to account for the reversible appearance and disappearance of 2-guaiacoxyacetophenone (**3.4**). This simulated model fit the experimental data for the disproportionation of **3.3**, suggesting that a radical reaction mechanism is possible (Figure 3).



Scheme 9. Possible mechanism for the catalytic radical disproportionation of **3.1**.

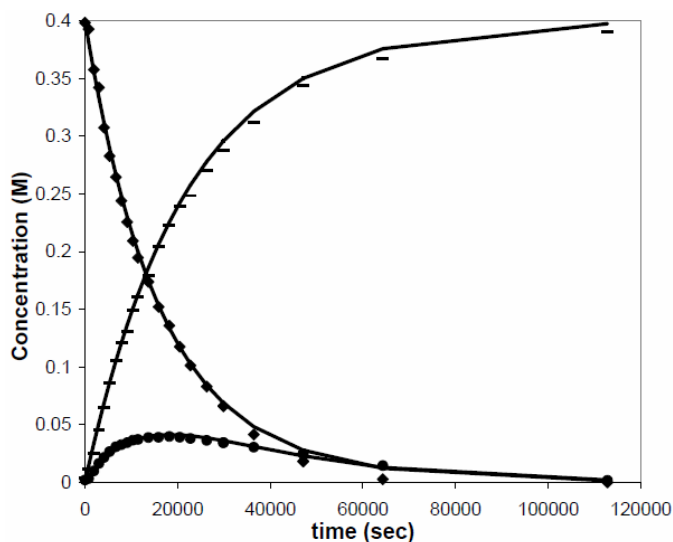
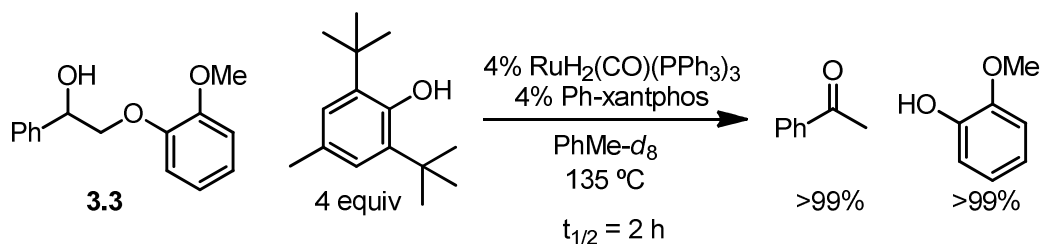


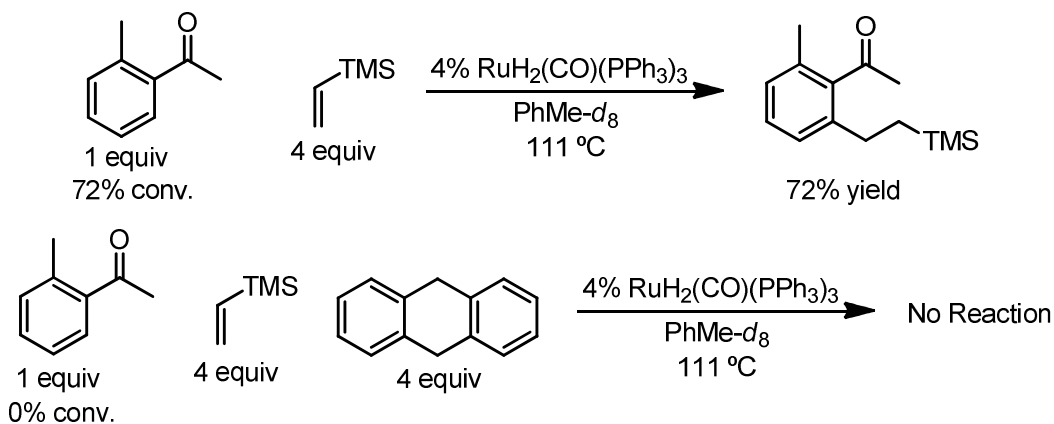
Figure 3. Experimental (data points) and simulated (lines) timecourses for the disproportionation of **3.3**. Simulated timecourse uses kinetic model shown in Scheme 9 along with a ruthenium-catalyzed dehydrogenation/hydrogenation. \blacklozenge = **3.3**; \bullet = **3.4**; $-$ = average concentration of acetophenone and guaiacol.

Despite the fact that the kinetic simulation described above suggests a radical pathway for the disproportionation of **3.3**, the following experiments did not confirm that mechanism. One of those experiments is that mentioned before using methyl ether **3.2** (Scheme 7). As the bond dissociation energy of the benzylic carbon-hydrogen bonds in **3.2** and **3.3** are not significantly different, abstraction of the benzylic hydrogen of either **3.2** or **3.3** by an aryloxy radical chain carrier should be equally likely. However, this is not the case, as conversion of **3.2** to phenol is not observed even in the presence of the disproportionation of **3.3** (Scheme 7). In addition, the presence of a large excess of the radical trap 2,6-di-*tert*-butyl-4-methylphenol (BHT) had no effect on the yield or rate of the disproportionation of **3.3** (Scheme 10). This experiment provides evidence against a mechanism proceeding through a phenoxy radical chain carrier.



Scheme 10. Disproportionation of **3.3** in the presence of the radical trap 2,6-di-*tert*-butyl-4-methylphenol.

Running the reaction in the presence of the radical trap 9,10-dihydroanthracene resulted in clean conversion of **3.3** to acetophenone and guaiacol. However, the reaction proceeded with a half-life of 18 h, three-fold more slowly than in the absence of dihydroanthracene. The sample of 9,10-dihydroanthracene used in this experiment, though recrystallized prior to use, was contaminated with 1% anthracene, which could be the cause of the rate deceleration. If the rate deceleration were due to radical scavenging by 9,10-dihydroanthracene, the result would be an increase in the concentration of anthracene. However, no change in the ratio of 9,10-dihydroanthracene to anthracene was observed *via* GC/MS analysis of the reaction mixture. In addition, as a test of its effect on other ruthenium-catalyzed reactions, 9,10-dihydroanthracene completely inhibited the $\text{RuH}_2(\text{CO})(\text{PPh}_3)_3$ -catalyzed alkylation of 2'-methylacetophenone with vinyltrimethylsilane, a reaction whose mechanism is thought to proceed through two-electron processes (Scheme 11).²⁴ It is possible that this alkylation also proceeds through a radical mechanism; however, production of anthracene is not observed in this reaction either. Though these results merit further study, we believe it is likely that 9,10-dihydroanthracene and anthracene are slowing or stopping these reactions not by trapping radical species, but by interacting with metal complex intermediates on the catalytic cycle.



Scheme 11. Alkylation of 2'-methylacetophenone is completely inhibited in the presence of 4 equivalents of 9,10-dihydroanthracene.²⁴

Attempts at Characterization of Catalyst Resting State: NMR

Analysis of the reaction mixtures of the above-described disproportionation reactions was carried out at room temperature. However, the catalytic reactions took place at 135 °C. In order to determine the nature of the resting state of the catalytic cycle, spectroscopic observation of the

reaction mixture at elevated temperatures is necessary. We first focused our attention on ^1H and ^{31}P NMR analysis. In order to monitor this disproportionation in toluene- d_8 at a temperature above that solvent's boiling point, the reaction mixture was assembled in a sealed glass capillary that was then immersed in a bath of mesitylene- d_{12} inside a J-Young NMR tube. This technique was developed initially by Michael Gribble, and adapted for this system by Dr. Jason Nichols. However, using 5% $\text{RuH}_2(\text{CO})(\text{PPh}_3)_3$ and 5% Ph-xantphos, the ^1H or ^{31}P resonances of the catalyst were not visible by *in situ* NMR analysis of the reaction mixture of **3.3** at 125 °C (the maximum temperature to which it is recommended to heat the probe of the spectrometer used). The only ^{31}P resonances observed at this temperature were those of the free PPh_3 liberated in the ligand exchange with Ph-xantphos.

Variable-temperature NMR experiments were carried out on a solution of $\text{RuH}_2(\text{CO})(\text{PPh}_3)_3$ using a 600 MHz spectrometer to determine the cause of the absence of catalyst resonances at elevated temperatures (Figure 4). Both the ^1H and ^{31}P resonances of this complex began to broaden at 67 °C, and were completely undetectable at 125 °C, an effect which was reversible, as the resonances again become distinguishable when lowering the temperature. The temperature at which the NMR resonances were visible was not affected by the addition of 20 equivalents of PPh_3 . These results suggest that a fluxional process that does not involve phosphine dissociation is occurring on the NMR timescale at these temperatures. The coalescence temperature did not change significantly by performing the experiment on a 400 MHz spectrometer. The same phenomenon was observed when using $\text{RuH}_2(\text{CO})(\text{PPh}_3)(\text{Ph-xantphos})$.²⁵

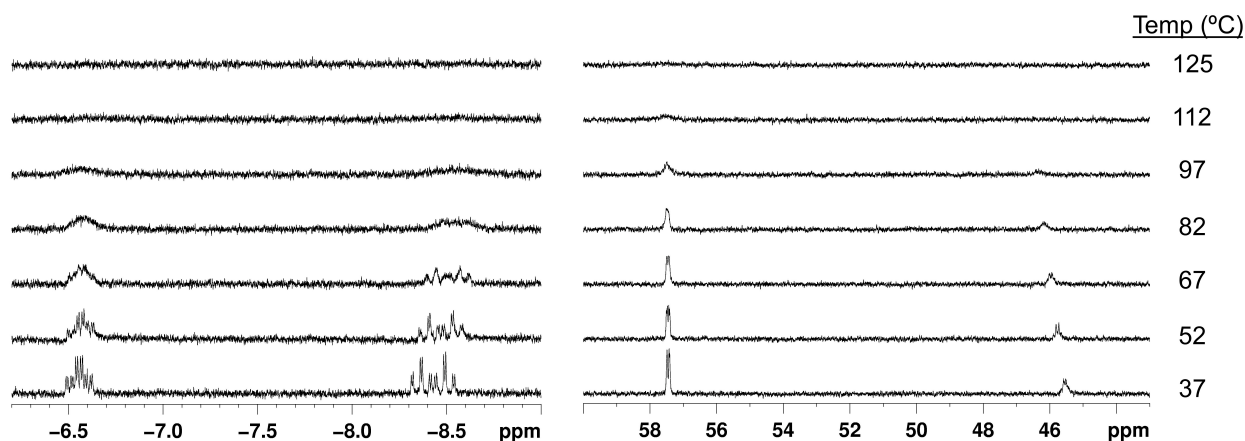
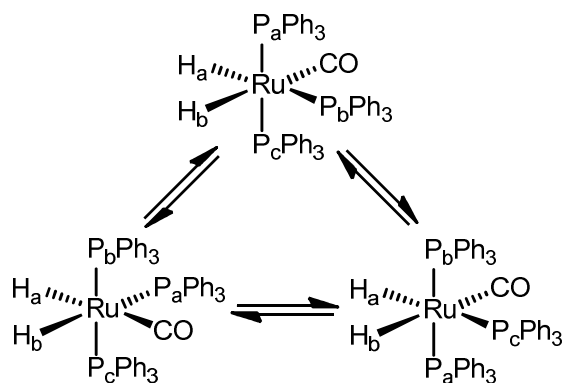


Figure 4. ^1H (left) and ^{31}P (right) NMR spectra of $\text{RuH}_2(\text{CO})(\text{PPh}_3)_3$ obtained on a 600 MHz spectrometer from 37-125 °C.

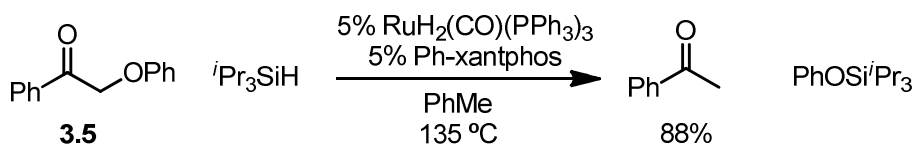
Intramolecular exchange of the hydride and phosphine ligands of $\text{RuH}_2(\text{CO})(\text{PPh}_3)_3$ has been postulated to occur *via* a non-dissociative “trigonal twist” mechanism (Scheme 12).²⁶ It is likely that a similar mechanism is the cause of the broadening observed in the above NMR experiments with both $\text{RuH}_2(\text{CO})(\text{PPh}_3)_3$ and $\text{RuH}_2(\text{CO})(\text{PPh}_3)(\text{Ph-xantphos})$.



Scheme 12. The proposed “trigonal twist” isomerization mechanism of $\text{RuH}_2(\text{CO})(\text{PPh}_3)_3$.²⁶

Attempts at Characterization of Catalyst Resting State: IR

As spectroscopic characterization of the catalyst resting state of the disproportionation reaction was unsuccessful *via* NMR, we turned our attention to *in situ* IR analysis. The IR probe of the Mettler Toledo ReactIR iC10 used in these studies is rated to a maximum temperature of 115 °C. At this temperature both $\text{RuH}_2(\text{CO})(\text{PPh}_3)_3$ and $\text{RuH}_2(\text{CO})(\text{PPh}_3)(\text{Ph-xantphos})$ ²⁵ exhibit clearly visible IR bands at 1943 cm^{-1} in toluene. This concurs with the reported stretch of 1940 cm^{-1} for $\text{RuH}_2(\text{CO})(\text{PPh}_3)_3$ in benzene.²⁷ The large volume of the IR reaction vessel used in these studies (100 mL) relative to that of the reaction mixture (2 mL) could cause unanticipated changes in the disproportionation reaction. To avoid that, we focused our attention on the hydrosilylation of 2-phenoxyacetophenone, a reaction discovered by Dr. Jason Nichols that avoids complications associated with the dehydrogenation pre-equilibrium of the disproportionation reaction (Scheme 13). We propose that the catalytic cycle of this hydrosilylation reaction will have relevance to that of the disproportionation reaction.



Scheme 13. Hydrosilylation of 2-phenoxyacetophenone, carried out by Dr. Jason Nichols. Yield obtained by GC/FID using an internal standard.

Analysis of the reaction mixture formed upon hydrosilylation of **3.5** at 115 °C revealed immediate disappearance of the band associated with the carbonyl stretch of the dihydrido ruthenium catalyst at 1943 cm^{-1} and growth of a new peak at 1936 cm^{-1} (Figure 5, A). Over the course of a few hours new peaks were observed between 1960-1900 cm^{-1} (Figure 5, B), and near reaction completion there were two major peaks at 1953 cm^{-1} and 1911 cm^{-1} (Figure 5, C). Based on these observations, it is clear that the resting state of the ruthenium catalyst is changing throughout the course of the hydrosilylation reaction. Monitoring the evolution of these peaks over the course of the reaction provides further support for this conclusion (Figure 6). Carrying out this experiment with $\text{RuH}_2(\text{CO})(\text{PPh}_3)(\text{Ph-xantphos})$ ²⁵ or in the presence of 20 equivalents of PPh_3 had no effect on this phenomenon. Due to the poor resolution of the IR spectrometer, structural characterization of the multiple species whose IR stretches are observed over the

course of this reaction would not be a straightforward matter. For this reason we did not pursue *in situ* IR analysis of the hydrosilylation reaction further.

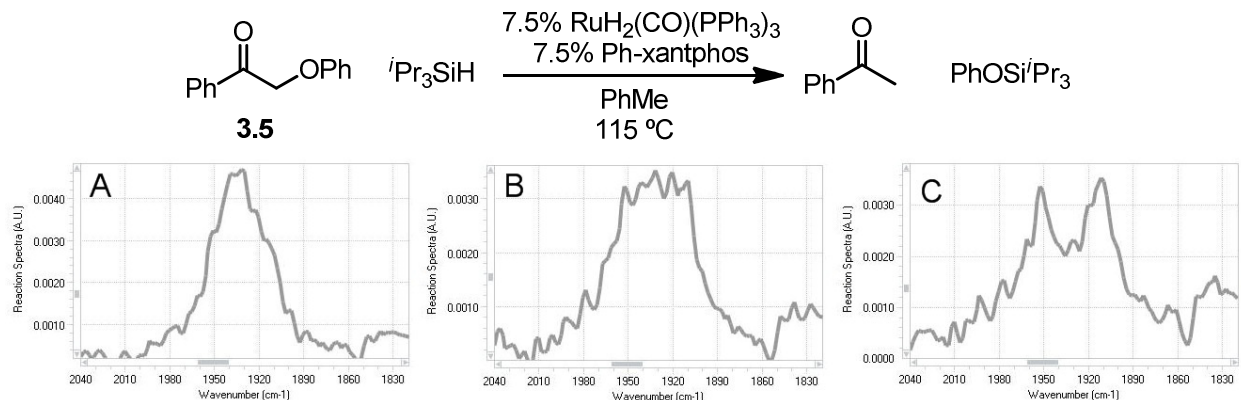


Figure 5. IR spectra from the *in situ* analysis of the ruthenium catalyst carbonyl stretch in the hydrosilylation of **3.5**. A = At 1.5 h (25% conversion of **3.5**), 1936 cm⁻¹; B = At 4.4 h (60% conversion of **3.5**), 1960-1900 cm⁻¹; C = At 17 h (90% conversion of **3.5**), 1953 cm⁻¹ and 1911 cm⁻¹.

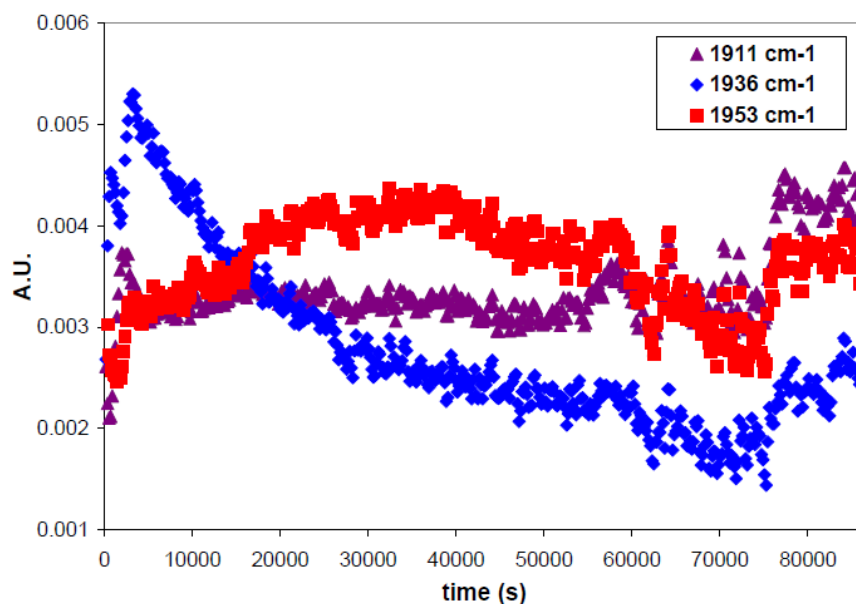
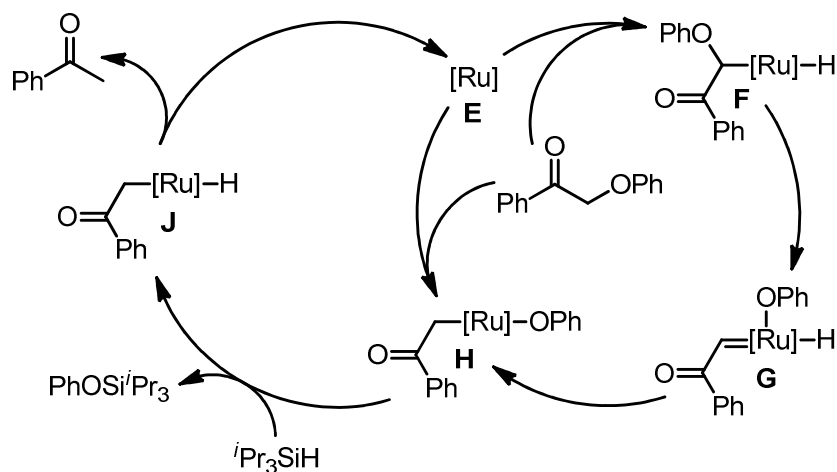


Figure 6. The change in the intensity of three representative ruthenium carbonyl stretches over the course of the hydrosilylation of **3.5**.

Deuterium-Labeling Experiment to Provide Evidence for a Ruthenium Enolate Intermediate

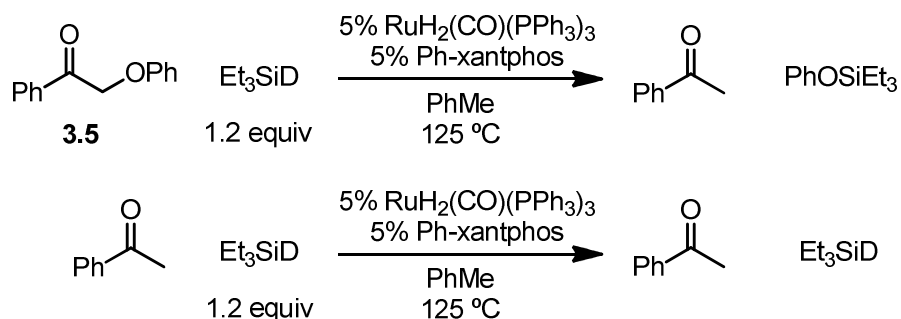
As *in-situ* spectroscopic characterization of species on the catalytic cycle was unsuccessful, we turned our attention to isotopic-labeling experiments to indirectly characterize these species. Based on literature precedent, we propose two possible mechanisms for the C-O bond cleavage reaction (Scheme 14). The first is a direct oxidative addition of the C-O bond to give phenoxy ruthenium enolate **H**, in analogy to the mechanism proposed for the reaction of pivalophenone derivatives with RuH₂(CO)(PPh₃)₃ discussed in the introduction.¹⁴ The second

proposed mechanism proceeds through oxidative addition of the α -carbon-hydrogen bond to give hydrido ruthenium enolate **F**, followed by α -phenoxide elimination to give **G** and 1,2-hydrogen migration to give **H**, in analogy to the iridium-mediated cleavage of the sp^3 C-O bond of anisole derivatives discussed in the introduction.¹⁸ Both mechanisms result in the formation of phenoxy ruthenium enolate **H**, which we propose forms hydrido ruthenium enolate **J** and silylated phenol in the presence of a silane. There are some examples in the literature of the isolation of O- and C-bound ruthenium enolates,²⁸⁻³⁰ as well as reactions thought to proceed through ruthenium enolate intermediates.^{23,31-39} In Scheme 14 only C-bound enolate species are shown for clarity. The final step of the proposed catalytic cycle is reductive elimination of acetophenone from **J** to regenerate ruthenium species **E**.



Scheme 14. Proposed mechanisms for the hydrosilylation of **3.5**.^{14,18} Only C-bound enolates are shown for clarity.

We hypothesized that the use of a silyl deuteride would provide a marker for the ruthenium enolate species by generating isotopically-labeled acetophenone. This experiment was carried out by subjecting **3.5** to the hydrosilylation conditions using triethylsilyl deuteride (Scheme 15, top). A control reaction was performed in parallel by subjecting acetophenone to identical reaction conditions (Scheme 15, bottom). The reaction of **3.5** was stopped at 75% conversion and analyzed *via* GC/MS. This revealed incorporation of multiple deuterium atoms into acetophenone in both the C-O bond cleavage and in the control reactions; the relative intensities of the molecular ions of acetophenone, corrected for ^{13}C , are listed in Table 1. The extent of deuteration in the C-O bond cleavage reaction was more significant than that observed in the control reaction.



Scheme 15. Isotopic-labeling C-O bond cleavage and control reactions.

Table 1. Relative intensities of the acetophenone (MW = 120 amu) molecular ions, corrected for ^{13}C and normalized to 120, as determined by GC/MS analysis of the reactions shown in Scheme 15. Standard deviation in parentheses.

Ion	Relative Intensity	
	C-O Cleavage	Control
120	100(0)	100(0)
121	85.7(6)	15.8(5)
122	16.6(5)	7.1(1)
123	10.4(8)	2.3(1)
124	6.7(4)	0.3(3)
125	0.9(3)	0.0(1)

The site of deuterium incorporation was established by concentrating the reaction mixtures *in vacuo*, dissolving the resulting residues in CD_2Cl_2 , and analyzing those solutions *via* ^2H NMR (Figure 7). This revealed resonances consistent with deuteration of the α -protons of acetophenone in both the C-O bond cleavage and control reactions. In addition, deuteration of the *ortho*- and *meta*-positions of acetophenone was observed in the control reaction. Presumably this deuterium incorporation is occurring *via* oxidative addition of the carbon-hydrogen bonds and proton-deuterium exchange, followed by reductive elimination. As the extent of deuteration in the C-O cleavage reaction is greater than that observed in the control reaction and only deuteration of the α -protons is observed *via* ^2H NMR in the C-O cleavage reaction, we conclude that the hydrosilylation likely proceeds through a ruthenium enolate intermediate. However, further experiments are necessary to distinguish between the direct and α C-H insertion pathways for ruthenium enolate formation (*vide infra*).

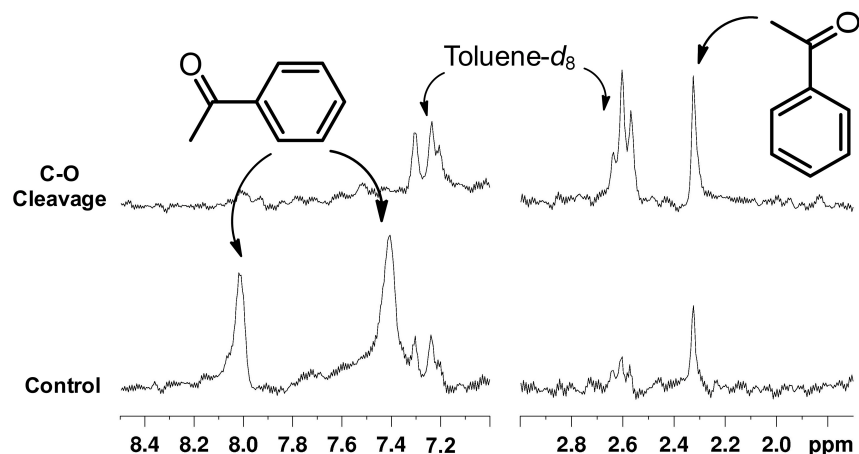
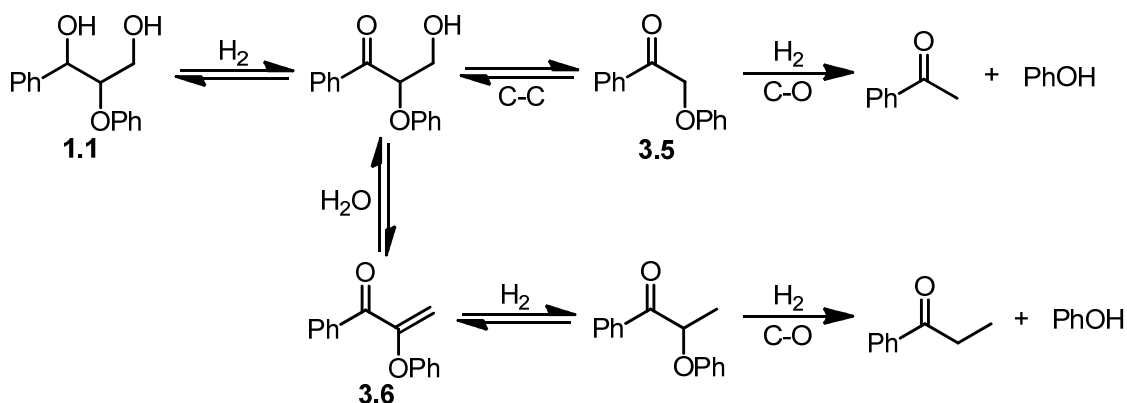


Figure 7. ^2H NMR spectra of the C-O bond cleavage (top) and control (bottom) reactions shown in Scheme 15.

Evidence for the Existence of a Novel Carbon-Oxygen Bond Activation Mechanism

^1H NMR analysis of the disproportionation of lignin model compound **1.1** (Scheme 3) at the early stages of the reaction reveals that propiophenone is formed at a much faster rate than is acetophenone. Our initial proposed mechanism for the formation of these products involved 2-phenoxypropiophenone and 2-phenoxyacetophenone undergoing rate-limiting reductive C-O bond cleavage (Scheme 16). We expected that there would be a steric predisposition against reductive cleavage of 2-phenoxypropiophenone and were surprised to observe the faster rate of formation of propiophenone in this reaction. While there are several possible explanations for this, we hypothesized that the production of acetophenone and propiophenone was most likely the result of different C-O bond cleavage mechanisms.

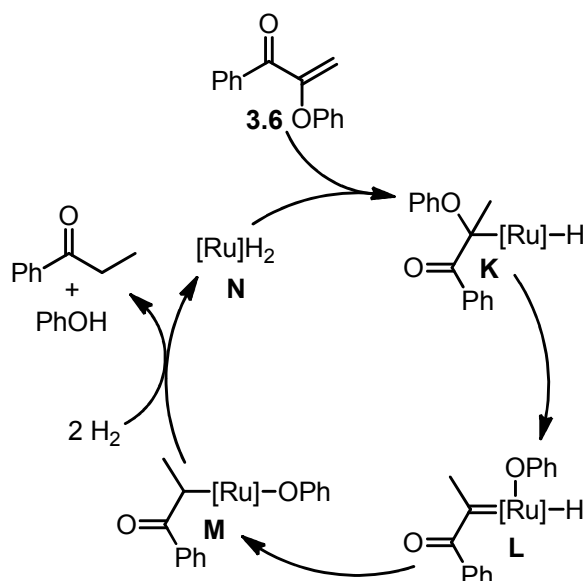


Scheme 16. Initially proposed mechanism for the formation of acetophenone and propiophenone from the disproportionation of **1.1**.

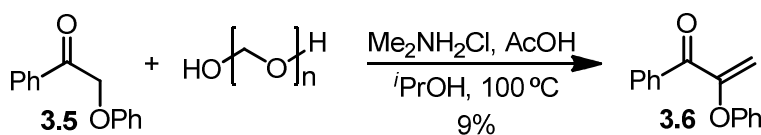
Rather than reduction of enone **3.6** to form 2-phenoxypropiophenone, we propose a mechanism that begins by migratory insertion of a hydrido ruthenium species (**N**) into **3.6** yielding hydrido ruthenium enolate **K**, based on several studies in which this step has been proposed with ruthenium catalysts as well as rhodium, palladium, and copper catalysts (Scheme 17).^{31,33,34,36-38,40,41} This ruthenium enolate species then undergoes α -phenoxy elimination to

give **L**, followed by 1,2-migration of a hydrogen atom to give **M**, in analogy to the proposed mechanism for the iridium-mediated C-O bond cleavage discussed in the introduction.¹⁸ Hydrogenolysis of the resulting phenoxy ruthenium enolate regenerates the dihydrido ruthenium catalyst.

To test whether propiophenone could indeed be obtained from **3.6** at a reaction rate consistent with that observed for the conversion of **1.1** to propiophenone, an authentic sample of **3.6** was prepared. Specifically, enone **3.6** was synthesized by Mannich reaction of **3.5**, paraformaldehyde, and dimethylammonium chloride followed by *in situ* elimination of the resulting α -amino ketone (Scheme 18).



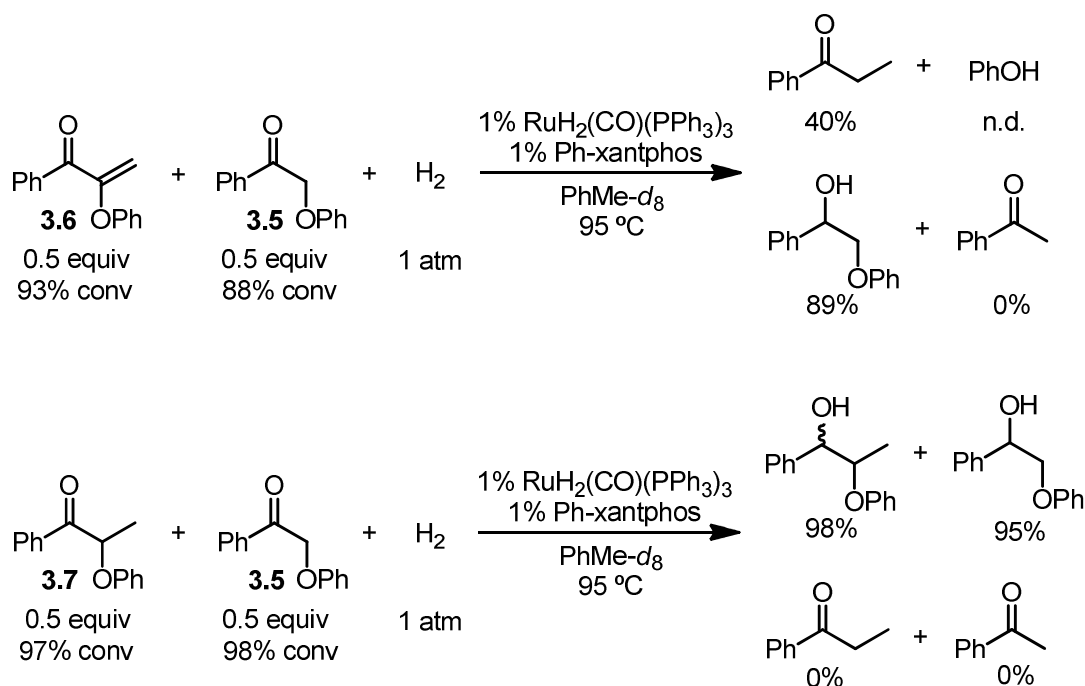
Scheme 17. Proposed mechanism for the formation of propiophenone from **3.6**. Only C-bound enolates are shown for clarity.



Scheme 18. Synthesis of enone **3.6**.

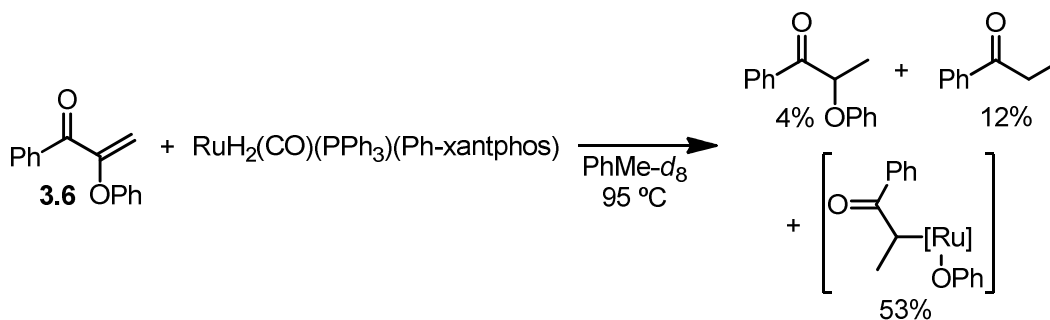
A direct competition experiment between **3.6** and 2-phenoxyacetophenone (**3.5**) supports the mechanism proposed in Scheme 17. When the consumption of the starting materials was almost complete (95 °C, 38 h 15 min), **3.6** results in a 40% yield of propiophenone while no acetophenone from reduction of **3.5** is detected by NMR or GC/MS analysis (Scheme 19, top). As **3.6** was observed to decompose upon storage at -30 °C, we propose that the imperfect mass balance for propiophenone formation is the result of non-specific decomposition of this enone. A mechanism alternative to that shown in Scheme 17 for propiophenone formation is the reduction of **3.6** to 2-phenoxypropiophenone followed by cleavage of the resulting sp^3 C-O bond. However, under conditions identical to those of the competition experiment between **3.6** and **3.5**, only carbonyl reduction of **3.7** and **3.5** was observed, which indicates that the C-O bond cleavage of **3.6** does not occur through reduction to **3.7** (Scheme 19, bottom). Based on these experiments

we propose that **3.6** is an intermediate in the formation of propiophenone in the disproportionation of **1.1** and that the rate of propiophenone formation from **3.6** is faster than that for the formation of acetophenone from **3.5**.



Scheme 19. Competition experiments indicating a novel mechanism for C-O bond cleavage of **3.6**, not passing through reduction to **3.7**. Yields were calculated by ^1H NMR using an external standard. n.d. = yield not determined.

Since these competition experiments suggested different mechanisms for the C-O bond cleavage of α -phenoxy enones and α -phenoxy ketones, we performed stoichiometric experiments in an effort to isolate intermediates in the C-O cleavage of **3.6**. As ^{31}P spectral analysis would be useful for the interpretation of the experimental results, we performed these experiments using independently synthesized $\text{RuH}_2(\text{CO})(\text{PPh}_3)(\text{Ph-xantphos})^{25}$ instead of generating that complex *in situ* as was done in the catalytic experiments. Accordingly, heating a solution of **3.6** and $\text{RuH}_2(\text{CO})(\text{PPh}_3)(\text{Ph-xantphos})$ to 95 °C resulted in complete consumption of **3.6** and 89% conversion of the ruthenium complex after 100 min (Scheme 20). ^1H NMR analysis of the reaction mixture did not show new ruthenium hydride signals. The production of small amounts of propiophenone and 2-phenoxypropiophenone was observed as well as species responsible for two new broad resonances at 2.88 and 2.25 ppm in a ratio of 1.67:1. These resonances are slightly below those that are reported for O-bound ruthenium enolates (4.25-3.41 ppm) and slightly above those that have been observed for C-bound ruthenium enolates (1.96-1.90 ppm).^{28,29} ^{31}P NMR analysis revealed the presence of free triphenylphosphine along with formation of two pairs of doublets in a ratio of 1.67:1 (46.7, 45.10 ppm and 31.9, 13.7 ppm). We hypothesize that these ^1H and ^{31}P NMR resonances are due to the presence of a mixture of O- and C-bound enolates or diastereomers of C-bound enolates. While much work still remains to definitively assign these resonances to ruthenium enolates, this proposal is supported by the fact that propiophenone is produced in this reaction, presumably *via* protonolysis of a ruthenium enolate intermediate.



Scheme 20. Stoichiometric reaction of **3.6** and $\text{RuH}_2(\text{CO})(\text{PPh}_3)(\text{Ph-xantphos})$, possibly yielding ruthenium enolates. Only a C-bound enolate is shown for clarity.

Summary & Conclusion

We have designed a number of model systems to investigate the C-O bond cleavage processes that are observed in the disproportionation of lignin model compound **1.1**. We have provided evidence that the benzylic hydroxyl group is essential for the observed reactivity in 2-aryloxy-1-phenylethanol substrates. While kinetic data suggest that a mechanism whereby benzylic alcohol oxidation is followed by ether bond reductive cleavage is incorrect, the data do support a mechanism whereby the 2-aryloxy-1-phenylethanol substrates are converted to a catalytic intermediate that can either dissociate 2-aryoxyacetophenone or form the propiophenone and aryl alcohol products. Radical trapping experiments suggest this mechanism does not proceed *via* radical intermediates, although aromatic compounds (some of which have been utilized as radical traps) retard the reaction, possibly by complexation to metal-based intermediates. Attempts at characterizing the catalyst resting state of the C-O bond cleavage reaction *via* both NMR and IR analysis were not successful. Deuterium tracer experiments suggest the C-O bond cleavage reaction observed in hydrosilylation of 2-phenoxyacetophenone proceeds through a ruthenium enolate intermediate. Finally, catalytic and stoichiometric experiments were carried out on a 2-phenoxy-1-phenylpropenone substrate, which indicate a novel mechanism is operative for the C-O bond cleavage of such substrates. At this stage, we propose that the C-O bond cleavage reactions of all substrates investigated proceed *via* ruthenium enolate intermediates.

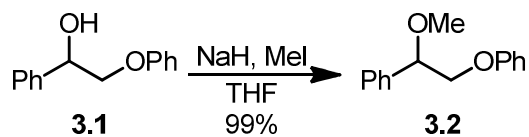
Future studies by others working on this project will focus on the isolation and characterization of catalytic intermediates in the C-O bond cleavage reactions of the 2-aryloxy-1-phenylethanol and 2-phenoxy-1-phenylpropenone substrates.

Experimental

General Information. All reactions and manipulations, unless otherwise noted, were carried out in an inert atmosphere (N_2) glovebox or using standard Schlenk and high vacuum techniques. Sealed NMR tubes were prepared by attaching the NMR tube directly to a Kontes high-vacuum stopcock via a cajon ultra-torr reducing union, then flame-sealing on a vacuum line. All glassware was dried in an oven at $150\text{ }^\circ\text{C}$ for at least 12 h prior to use or was flame-dried under reduced pressure. ^1H NMR and ^{13}C NMR spectra were recorded on Bruker DRX-500 (500

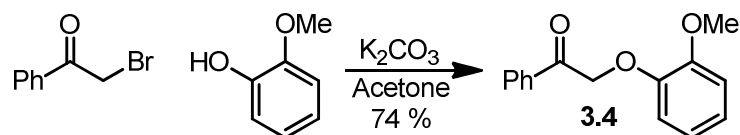
MHz), AV-500 (500 MHz), AVB-400 (400 MHz), AVQ-400 (400 MHz), and AV-300 (300 MHz) spectrometers as indicated. ^1H NMR chemical shifts (δ) are reported in parts per million relative to residual protiated solvent. Data are reported in the following format: (s = singlet, d = doublet, t = triplet, q = quartet, m = multiplet; coupling constant; integration). ^{13}C NMR chemical shifts (δ) are reported in parts per million relative to the carbon resonance of the deuterated solvent. Column chromatography was performed using a Biotage SP1 MPLC purification system and pre-packed silica gel and C18 reverse-phase columns. IR spectra of products were obtained on neat samples on NaCl plates using a ThermoNicolet Avatar 370 FT-IR spectrometer. IR spectra of reaction mixtures and ruthenium catalysts in solution were obtained using a Mettler Toledo ReactIR iC10 equipped with a 9.5 mM AgX Fiber Conduit. GC/MS analysis was carried out using an Agilent Technologies 6890 network GC system coupled with an Agilent technologies 5973 network mass selective detector. The temperatures of the NMR probe in the variable temperature experiments were determined from the ^1H NMR chemical shifts of ethylene glycol and MeOH samples.

Materials. Tetrahydrofuran and toluene were dried and purified by passage through a column of activated alumina under N_2 pressure followed by sparging with N_2 .⁴² CDCl_3 , PhMe- d_8 , and CD_2Cl_2 were obtained from Cambridge Isotope Labs, Inc. CDCl_3 was stored over K_2CO_3 . PhMe- d_8 was sparged with N_2 and stored over activated 4 Å molecular sieve pellets overnight. CD_2Cl_2 was used without further purification. The 4 Å molecular sieve pellets were obtained from Sigma-Aldrich and activated by heating at 150 °C under vacuum for 24 h. 9,10-dihydroanthracene was obtained from Sigma-Aldrich and recrystallized from ethanol. Vinyltrimethylsilane was obtained from Sigma-Aldrich and was stored over activated 4 Å molecular sieve pellets overnight. 2'-methylacetophenone was obtained from Sigma-Aldrich and was distilled. Tri-*iso*-propylsilane was obtained from Sigma-Aldrich and distilled. Acetophenone was obtained from Eastman Chemical Company and distilled. Sodium hydride, iodomethane, 2-bromoacetophenone, 2,6-di-*tert*-butyl-4-methylphenol, paraformaldehyde, and dimethylammonium chloride were obtained from Sigma-Aldrich; potassium carbonate was obtained from EMD Chemicals; guaiacol was obtained from Acros Organics; acetone, *iso*-propanol, and acetic acid were obtained from Fisher Scientific; triethylsilyl deuteride (97% D) was obtained from Isotec; these reagents were used without further purification. 2-phenoxy-1-phenylethanol,¹⁹ 2-phenoxyacetophenone,⁴³ 2-phenoxypropiophenone,^{44,45} and $\text{RuH}_2(\text{CO})(\text{PPh}_3)(\text{Ph-xantphos})$ ²⁵ were synthesized according to literature procedures. Characterization data for these compounds agree with literature values.

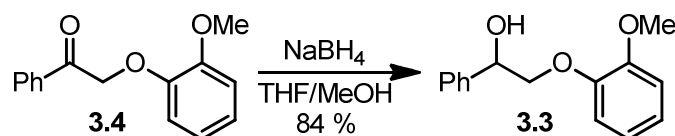


Synthesis of 2-methoxy-1-phenoxy-1-phenylethane (3.1). A round bottom flask was charged with 2-phenoxy-1-phenylethanol (505 mg, 2.35 mmol) and tetrahydrofuran (12 mL). The resulting solution was cooled to 0 °C and sodium hydride (94 mg, 60 wt% in mineral oil, 2.35 mmol) was added in one portion. The resulting suspension was stirred at 0 °C for 1.5 h after which iodomethane (0.15 mL, 2.47 mmol) was added dropwise. The reaction mixture was allowed to warm to room temperature, stirred overnight, and quenched with half-saturated aqueous sodium bicarbonate solution. The aqueous layer was extracted twice with ethyl acetate.

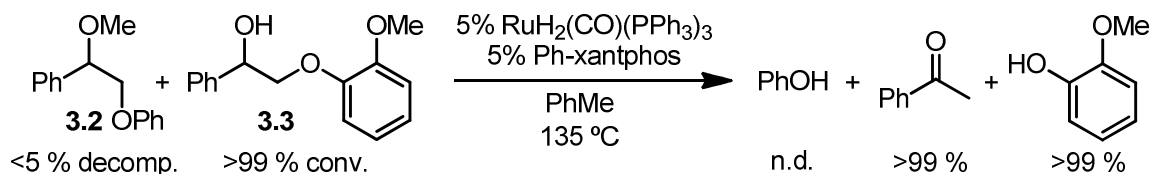
The combined organic extracts were washed twice with brine, dried over MgSO₄, filtered, concentrated *in vacuo*, and purified by silica gel chromatography (5-12% EtOAc in hexanes) yielding 534 mg **3.2** as a yellow oil (99%). ¹H NMR (500 MHz, CDCl₃): δ 7.44-7.32 (m, 5H), 7.27 (t, *J* = 8.0 Hz, 2H), 6.97-6.90 (m, 3H), 4.61 (dd, *J* = 3.6, 7.9 Hz, 1H), 4.19 (dd, *J* = 8.0, 10.3 Hz, 1H), 4.02, (dd, *J* = 3.6, 10.3 Hz, 1H) ppm; ¹³C NMR (125 MHz, CDCl₃): δ 158.8, 138.7, 129.6, 128.8, 128.4, 127.2, 121.1, 114.9, 82.4, 72.4, 57.4 ppm; HRMS (FAB⁺) Exact mass calcd for C₁₅H₁₆O₂ [M]⁺: 228.1150, found 228.1152.



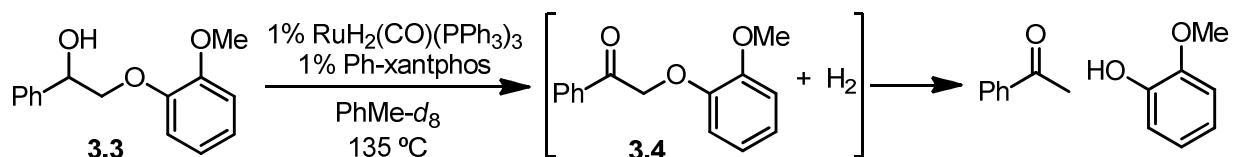
Synthesis of 2-guaiacoxy-acetophenone (3.4). A round bottom flask equipped with a reflux condenser was charged with 2-bromoacetophenone (11.8 g, 59.4 mmol), potassium carbonate (12.3 g, 89.1 mmol), guaiacol (8.2 mL, 74.2 mmol), and acetone (250 mL). The resulting suspension was stirred and heated to reflux for 3 h, after which it was filtered through a plug of Celite and concentrated *in vacuo*. The resulting solid was crystallized from ethanol to give 10.6 g **3.4** as white crystals (74%). ¹H NMR (100 MHz, CDCl₃): δ 7.99 (d, *J* = 7.5 Hz, 2H), 7.59 (t, *J* = 7.5 Hz, 1H), 7.47 (t, *J* = 7.6 Hz, 2H), 6.99-6.81 (m, 4H), 5.33 (s, 2H), 3.86 (s, 3H) ppm; ¹³C NMR (100 MHz, CDCl₃): δ 194.8, 150.0, 147.7, 134.8, 134.0, 129.0, 128.3, 122.7, 121.0, 115.1, 112.4, 72.3, 56.1 ppm; LRMS (EI⁺) Mass calcd for C₁₅H₁₄O₃ [M]⁺: 242, found 242.



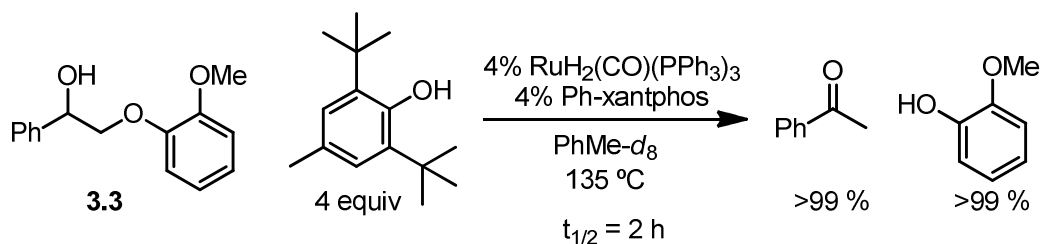
Synthesis of 2-guaiacoxy-1-phenylethanol (3.3). A round bottom flask was charged with 2-(guaiacoxy)-acetophenone (8.2 g, 34.0 mmol), tetrahydrofuran (170 mL), and methanol (60 mL). To the resulting solution was added sodium borohydride (1.9 g, 51.0 mmol) in portions over 5 minutes, after which the reaction mixture was stirred for 16 h at room temperature. The reaction was quenched with water (170 mL), and the resulting mixture was extracted twice with ethyl acetate. The combined organic extracts were washed twice with brine, dried over MgSO₄, filtered, and concentrated *in vacuo* to give a clear oil. The oil was lyophilized from benzene to give 6.97 g **3.3** as a white solid (84%). ¹H NMR (600 MHz, CDCl₃): δ 7.43 (d, *J* = 7.5 Hz, 2H), 7.36 (t, *J* = 7.6 Hz, 2H), 7.30 (t, *J* = 7.3 Hz, 1H), 6.98 (t, *J* = 7.8 Hz, 1H), 6.94-6.87 (m, 3H), 5.11 (d, *J* = 9.37 Hz, 1H), 4.17 (dd, *J* = 2.92, 10.1 Hz, 1H), 3.98 (t, *J* = 9.7 Hz, 1H), 3.86 (s, 3H), 3.58 (d, *J* = 1.8 Hz, 1H) ppm; ¹³C NMR (150 MHz, CDCl₃): δ 150.3, 148.2, 139.7, 128.6, 128.2, 126.5, 122.7, 121.2, 116.2, 112.1, 76.4, 72.5, 56.0 ppm; HRMS (ESI⁺) Exact mass calcd for C₁₅H₁₆O₃Na [M+Na]⁺: 267.0992, found 267.0996.



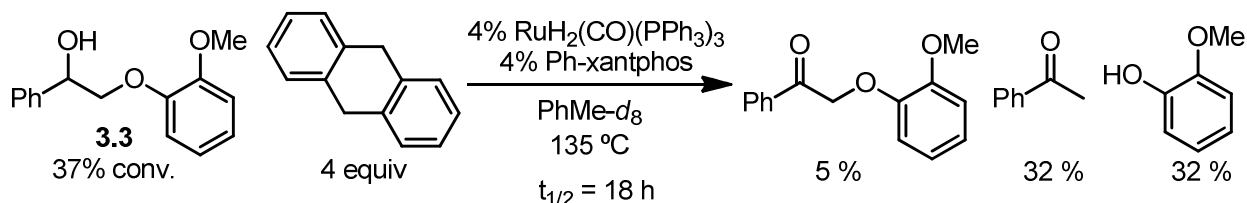
Control reaction showing the necessity of a free hydroxyl group for successful disproportionation. An NMR tube was charged with $\text{RuH}_2(\text{CO})(\text{PPh}_3)_3$ (7.3 mg, 0.008 mmol), 4,5-bis(diphenylphosphino)-9,9-dimethylxanthene (4.6 mg, 0.008 mmol), **3.3** (9.8 mg, 0.040 mmol), toluene- d_8 (350 μL), and a glass capillary containing 4-trifluoromethylpyridine. The NMR tube was sealed under vacuum and heated at 135 $^\circ\text{C}$ for 18 min, after which 33% conversion of **3.3**, 26% yield of acetophenone, and 7% yield of guaiacol were observed by ^1H NMR. The NMR tube was then opened and a solution of **3.2** (150 μL , 800 mM in toluene- d_8 , 0.120 mmol) was added. The NMR tube was sealed under vacuum, heated at 135 $^\circ\text{C}$, and monitored periodically *via* ^1H NMR. After 3.45 h of heating, quantitative conversion of **3.3** to acetophenone and guaiacol and less than 5% decomposition of **3.2** were observed. No phenol was detected by GC/MS analysis of the reaction mixture. The diagnostic resonances used to determine yields by comparison to the external standard are as follows: ^1H NMR (600 MHz, $\text{PhMe-}d_8$): 2-guaiacoxy-1-phenylethanol – δ 4.98 (d, $J = 9.0$ Hz, 1H), 3.89 (dd, $J = 3.0, 9.6$ Hz, 1H), 3.56 (s, 1H) ppm; 2-guaiacoxyacetophenone – δ 4.80 (s, 2H) ppm; acetophenone – δ 2.14 (s, 3H) ppm; guaiacol – δ 5.57 (s, 1H), 3.20 (s, 3H) ppm; 2-methoxy-1-phenoxy-1-phenylethane – δ 4.41 (dd, $J = 3.9, 7.6$ Hz, 1H), 4.03 (dd, $J = 7.8, 9.9$ Hz, 1H), 3.16 (s, 3H) ppm. The diagnostic resonance of the 4-trifluoromethylpyridine external standard is as follows: ^1H NMR (600 MHz, neat): δ 8.82 (d, $J = 4.8$ Hz, 2H) ppm.



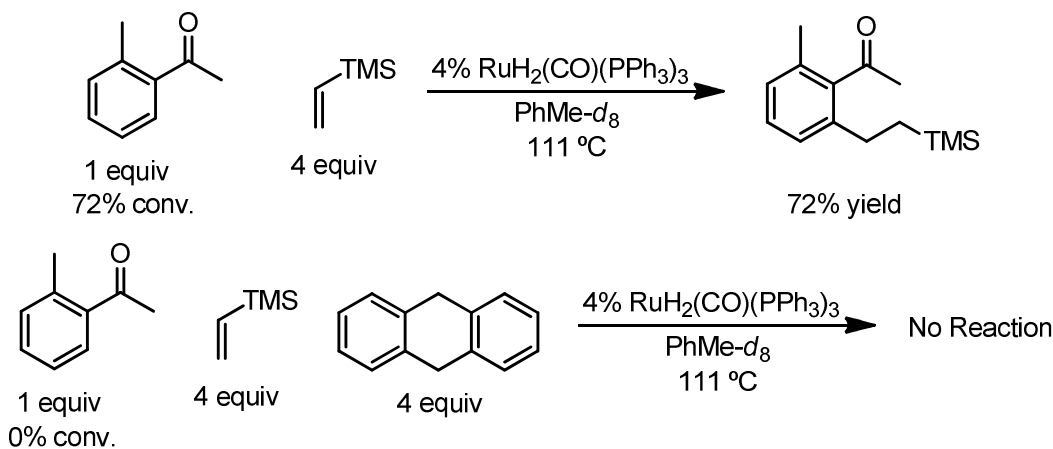
Kinetic analysis of the disproportionation of 3.3. A solution of **3.3** (250 μL , 640 mM in toluene- d_8 , 0.160 mmol) and a solution containing $\text{RuH}_2(\text{CO})(\text{PPh}_3)_3$ and 4,5-bis(diphenylphosphino)-9,9-dimethylxanthene (50 μL , 32 mM in both, 0.0016 mmol of both) were combined in an NMR tube with toluene- d_8 (100 μL) and a glass capillary containing 4-trifluoromethylpyridine. The NMR tube was sealed under vacuum and the reaction mixture was analyzed *via* ^1H NMR on an AV-500 spectrometer to verify that the catalyst loading was 1 mol%. Kinetic analysis of the reaction was carried out in the following fashion: the NMR tube was completely submerged in a circulating oil bath equilibrated to 135 $^\circ\text{C}$; the tube was removed from the oil bath and cooled under a stream of hexanes; the reaction mixture was monitored for disappearance of **3.3**, appearance and disappearance of **3.4**, and appearance of acetophenone and guaiacol (*via* single-scan ^1H NMR spectroscopy using an AVQ-400 spectrometer); the tube was replaced in the oil bath. Only time spent in the oil bath was included in the concentration versus time plots. The timecourse obtained in this fashion is shown in Figure 1. The diagnostic resonances used to determine yields by comparison to the external standard are as listed above for the disproportionation of **3.3** in the presence of **3.2**. The temperature of the circulating oil bath was measured using a calibrated mercury thermometer, and varied ± 0.1 $^\circ\text{C}$.



Disproportionation of 3.3 in the presence of radical trap 2,6-di-tert-butyl-4-methylphenol. A solution of **3.3** (200 μL , 200 mM in toluene- d_8 , 0.040 mmol) and a solution containing $\text{RuH}_2(\text{CO})(\text{PPh}_3)_3$ and 4,5-bis(diphenylphosphino)-9,9-dimethylxanthene (50 μL , 32 mM in both, 0.0016 mmol of both) were combined in an NMR tube with 2,6-di-tert-butyl-4-methylphenol (35 mg, 0.160 mmol), toluene- d_8 (150 μL), and a glass capillary containing 4-trifluoromethylpyridine. The NMR tube was sealed under vacuum, heated at $135\text{ }^\circ\text{C}$, and monitored periodically *via* ^1H NMR, which after 15 h of heating indicated complete consumption of **3.3**. The approximate half-life of the reaction was 2 h. The diagnostic resonances used to determine yields by comparison to the external standard are as listed above for the disproportionation of **3.3** in the presence of **3.2**. A control reaction was carried out in an identical fashion omitting the addition of 2,6-di-tert-butyl-4-methylphenol, and proceeded with an approximate half-life of 2 h.

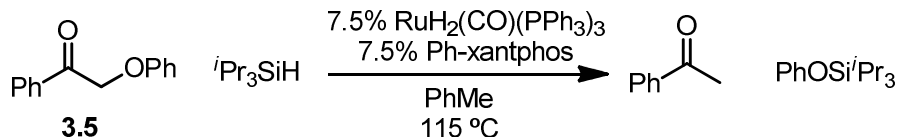


Disproportionation of 3.3 in the presence of radical trap 9,10-dihydroanthracene. A solution of **3.3** (200 μL , 200 mM in toluene- d_8 , 0.040 mmol) and a solution containing $\text{RuH}_2(\text{CO})(\text{PPh}_3)_3$ and 4,5-bis(diphenylphosphino)-9,9-dimethylxanthene (50 μL , 32 mM in both, 0.0016 mmol of both) were combined in an NMR tube with 9,10-dihydroanthracene (29 mg, 0.160 mmol), toluene- d_8 (150 μL), and a glass capillary containing 4-trifluoromethylpyridine. The NMR tube was sealed under vacuum, heated at $135\text{ }^\circ\text{C}$, and monitored periodically *via* ^1H NMR, which after 15 h of heating indicated 37% consumption of **3.3**. The approximate half-life of the reaction was 18 h. The diagnostic resonances used to determine yields by comparison to the external standard are as listed above for the disproportionation of **3.3** in the presence of **3.2**. A control reaction was carried out in an identical fashion omitting the addition of 9,10-dihydroanthracene, and proceeded with an approximate half-life of 2 h.

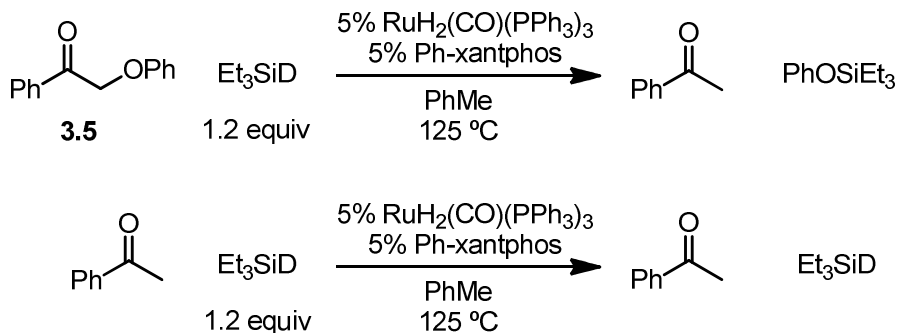


Alkylation of 2'-methylacetophenone in the presence and absence of 9,10-dihydroanthracene. An NMR tube was charged with 9,10-dihydroanthracene (28.8 mg, 0.160 mmol), 2-methylacetophenone (5.2 μL , 0.040 mmol), vinyltrimethylsilane (23.4 μL , 0.160 mmol), a solution of $\text{RuH}_2(\text{CO})(\text{PPh}_3)_3$ (100 μL , 16 mM in toluene- d_8 , 0.0016 mmol), toluene- d_8 (272 μL), and a glass capillary containing 4-trifluoromethylpyridine. The NMR tube was sealed under vacuum, heated at 111 °C, and monitored periodically *via* ^1H NMR. A control reaction was carried out in an identical fashion omitting the addition of 9,10-dihydroanthracene. After 2 h 40 min of heating, ^1H NMR analysis of the reaction mixture containing 9,10-dihydroanthracene indicated no conversion of 2'-methylacetophenone and no production of 2'-methyl-6'-(2-(trimethylsilyl)ethyl)acetophenone. After 2 h 40 min of heating, ^1H NMR analysis of the control reaction indicated 72% conversion of 2'-methylacetophenone and 72% yield of 2'-methyl-6'-(2-(trimethylsilyl)ethyl)acetophenone. The diagnostic resonances used to determine yields by comparison to the external standard are as follows: ^1H NMR (400 MHz, $\text{PhMe-}d_8$): 2'-methylacetophenone – δ 2.53 (s, 3H) ppm; vinyltrimethylsilane – δ 5.92 (dd, $J = 3.9, 14.7$ Hz, 1H), 5.67 (dd, $J = 4.0, 20.6$ Hz, 1H) ppm; 2'-methyl-6'-(2-(trimethylsilyl)ethyl)acetophenone – δ 2.51-2.44 (m, 2H), 2.06 (s, 3H), 0.86-0.78 (m, 2H) ppm. The diagnostic resonance of the 4-trifluoromethylpyridine external standard is as follows: ^1H NMR (400 MHz, neat): δ 8.82 (d, $J = 4.8$ Hz, 2H) ppm.

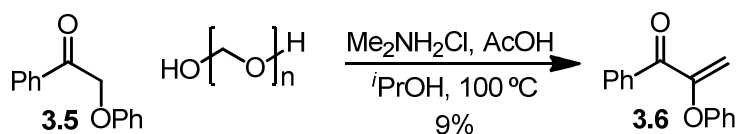
Variable-temperature NMR analysis of $\text{RuH}_2(\text{CO})(\text{PPh}_3)_3$ and $\text{RuH}_2(\text{CO})(\text{PPh}_3)(\text{Ph-xantphos})$. A 2.97 mm outer-diameter, 1.96 mm inner-diameter Wilmad-Labglass coaxial NMR insert was charged with a solution of $\text{RuH}_2(\text{CO})(\text{PPh}_3)_3$ or $\text{RuH}_2(\text{CO})(\text{PPh}_3)(\text{Ph-xantphos})$ (80 μL , 19.5 mM in toluene- d_8 , 0.00156 mmol) and toluene- d_8 (20 μL). The coaxial insert was sealed under vacuum 1 cm above the level of the solvent meniscus and inserted into a 4.96 mm outer-diameter, 3.43 mm inner-diameter J-Young NMR tube containing mesitylene- d_{12} (250 μL) and 4-trifluoromethylpyridine (10 μL). The J-Young NMR tube was placed in an AV-600 NMR probe pre-equilibrated to 37 °C. The probe was then heated in intervals of 15 °C to a maximum of 125 °C and allowed to cool to 37 °C. The reaction mixture was analyzed at each temperature *via* single-scan ^1H NMR spectroscopy and 64-scan ^{31}P NMR spectroscopy. The results of these experiments can be found in Figure 4. An additional experiment was conducted in an analogous fashion by combining a solution of $\text{RuH}_2(\text{CO})(\text{PPh}_3)_3$ and PPh_3 (80 μL , $[\text{RuH}_2(\text{CO})(\text{PPh}_3)_3] = 19.5$ mM, $[\text{PPh}_3] = 390$ mM, in toluene- d_8 , 0.00156 mmol $\text{RuH}_2(\text{CO})(\text{PPh}_3)_3$, 0.03120 mmol PPh_3) and toluene- d_8 (20 μL) in the Wilmad-Labglass coaxial NMR insert.



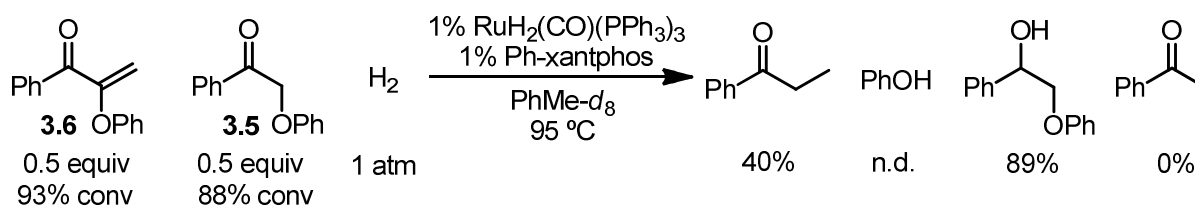
IR observation of the ruthenium catalyst during the hydrosilylation of 3.5. In an inert atmosphere glovebox, a 100 mL Schlenk tube was charged with $\text{RuH}_2(\text{CO})(\text{PPh}_3)_3$ (6.9 mg, 0.0075 mmol), 4,5-bis(diphenylphosphino)-9,9-dimethylxanthene (4.4 mg, 0.0075 mmol), 2-phenoxyacetophenone (21.2 mg, 0.100 mmol), tri-*iso*-propylsilane (20.5 μL , 0.100 mmol), and toluene (2.0 mL). The Schlenk tube was sealed with a rubber septum and removed from the glovebox, after which the septum was removed under positive nitrogen pressure and replaced with the ReactIR Fiber Conduit. The Schlenk tube was submerged in a circulating oil bath equilibrated to 122 $^\circ\text{C}$. IR spectral analysis was commenced after allowing 5 minutes for the temperature of the reaction mixture to equilibrate. The temperature of the reaction mixture was established to be 115 ± 1 $^\circ\text{C}$ by repeatedly, over the course of a number of days, submerging an identical Schlenk tube containing toluene (2.0 mL) into the same circulating oil bath equilibrated to 122 $^\circ\text{C}$ and inserting an IKA ETS-D4 thermocouple through a rubber septum in order to measure the temperature of the toluene. The results of these experiments can be found in Figures 5 and 6.



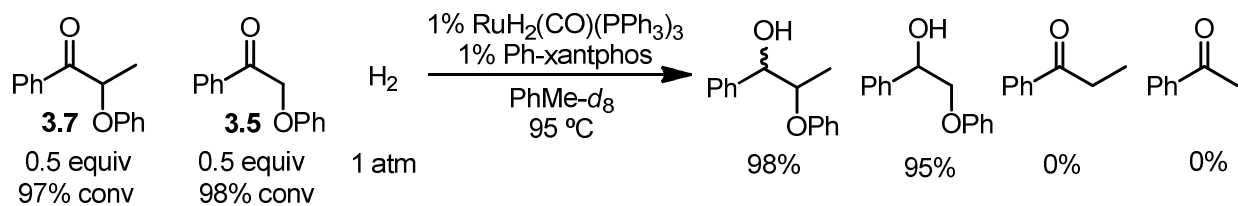
Deuterium tracer experiment in the hydrosilylation of 3.5. An NMR tube was charged with $\text{RuH}_2(\text{CO})(\text{PPh}_3)_3$ (7.3 mg, 0.008 mmol), 4,5-bis(diphenylphosphino)-9,9-dimethylxanthene (4.6 mg, 0.008 mmol), 2-phenoxyacetophenone (34.0 mg, 0.160 mmol), triethylsilyl deuteride (30.6 μL , 0.192 mmol, 97% D), and toluene- d_8 (400 μL). The NMR tube was sealed under vacuum, heated at 125 $^\circ\text{C}$, and monitored periodically *via* ^1H NMR, which after 50 min indicated 79% conversion of 3.5. A control reaction was carried out in an identical fashion, charging the NMR tube with acetophenone (18.7 μL , 0.160 mmol) instead of 2-phenoxyacetophenone. The isotopic distributions of the molecular ion of acetophenone obtained from this experiment were measured *via* GC/MS analysis of the crude reaction mixtures and integration of the mass spectral signals at m/z values of 120, 121, 122, 123, 124, and 125 in the region ± 1 minutes of the acetophenone retention time (Table 1). ^2H NMR spectra were obtained by concentrating the reaction mixtures *in vacuo*, dissolving the residues in CD_2Cl_2 , and scanning the resulting solutions on an AVB-400 spectrometer (Figure 7).



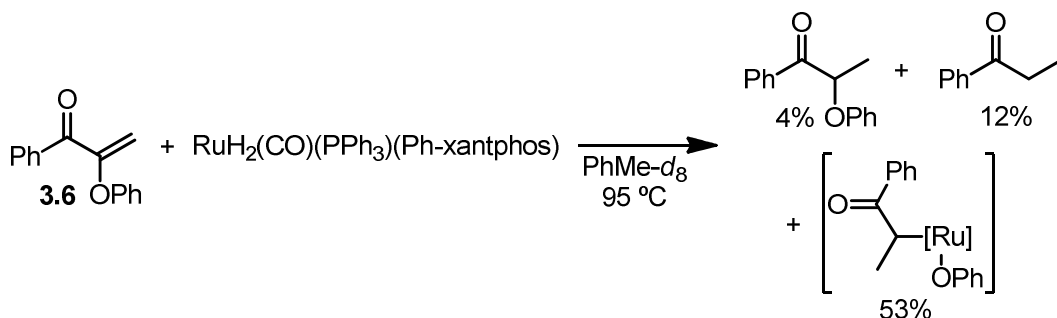
Synthesis of enone 3.6. *Caution:* this procedure should be performed behind a blast shield and not be performed on a scale larger than that described herein, as the procedure involves heating a sealed vessel in which formaldehyde gas is evolved and consumed. A 100 mL round bottom flask was charged with 2-phenoxyacetophenone (1.10 g, 5.17 mmol), paraformaldehyde (155 mg, 5.17 mmol), dimethylammonium chloride (958 mg, 11.7 mmol), *iso*-propanol (1.2 mL), and acetic acid (100 μ L). The flask was sealed with a greased glass stopper which was secured *via* rubber bands to the round bottom flask, and the reaction mixture was heated to 100 $^{\circ}$ C for 2 h. The reaction mixture was cooled to room temperature, after which the stopper was removed from the flask and water (50 mL) and saturated aqueous sodium bicarbonate (6.25 mL) were added. The flask was re-sealed and the resulting suspension was stirred at 100 $^{\circ}$ C for 30 min and cooled to room temperature. The stopper was then removed from the flask and the reaction mixture was extracted thrice with dichloromethane. The combined organic extracts were washed once with brine, dried over MgSO_4 , filtered, and concentrated *in vacuo* and purified by silica gel chromatography (4-6% EtOAc in hexanes) yielding a red oil. The oil was further purified by C18 reverse-phase chromatography (50-95% acetonitrile in water, both aqueous and organic phases containing 0.1% trifluoroacetic acid) to yield 101 mg **3.6** as a yellow oil (9%). $^1\text{H NMR}$ (600 MHz, CDCl_3): δ 7.91 (d, $J = 7.5$ Hz, 2H), 7.56 (t, $J = 7.2$ Hz, 1H), 7.44 (t, $J = 7.4$ Hz, 2H), 7.33 (t, $J = 7.5$ Hz, 2H), 7.11 (t, $J = 7.3$ Hz, 1H), 7.06 (d, $J = 7.7$ Hz, 2H), 5.38 (s, 1H), 5.11 (s, 1H) ppm; $^{13}\text{C NMR}$ (150 MHz, CDCl_3): δ 191.7, 157.4, 155.3, 136.5, 133.3, 130.1, 129.9, 128.5, 124.6, 119.7, 105.7 ppm; **IR** 1668, 1590, 1489, 1212, 963, 689 cm^{-1} ; **HRMS** (EI^+) Exact mass calcd for $\text{C}_{15}\text{H}_{12}\text{O}_2$ $[\text{M}]^+$: 224.0837, found 224.0831.



Competition experiment between 3.6 and 3.5. A solution of **3.6** (200 μ L, 400 mM in toluene- d_8 , 0.080 mmol) and a solution containing $\text{RuH}_2(\text{CO})(\text{PPh}_3)_3$ and 4,5-bis(diphenylphosphino)-9,9-dimethylxanthene (50 μ L, 32 mM in both, 0.0016 mmol of both) were combined in an NMR tube with 2-phenoxyacetophenone (17.0 mg, 0.080 mmol) and toluene- d_8 (150 μ L). The NMR tube was sealed under vacuum, heated at $95\text{ }^{\circ}\text{C}$, and monitored periodically *via* $^1\text{H NMR}$, which after 38 h 15 min indicated 93% conversion of **3.6**, 88% conversion of **3.5**, 40% yield of propiophenone, 89% yield of 2-phenoxy-1-phenylethanol, and no detectable amount of acetophenone. No acetophenone was detected by GC/MS analysis. The diagnostic resonance used to determine yield of acetophenone by comparison to the external standard are as listed above for the disproportionation of **3.3** in the presence of **3.2**. Those for other compounds are as follows: $^1\text{H NMR}$ (500 MHz, $\text{PhMe-}d_8$): 2-phenoxy-1-phenylpropenone – δ 5.24 (d, $J = 2.0$ Hz, 1H), 4.84 (d, $J = 2.1$ Hz, 1H) ppm; 2-phenoxyacetophenone – δ 4.66 (s, 2H) ppm; propiophenone – δ 2.43 (q, $J = 7.2$ Hz, 2H), 1.07 (t, $J = 7.2$ Hz, 3H) ppm; 2-phenoxy-1-phenylethanol – δ 4.86 (t, $J = 5.8$ Hz, 1H), 3.71 (d, $J = 5.9$ Hz, 2H) ppm. The diagnostic resonance of the 4-trifluoromethylpyridine external standard is as follows: $^1\text{H NMR}$ (500 MHz, neat): δ 8.82 (d, $J = 4.8$ Hz, 2H) ppm.



Competition experiment between 3.7 and 3.5. A solution containing $\text{RuH}_2(\text{CO})(\text{PPh}_3)_3$ and 4,5-bis(diphenylphosphino)-9,9-dimethylxanthene (50 μL , 32 mM in both, 0.0016 mmol of both) was combined in an NMR tube with 2-phenoxyacetophenone (17.0 mg, 0.080 mmol), 2-phenoxypropioacetophenone (18.1 mg, 0.080 mmol), and toluene- d_8 (350 μL). The NMR tube was sealed under vacuum, heated at 95 $^\circ\text{C}$, and monitored periodically *via* ^1H NMR, which after 38 h, 15 min indicated 97% conversion of 3.7, 98% conversion of 3.5, 98% yield of 2-phenoxy-1-phenylpropanol, 95% yield of 2-phenoxy-1-phenylethanol, and no detectable amounts of propiophenone or acetophenone. No propiophenone or acetophenone was detected by GC/MS analysis. The diagnostic resonance used to determine yield of acetophenone by comparison to the external standard are as listed above for the disproportionation of 3.3 in the presence of 3.2 and the competition experiment between 3.6 and 3.5. Those for other compounds are as follows: ^1H NMR (500 MHz, $\text{PhMe-}d_8$): 2-phenoxypropioacetophenone – δ 5.13 (q, $J = 6.7$ Hz, 1H), 1.44 (d, $J = 6.7$ Hz, 3H) ppm; 2-phenoxy-1-phenylpropanol – δ 1.11 (d, $J = 6.1$ Hz, 3H), 0.91 (d, $J = 6.0$ Hz, 3H) ppm. The diagnostic resonance of the 4-trifluoromethylpyridine external standard is as follows: ^1H NMR (500 MHz, neat): δ 8.82 (d, $J = 4.8$ Hz, 2H) ppm.



Stoichiometric reaction of 3.6 and $\text{RuH}_2(\text{CO})(\text{PPh}_3)(\text{Ph-xantphos})$. A solution of 3.6 (20.6 μL , 400 mM in toluene- d_8 , 0.00824 mmol) was combined in an NMR tube with $\text{RuH}_2(\text{CO})(\text{PPh}_3)(\text{Ph-xantphos})$ (8.0 mg, 0.00824 mmol) and toluene- d_8 (379.4 μL). The NMR tube was sealed under vacuum, heated at 95 $^\circ\text{C}$, and monitored periodically *via* ^1H NMR, which after 100 min indicated complete consumption of 3.6, 89% conversion of $\text{RuH}_2(\text{CO})(\text{PPh}_3)(\text{Ph-xantphos})$, 4% yield of 2-phenoxypropioacetophenone, 12% yield of propiophenone, and 53% yield of the presumed ruthenium enolate species. The NMR tube was opened and the reaction mixture analyzed *via* GC/MS, which revealed no products aside from phenol that were not assigned above *via* ^1H NMR analysis. The diagnostic resonance used to determine yield of acetophenone by comparison to the external standard are as listed above for the competition experiment between 3.6 and 3.5 and the competition experiment between 3.7 and 3.5. Those assigned to the presumed ruthenium enolate species are as follows: ^1H NMR (400 MHz, $\text{PhMe-}d_8$): δ 2.88 (broad, 1.67H), 2.25 (broad, 1H) ppm; ^{31}P NMR (162 MHz, $\text{PhMe-}d_8$): δ 46.7 (d, $J = 7.2$ Hz, 1.67H), 45.1 (d, $J = 7.2$ Hz, 1.67H), 31.9 (d, $J = 2.0$ Hz, 1H), 13.7 (s) ppm.

References

- (1) Brieger, G.; Nestruck, T. J. *Chem. Rev.* **1974**, *74*, 567.
- (2) Samec, J. S. M.; Bäckvall, J. E.; Andersson, P. G.; Brandt, P. *Chem. Soc. Rev.* **2006**, *35*, 237.
- (3) Zassinovich, G.; Mestroni, G.; Gladdiali, S. *Chem. Rev.* **1992**, *92*, 1051.
- (4) Dobson, A.; Robinson, S. D. *J. Organomet. Chem.* **1975**, *87*, C52.
- (5) Dobson, A.; Robinson, S. D. *Inorg. Chem.* **1977**, *16*, 137.
- (6) Dobson, A.; Robinson, S. D. *Inorg. Chem.* **1977**, *16*, 1321.
- (7) Wenkert, E.; Michelotti, E. L.; Swindell, C. S. *J. Am. Chem. Soc.* **1979**, *101*, 2246.
- (8) Wenkert, E.; Michelotti, E. L.; Swindell, C. S.; Tingoli, M. *J. Org. Chem.* **1984**, *49*, 4894.
- (9) Bryndza, H. E.; Tam, W. *Chem. Rev.* **1988**, *88*, 1163.
- (10) van der Boom, M. E.; Liou, S.-Y.; Ben-David, Y.; Vigalok, A.; Milstein, D. *Angew. Chem. Int. Ed.* **1997**, *36*, 625.
- (11) van der Boom, M. E.; Liou, S.-Y.; Ben-David, Y.; Shimon, L. J. W.; Milstein, D. *J. Am. Chem. Soc.* **1998**, *120*, 6531.
- (12) Dankwardt, J. W. *Angew. Chem. Int. Ed.* **2004**, *43*, 2428.
- (13) Kakiuchi, F.; Usui, M.; Ueno, S.; Chatani, N.; Murai, S. *J. Am. Chem. Soc.* **2004**, *126*, 2706.
- (14) Ueno, S.; Mizushima, E.; Chatani, N.; Kakiuchi, F. *J. Am. Chem. Soc.* **2006**, *128*, 16516.
- (15) Guan, B.-T.; Xiang, S.-K.; Wang, B.-Q.; Sun, Z.-P.; Wang, Y.; Zhao, K.-Q.; Shi, Z.-J. *J. Am. Chem. Soc.* **2008**, *130*, 3268.
- (16) Guan, B.-T.; Xiang, S.-K.; Wu, T.; Sun, Z.-P.; Wang, B.-Q.; Zhao, K.-Q.; Shi, Z.-J. *Chem. Commun.* **2008**, 1437.
- (17) Tobisu, M.; Shimasaki, T.; Chatani, N. *Angew. Chem. Int. Ed.* **2008**, *47*, 4866.
- (18) Choi, J.; Choliy, Y.; Zhang, X.; Emge, T. J.; Krogh-Jespersen, K.; Goldman, A. S. *J. Am. Chem. Soc.* **2009**, *131*, 15627.
- (19) Kandamarachchi, P. H.; Autrey, T.; Franz, J. A. *J. Org. Chem.* **2002**, *67*, 7937.
- (20) Hoops, S.; Sahle, S.; Gauges, R.; Lee, C.; Pahle, J.; Simus, N.; Singhal, M.; Xu, L.; Mendes, P.; Kummer, U. *Bioinformatics* **2006**, *22*, 3067.
- (21) For further information or to download Copasi, see: <http://www.copasi.org/tiki-index.php>.
- (22) Nagashima, H. Ruthenium-Promoted Radical Reactions. In *Ruthenium in Organic Synthesis*; Murahashi, S.-I., Ed.; Wiley-VCH: Weinheim, 2004.
- (23) Trost, B. M.; Toste, F. D.; Pinkerton, A. B. *Chem. Rev.* **2001**, *101*, 2067.
- (24) Kakiuchi, F.; Sekine, S.; Tanaka, Y.; Kamatani, A.; Sonoda, M.; Chatani, N.; Murai, S. *Bull. Chem. Soc. Jpn.* **1995**, *68*, 62.
- (25) Ledger, A. E. W.; Slatford, P. A.; Lowe, J. P.; Mahon, M. F.; Whittlesey, M. K.; Williams, J. M. J. *J. Chem. Soc. Dalton Trans.* **2009**, 716.
- (26) Ball, G. E.; Mann, B. E. *J. Chem. Soc. Chem. Commun.* **1992**, 561.
- (27) Colombo, M.; George, M. W.; Moore, J. N.; Pattison, D. I.; Perutz, R. N.; Virrels, I. G.; Ye, T.-Q. *J. Chem. Soc. Dalton Trans.* **1997**, 2857.
- (28) Hartwig, J. F.; Andersen, R. A.; Bergman, R. G. *J. Am. Chem. Soc.* **1990**, *112*, 5670.
- (29) Hartwig, J. F.; Bergman, R. G.; Andersen, R. A. *Organometallics* **1991**, *10*, 3326.
- (30) Rasley, B. T.; Rapta, M.; Kulawiec, R. *J. Organometallics* **1996**, *15*, 2852.

- (31) Matsuda, I.; Shibata, M.; Sato, S. *J. Organomet. Chem.* **1988**, *340*, C5.
- (32) Trost, B. M.; Portnoy, M.; Kurihara, H. *J. Am. Chem. Soc.* **1997**, *119*, 836.
- (33) Berger, D.; Imhof, W. *Tetrahedron* **2000**, *56*, 2015.
- (34) Chang, S.; Na, Y.; Choi, E.; Kim, S. *Org. Lett.* **2001**, *3*, 2089.
- (35) Wang, M.; Yang, X.-F.; Li, C.-J. *Eur. J. Org. Chem.* **2003**, 998.
- (36) Doi, T.; Fukuyama, T.; Horiguchi, J.; Okamura, T.; Ryu, I. *Synlett* **2006**, *5*, 721.
- (37) Doi, T.; Fukuyama, T.; Minamino, S.; Husson, G.; Ryu, I. *Chem. Commun.* **2006**, 1875.
- (38) Doi, T.; Fukuyama, T.; Minamino, S.; Ryu, I. *Synlett* **2006**, *18*, 3013.
- (39) Bartoszewicz, A.; Livendahl, M.; Martín-Matute, B. *Chem. Eur. J.* **2008**, *14*, 10547.
- (40) Jang, H.-Y.; Huddleston, R. R.; Krische, M. J. *J. Am. Chem. Soc.* **2002**, *124*, 15156.
- (41) Nishiyama, H.; Shiomi, T. *Top. Curr. Chem.* **2007**, *279*, 105.
- (42) Alaimo, P. J.; Peters, D. W.; Arnold, J.; Bergman, R. G. *J. Chem. Ed.* **2001**, *78*, 64.
- (43) Banerjee, A.; Lee, K.; Falvey, D. E. *Tetrahedron* **1999**, *55*, 12699.
- (44) Fabbri, C.; Bietti, M.; Lanzalunga, O. *J. Org. Chem.* **2005**, *70*, 2720.
- (45) Shindo, M.; Yoshikawa, T.; Itou, Y.; Mori, S.; Nishii, T.; Shishido, K. *Chem. Eur. J.* **2006**, *12*, 524.